MESOSCALE CIRCULATION IN THE BLACK SEA: A STUDY COMBINING NUMERICAL MODELLING AND OBSERVATIONS
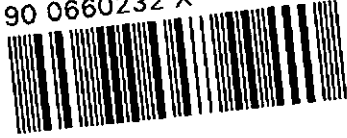
by

CECILIA ELIZABETH ENRIQUEZ ORTIZ

A thesis submitted to the University of Plymouth
in partial fulfilment for the degree of

DOCTOR OF PHILOSOPHY

School of Earth, Ocean and Environmental Sciences
Faculty of Science

April, 2005

MESOSCALE CIRCULATION IN THE BLACK SEA: A STUDY COMBINING NUMERICAL MODELLING AND OBSERVATIONS

by Cecilia Elizabeth Enriquez Ortiz

ABSTRACT

Mesoscale dynamics play a major role in the general circulation throughout the ocean. Mesoscale eddies promote the exchange of material and physical properties between different areas of the ocean such as continental shelves and the deep seas. Despite the increasing number of studies on mesoscale processes, there are further important questions unanswered concerning the origin and evolution of eddies, the mechanisms enhancing mesoscale activity and the detachment of eddies from the coast.

The present research contributes to the understanding of the mesoscale circulation in the Black Sea basin by combining hydrodynamic numerical modelling with observational data analysis. Within this research: i) A fully working eddy resolving Black Sea model was set up using the POLCOMS 3-D numerical code. ii) The mesoscale circulation in the Black Sea during October-November 2004 was characterised from *in situ* CTD measurements and from satellite-derived sea surface temperature data. iii) The Black Sea model was tested and validated against observational data. iv) The model was used to simulate the Black Sea hydrodynamics and to investigate the effects of the variability of the wind on the mesoscale activity of the basin. The detailed spatial and temporal variability of the wind field was included in the model forcing by using NCEP re-analysis wind data.

It was demonstrated that the model accurately resolves the thermo-haline structure, general circulation and mesoscale dynamics of the Black Sea basin. The model results showed that the interannual wind variability had a significant effect on the mesoscale activity and hence on the general circulation of the Black Sea basin. The mesoscale activity is very low when the wind forcing has long lasting strong cyclonic events which reinforce the large scale circulation. On the other hand, the large scale circulation is less intense and the mesoscale activity increases when the wind is weak and even more when it is anticyclonic. This study highlights the importance of taking into account the wind variability in numerical modelling studies to avoid underestimating the contribution of some important physical processes that control the ocean response to the atmospheric forcing.

CONTENTS

FIGURES

TABLES

ACKNOWLEDGEMENTS

AUTHOR'S DECLARATION

At no time during the registration for the degree of Doctor of Philosophy has the author been registered for any other University award.

The text in this thesis (excluding lists of contents, figures and references) has a total of 34,745 words.

The PhD academic program included:

- Postgraduate courses on Research Skills, Sediment dynamics, Modelling Marine Processes, Remote Sensing and Geographical Information Systems and Teaching Methods imparted by the University of Plymouth.
- Postgraduate Modelling Course imparted by Proudman Oceanographic Laboratory
- A series of Altimeter ERS/TOPEX PPOSEIDON seminars at Plymouth Marine Laboratory.

The author attended the following international courses:

- Summer School in Remote Sensing applied to Oceanography, imparted by EURISY (European Association for the Space Year); (Spain, June 2003).
- Oceanographic Campaign Baltic Floating University Cruise and International Course on the environment of the Baltic Sea On board the research vessel SIBIRYAKOV; (Baltic Sea, August, 2001).

Publications:

Enriquez, C.; Shapiro, G.; Souza, A; Zatzepin, A.; Hydrodynamic Modelling of Mesoscale Eddies in the Black Sea. In Physics of Estuaries and Coastal Seas Abstracts; No. O-26. Merida, Mexico.

Enriquez, C.; Shapiro, G.; Souza, A.; Modelling the general baroclinic circulation and thermohaline structure of the Black Sea; In 11th Postgraduate Research in Marine and Earth Science Meeting (PRMES) Abstracts; No. 6; Page 9; Southampton, UK.

Enriquez, C.; Shapiro, G.; Zatzepin, A. 2002. Mesoscale circulation in the Black Sea from remote and in situ data in November 2000. In Geophysical Research Abstracts; No. EGS02-A-00069; 127th General Assembly of the European Geophysical Society; Nice, France.

Enriquez, C.; Shapiro, G.; Zatzepin, A. 2002. Mesoscale circulation in the Black Sea from remote and in situ data in November 2000. In the Challenger Centenary Converence Marine Science, 2002 Book of Abstracts. No. P59. page 187.

Conferences Attended:

XII International Biennial Conference on Physics of Estuaries and Coastal Seas (PECS);
    (Merida, Mexico; October, 2004).

11th Annual Post-graduate Research in Marine and Earth Sciences Meeting (PRMES);
    (Southampton, UK; March 2003).

Challenger Centenary Conference for Marine Science; (Plymouth, U.K.; September, 2002)
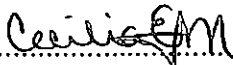
XXVII General Assembly of the EGS. (Nice, France; April, 2002)

External Contacts:

Proudman Oceanographic Laboratory, U.K. (Visited in November, 2001)
Plymouth Marine Laboratory and Marine Biological Association; Plymouth, U.K.
Shirshov Institute of Oceanology; Moscow, Russia. (Visited in January, 2004).

Signed: ....

Date: ...26 - APRIL - 2005....

CHAPTER 1. INTRODUCTION

1.1. Background and motivation

Mesoscale circulation plays a major role in the whole circulation picture all around the ocean. It is known that it influences significantly the large scale circulation (Wilson and Williams, 2004). Mesoscale eddies and meanders have spatial and temporal scales which place them as the main link between different zones of the ocean. For example, they link the coastal environment with the open ocean and because it is known that they are related to mass transfer (Shapiro *et al.*, 1995; Shapiro and Meschanov, 1996) they may provide a source of nutrient rich material from the coast to an oligotrophic and unproductive environment (deep sea). Alternatively, they may aid in voiding excess or waste suspended matter from the coastal environment, especially where eutrophication problems exist. It has been shown that mesoscale eddies and meanders are important mechanisms for shelf-deep sea transport (e.g. Huthnance, 1995; Shapiro *et al.*, 2000).

In the Black Sea the combination of many quasi-synoptic surveys, the availability of satellite data analysis (e.g. Kazmin and Sklyarov, 1982; Federov and Ginzburg, 1992; Sur and Ilyin, 1997; Oguz and Besiktepe, 1999; Ginzburg *et al.*, 2000; Zatsepin *et al.*, 2002) and the progress in eddy resolving models (e.g. Ibraev, 2001; Besiktepe *et al.*, 2001; Stanev and Staneva, 2001; Staneva *et al.*, 2001; Stanev *et al.*, 2003) have revealed the strong mesoscale activity in the hydrodynamics. This has dramatically changed the concept of the Black Sea circulation which was accepted for years as a relatively permanent distribution of currents delimiting areas and separating water masses. It is now known that the circulation is considerably more complicated, that the surface layer is controlled by mesoscale currents and that the water properties are influenced by the exchange resulting from the mesoscale activity (Ginzburg *et al.*, 2002; Zatsepin *et al.*, 2003).

Despite the increasing availability of studies of mesoscale processes by observations and modelling, they are still not fully understood. There are further important questions to answer such as the process of formation and evolution of eddies, circumstances for mesoscale activity enhancement and the separation of eddies from the coast.

1.2. Objectives

The aim of the present research is to contribute to the effort of understanding mesoscale currents particularly in the Black Sea. To achieve this, the objectives are to characterise the 3-dimensional structure of eddies, identify mechanisms involved in the process of formation of eddies and circumstances involved in their evolution.

This study combines analysis of observational data (*in situ* measurements and satellite imagery) and numerical modelling using the Proudman Oceanographic Laboratory Coastal Ocean Modelling System (POLCOMS) to study the hydrodynamics.

The Black Sea was chosen as a convenient basin to investigate circulation for its reasonably simple coastline, it has no influence of tides and moreover, because it has been widely studied both from observations and modelling providing good background information to compare results.

During this investigation we addressed the following questions:

- How important is the mesoscale circulation in determining the inter-annual variability of the large scale circulation?

- Is there a clear relationship between the stability of the macro-scale circulation with the interannual variability of the wind forcing?

- To what degree is the stability of the general circulation a determining factor for the level of mesoscale structure formation and therefore how is the mesoscale circulation affected by the wind forcing?

1.3. Outline of the thesis

This thesis starts with a review of the Black Sea dynamics in **Chapter 2** covering general aspects of the meteorology and oceanography of the study area.

Chapter 3 gives a detailed description of the materials (data) used for this study. It outlines the methodology for the data treatment. This chapter also includes the description of the numerical model used to study the hydrodynamics (POLCOMS model) and its set up for modelling the Black Sea.

Chapter 4 presents the results of the analysis of observational data. These include CTD measurements in the north-eastern region of the Black Sea and sea surface temperature satellite images covering the whole basin.

Chapter 5 shows the results of the sensitivity tests and calibration of the numerical model. The sensitivity tests were applied to the grid resolution, bathymetry, time steps and horizontal diffusion coefficient.

In **Chapter 6** we describe the process of geostrophic adjustment and the validation of the model. To validate, the modelled velocities were compared with measurements and the major circulation elements and thermo-haline structure were qualitatively verified.

Chapter 7 analyses the results of the modelled hydrodynamics from 3 sets of 2-month runs using wind data from 3 different years: 1998, 1999 and 2000. The inter-annual variability of the wind and its influence in the mesoscale circulation are considered in this chapter.

Chapter 8 provides a discussion of the results and the conclusions.

The **Appendix** compiles the Fortran and Matlab subroutines developed for this study. Figures showing the wind fields and the modelled results are compiled on a CD-ROM (attached).

1.4. Individual contribution and external collaboration

The contribution to this project from collaborators is as follows:

- The Director of Studies, G. Shapiro[1], suggested the hypothesis to test and the methodologies, participated in defining the objectives and in scientific discussions.

- The second supervisor, S. Bass[1], was involved in discussions and offered advice.

- The external advisor, A. Souza[2], helped transferring the POLCOMS model from UNIX to Windows environment and gave technical support and advice to solve problems encountered with the model.

- A. Zatsepin[3] provided raw *in situ* data and the wind data. He was also involved in discussions and contributed ideas towards the formulation of the hypothesis.

- J. Staneva[4] provided some of the initial and forcing data for the modelling.

The **individual contribution** of the candidate includes:

- Processing and analysis of *in situ* data.

- Compilation and analysis of remote sensing data.

- Development of specialist software for pre- and post-processing.

- Pre-processing of all the data for the model.

- Modification of the POLCOMS code to suit the nature of this research.

- Execution of all the modelling work, including sensitivity tests, calibration, validation and the numerical experiments.

- Post-processing of the model output data and the analysis and interpretation of the results.

[1] University of Plymouth, UK. [2] Proudman Oceanographic Laboratory, UK. [3] Shirshov Institute of Oceanology, Moscow. [4]. University of Sofia, Bulgaria.

CHAPTER 2. LITERATURE REVIEW

2.1. General aspects about the Black Sea

The Black Sea (Figure 2-1) is an enclosed basin with a maximum zonal length of approximately 1,150 km and maximum meridional length of approx 618 km. It has an area excluding its northern arm, the Sea of Azov, of 420,000 km^2 and a volume of 5.3 x 10^5 km^3 (Leonov, 1960). It has a very dramatic bottom topography which can be divided into four physiographic provinces, shelf, basin slope, basin apron and abyssal plain. There are 2 main types of slopes in the Black Sea basin, a steep highly dissected slope where erosion was dominant in the past and a smooth slope where deposition has been predominant (in the widest shelf). The Crimean Peninsula projects into the Black Sea from the north, forming the shallow Sea of Azov on the east and the Karkinitskiy Gulf on the west (Ozsoy and Unluata, 1997). Continental shelves (depth < 200 m) constitute about 25% of the total area. The maximum development of the shelf is at the west of the Crimean Peninsula, being over 200 km wide and with depth ranging from 0 to 100 m. The continental shelf is narrow in the remaining part of the Black Sea rarely exceeding a width of 20 km. It occurs as narrow stretches along the coasts of Anatolia, Caucasus and Kerch, often separated by canyons or steep slopes adjoining the land. Most of the central part of the basin is deeper than 2,000m.

The Black Sea is connected to the Mediterranean Sea through the Strait of Bosphorus, the Sea of Marmara and the Strait of Dardanelles. The Bosphorus Strait is an elongated channel with an approximate length of 31 km, about 0.7-3.5 km wide and 35.8 m average depth (Gunnerson and Ozturgut, 1974). In the north-eastern part the Black Sea is connected to the Sea of Azov through the Kerch Strait, which is a narrow and shallow channel with 5 to 18 m depth.

5
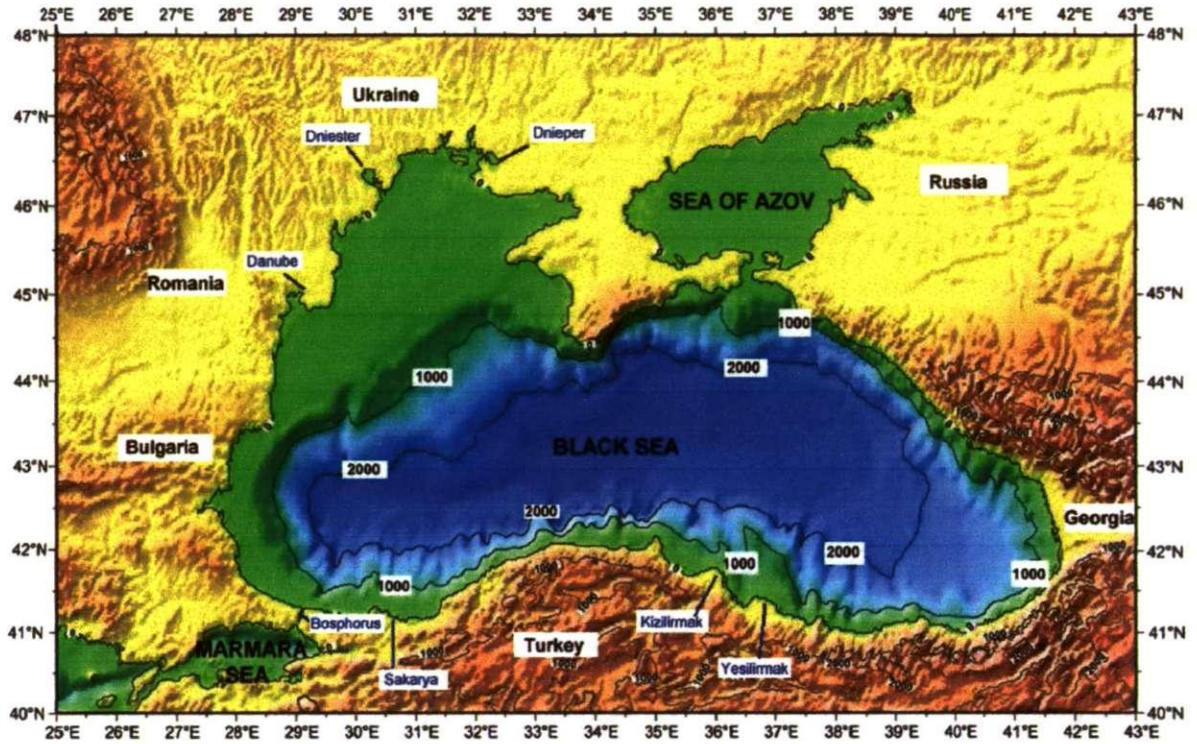
Figure 2-1 Map of the Black Sea showing the major rivers, coastal countries and topography

This degree of isolation together with the absence of tides, the low salinity and low winter water temperatures generate strong density stratification and weak vertical mixing. The Black Sea basin is almost completely anoxic, containing oxygen in the upper 90 to 200 m depth (13% of the volume of the sea) and hydrogen sulphide in deeper waters (Ozsoy and Unluata, 1997; Konovalov et al., 1999). Furthermore, the unique ecosystem of the Black Sea has been severely damaged due to eutrophication from human activities in all the 17 countries that are part of its catchment area. The catchment area covers about one third of the European continent and includes 3 of Europe's most significant riverine systems: the Danube, Dnieper and Don rivers.

The Black Sea coastline is shared by six countries and is used by each one of them for recreation, trading ports, fishing, urban development and industry. All these industries are expanding and thereby increasing the pollution of the sea (Mee, 2001).

2.2. History of the Black Sea studies

Systematic studies of the Black and Azov Seas started on 1696 by the order of the Russian Tsar Peter the Great when the coastal areas of the Azov Sea were conquered. The main interest was on navigation and measurements of the coast line were carried out by the naval boat 'Kriepest'. As a result, in 1703 the first navigational atlas of the Black and Azov Seas was published.

After this date there were no active studies until the end of the 18th century when the famous Russian zoologist Pyotr Pallas, Professor at the St. Petersburg Academy of Science, visited the Crimea in the year 1793 and studied the local fauna, especially the fish. After the Russians took the Crimean peninsula and the northern coast of the Black Sea, they built a powerful fleet and started systematic hydrographic studies of the Black Sea this time measuring not only the coastline but also the depth. The special expedition took 11 years (1825-1836) and was lead by Admiral Yegor Manganari. From their results a detailed hydrographic atlas of the Black and the Azov Seas was produced.

The next important discovery was in 1842 when the Russian chemist I. Gebel discovered that the salinity in the Black Sea is significantly lower than in the open ocean (~ 35 *psu*) and he measured it as 17.7 *psu*.

More comprehensive studies of the Black Sea, its shores and waters, began in the second half of the 19th century. Studies of the hydrology of the Black Sea were made by Admiral S. Makarov in 1880, and later in 1890 by a special deep-sea expedition organized by N. Andrusov and I. Spindler. Their studies describe the main features of the origin,

morphometry, circulation, chemistry and zoogeography of the sea up to the beginning of the 20th century. During the late 19th century there were important findings such as the existence of the hydrogen sulphide zone by N. Andrusov in 1890.

Later, extensive studies of hydrology and hydrochemistry were performed by a special Azov-Black Sea expedition of the Academy of Science of the USSR in 1927 – 1930 under the leadership of N. Knipovich (1932).

The main features of the geological history of the basin were delineated by Arkhangelski and Strakhov in 1938. The number of studies of the hydrology of the Black Sea increased substantially during that time (e.g. Antipa, 1941; Neumann, 1942; Vodyanitzki, 1948; Caspers, 1957; Bogdanova, 1959b; Vladimirtzev, 1961; Filippov, 1968).

Overall, before the 1960's the Black Sea studies were mainly carried out by the Russians and from the 60's the countries of the communist block joined in the investigation of the area. The knowledge of the hydrometeorology of the Black Sea is summarized in (Leonov, 1960) and (Blatov et al., 1984).

The importance of the Black Sea and the uniqueness of its nature attracted international attention and the USA joined in the studies with an expedition lead by Woods Hole Oceanographic Institution in 1969. Their results are given in (Degens E.T. and Ross D.A., 1974).

Since then, the surveys have been growing in coverage, resolution and quality of data as a number of international programs tasked with the study of the Black Sea area have been developed. Examples of these programs are:

The Co-operative Marine Science Programme for the Black Sea (CoMSBlack) international program starting in the year 1991. It was the first multinational program implemented in the Black Sea. It was recognized and supported by the Intergovernmental Oceanographic Commission (IOC) and UNESCO. The participating countries in

CoMSBlack were Bulgaria, Romania, Ukraine, the Russian Federation, Turkey and the USA. The NATO TU – Black Sea program which was the first highly significant NATO attempt to establish scientific collaboration with the central and eastern European countries [http://sfp1.ims.metu.edu.tr/TU-BlackSea]. The Black Sea Regional Committee (BSRC) was established in 1995 with joint international planning and implementation of operational oceanography, including ocean monitoring, promoting the development of the scientific and technological means to carry out joint programs assessing the economic and social benefits and the impacts of their activities on the region [http://www.gosic.org/goos/BLACKSEA_program_overview.htm].

A currently active program is the Black Sea Ecosystem Recovery Program, (BSERP) [http://www.blacksea-environment.org/text/default.htm]. It was initiated in the year 2002 by the Black Sea Commission and the International Commission for the Protection of the Danube River Basin with a view to develop legal, policy and technical measures to reduce the discharges of nutrients and other toxic substances in the Danube and in the Black Sea itself. It focuses on the most impacted areas (e.g. the north-western shelf). Part of this research project will contribute to the BSERP program by providing modelling results to complement the measurements obtained during the hydrographic campaign carried out in April 2004.

These programs, among others, contribute to the existence of wide data sets and scientific knowledge in the continuous and unfinished search of understanding the Black Sea environment.

2.3. Water balance of the Black Sea

The high degree of isolation from the ocean, the extensive drainage basin and the large number of incoming rivers all contribute to the unique water balance of the Black Sea. Its

components are: river discharge, precipitation, evaporation and exchange via the Bosphorus and the Kerch Straits. The characteristics of the surface waters in the Black Sea are mainly controlled by the freshwater inflow and the restricted exchange across the shallow Bosphorus Strait (described in Section 2.3.3). For many years the average fresh water input has exceeded the evaporation with considerable annual and seasonal fluctuations mainly caused by variations in the river discharges (Simonov and Altman, 1991).

The water balance of the Black Sea has been studied for many years and there is considerable controversy over the magnitude of its terms with figures of total inflow ranging from 171 km^3/yr (Altman and Kumish, 1986) to 611 km^3/yr (Unluata et al., 1990) and of total outflow between 190 km^3/yr (Sitnikov, 1972) and 612 km^3/yr (Unluata et al., 1990). These values were taken from the comparison between estimates of the Black Sea water balance presented in Degens and Ross (1974).

2.3.1. Rivers

The largest volume of river inflow to the Black Sea comes from the north-western part of the basin and most of this inflow comes from the Dnieper, Dniester, and Danube. These three rivers, together with the Sakarya, Kizilirmak and Yesilirmak, discharging along the Anatolian coast, account for 90 % of the river runoff of the entire basin. Therefore, only these six rivers were included in the numerical modelling part of this project. Their location is shown in Figure 2-1. The discharge volumes used in the model were taken from Altman and Kumish (1986) and from Jaoshvili (2002) and the figures are shown in Chapter 3 - Table 3.

Nevertheless there are about one thousand rivers that flow into the Black Sea but most of them are small rivers and many are seasonal, short lived watercourses. Long-term hydrological observations are available for the majority of rivers in the USSR and other

communist countries, while the data sets available for the rivers along the Anatolian coastline are sporadic and static observations of some of the major rivers which began only recently. As with the total water balances, the figures of the total discharge into the Black Sea vary between different databases ranging from 294 km^3/yr (Pora and Oros, 1974) to 480 km^3/yr (Vodyanitski, 1948). A comprehensive revision and up to date information about the rivers of the Black Sea is given in Jaoshvili (2002).

2.3.2. Evaporation – Precipitation

Overall the Black Sea has a positive water balance. There is an excess of evaporation over precipitation which is balanced by the water input from the major rivers and the net outflow through the Bosphorus Strait. Recent estimates amount to 225 km^3/yr for precipitation and 370 km^3/yr for evaporation (Reshetnikov, 1992 in (Jaoshvili, 2002)).

The seasonal trend shows that during December and January there is a balance between evaporation and precipitation, followed by an excess of precipitation of about 15 mm/month during February-April. Evaporation begins to dominate after May, with a maximum of about 150 mm/month in August and it starts decreasing by November and December as shown in Figure 2-2 which shows values derived from observations in Oguz and Malanotte-Rizzoli (1996).

There is also an important spatial variability as shown in Figure 2-3 and 2-4 which present modelling data from Staneva and Stanev (1998) (the description of these data is given in Chapter 3- Section 3.4). The greatest rate of evaporation occurs in the western and eastern zones between latitudes 44 °N and 45 °N. The south-eastern region receives the largest amount of precipitation which is generally caused by cyclonic activity and cyclones pass mainly from west to east through the southern part of the sea.
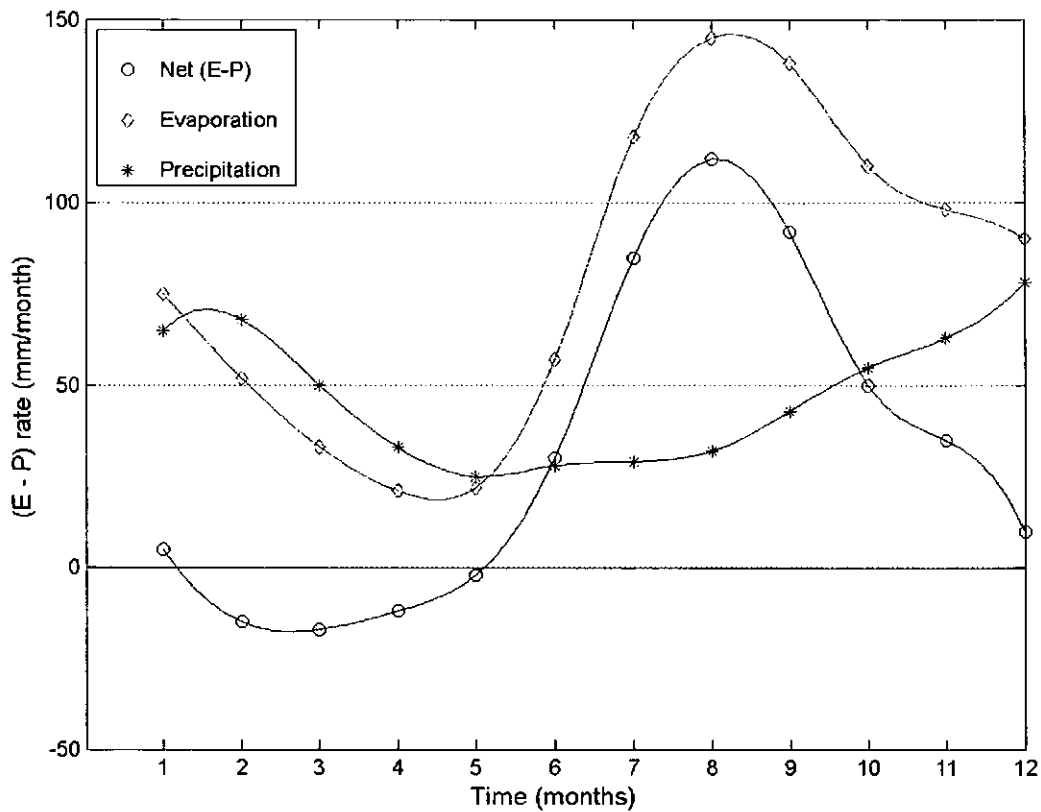
Figure 2-2 The Black Sea averaged climatological monthly variations of the evaporation – precipitation (data taken from [Oguz and Malanotte-Rizzoli, 1996]).

Overall, from October to April, the northern half of the Black Sea has an excess of evaporation over precipitation and the southern part has an excess of precipitation, being more intense in the south-eastern part of the basin. This situation persists until May when precipitation weakens. During the summer, the maximum evaporation happens near the north-western shelf and in the northern part of the centre of the basin. From May until September, nearly all the basin has an excess of evaporation over precipitation, except for the south-eastern corner.
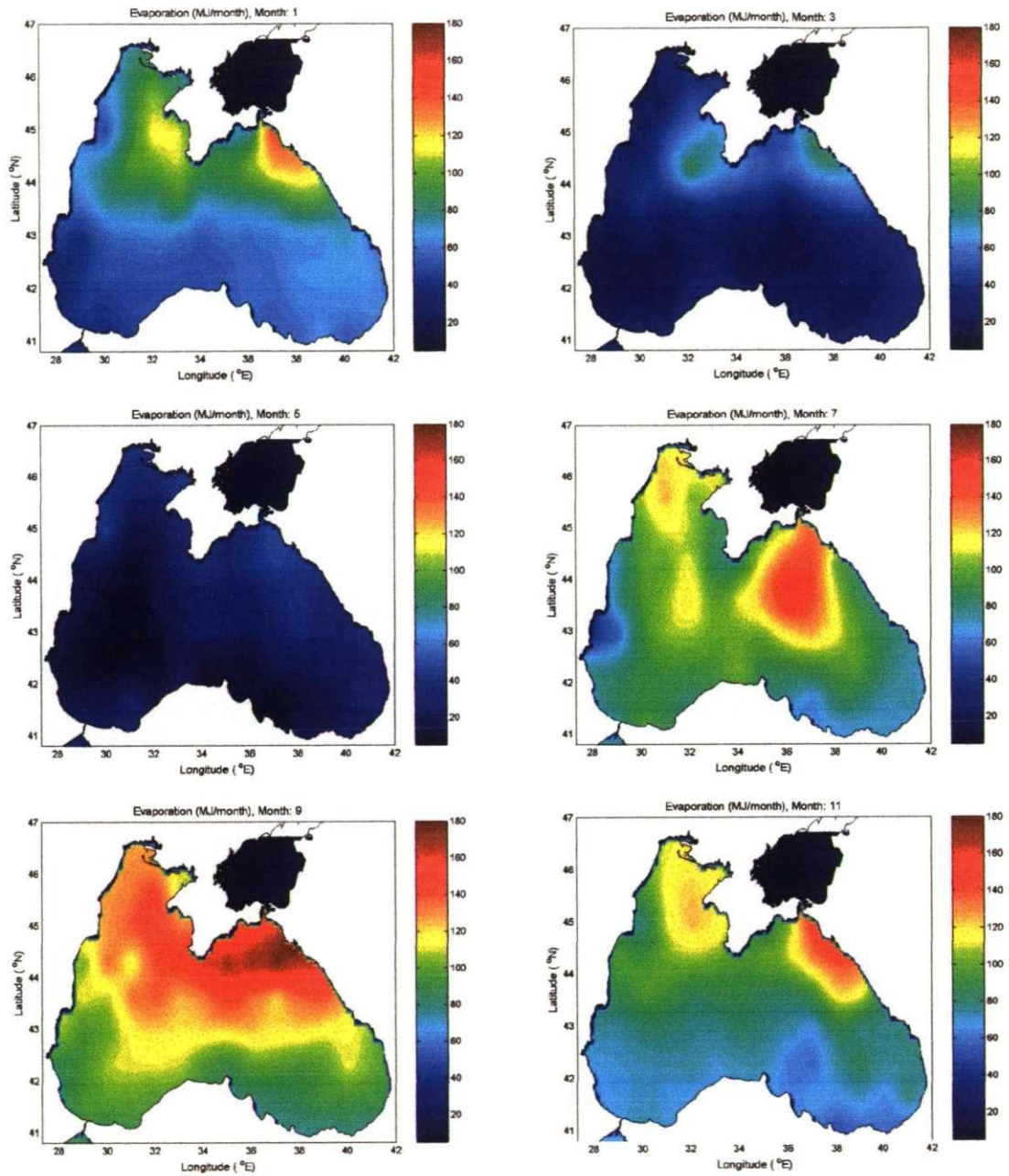
Figure 2-3 Maps of climatic evaporation distribution in the Black Sea (MJ/month) for January, March, May, July, September and November. Modelling data (Staneva and Stanev, 1998).

13
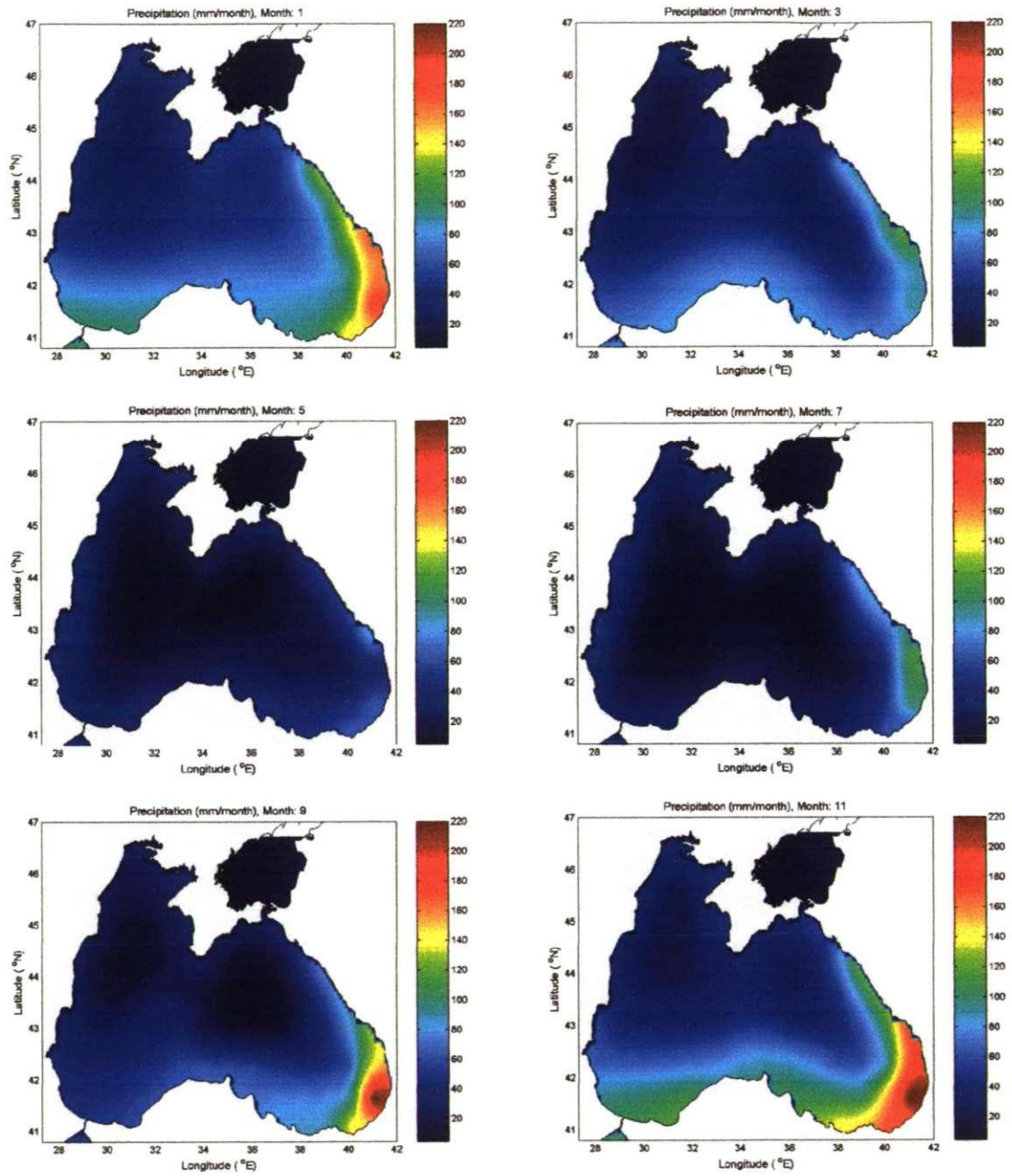
Figure 2-4 Maps of climatic precipitation distribution in the Black Sea (mm/month) for January, March, May, July, September and November Modelling data (Staneva and Stanev, 1998).

2.3.3. Exchange through the Bosphorus and Kerch straits

The Bosphorus Strait has a two-layered circulation: in the surface layer low saline water (<18 *psu*) flows southward from the Black Sea to the Marmara Sea and in the deep layer more saline water (~35 *psu*), which originates from the Mediterranean Sea, flows northward into the Black Sea. The Mediterranean water is always present in the Bosphorus Strait and it extends as a salt wedge into the Black Sea. There is a sharp intermediate transition layer in this two-layered current in the Strait.

Blocking of the flows in either layer occurs during extraordinary events, lasting for a few days each time. For example, the Mediterranean water flows into the Black Sea except under an adverse combination of strong northerly winds and extreme sea-level difference (Yuce, 1996). This lower layer blocking typically occurs during the spring and summer months, when the net freshwater influx into the Black Sea increases. The upper layer blocking events occur in the autumn and winter months, when the surface flow reverses (Ozsoy and Unluata, 1997).

The exchange flows through the Bosphorus have been estimated in various literature sources. The inflow estimates range between 100 and 300 km^3/yr and the outflow between 200 and 575 km^3/yr and a critical review of different estimates are given by Unluata et al. (1990). For modelling the Black Sea hydrodynamics in the present study, the fluxes across the Bosphorus Strait (net outflow of 197.7 km^3/yr) and Azov Sea (inflow of 17.2 km^3/yr) are taken from Altman and Kumish (1986).

2.4. Wind

The monthly distributions of wind stress are all dominated by the northerlies in the western basin, veering cyclonically towards the eastern basin where they become north-westerlies. North-easterly winds usually prevail in the southern part of the western basin. The winds

tend to be stronger in the western part and weaken toward the eastern end of the sea. The typical monthly mean wind speed is 5 m/s during the summer period, increasing to 8 m/s during the winter months (Figure 2-5). These values correspond to wind stress values ranging between 0.03 and 0.08 Pascals (using a drag coefficient, *CD,* of 0.0013). The annual mean wind field is smoother than the monthly mean, particularly in the western part of the sea where the seasonal variation is higher, while the pattern in the eastern Black Sea does not change qualitatively throughout the year (Staneva and Stanev, 1998). Accordingly, the monthly mean wind field is smoother than the weekly mean field and this is smoother than the real wind without averaging. The process of averaging removes the high variability both in magnitude and direction of the wind which is expected to have an important influence on the mesoscale activity of the currents of the sea.

The spatial variability of the wind field is shown in Figure 2-6 by plotting the averages of January, May and September of the year 2000 taken from NCEP re-analysis data.
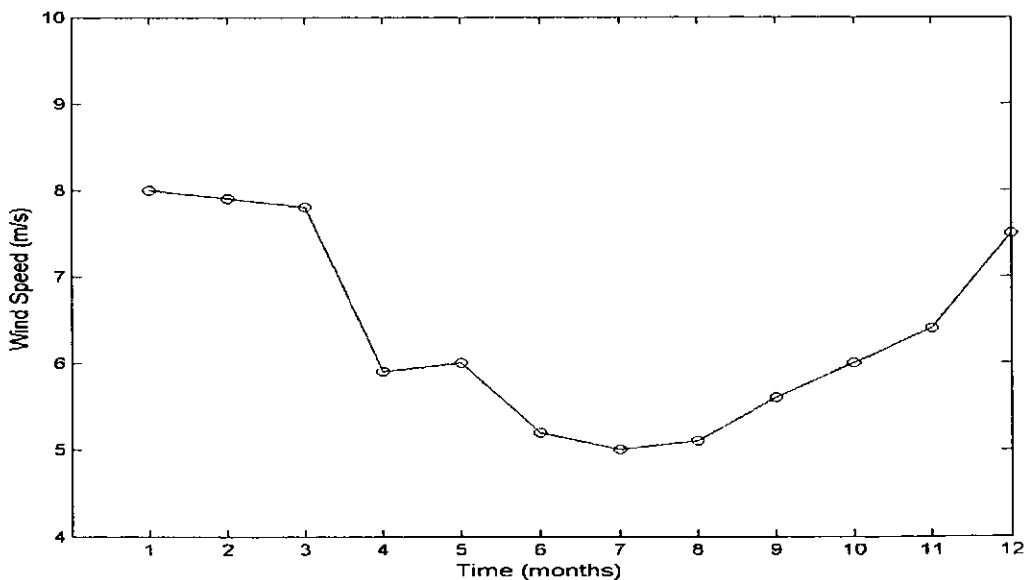
Figure 2-5 The Black Sea averaged climatological monthly variations of the wind speed (data taken from Oguz and Malanotte-Rizzoli (1996)).
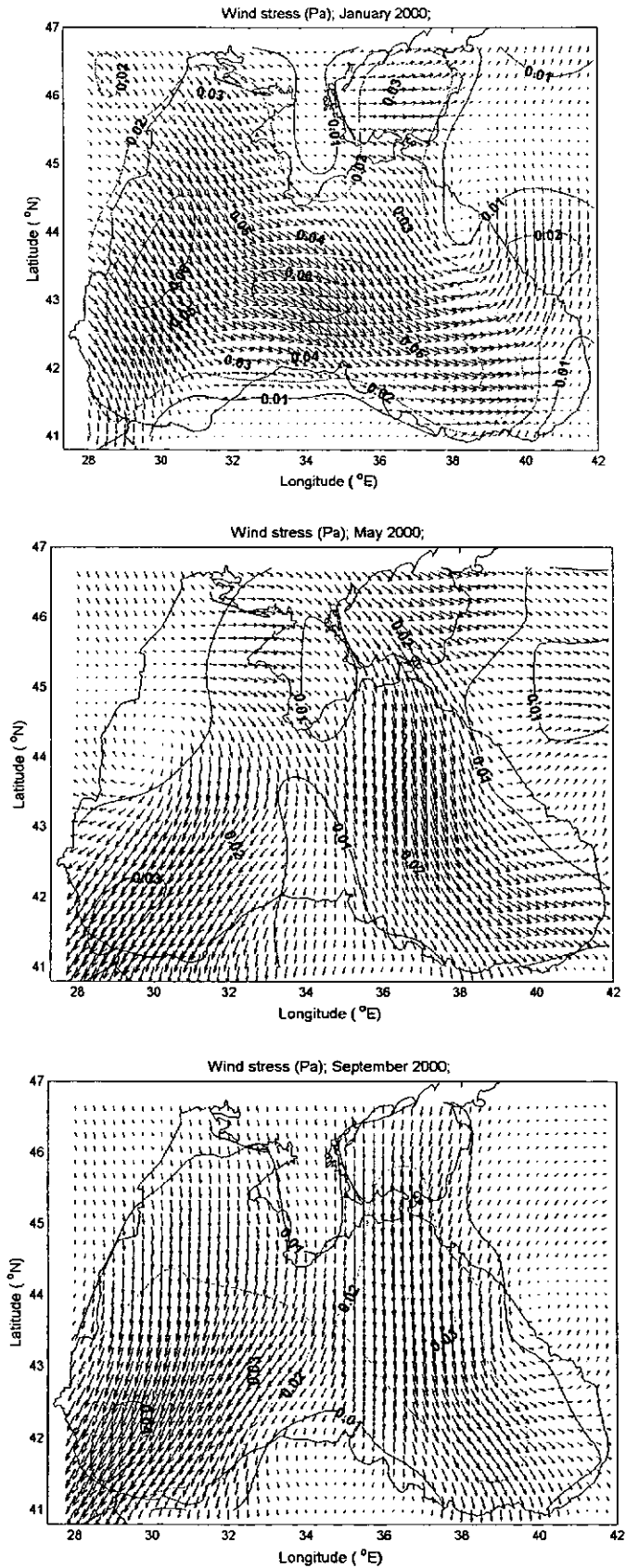
*Figure 2-6 Averaged wind stress fields for a) January, b) May and c) September 2000.
(Data taken from NCEP reanalysis)*

17

2.5. Heat fluxes

The net heat flux, QH, is the net radiative flux (Rn), defined by the sum of short-wave incoming radiation and long-wave back radiation.

According to the climatological data given by Efimov et al. (1985) the basin-averaged net heat flux variations may be described as follows: There is a cooling trend from the beginning of September to the end of February with greatest cooling rates of $\sim$150 W/m^2 occurring in December and January. From March to August there is a warming cycle of heat flux with maximum value of $\sim$150 W/m^2 during June. Overall, the heat flux is nearly balanced (Figure 2-7). The sea gains a net heat from the atmosphere of $\sim$0.4 W/m^2, which is compensated by the advective heat loss through the Bosphorus (Oguz et al., 1995).

During the cooling season (October – February), there is considerable spatial variability of net heat flux patterns within the basin as can be seen in Figure 2-8 showing the fields derived from Staneva and Stanev (1998). The maximum cooling takes place in the north-western shelf area and the minimum near the south-east. During April the basin has mainly uniform distribution of heat flux followed by a rapid warming during May. The strongest warming happens in the centre of the basin during June-July and starts to decrease slightly in August.
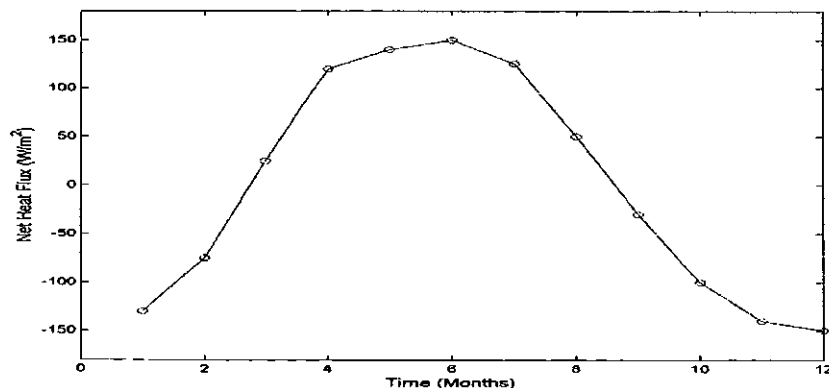
Figure 2-7 The basin averaged climatological monthly variations of the net heat flux during the year. Data taken from (Efimov and Timofeev, 1990).
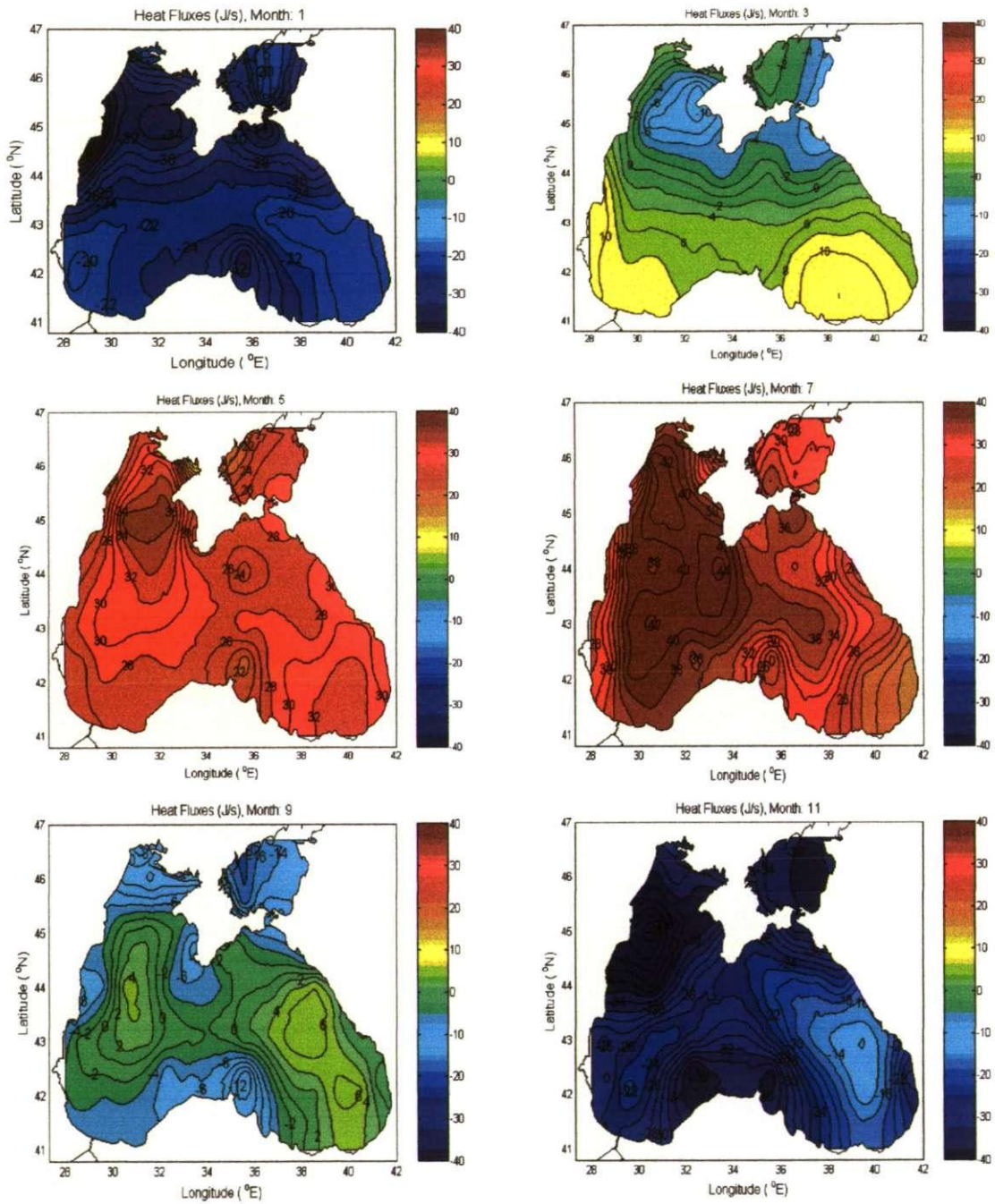
Figure 2-8 Maps of climatic heat flux distribution in the Black Sea (J/s) for January, March, May, July, September and November (Staneva and Stanev, 1998).

19

2.6. Physical oceanography of the Black Sea

2.6.1. Water masses and thermo-haline distribution

The Black Sea has three different water masses: surface layer, cold intermediate layer (CIL) and bottom layer (Filippov, 1965). Vertical transects of temperature, salinity and sigma-t are shown in Figure 2-9.

The top layer is a surface mixed layer, which responds strongly to seasonal heating and cooling at the surface. This layer has the freshest water and in the summer, the highest temperature of the water column.

Below this surface layer the cold intermediate layer is located. It is shown in Figure 2-10, and contains the coldest water of the sea characterised by the 8 °C limiting isotherm and minimum temperature of 6-7 °C in most areas of the Black Sea. It is located within a typical depth range of about 50 – 180 m overlying the main pycnocline, where vertical stratification is maintained by the salinity gradient. The major part of the circulation is confined to the surface and intermediate layers.

The heavily saline bottom layer is isolated from the surface layers. The strong density gradient results from the fresh water input due to precipitation and rivers and the input of more saline water through the Bosphorus together with the topography of the basin. Figure 2-9 shows the vertical structure of the water column in the Black Sea. The vertical mixing and seasonal turnover of the water column is limited to the upper layer down to the halocline. Under such circumstances, organic materials accumulate in the deep water and, as they are decomposed, the oxygen of the water is exhausted and hydrogen sulphide is formed. Another hypothesis suggests that the hydrogen sulphide is released by underwater volcanoes (Konovalov et al., 1999).

The halocline and the pycnocline coincide at a typical depth interval of 100-200 m, approximately where the lower boundary for the CIL is located.

There are different hypothesis on the formation of the CIL. One states that it is formed as a result of advective and convective contributions taking place along convergence zones (anticyclonic regions) of the Black Sea, mainly originating from the shelf and the continental slope area during winter and spreading during spring and summer (Ozsoy and Unluata, 1997). More recent studies (Stanev et al., 2003) show that the cold water mass is formed over the entire Black Sea but with a pronounced regional dependency so that approximately 42 % is formed in the continental slope in the north-western part of the sea, 28 % in the interior deep basin, 20 % in the north-western shelf and 10 % in the eastern basin. Stanev and Staneva (2001) demonstrated that the coastal anticyclones formed between the interior Rim Current and the coast enhance the rates of CIL penetration into the pycnocline. However this does not necessarily imply penetration from above, but rather laterally from areas possessing strong coastal eddies.

A suboxic layer, SOL, is located below the CIL with a maximum mesoplankton concentration. The pycnocline is located below the SOL, restricting the propagation of seasonal signal from the surface so that the seasonal and interannual temperature and salinity variations are only present in the upper layers above the pycnocline (Stanev et al., 1997). Waters below 500 m depth are essentially stagnant, showing little sign of change in properties, except near the boundaries where local instabilities are able to produce fine structures (Ozsoy et al., 1995)

Below a depth of 1700 m, a bottom convection layer is driven by geothermal heating from the sea floor (Besiktepe et al., 1995).This bottom layer has potential temperature of 8.893 °C and salinity of 22.3 *psu* with variations of less than 0.001 units in both potential temperature and salinity across the basin (Ivanov and Shkvorets, 1995; Oguz et al., 1993)
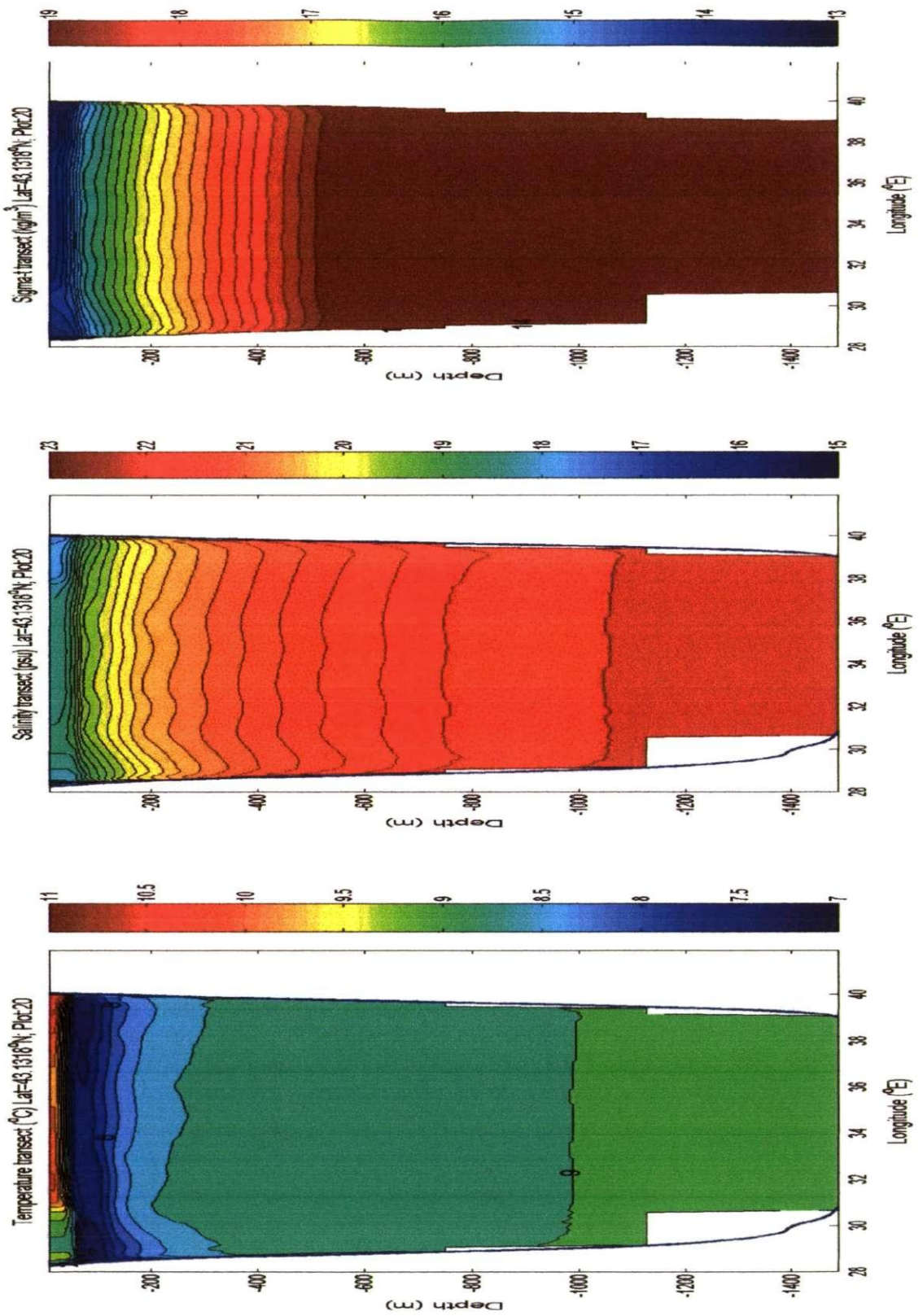
*Figure 2-9 Vertical zonal transect of the Black Sea basin at latitude 43.13 °N showing a)
temperature b) salinity and c) sigma-t; Plots show modelled output data corresponding to
the 14 of May of the year 1998 from this study to illustrate the vertical distribution.*

22
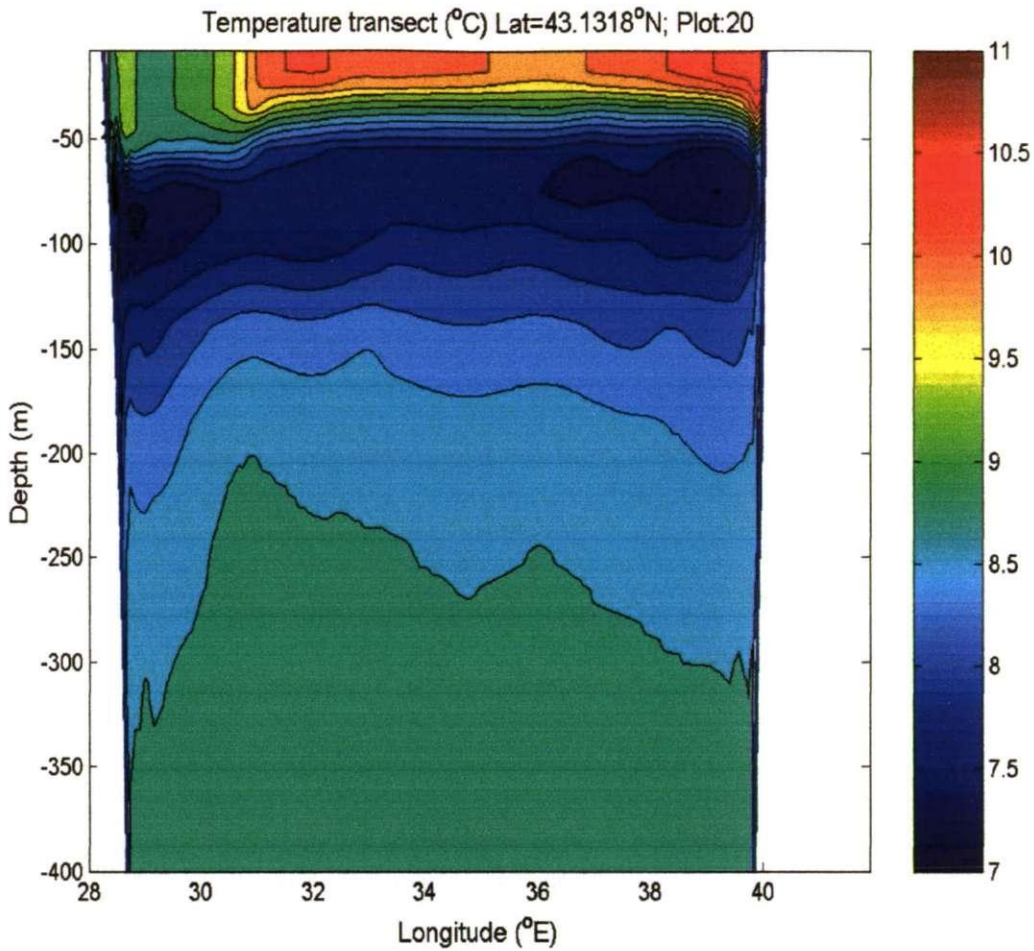
Figure 2-10 Temperature transect showing the Cold Intermediate Layer (CIL). The plot shows this study's modelled output data corresponding to the 14 of May of the year 1998.

The horizontal variability of the salinity and temperature stratification is mainly associated with the motion fields. There is a pronounced lateral salinity gradient from the western coast due to freshwater discharges from rivers as can be seen in Figure 2-11. Along the south-eastern coast there is a similar but weaker salinity gradient, extending north-westward along the Caucasian coast in the direction of the Rim Current. The rest of the basin shows a more uniform salinity distribution.

The horizontal temperature fields exhibit a more pronounced seasonal variability (Figure 2-12).
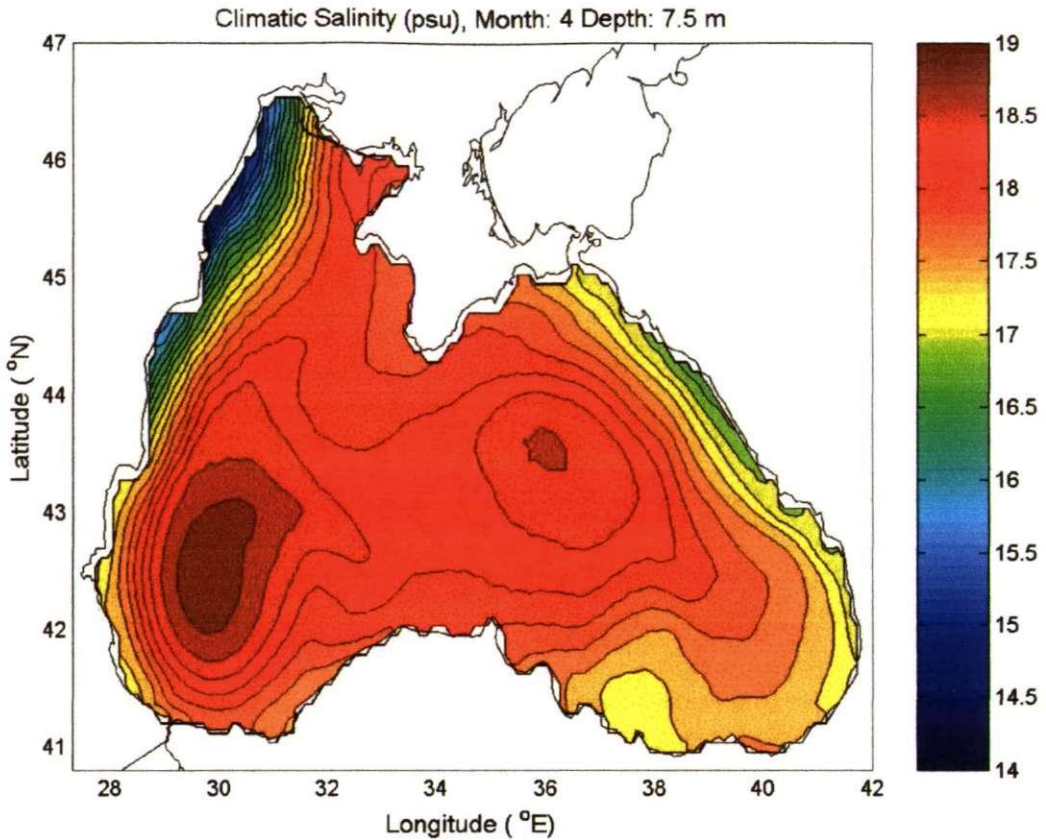
Figure 2-11 Map of salinity for the month of April from monthly climatic data (Staneva and Stanev, 1998).

During the winter, the north-western shelf is characterised by minimum temperature values of the order of 3 °C, increasing to 7 °C within the outer shelf and also increasing toward the east. During this season, the centre of the Black Sea has a spatially uniform temperature distribution. During the summer the north-west is also the colder area, with temperatures around 22 °C and the east is warmer with temperatures of ~24 °C although the centre of the basin presents a zonal gradient of temperature distribution.

Because diapycnal mixing is limited and decays rapidly with depth, the horizontal density variations at the pycnocline are mainly associated with the geostrophic currents. The changes in depth and structure of the pycnocline occur between the cyclonic central part and the anticyclonic regions near the basin boundary, as well as within the eddy fields (Oguz et al, 1993; Saydam et al 1993; Bingel et al 1994).
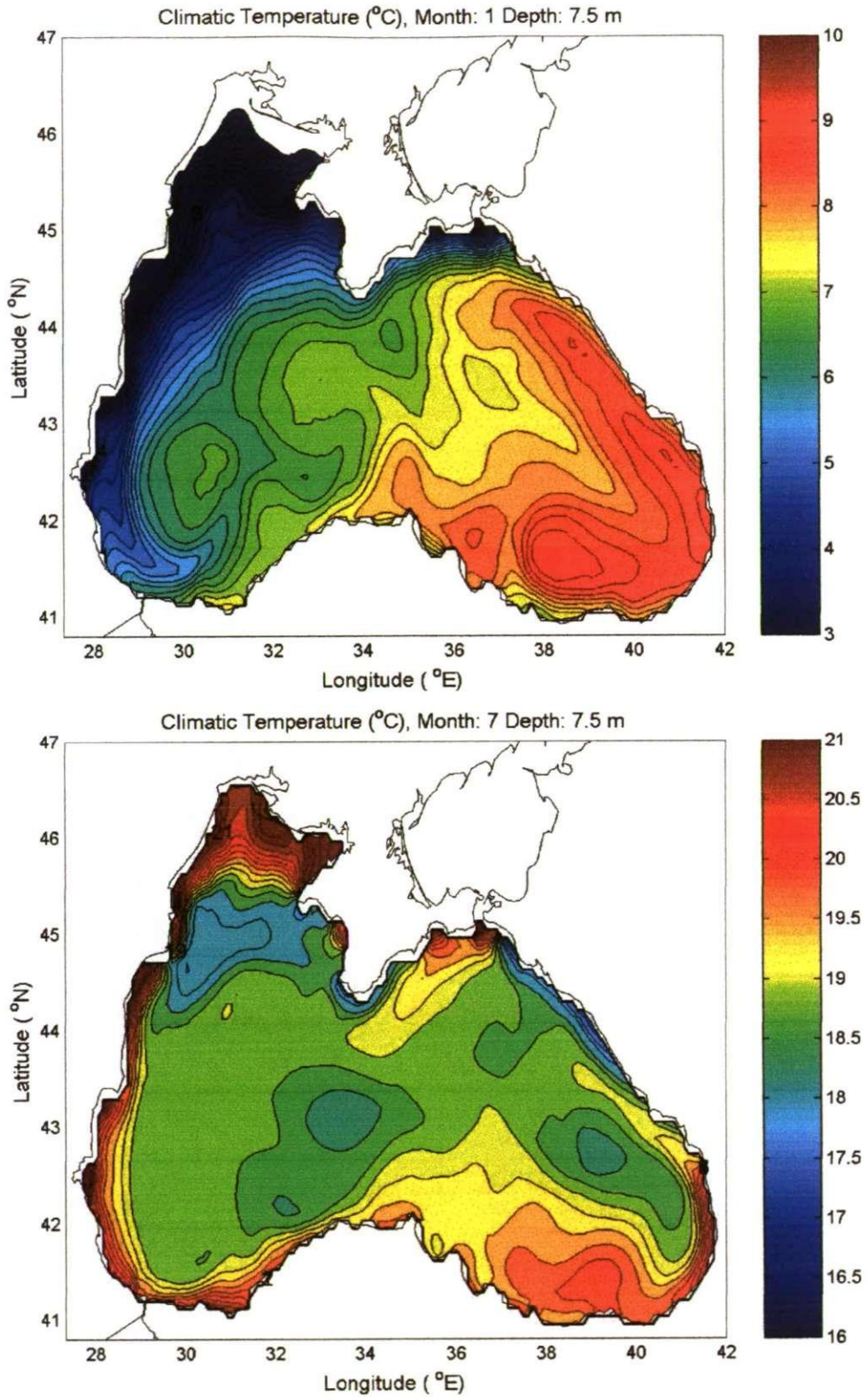
Figure 2-12 Maps of climatic temperature for a) January and b) July. Note the change in the scale of the colourbar to allow the temperature gradient visualisation.

2.6.2. General circulation

The scheme of the Black Sea circulation has evolved through time increasing in complexity. The general picture includes:

1. A boundary current (Rim Current)

2. Cyclonic gyres in the open sea

3. Near shore anticyclonic eddies (NAEs)

The Rim Current is a basin scale current flowing cyclonically around the sea with velocities of up to 1 m/s. It has a width of about 50 km and develops meanders and undulations near the coast.

The general cyclonic circulation has been attributed to the cyclonic nature of the wind field (positive curl of wind stress) first described by Knipovich in 1932. However numerous descriptions and further investigation of the circulation have been carried out since then. Results of numerical studies (Stanev, 1990; Oguz and Malanotte-Rizzoli, 1996) indicate that the combination of the seasonal thermohaline circulation driven by non-uniform surface fluxes, the wind, and the topography of the basin are altogether the crucial factors in controlling the pattern of the circulation. The freshwater inflow from the rivers, winter convection in the north-western shelf and intrusions of dense Mediterranean inflow in the Bosphorus vicinity generate lateral buoyancy fluxes, also contributing to the general Black Sea circulation (Ozsoy and Unluata, 1997; Stanev, 1990).

The temporally and spatially variable sub-basin scale features are typically cyclonic gyres in the deep sea and several anticyclones located at the shelf break between the Rim Current and the coast (Figure 2-13a) with spatial scale ranging from 20 to 60 km for the mesoscale eddies and approximately 100 to 250 km for the sub-basin gyres (Stanev and Rachev, 1999).

The semi-permanent features are schematised in Figure 2-13b and starting from the north in a clockwise direction they are the Crimea eddy at the east of the Crimean peninsula, the Caucasus eddy in the north-eastern coast, the Batumi eddy in the south-eastern corner of the basin, a series of anticyclones along the Anatolian coast including the Sakarya, Sinop and Kizilirmak eddies, the Bosphorus and Kali-Akra eddies in the western coast and the Sevastopol eddy at the west of the Crimean peninsula.

2.6.3. Mesoscale circulation

In the seas all around the world there is a great component of mesoscale circulation (Meschanov and Shapiro, 1998; Shapiro and Meschanov, 1996; Shapiro and Meschanov, 1991; Robinson and Golnaraghi, 1993; Whitney and Robert, 2002). In other words, the ocean is turbulent. Viewed either with a microscope or from an orbiting satellite, the movements of seawater shift and meander, and eddying motions are almost everywhere. Eddies fragment and mix the flow, and transport quantities like heat and trace chemicals across it. In the oceans the smallest circulations are just a few millimetres in size, yet the largest are in the order of 10,000 km in diameter. This represents a range in scale of about ten billion (10^{10}), between the smallest and the largest. There is thus room for many sizes of motion, each with a distinct dynamical nature: from tiny eddies that strongly feel viscosity, to 'mesoscale eddies', which feel the Earth's rotation, to great 'gyres' of circulation filling entire oceans, that also feel the curvature of the Earth.

The horizontal scales of mesoscale eddies vary with latitude and other factors of their environment such as energy level, nearby bottom topography, and the nature of their generation. More specifically, mesoscale eddies have sizes of the order of the local Rossby radius of deformation and characteristic time scales exceeding the pendulum-related day (Shapiro et al., 2000). Width of eddies, λ is approximately given by $\lambda = NH/f$ (Rossby

radius of deformation), where N is the buoyancy frequency or Brunt-Vaisala frequency, H is the vertical scale of the eddy and f is the Coriolis parameter (Rhines, 2004). In this way, for eddies with vertical scales comparable with the ocean depth, the size λ ranges from a few hundred kilometres in the tropics to 10 km or so at high latitudes. This great range of variation comes from the tendency for the high-latitude ocean to have weaker density stratification (Sherwin et al., 2002) and larger Coriolis frequency (f).

There is frequent formation of mesoscale eddies almost everywhere in the ocean. They are often generated by unstable meandering of an intense current where the waving deflection of the current is itself a form of latent eddy, which may eventually grow and 'break' to form a circular eddy (as an ocean surface-wave grows and 'breaks' at a beach). The kinetic energy of the eddies is comparable with that of the mean ocean circulation. Mesoscale eddies are typically as energetic as the currents that generate them, yet they may owe their existence to several sources other than meandering of strong currents. For example, direct generation by winds or cooling at the sea surface, flow over a rough sea-floor or past islands and coastal promontories, or generation by mixing or waves of smaller scale.

Mesoscale eddies are crucial mechanisms of transport of momentum, heat and trace water properties including chemicals, biological communities, oxygen and nutrients relating to life in the sea. This transfer of heat and dynamic tracers, such as potential vorticity significantly affects the mean circulation (Wilson and Williams, 2004) sometimes even far away from the eddy formation site. Therefore mesoscale eddies are regarded as one of the most powerful mechanisms of horizontal water and admixture exchange. They are active in air-sea interaction and because they have deep 'roots', the transport of energy, momentum, etc. is also in the vertical. The extent of their influence depends on the speed and direction of the eddy propagation, as well as on their life span.

In the Black Sea, the increased resolution obtained from oceanographic surveys (Sur et al., 1994; Krivosheya et al., 1997; Krivosheya et al., 1998; Oguz et al., 1994) and the availability of satellite data (Ginzburg et al., 2000; Ginzburg et al., 2002a; Ginzburg et al., 2002b) added significant detail to the description of the Black Sea circulation. It has been shown that the traditional circulation is not as steady as previously thought and that there is an intense mesoscale activity in the region.

Mesoscale eddies in the Black Sea normally have diameters of about 80 – 100 km and they penetrate deeply into the pycnocline (down to 300 – 400 m). Their typical orbital velocity near the sea surface is about 0.15 – 0.50 m/s (Zatsepin et al., 2003b). It is now known that the Rim Current is not a permanent barrier inhibiting the water exchange between the coast and open sea (Zhurbas et al., 2004; Zatsepin et al., 2003a). It has been observed that under specific circumstances, mesoscale anticyclonic eddies which were formed in the coastal area travelled to the central part of the Black Sea (Ginzburg et al., 2002b; Zatsepin et al., 2003c). This link between the coastal environment and the open ocean has very important implications as it is known that the mesoscale eddies are related to mass transfer (Shapiro and Meschanov, 1996; Shapiro et al., 1995) and the resulting exchange may provide shelf-deep sea transport of material or properties.
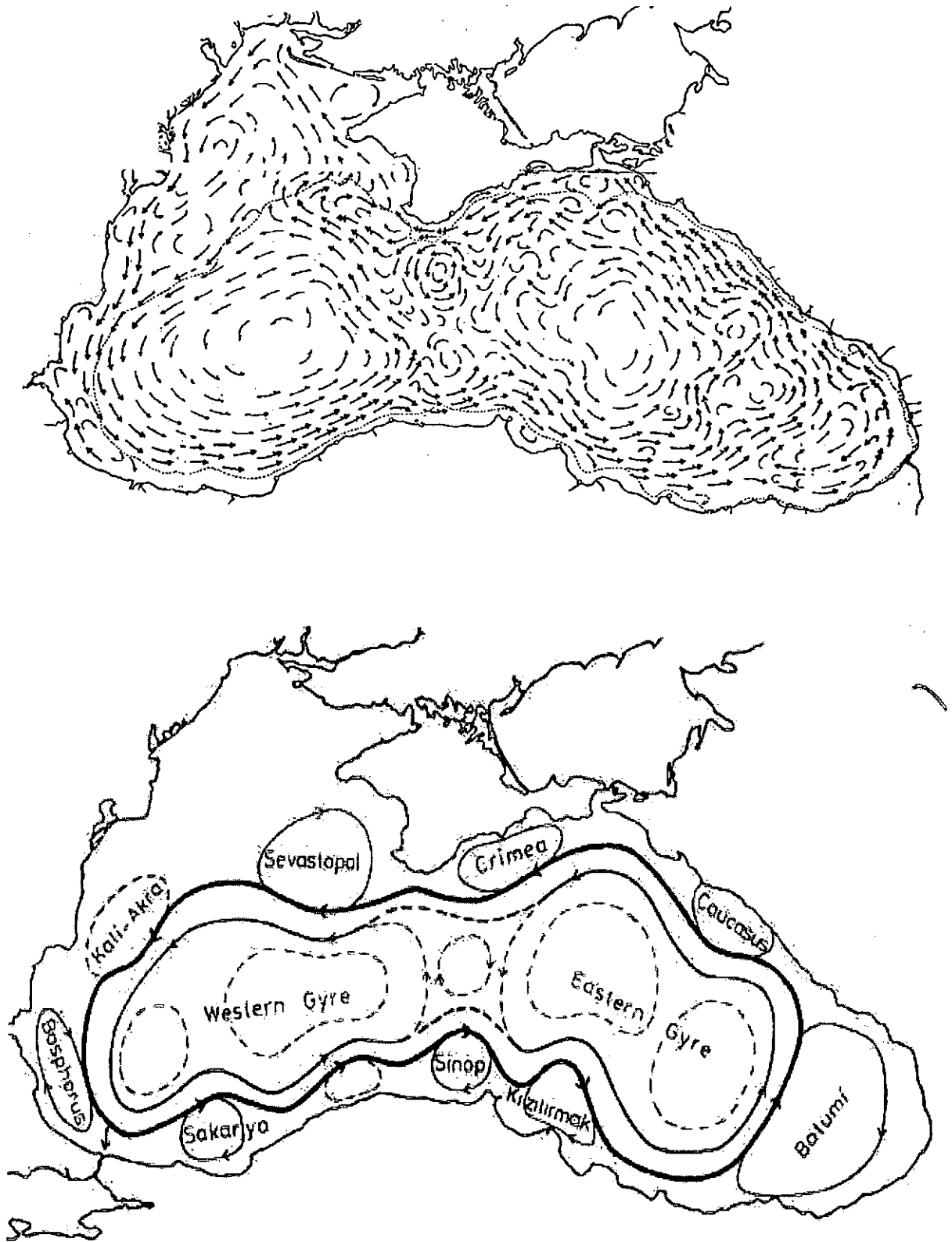
Figure 2-13 Schematization of the main features of the upper layer general circulation from (Neumann, 1942) at the top and (Oguz et al., 1993) at the bottom.

2.7. Modelling of the Black Sea

The Black Sea circulation has been studied using a diversity of numerical models, amongst others the Bryan-Cox primitive equation model (e.g. Stanev 1995), the Geo-Hydrodynamics and Environment Research model, GHER-3D (Stanev and Beckers, 1999), the Dietrich-Centre for Air-Sea Technology hydrodynamic model DieCAST (Staneva et al., 2001), the Princeton Ocean Model, POM (Oguz et al., 1995), the Bryan-Semtner-Cox Modular Ocean Model, MOM (Stanev et al., 2005) and the Harvard Ocean Prediction System, HOPS (Besiktepe et al., 2001).

Early studies were concerned mainly with large spatial scales and seasonal variations and there has been an increase in number and complexity of the studies.

Stanev (1995) studied the response of the basin scale circulation to atmospheric forces using a relatively low resolution ($1°$) rigid lid model. Further progress, particularly in examining low frequency oscillations, was achieved by using free-surface models (Stanev and Beckers, 1999). Reduced gravity models with altimeter data assimilation (Korotaev et al., 2003) allowed improving the forecast of large scale currents. Inaccuracies introduced by z-coordinate models were partly cured by setting up the sigma-coordinate models for the Black Sea (Oguz et al., 1995; Stanev et al., 2005; Besiktepe et al., 2001). Many of these studies targeted processes other than mesoscale phenomena including among others the following topics: water mass formation (e.g. Stanev et al., 2003; Stanev et al., 1997; Ivanov and Samodurov, 2001; Stanev et al., 2004); sensitivity studies to atmospheric forcing, lateral forcing and topography (e.g. Oguz et al., 1995; Stanev et al., 1995; Oguz and Malanotte-Rizzoli, 1996; Staneva and Stanev, 1998; Stanev et al., 2000); studies of the circulation and thermo-haline structure (e.g. Trukhchev and Sarkisyan, 1995; Oguz and Malanotte-Rizzoli, 1996; Besiktepe et al., 2001 Staneva et al., 2001); studies on the

oscillations of the Black Sea (Stanev and Rachev, 1999; Stanev and Beckers, 1999); circulation and transport of oil spills in the Black Sea (Korotenko et al., 2003).

Some of the initial and forcing data used for the modelling part of this research (detailed in Section 3.4) were produced by Staneva and Stanev (1998). They compiled climatic and atmospheric data sets from different sources and incorporated them into a Black Sea numerical model based on the Bryan-Semtner-Cox Modular Ocean Model. The model was forced with twice daily data of temperature, relative humidity and wind velocity (u and v components) from the 1st of June 1991 to the 31st of May 1995. These data were obtained from Hadley Centre [http://www.meto.gov.uk/research/hadleycentre/]. A more detailed description of the nature of the data is available in (Staneva and Stanev, 1998).

2.8. Summary

The enclosed Black Sea basin has a very restricted communication with the open ocean. Its catchment area includes 17 countries covering about one third of the European continent and includes three of Europe's most significant riverine systems: the Danube, Dnieper and Don rivers. The impact received by the Black Sea from all its surroundings is enormous so that the interest in studying and monitoring this basin is no longer contained to the regional countries but to the international community.

Studies of the Black Sea started from the end of the 17th century and up to the 1960s nearly all the research was carried out by the USSR. From the 60s other countries of the communist bloc contributed to the investigations and since the late 80s the Black Sea has been studied by international groups.

The water balance of the Black Sea is determined by river discharges, precipitation, evaporation and exchange via the Bosphorus and the Kerch Straits. Overall there is a

positive water balance: the input from the rivers and precipitation exceeds the evaporation, therefore the net flow in the Bosphorus is negative. Low salinity water from the Black Sea (< 18 *psu*) flows southwards, towards the Marmara Sea, in the surface layers of the Bosphorus strait and more saline deep water (~ 35 *psu*) from the Mediterranean Sea flows into the Black Sea.

The fresh water input from rivers and the input of more saline water through the Bosphorus together with the steep topography of the basin results in a sharp pycnocline which separates the active layer from the bottom layer. The active layer includes a surface mixed layer with the lowest salinity and maximum temperature of the water column. Below the surface layer a cold intermediate layer is located having the minimum temperature of the water column. The deep layer has no movement so that organic materials accumulate in it and, as they are decomposed, the oxygen of the water is exhausted and hydrogen sulphide is formed.

The horizontal variability of the salinity and temperature stratification is mainly associated with the motion fields. The lateral salinity gradients are mainly from the coast due to freshwater discharges from rivers. The temperature gradient in general is characterised by low temperature in north-western shelf and increasing toward the south-east.

The current system in the Black Sea, as in the seas all around the world has an important mesoscale component. In general, mesoscale eddies have horizontal scales varying with latitude and other factors of their environment such as energy level, nearby bottom topography, and the nature of their generation. Typically their diameters range from a few hundred km. in the tropics to 10 km or so at high latitude. They are constantly formed almost everywhere in the ocean, often by unstable meandering of an intense current but other eddy generation mechanisms include direct generation by winds, cooling at the sea surface, flow over a rough sea-floor or past islands and coastal promontories.

Eddies are crucial mechanisms of transport of momentum, heat and trace water properties, significantly affecting the mean circulation sometimes even far away from their formation site.

The general circulation in the Black Sea includes a basin scale current flowing cyclonically around the sea (Rim Current) and temporally and spatially variable mesoscale features. These are typically cyclonic in the open sea and anticyclonic in the coast.

Eddies in the Black Sea normally have diameters of about 80 – 100 km and they penetrate deeply into the pycnocline (at least down to 300 – 400 m). Their typical orbital velocity near the sea surface is about 0.15 – 0.50 m/s (Zatsepin et al., 2003b).

The circulation is controlled by the combination of the seasonal thermohaline circulation, which is driven by non-uniform surface fluxes, inflow from the rivers and dense Mediterranean inflow from the Bosphorus, the wind forcing either reinforcing the Rim Current by its dominating cyclonic nature or weakening the general circulation with its variability, and the topography of the basin.

The increased resolution obtained from oceanographic surveys and the availability of satellite data has revealed that the mesoscale activity is more intense than previously thought and that the Rim Current is not a permanent barrier inhibiting the water exchange between the coast and open sea (Zhurbas et al., 2004; Zatsepin et al., 2003a).

CHAPTER 3. MATERIALS AND METHODS

3.1. Introduction

This chapter covers the description of the materials and methods used for this study. Materials include all available data and can be divided into:

1. Observational data of the Black Sea for model verification and characterisation of the dynamics

2. Data for the model initialisation and forcing

The methods include:

1. The analysis applied to the observational data

2. The pre-processing treatment applied to the data for the model

3. The set up of the hydrodynamic numerical model (POLCOMS) to the Black Sea.

4. The methods of post-processing which were applied to all the modelled output data.

This chapter does not cover the methodologies describing analysis techniques applied to aid the interpretation of the results. In such cases, the methodology will be described together with the corresponding result.

3.2. Observational data

3.2.1. In situ data (CTD)

The CTD data used in this study is part of a project carried out by the Shirshov Institute of Oceanography in Russia which periodically takes measurements in the north-eastern part of the Black Sea. The data set from the year 2000 is the one included in this study and was provided by Prof. Andrei Zatsepin. The measurements were carried out from the 17 to 20 of November 2000. The data consist of 40 CTD profiles measured on an almost regular grid (Figure 3-1), collected using a Sea-Bird CTD probe (SBE 9 plus CTD Underwater

Unit, S/N 09 P8970-0347). CTD casts were deployed to a few metres above the seabed in the areas with depths between 10 and 510m, and up to 510 - 540 meters depth in deeper areas. The typical distance between CTD stations is 10 to 20 nautical miles. The pooled data consist of vertical profiles of temperature, salinity and specific density with 1 m vertical resolution at each station.
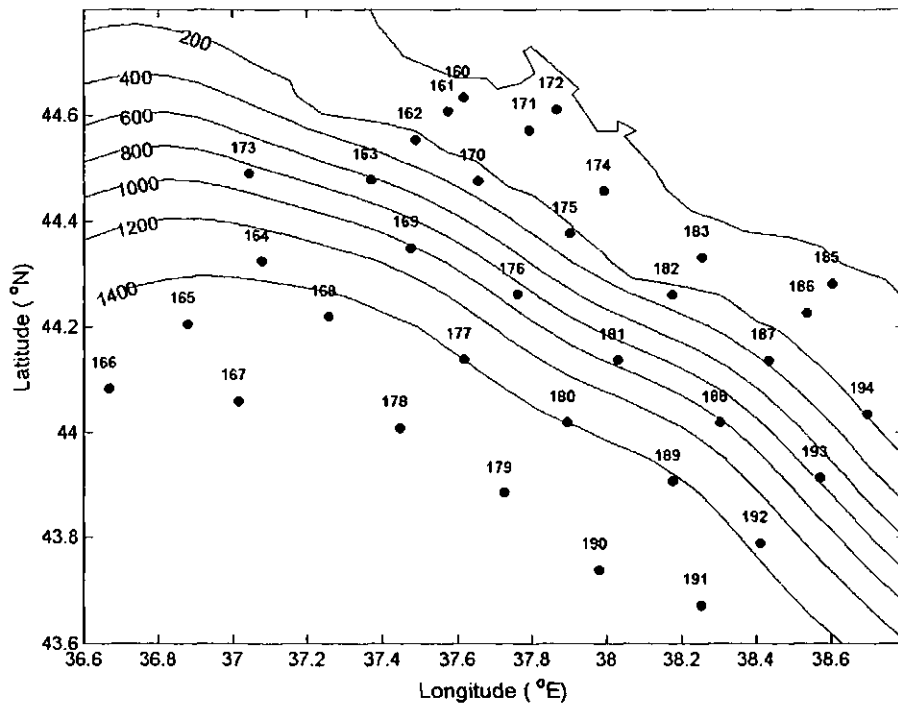
Figure 3-1 Location of CTD deployments during hydrographic campaign in November 2000. The map also presents isolines of bathymetry (m). Data provided by Andrei Zatsepin from Shishov Institute of Oceanology, Moscow.

3.2.2. Methods for CTD data treatment

Most of the procedures used for the CTD data treatment analysis are standard, well established methods and the procedure will be omitted. Hence here we will only mention which kinds of analysis were performed and we will give details only on the approach followed to calculate the geostrophic currents.

The dynamic height, ζ, was calculated at different a levels relative to a depth b of 500 m,

by: $$\zeta(x,y,a) = -\frac{g}{\rho_0} \int_b^a (\rho(x,y,z) - \overline{\rho}(z))dz,$$

where x, y and z are the cartesian coordinates, g is the acceleration due to gravity, taken as

9.80 m/s², ρ is the *in-situ* density, $\overline{\rho}$ is the calculated average density at depth z, and ρ_0 is

1000 kg/m³.

The dynamic heights were linearly interpolated for the area and were used to compute the

geostrophic velocities with:

$$u = -\frac{g}{f}\left(\frac{d\zeta}{dy}\right) \qquad \text{and} \qquad v = \frac{g}{f}\left(\frac{d\zeta}{dx}\right)$$

where f is the Coriolis parameter $= 2\Omega \sin \phi$ in which Ω is the angular speed of rotation of

the Earth and ϕ is the latitude.

3.2.3. Remote sensing data (SST images)

To complement the *in situ* measurements, a series of NOAA AVHRR (Advanced Very

High Resolution Radiometer) Sea Surface Temperature images were gathered. Images

from 23 October 2000 to 25 November 2000, concurrent with the period of the

oceanographic survey in the north-eastern part of the Black Sea were used.

The SST maps were collected online from the German Remote Sensing Data Centre (DFD)

Earth Observation Information Service (EOWEB, 2000) [http://eoweb.dlr.de/Products]. The

maps consist of daily composites covering the entire Black Sea, from 40 to 48° latitude

north and from 26 to 42° longitude east as shown in Figure 3-2.

Figure 3-2 AVHRR image from the NOAA 14 satellite for 1 Nov 2000, showing the Sea Surface Temperature of the Black Sea.

3.2.4. Methods for remote sensing data treatment

The basis of image processing is the quantification of intensity variability of an image into a two-dimensional array of picture elements or pixels. The image samples were taken daily and were already processed, calibrated, cloud screened, remapped and ocean masked. The available maps have a geometrical resolution of 1.1 km at nadir and are images in 8-bit MCSST integer format, with radiometric resolution of 0.125 °C. In this way, the grey value of 0 corresponds to land, 255 corresponds to clouds and/or missing data and the range of greys from 1 to 254 are the temperatures from 0.125 °C to 31.75 °C respectively (EOWEB, 2000).

To analyse the SST images we applied several standard techniques to extract information, such as histogram calculations, filtering and stretching. For this research the main interest is to enhance the contrast of the image and be able to determine the sea surface temperature at any point of the image. These are well known procedures commonly used for image processing which can now be performed with a range of image processing software. For this study UNESCO WinBilko version 2.0 and Matlab were used.

Because the sea surface temperature patterns are shaped by the movement of heat in ocean currents, the sea surface temperature satellite images are a very useful tool to study mesoscale currents having the spatial and temporal coverage needed for these studies.

By detecting sharp temperature gradients in the satellite images, several mesoscale features including fronts, meanders, filaments and eddies were identified in the Black Sea. Their size and shape were obtained from the images and by compiling time series of images it was possible to see the movement of the currents and to estimate the orbital and drifting velocity of some mesoscale eddies.

3.3. POLCOMS model

The main part of this research is to use a numerical model as a tool to explore and study the hydrodynamics of the Black Sea. For this purpose the Proudman Oceanographic Laboratory Coastal Ocean Modelling System (POLCOMS) was used. It is a three dimensional baroclinic model developed in Proudman Oceanographic Laboratory [http://www.pol.ac.uk/home/research/polcoms/]. A full description is given by Holt and James (2001).

One of the main features of POLCOMS is its advection scheme which is the piecewise parabolic method, PPM, (Colella and Woodward, 1984; James, 1996). The PPM maintains horizontal gradients and minimizes numerical diffusion having excellent feature preserving

properties. Hence it is ideal for the simulation of baroclinic features such fronts and the transport of tracers from localized sources on the shelf, at the shelf slope and in ocean regions. Another characteristic of the model is the use of a refinement of the σ-coordinate scheme which allows higher resolution in the vertical at particular areas of interest (s-coordinate system, described in Section 3.5.2) and at the same time the method of estimating the horizontal pressure gradient term which allows steep topographic changes.

3.3.1. Equations

The model is formulated in spherical polar sigma coordinates: χ (eastward), ϕ (northward) and σ (vertical), with $\sigma = \dfrac{(z-\zeta)}{(h+\zeta)}$, where z is the cartesian vertical coordinate, h is the water depth relative to the reference sea level ($z = 0$), and ζ is the elevation above the reference sea level. The total water depth is $H = h + \zeta$.

The model solves the incompressible, hydrostatic, Boussinesq equations of motion and allows time splitting between barotropic and baroclinic components. The equations are divided into depth independent and depth varying parts; so the eastward velocity is $u = \bar{u}(\chi,\phi,t) + u_r(\chi,\phi,\sigma,t)$ and the northward velocity is $v = \bar{v} + v_r$.

The depth mean equations are:

$$\frac{\partial \bar{u}}{\partial t} = f\bar{v} - (R\cos\phi)^{-1}\left(g\frac{\partial \zeta}{\partial \chi} + \rho_0^{-1}\frac{\partial P_a}{\partial \chi} \right) + H^{-1}(F_S - F_B) + NLB_\chi \quad \text{and}$$

$$\frac{\partial \bar{v}}{\partial t} = -f\bar{u} - (R)^{-1}\left(g\frac{\partial \zeta}{\partial \phi} + \rho_0^{-1}\frac{\partial P_a}{\partial \phi} \right) + H^{-1}(G_S - G_B) + NLB_\phi$$

and the depth varying components are:

$$\frac{\partial u_r}{\partial t} = -L(u) + fv_r + \frac{uv\tan\phi}{R} - \Pi_\chi + D(u) - H^{-1}(F_S - F_B) - NLB_\chi + HD \quad \text{and}$$

$$\frac{\partial v_r}{\partial t} = -L(v) - fu_r - \frac{u^2 \tan\phi}{R} - \Pi_\phi + D(v) - H^{-1}(G_S - G_B) - NLB_\phi + HD$$

where R is the radius of the earth, HD the horizontal diffusion and the buoyancy terms are:

$$\Pi_\chi = (R\cos\phi)^{-1} \frac{\partial\psi}{\partial\chi}\bigg|_z \qquad \Pi_\phi = (R)^{-1} \frac{\partial\psi}{\partial\phi}\bigg|_z$$

where $\partial\psi$ are the pressure gradients estimated along the edges of the horizontal plane.

The depth means of the nonlinear and buoyancy terms are

$$NLB_\chi = \int_{-1}^{0}\left[-L(u) + \frac{uv\tan\phi}{R} - \Pi_\chi\right]d\sigma \qquad NLB_\phi = \int_{-1}^{0}\left[-L(v) + \frac{u^2\tan\phi}{R} - \Pi_\phi\right]d\sigma$$

The advection terms are given by:

$$L(a) = \frac{u}{R\cos\phi}\frac{\partial a}{\partial\chi} + \frac{v}{R}\frac{\partial a}{\partial\phi} + \Omega\frac{\partial a}{\partial\sigma}$$

where $\Omega = -\frac{\sigma}{H}\frac{\partial\zeta}{\partial t} - (HR\cos\phi)^{-1} \times \left[\frac{\partial}{\partial\chi}\left(H\int_0^\sigma u\,d\sigma\right) + \frac{\partial}{\partial\phi}\left(H\cos\phi\int_0^\sigma v\,d\sigma\right)\right]$

The vertical gradients of the stresses are replaced by a diffusion term:

$$D(a) = H^{-2}\frac{\partial}{\partial\sigma}\left(K_z\frac{\partial a}{\partial\sigma}\right)$$

where K_z is the eddy viscosity.

The equation for the free surface is

$$\frac{\partial\zeta}{\partial t} = -(R\cos\phi)^{-1}\left[\frac{\partial}{\partial\chi}(H\bar{u}) + \frac{\partial}{\partial\phi}(H\cos\phi\bar{v})\right]$$

The model uses slip vertical boundary conditions and the components of stress and the corresponding friction coefficients for the bottom are given by:

$$(F_B, G_B) = c_B(u_B, v_B)\sqrt{u_B^2 + v_B^2}$$

41

where $c_B = \left(\kappa^{-1} \log\left(\dfrac{\delta}{z_0}\right) \right)^{-2}$, $c_B \rangle 0.005$, following (Blumberg and Mellor, 1987)

The near bed velocity is defined at a depth δ above the sea bed, the roughness length is taken to be $z_0 = 0.003m$ and $\kappa = 0.4$ is the von Karman's constant.

The transport equation for temperature, T, and salinity, S, is

$$\frac{\partial T}{\partial t} = -L(T) + D(T)$$

This uses the eddy diffusivity K_H estimated within the Mellor-Yamada-Galperin level 2.5 turbulence closure scheme (Mellor and Yamada, 1974; Galperin et al., 1988).

The density is defined by an approximation to the full UNESCO equation of state:

$$\rho(T,S,p) = \rho(T,S,0) + \rho'(T,S,p)$$

where T is the potential temperature (°C), S is salinity (practical salinity units (*psu*)), p is the pressure relative to the sea surface, $\rho(T,S,0)$ is taken from the UNESCO equation of state and $\rho'(T,S,p) = 10^4 \dfrac{p}{c^2}\left(1 - 0.20\dfrac{p}{c^2}\right)$

with $c = 1449.2 + 1.34(S - 35) + 4.55T - 0.045T^2 + 0.00821p + 15.0x10^{-9}p^2$, following (Mellor, 1991).

The buoyancy is defined by: $b = b_0 + b'$ being b_0 the potential buoyancy $\left(b_0 = g\left[\dfrac{\rho_0 - \rho(T,S,0)}{\rho_0}\right]\right)$, ρ_0 the reference density $\left(\rho_0 = 1027\dfrac{kg}{m^3}\right)$ and the variation of compressibility with temperature and salinity is accounted for by

$b' = g\dfrac{\left[\rho'(Z) - \rho'\right]}{\rho_0}$, with $Z = z - \zeta = \sigma H$

3.3.2. Changes to the code

The subroutines which were modified for this study are the following:

1. The subroutine that reads the meteorological data (*metset.for*) was modified as follows:

   - To read the forcing data available for the Black Sea: Wind stress, Evaporation less Precipitation and Heat fluxes.

   - To include different meteorological counters according to the sampling frequency of this study's forcing data.

   - To interpolate each of the meteorological variables linearly in time to each time step.

   - To convert units of the evaporation-precipitation data from mm/month to m/s.

   - To begin reading forcing data from the start of the simulations. (Before it was set to read first forcing data after 24 hrs).

2. The subroutine which sets the values for the heat fluxes (*heatin.for*). In previous studies the model did not read heat flux data, for this study:

$$heat = {Q_{tot}} / {\left(c_p \times \rho \right)}$$

where Q_{tot} is the total heat flux $\left(W/m^2 \right)$ introduced to the model every 24 hrs produced by Staneva and Stanev (1998); $c_p = 4086$ is the specific heat of the sea with units J/kg°K and ρ is the density. The heat flux is assigned to a variable (*heatin* or *heatout*) depending on the direction of the flow (Q_{tot} positive or negative respectively).

43

3. The subroutine which sets the vertical *s*-coordinate system (*al_init.for*) according to the predefined input parameters. The modification consisted in changing the value of *hc* to be consistent with the one defined in the input file (for this study *hc* = 300 as described in Section 3.5.2).

4. The subroutine which performs the barotropic calculations in the model (*barot.for*). The amendment was to avoid calling the subroutine which updates boundary elevations by volume flux and radiation because this study does not include open boundaries and therefore it is not needed.

5. The subroutine which is called at the end of each time step (*endstep.for*) to update counters and to call the subroutines which renew the atmospheric variables.

6. The subroutine which outputs data when required (*tidemeanout.for*). It was modified so that the output is released either hourly (snapshots) or every 17 hours (residuals) to filter the inertial oscillations.

3.4. Data for the model

To model the Black Sea hydrodynamics a complete set of data was gathered consisting of: bathymetry, wind, heat fluxes, water fluxes (evaporation-precipitation and rivers), and initial condition of temperature and salinity throughout the water column. No initial current velocities were available and in this case a common procedure is to initialise with zero velocities and pre-run the model with the thermohaline distribution and the bathymetry of the area without any other forcing. This is to achieve quasi-geostrophic adjustment between the given density and the velocity fields. The quasi-geostrophic adjustment procedure is described in detail in Chapter 4.

The initial condition of temperature and salinity together with some forcing data (heat fluxes, evaporation and precipitation), were produced by Staneva and Stanev (1998) as described in Section 2.7 and hereafter will be referred as Staneva's data.

All the initial and forcing data were interpolated to fit the mesh of this study (Table 3-1) and the input data files were organized for POLCOMS starting from the south-western corner and increasing first in zonal direction. For the 3-D data the horizontal structure of each vertical layer is the same as the 2-D data and the layers are organized from bottom to surface as shown in Figure 3-3.

	Western grid point	Southern grid point	Longitudinal Resolution	Latitudinal Resolution	Approx dx	Mesh size
Bathymetry	27.25	40.41	1/12°	1/12°	-	(178 x 92)
Staneva's data	27.38° E	40.45° N	1/9°	1/12°	9 km	(133 x 76x24)
Wind data	27	40	1°	1°	-	(16 x 9)
This study's domain	28° E	41° N	1/12°	1/16°	6.5 km	(168 x 92x24)

Table 3-1 Horizontal spatial characteristics of the data for the model.
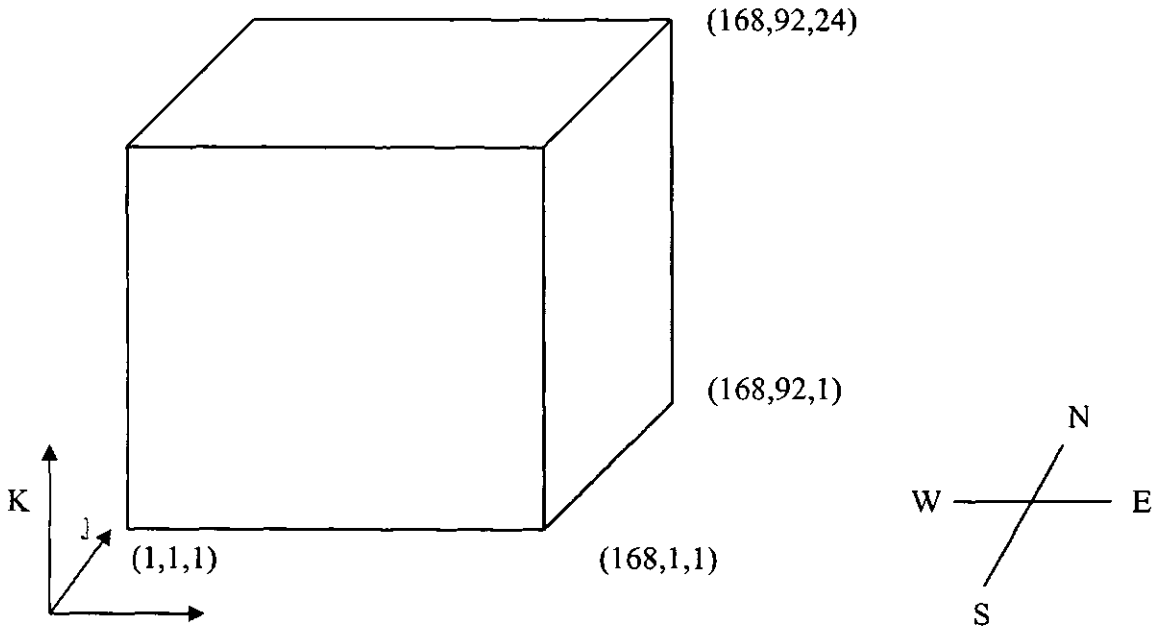
Figure 3-3 Schematic distribution of the geometry of the model used for this study.

3.5. Model set up for the Black Sea

3.5.1. Horizontal discretisation

The model is formulated on an Arakawa B grid and the domain ranges from 41 to 46.7 °N and from 28 to 42 °E, covering the whole Black Sea basin except the areas with less than 10 m depth. It has a horizontal resolution of 1/12° in longitudinal direction and 1/16° in latitudinal direction. At the centre of the Black Sea [latitude 43° N] this resolution is approximately equivalent to a *dx* of 6.7 km and *dy* of 6.9 km. The mesh has 92 latitudinal grid points, 168 longitudinal grid points (Figure 3-4).

46
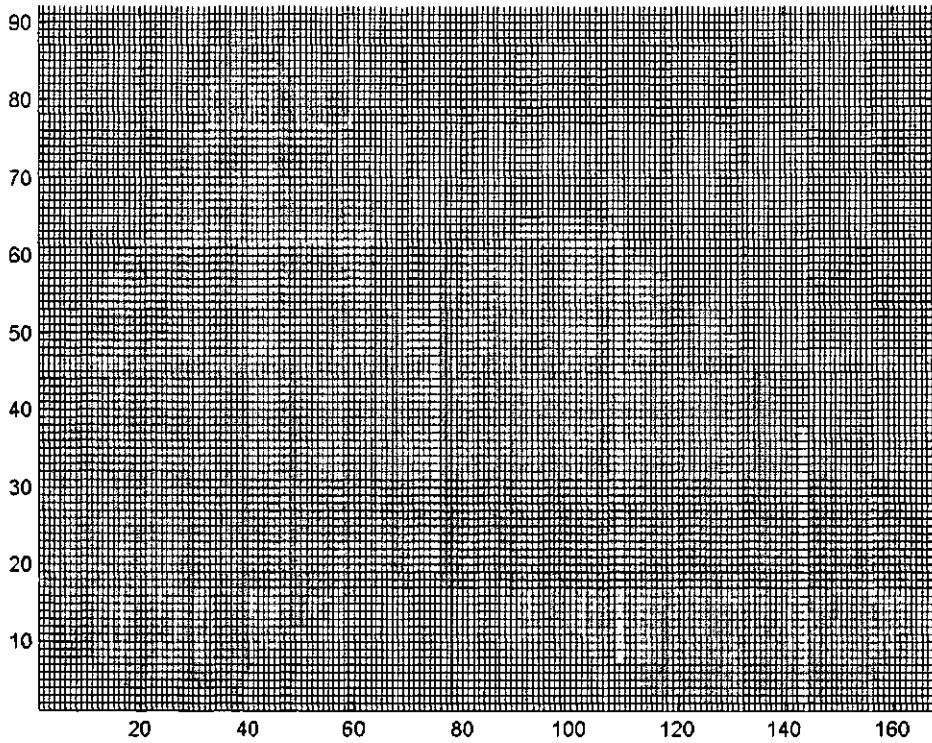
Figure 3-4 Space discretisation of the grid (Inverse latitudinal and longitudinal resolution 12 ° and 16.14 ° respectively).

3.5.2. Vertical discretisation: s-coordinates

The water column is divided into 24 vertical s-coordinate levels as shown in Figure 3-5. The s-coordinate system is a non-linear function of z which allows high resolution in specific regions while mapping the varying topography. The s-coordinate scheme was originally introduced by Song and Haidvogel (1994) and it consists of three terms:

$$z = \zeta(1+s) + h_c s + (h - h_c)C(s)$$

where s varies from -1 to 0 so that the sea surface $z = \zeta$ is at $s = 0$ and the sea bed $z = -h$ is at $s = -1$. h_c is a constant chosen to meet the layer in which a higher resolution is required and $C(s)$ is a set of s-curves, defined by:

47

$$C(s) = (1-b)\frac{\sinh(\theta s)}{\sinh\theta} + b\frac{\tanh\left[\theta\left(s + \frac{1}{2}\right)\right] - \tanh\left[\left(\frac{1}{2}\right)\theta\right]}{2\tanh\left[\left(\frac{1}{2}\right)\theta\right]}$$

where θ and b are the surface and bottom control parameters. For a full description of the system refer to Song and Haidvogel (1994). For this study, the parameters are $\theta=8$, $b=1$ and $hc=300$ to give compression at the surface and at the bottom of the water column at each point.
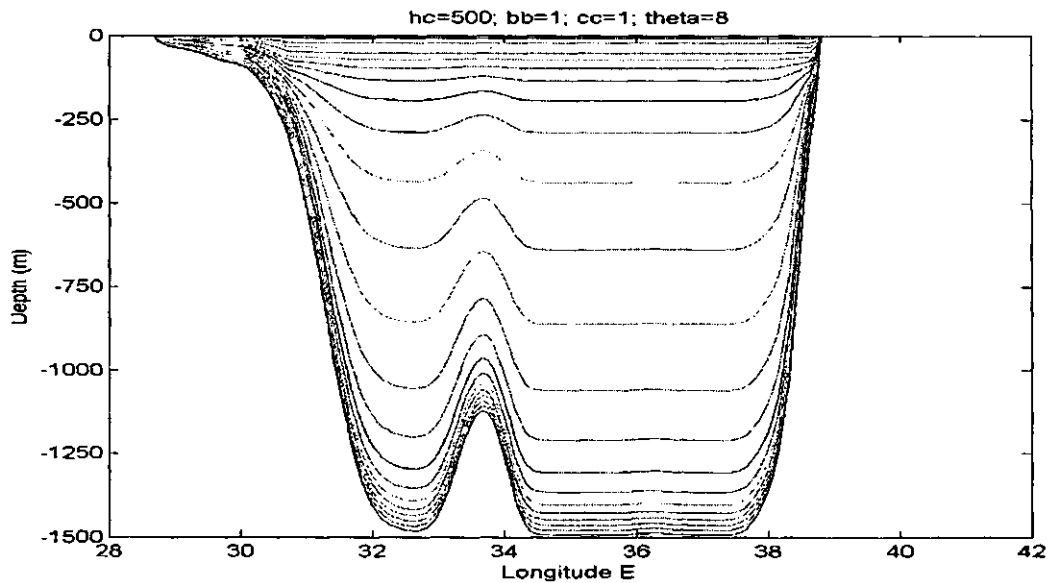
Figure 3-5 Zonal transect of the vertical s-level at 44°N

3.5.3. Bathymetry

The source of the bathymetry used for this study is the ETOPO5 database. The bathymetry of the Mediterranean Sea (from longitude -9 to 42 °E and from latitude 30 to 48 °N), containing bathymetric and elevation data, was obtained online from the Mediterranean Oceanic Database Project, MODB [http://modb.oce.ulg.ac.be/mirror/pub/MODB/]. The Black Sea domain was extracted from it.

3.5.4. Methods for bathymetric data treatment

The route followed to process the bathymetric data is presented in Figure 3-6. The data were linearly interpolated from the original 5 minute resolution grid to fit the grid of this study (detailed in Table 3-1). Special care needs to be taken when using a σ-coordinate system in regions with steep topography and strong stratification to avoid errors resulting from the pressure gradient formulation (Stanev and Rachev, 1999). This is exactly the case for the Black Sea basin where the bottom topography is very complicated particularly in the southern area (Figure 3-7a) featuring a number of small scale canyons and the vertical density gradients there are larger than in the ocean. A common method used in 3-D modelling to avoid the possible errors arising from this situation is to smooth the bathymetry. Because this study is aimed at mesoscale phenomena with greater scales than the scale of the canyons, smoothing the bathymetry was not expected to significantly alter the results of the model but to considerably improve the efficiency and performance of the modelling. The bathymetry was smoothed by running average filtering using the function 'filter2' from Matlab with window size of 5 by 5 (convolution kernel of 1/25).

The bathymetry was then cut to a maximum depth of 1500 m. The purpose of this is to allow the use of a longer barotropic time step saving a considerable amount of computational time. This does not alter the results as it is known that in the Black Sea the water dynamics are limited to the upper layer by the strong pycnocline so that from depths of about 700 m there is no motion. The bathymetry used for the modelling is shown in Figure 3-7b and c.

3.5.5. Land mask

The land mask is a file which tells the model if the grid points correspond to land or sea at the surface ($z = 0$).
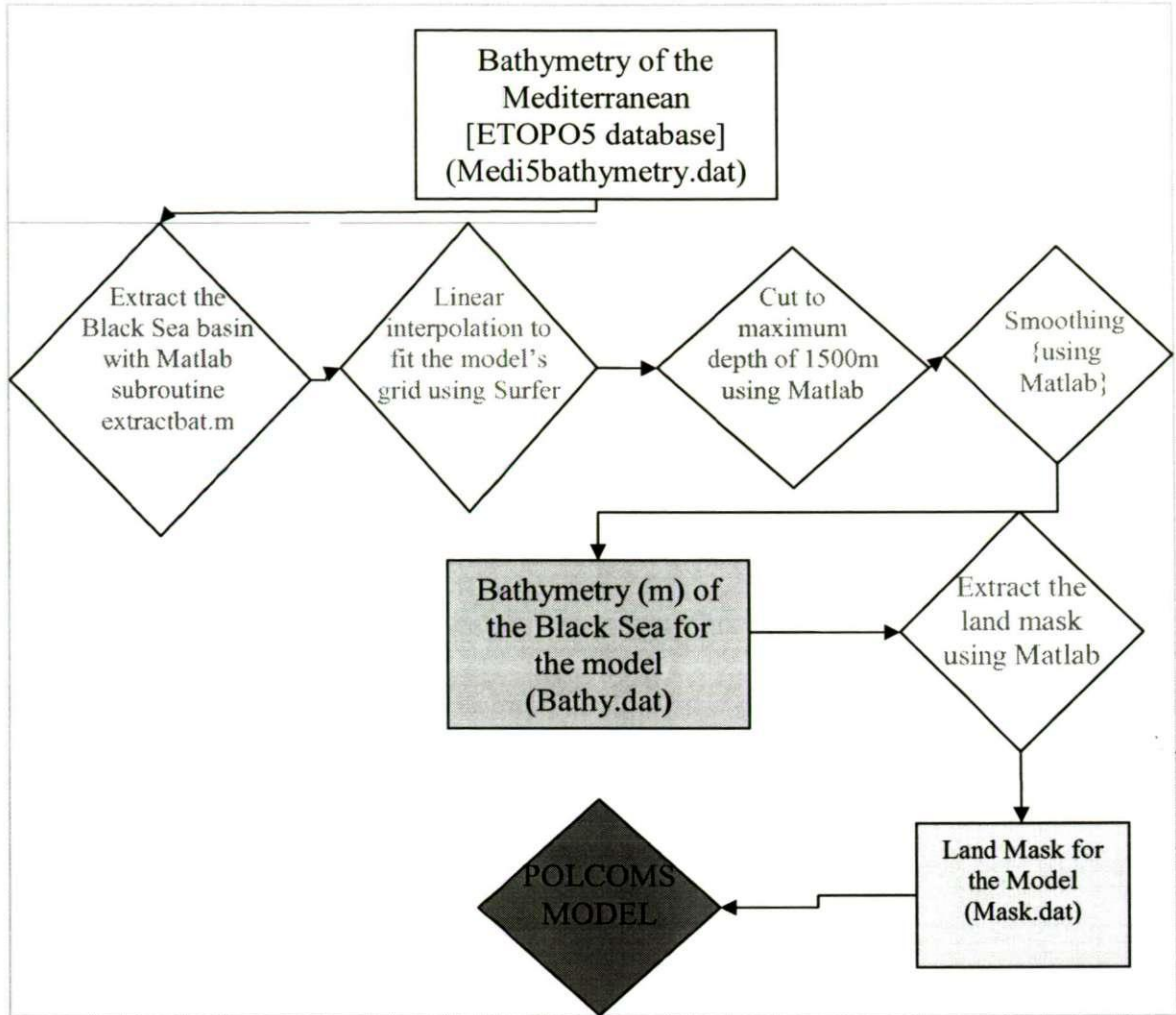
Figure 3-6 Flow chart showing the pre-processing route for the bathymetry and land mask

a)

b)

c)
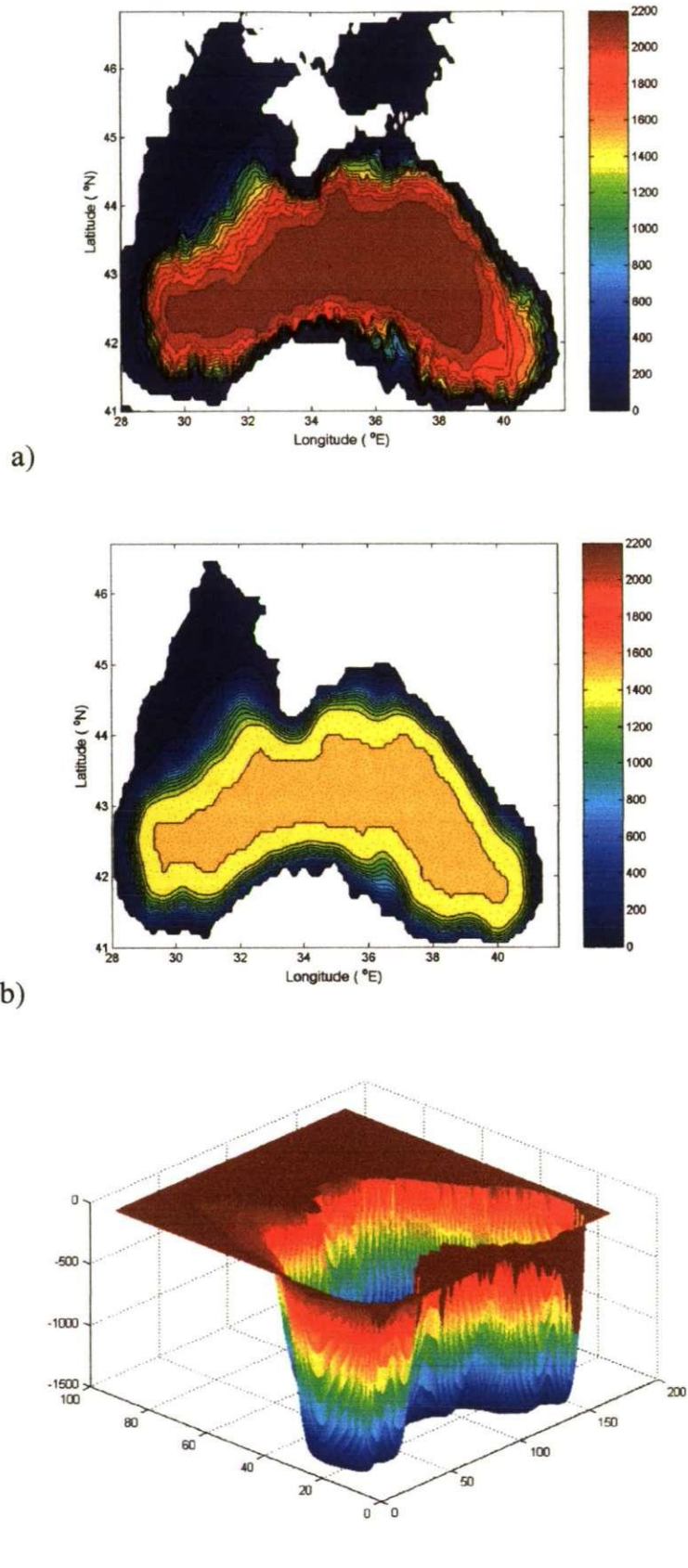
Figure 3-7 Black Sea bathymetry a) contour map before processing b) contour map after processing c) 3-D view of the bathymetry for the model. (Depths are in meters).

3.5.6. Methods for creating the land mask

The land mask is built from the bathymetry, assigning number 1 to the wet points and number 0 to the land. Then attention should be paid to check that every wet point has a corresponding initial temperature and salinity value (different from zero), and otherwise set it as land.

3.5.7. Initial temperature and salinity distribution

The model is initialised with a 3-dimensional distribution of temperature and salinity from Staneva's data (Staneva and Stanev, 1998). The data provided are climatic monthly temperature and salinity distribution from which the month of May was extracted to initialise the experiments carried out during this study. The origin of this data is explained in Section 2.7. The horizontal geometry of the data is detailed in Table 3-1. In the vertical, the data has 24 z-levels (Table 3-2).

z-level	1	2	3	4	5	6	7	8	9	10	11	12	13
Depth (m)	2.5	7.5	12.5	17.5	25	35	45	55	65	75	85	105	140

z-level	14	15	16	17	18	19	20	21	22	23	24
Depth (m)	185	240	310	400	515	750	1125	1485	1755	1940	2070

Table 3-2 Vertical discretisation of the initial temperature and salinity data (Staneva's data, z-coordinates).

3.5.8. Methods for initial T-S data treatment

The pre-processing route for the initial temperature and salinity data is shown in Figure 3-9. The first step was to extract from the available data set the month of May, which was used to initialise the model. Then the data of each one of the vertical levels was interpolated in the horizontal to fit the model's grid (Table 3-1). The horizontal interpolation was performed with Surfer using the kriging method with the default parameters: linear variogram, slope = 1, anisotropy = 1.0 and no nugget. The resulting processed levels are 20 in total, from level 1 at 2.5 m depth to level 20 at 1125 m depth. Deeper data were not usable within Surfer because they were too sparse. Therefore levels 20 to 24 were generated manually by looking at the values from the original data files, which at this depth are nearly spatially constant.

To produce a 3-D mesh of *s*-coordinate depths for the model's domain, the T and S data were linearly interpolated in the vertical from the original z-depths to the *s*-coordinate depths. For this process the Matlab routines interscoord1.m and interscoord2.m were developed (Appendix). The first one generates a 3-D array of depths at which each grid point of this study's mesh is located based on the bathymetry and the parameters determined for the set up of the *s*-coordinate levels (described in Section 3.5.2). The second one interpolates in one dimension from the original z-level depths to the 24 *s*-level depths corresponding to each grid point.

The processed initial temperature and salinity fields which are the model input for this study in Figures 3-10 to 3-15.

A total of 6 transects were selected as representative of the different regions of the Black Sea basin. The vertical cross-sections of different parameters displayed from this point onwards are on these locations, which are shown in Figure 3-8, unless stated otherwise.
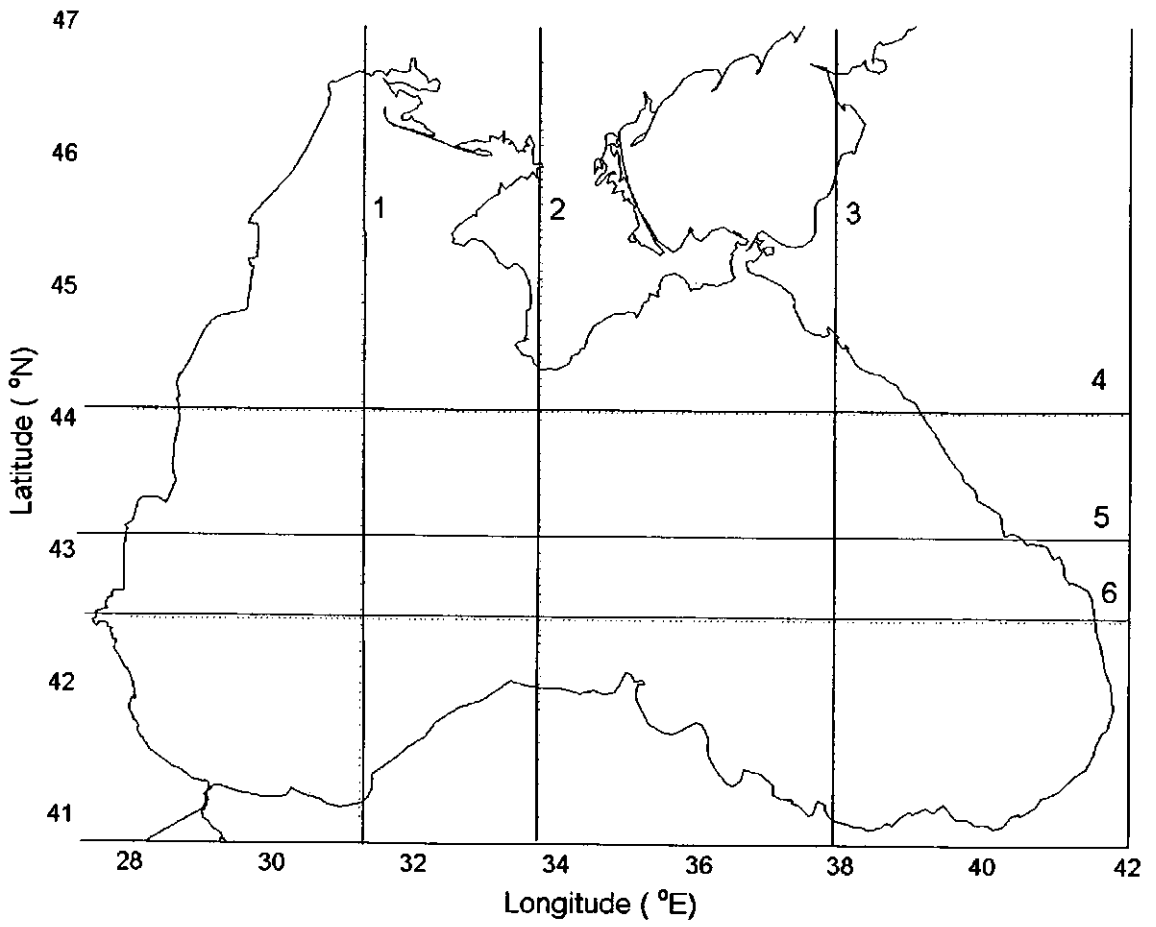
Figure 3-8 Location of the vertical transects for plotting

Climatic monthly 3-D temperature
and salinity distribution
from MOM model
[Staneva and Stanev, 1997]
(tem.dat) (sal.dat)

Separate data in 12
files with Matlab
subroutines
readsal.m and
readtem.m

For the month of
May prepare files for
interpolation with
Matlab subroutine
surfout.m

Horizontal
interpolation to fit
this study's grid.
kriging method
using Surfer

12 files (one/month)
for each variable:
sal1.mat   tem1.mat
sal2.mat   tem2.mat
...   ...
sal12.mat tem12.mat

24 files
(one/vertical level)
temsal01.dat
temsal02.dat
...
temsal24.dat

20 files (one/vertical
level) for each variable:
salkr01.dat   temkr01.dat
salkr02.dat   temkr02.dat
...
salkr20.dat   temkr20.dat

Bathymetry
and Land
mask from
mascara.mat

Generate 3-D
array of depths for the
S-coordinates with
Matlab subroutine
Interscoord1.m

Import data into
Matlab with surfin.m
and manually fill 4
remaining vertical
levels

Variable zzz3 added
to the file
mascara.mat

1 file with the interpolated T and
S data with 24 vertical Z-levels:
TsextrapolZlevels.mat

Linear vertical
interpolation converting from Z
to S-coordinates: Matlab
subroutine Interscoord2.m

Write file
for model input
using Matlab
subroutine
wts.m

POLCOMS
MODEL

1 file with the
interpolated T and S data
with 24 vertical Z-levels:
TS_S_levels.mat

Initial T (°C) and S
(psu) for May for the
model
(TSini.dat)

Figure 3-9 Flow chart showing the pre-processing applied to the initial TS distribution for POLCOMS model.

Colour code: ☐ *Original data* ☐ *Process* ☐ *Data* ☐ *Model input data*
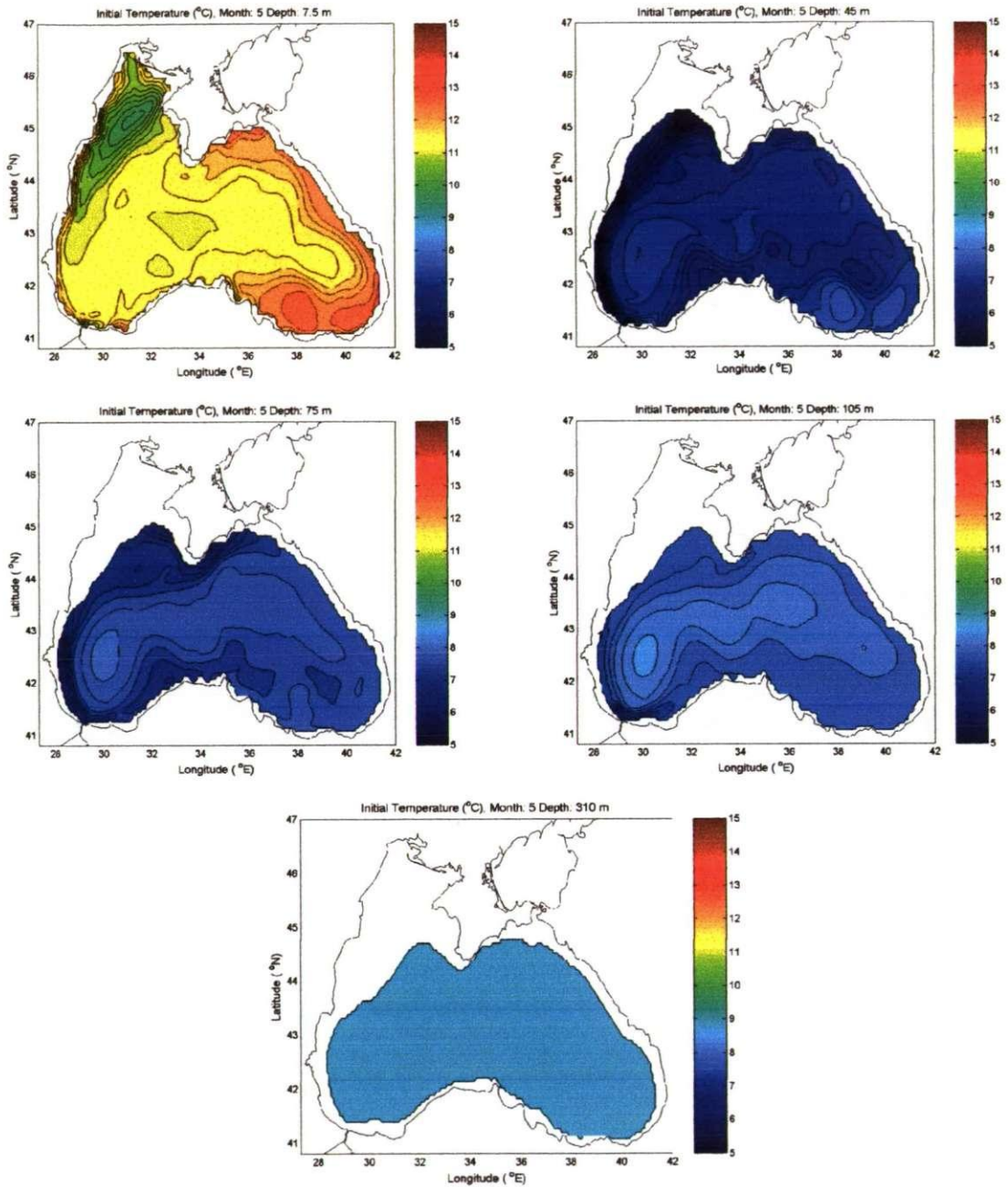
Figure 3-10 Maps showing the initial temperature distribution (°C) used in the modelling at depths: 7.5, 45, 75, 105 and 310m. (Staneva and Stanev, 1998)
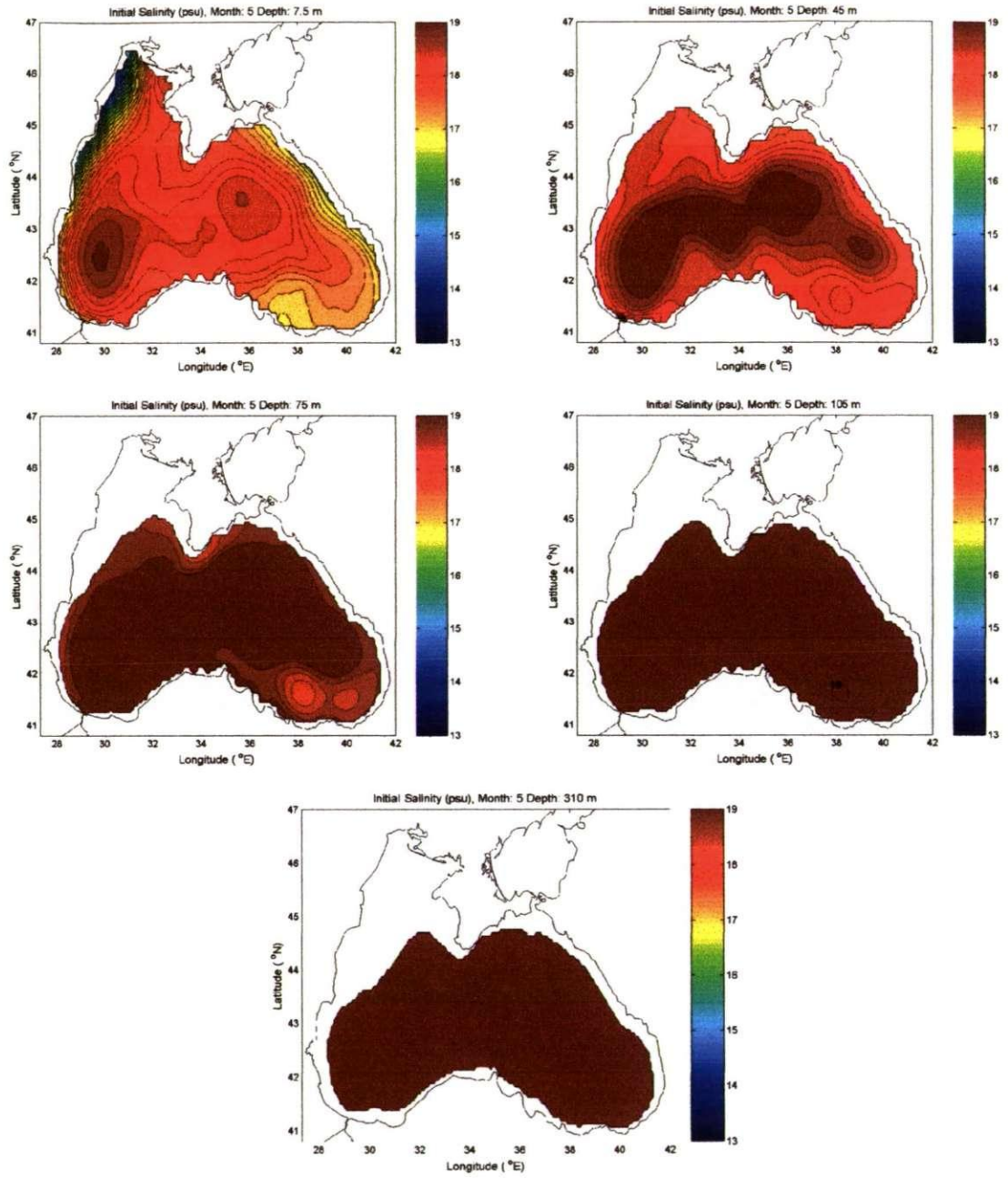
Figure 3-11 Maps showing the initial salinity distribution (psu) used in the modelling at depths: 7.5, 45, 75, 105 and 310m. (Staneva and Stanev, 1998)
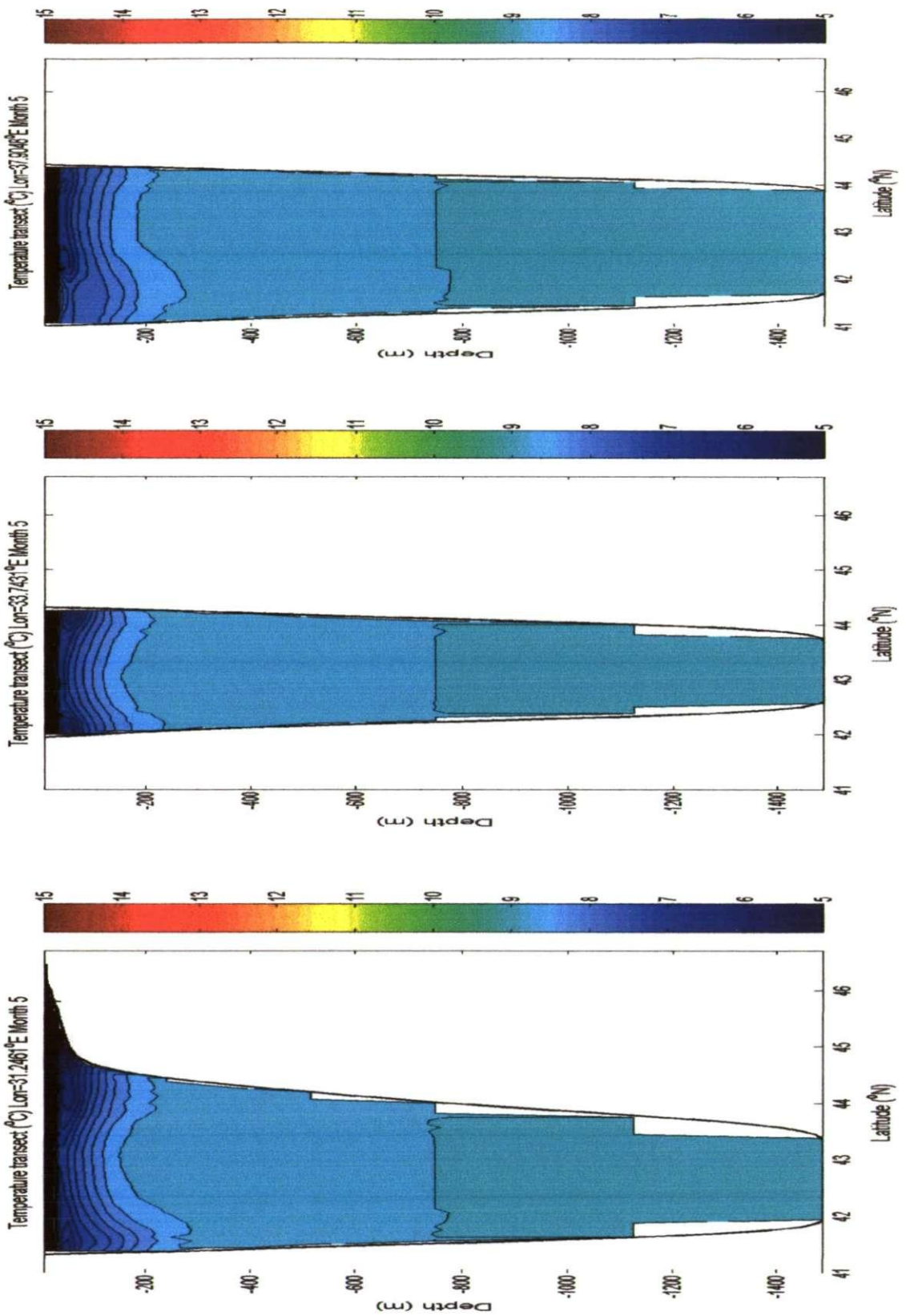
Figure 3-12 Meridional temperature transects1,2 and 3 showing the initial data for the modelling (Staneva and Stanev, 1998)
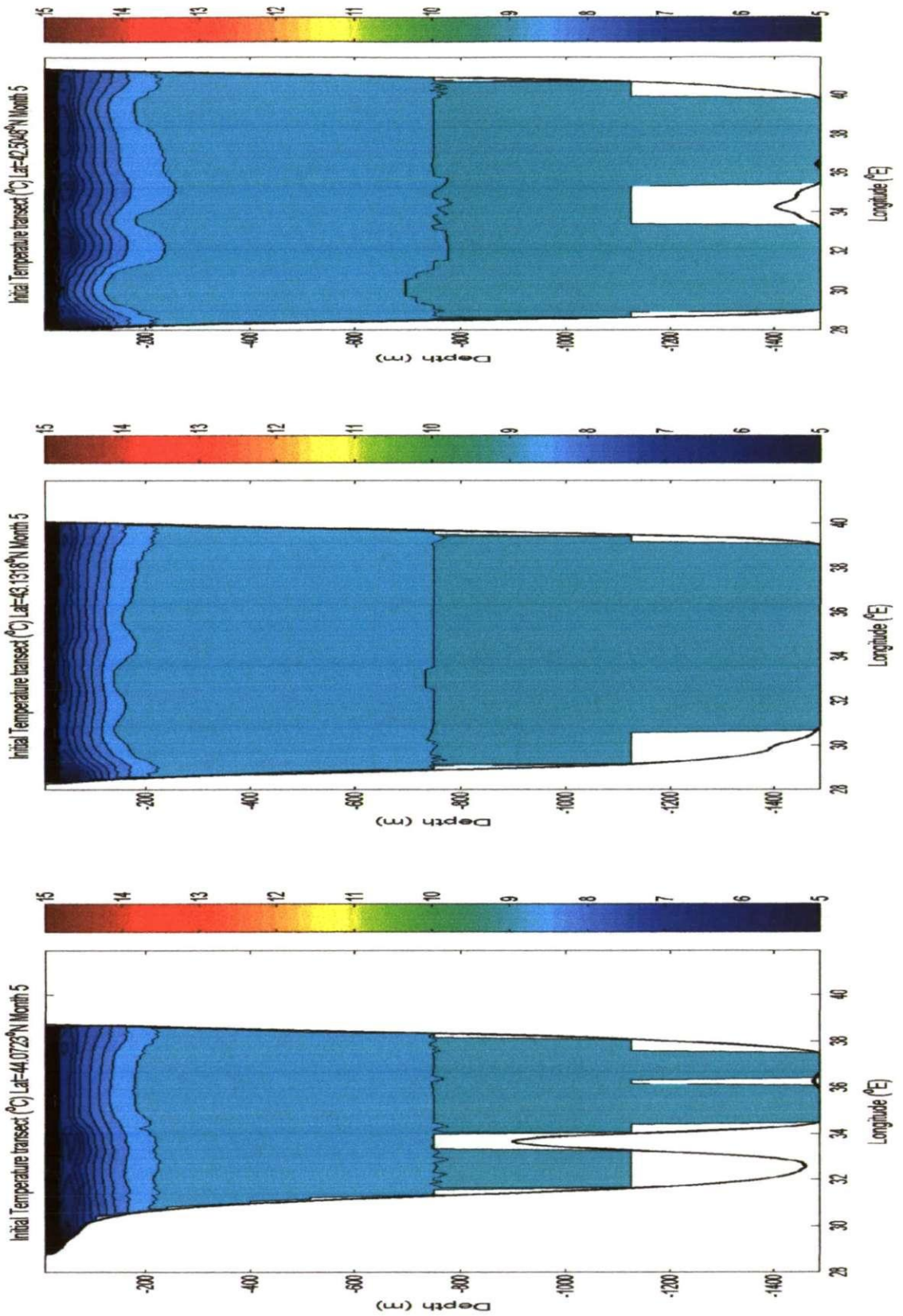
Figure 3-13 Zonal temperature transects 4, 5 and 6 showing the initial data for the modelling (Staneva and Stanev, 1998)
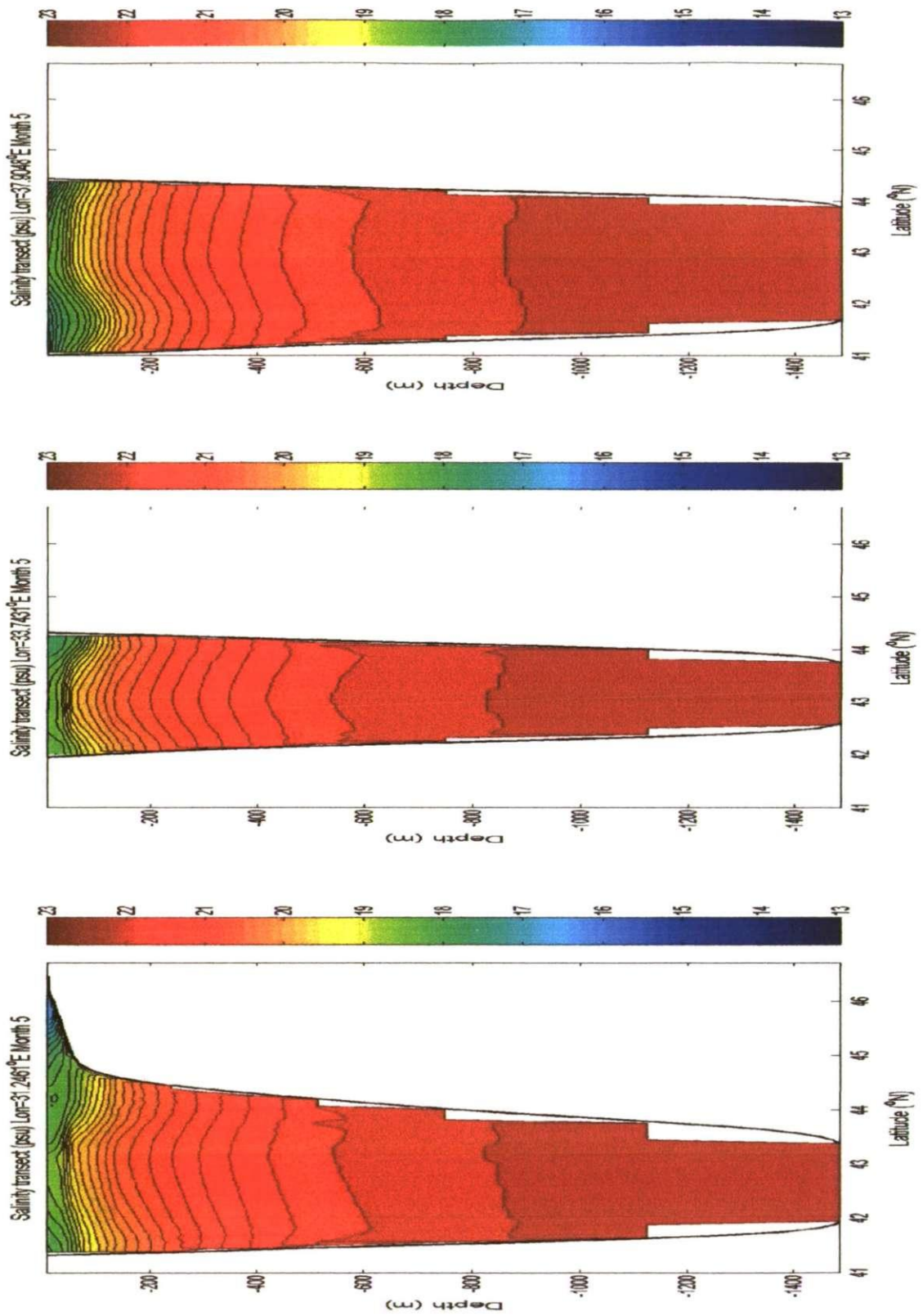
Figure 3-14 Meridional salinity transects 1,2 and 3 showing the initial data for the modelling (Staneva and Stanev, 1998)
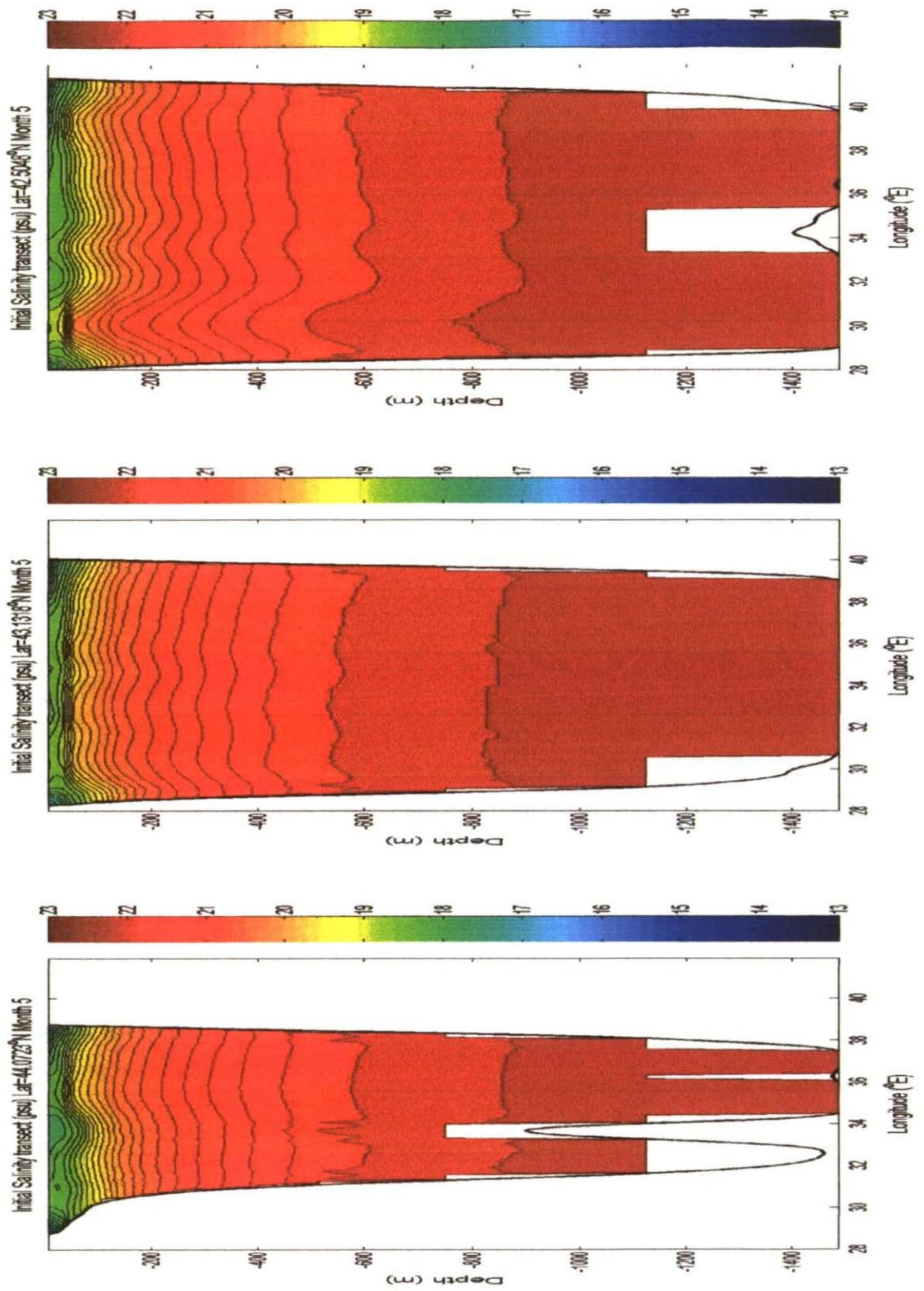
Figure 3-15 Zonal salinity transects 4, 5 and 6 showing the initial data for the modelling (Staneva and Stanev, 1998)

3.6. External forcing

3.6.1. Heat fluxes

One of the forces included in the model is the heat flux at the surface. The data are climatic monthly heat fluxes provided by Staneva and Stanev (1998). The horizontal geometry of these data is detailed in Table 3-1.

3.6.2. Methods for heat flux data treatment

The processing route for the heat flux data is presented in Figure 3-17. The first step was the unit converson. The units of the provided data are MJ/month and were converted to Watts using Matlab subroutine MJ2W.m (Appendix). Then the data were interpolated to fit the grid of this study (Table 3-1). The interpolation was performed in Surfer using the kriging method with the default parameters (linear variogram, slope=1, anisotropy = 1.0 and no nugget). Then the 12 data files containing climatic monthly heat fluxes were linearly interpolated in time to obtain daily data sets. This was done using FORTRAN subroutine qtfine.f90 (Appendix). Figure 3-16 shows the climatic heat flux at the surface for the months of May and June from which the data for the numerical experiments were obtained.

3.6.3. Evaporation – Precipitation

The model is also forced with water fluxes which at the surface are the evaporation and precipitation. The climatic monthly evaporation and precipitation data are taken from Staneva's data with horizontal geometry as stated in Table 3-1.
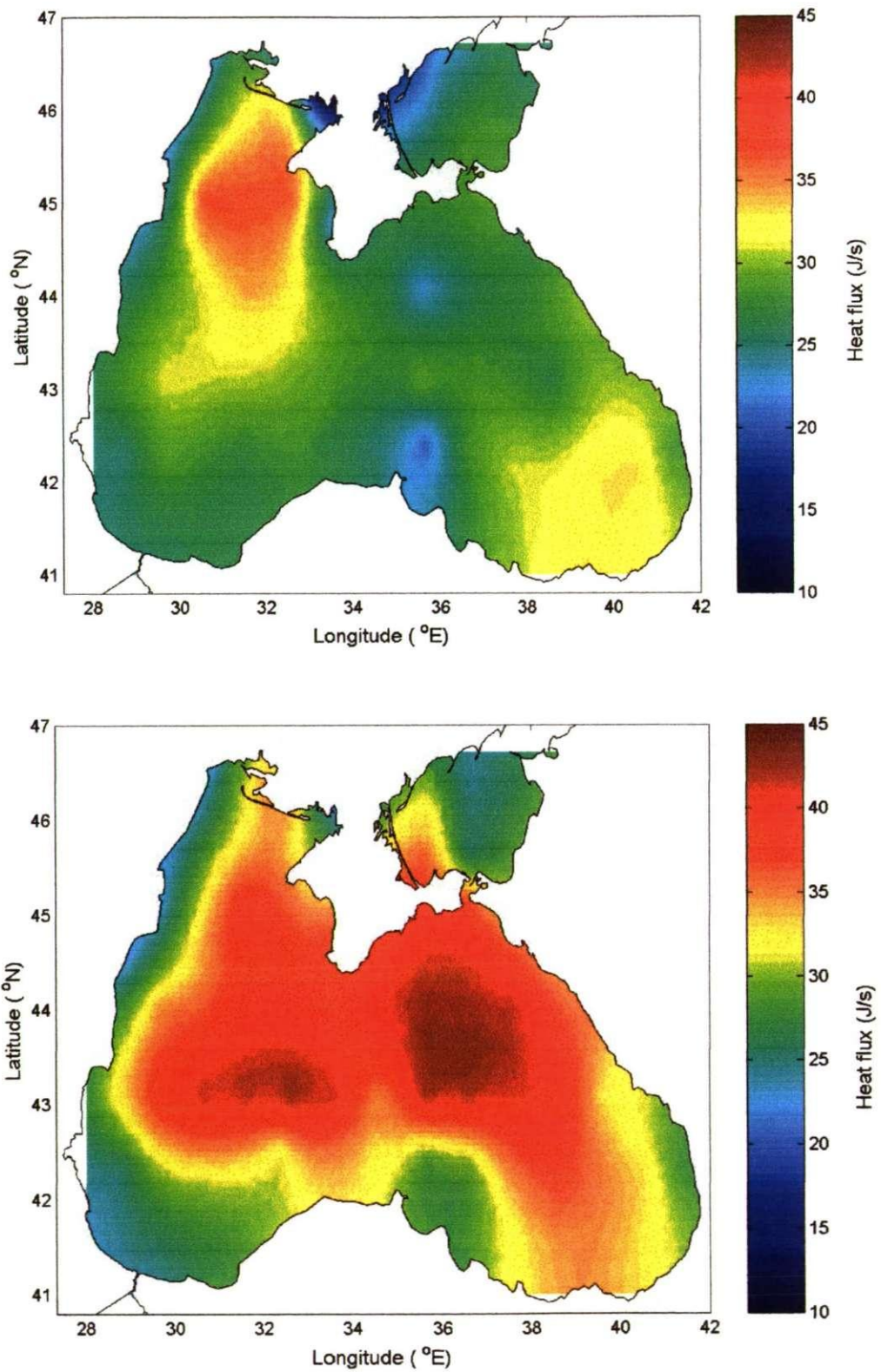
Figure 3-16 Climatic heat flux at the surface (J/s) a) May and b) June. Positive values mean sea surface receives heat from the atmosphere (Staneva and Stanev, 1998).

Climatic monthly 2-D Heat flux
[Staneva and Stanev, 1997]
(QTOT.dat)

Convert units
[MJ/month to J/s] and
prepare files for
interpolation using
Matlab subroutine
MJ2W.m

Horizontal
interpolation to fit
this study's grid.
kriging method
using Surfer

Import data into
Matlab produce 12
files for interpolation
in time using Matlab
subroutine wqt.m

12 files (one/month)
qtout1.dat
qtout2.dat
...
qtout12.dat

12 files (one/month) :
qtkr01.dat
qtkr02.dat
...
qtkr12.dat

12 files (one/month)
QT1.dat
QT2.dat
...
QT12.dat

Linear interpolation in
time to daily heat flux
data and writing file for
model input.
Using Fortran program
Qtfine.f90

Heat Flux ($Js^{-1}m^{-2}$)
during the month
of May for the
model
(QTmay.dat)

POLCOMS
MODEL

Figure 3-17 Flow chart showing the pre-processing treatment applied to the heat flux data for POLCOMS model.

Colour code: ☐ *Original data* ☐ *Process* ☐ *Data* ☐ *Model input data*

64

3.6.4. Methods for evaporation-precipitation data treatment

The processing route for the evaporation less precipitation data is presented in Figure 3-18. The first step was the unit conversion. Staneva's evaporation data has units of MJ/month and the precipitation data is given in mm/month. The evaporation data are converted to mm/month with

$$Evaporation\left(^{mm}\!/_{month}\right) = \frac{Evaporation\left(^{J}\!/_{(month)(m^2)}\right)}{(L_{lv})(\rho)} x\left(1x10^9\right)$$

where L_{lv} is the latent heat of evaporation: $2.5 \times 10^6 \, ^{J}\!/_{kg}$ and ρ is the density of sea water $\left(1027 \, ^{kg}\!/_{m^3}\right)$. Then the precipitation is subtracted from the evaporation to obtain evaporation less precipitation data files. These two steps are performed using the Matlab subroutine ep.m (Appendix). The monthly evaporation less precipitation data were linearly interpolated to fit the model's grid (Table 3-1). This was performed in Surfer using the kriging method with the default parameters: linear variogram, slope=1, anisotropy = 1.0 and no nugget. Finally the 12 data files containing climatic monthly evaporation less precipitation were linearly interpolated in time to obtain daily data sets. This was done using FORTRAN subroutine epfine.f90 (Appendix).

Figure 3-19 shows the climatic evaporation less precipitation data at the surface for the months of May and June from which the data for the numerical experiments were obtained.
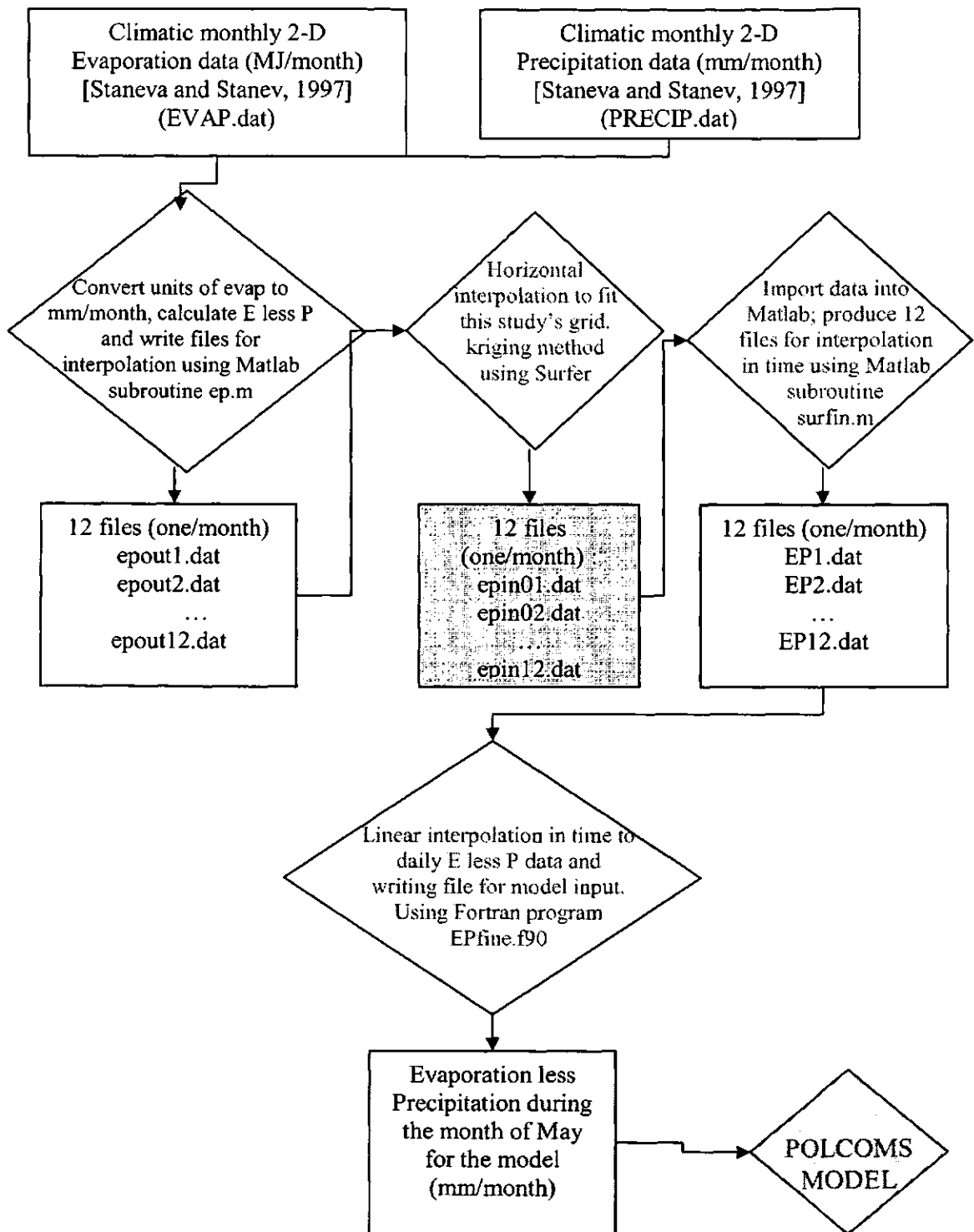
Figure 3-18 Flow chart showing the pre-processing treatment applied to the evaporation and precipitation data for POLCOMS model.

Colour code: □ *Original data* □ *Process* □ *Data* □ *Model input data*
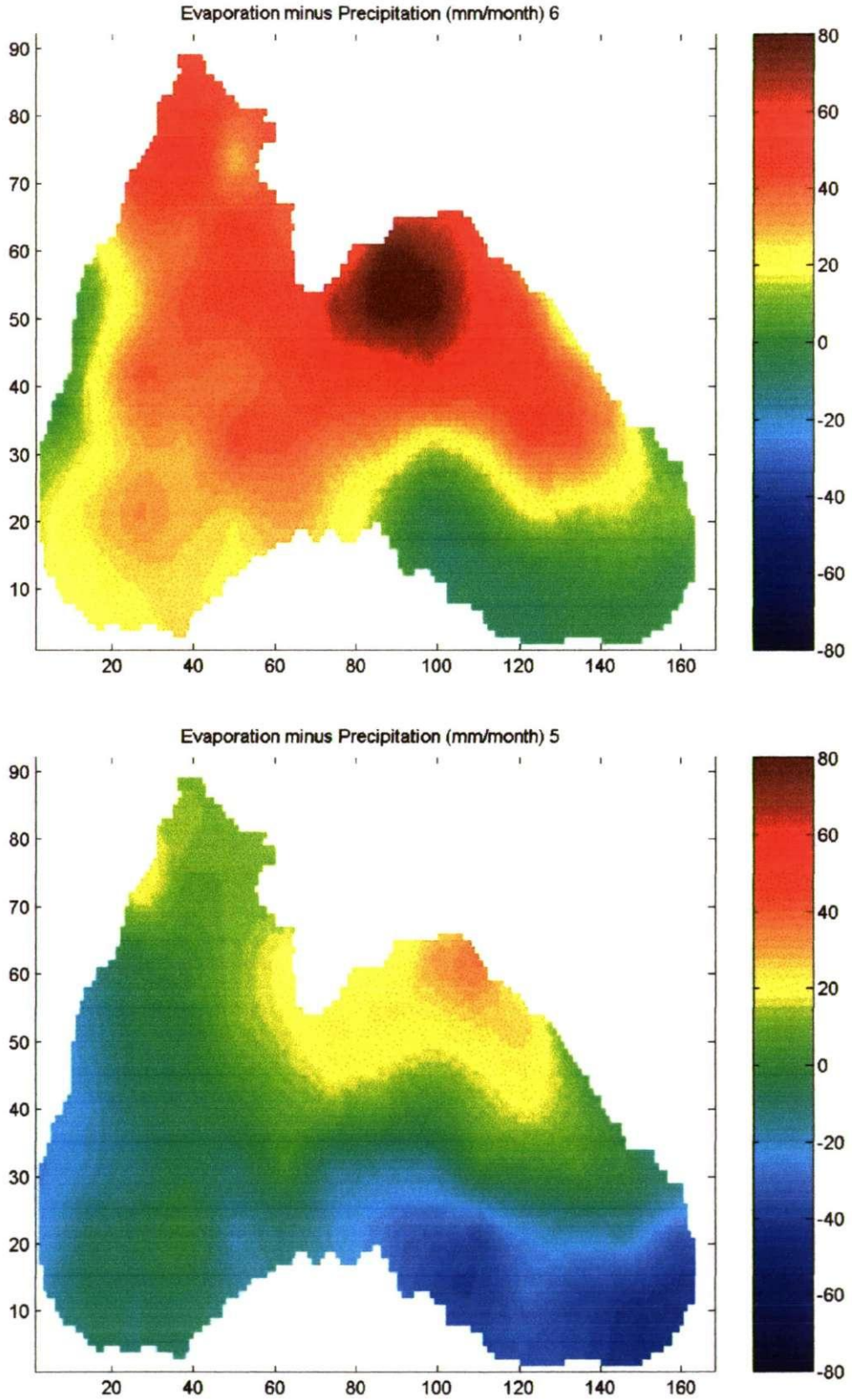
Figure 3-19 Climatic water flux at the surface (Evaporation less precipitation in mm/month) during a) May and b) June. Positive values mean excess of evaporation. (Staneva and Stanev, 1998)

3.6.5. Rivers

Another important forcing in the Black Sea is the river input and the water exchange in the Bosphorus Strait and with the Azov Sea. This study includes lateral water exchange from 6 rivers:

- The Danube, Dniepr, Dniestr which are the 3 main rivers and they all discharge to the north-western area.

- The Sakarya, Kizilirmak and Yesilirmak rivers which discharge to the southern part of the Black Sea.

These 6 rivers account for more than 90% of the total river discharge into the Black Sea basin. Their locations are presented in Figure 3-20. The river discharge data were obtained from a technical report the Rivers of the Black Sea (Jaoshvili, 2002) and the exchange at the Bosphorus and Azov seas were taken from (Altman and Kumish, 1986). The temperature of each one of them was approximated by taking the temperature value of the sea at the closest location from the climatic monthly temperature distribution of Staneva's data (Staneva and Stanev, 1998). The discharge was assumed uniform throughout the year because the interannual variability was not available. The volume and temperature at each one of the rivers included in the modelling is detailed in Table 3-3.

3.6.6. Wind

Finally, the wind forcing is included in this research as the main object of our study. While all the other forcing data are monthly averaged, the wind data used has high frequencies with 6 hour sampling interval. It is reanalysis data from the National Centre for Environmental Prediction, NCEP, [http://wwwt.ncep.noaa.gov/] consisting of wind speed data at 10 m height and 1° resolution. The cooperation of Yuriy Ratner in the extraction and pre-processing of the wind data is gratefully acknowledge.
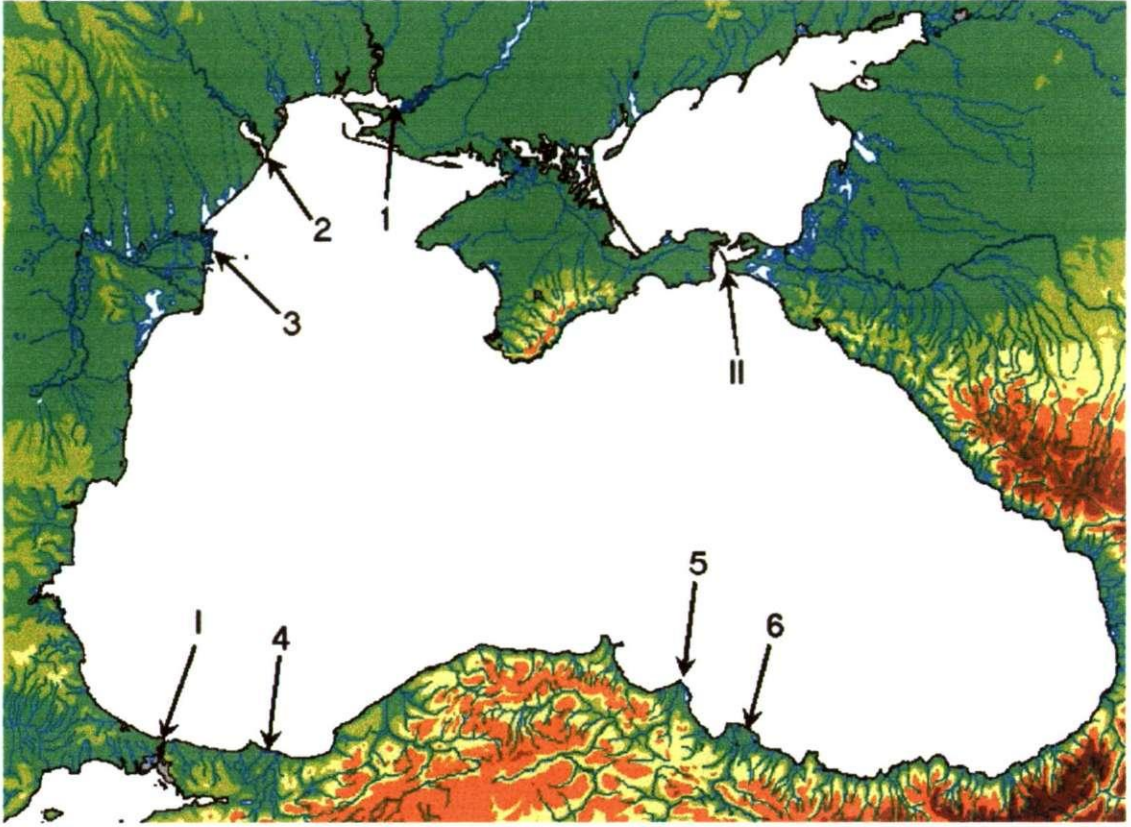
Figure 3-20 Location of the rivers included in the modelling and the exchanges with the Bosphorus strait and Sea of Azov. Map taken from (Suvorov et al., 2004) (The volume exchange and temperature are given in Table 3-3).

3.6.7. Methods for wind data treatment

From the wind speed, the components of the zonal (x) and meridional (y) wind stress were calculated by $\tau_x = c_D \rho_a u \sqrt{(u^2 + v^2)}$ and $\tau_y = c_D \rho_a v \sqrt{(u^2 + v^2)}$, where u and v are the zonal and meridional components of the wind speed at 10 m above the sea level and using a wind drag coefficient $c_D = 0.001$ and air density $\rho_a = 0.00129 \; {}^g/_{cm^3}$. The data were then interpolated from the one degree mesh by bicubic splines to fit the grid of this study (Table 3-1). The flow chart showing the pre-processing route for the wind data is shown in Figure 3-21. The data were converted from ${}^{din}/_{cm^2}$ to Pascals and written in the proper order for POLCOMS model.

No.	River Name	Volume Discharge m³/s	Jan	Feb	Mar	Apr	May	Jun	Jul	Aug	Sep	Oct	Nov	Dec
1	Dniepr	1398.5	0	0	1.9	6.4	11.9	18.2	21.5	23.4	20.1	14.7	6.1	1.4
2	Dnestr	292.56	0	0	2.3	7.3	13.2	19.1	22.4	23.9	20.4	15.1	6.5	1.7
3	Danube	6430	0	0.3	2.7	7.8	13.7	19.6	22.8	24.2	20.6	15.6	7.3	2.2
4	Sakarya	180	7.5	5.5	6.9	9.7	14.1	19.0	22.1	23.2	21.4	19.1	15.0	11.1
5	Kizilirmak	189.6	8.4	6.8	7.2	10.0	13.2	17.4	21.2	23.0	21.3	18.9	14.9	11.0
6	Yesilirmak	170.39	8.2	6.8	7.3	10.2	13.4	17.4	21.1	23.0	21.4	19.0	15.1	11.2
I	Bosphorus	-6269.2	6.4	5.4	6.1	8.4	10.8	17.5	21.1	22.5	20.7	18.0	13.6	9.2
II	Azov	546.6	1.4	0.8	3.5	8.5	14.0	20.1	23.4	24.6	21.0	15.6	6.5	2.8

Table 3-3 Lateral water exchange used for modelling. Volume discharges are positive for input of water to the Black Sea. Discharges taken from (Altman and Kumish, 1986) and temperature data taken from (Staneva and Stanev, 1998).
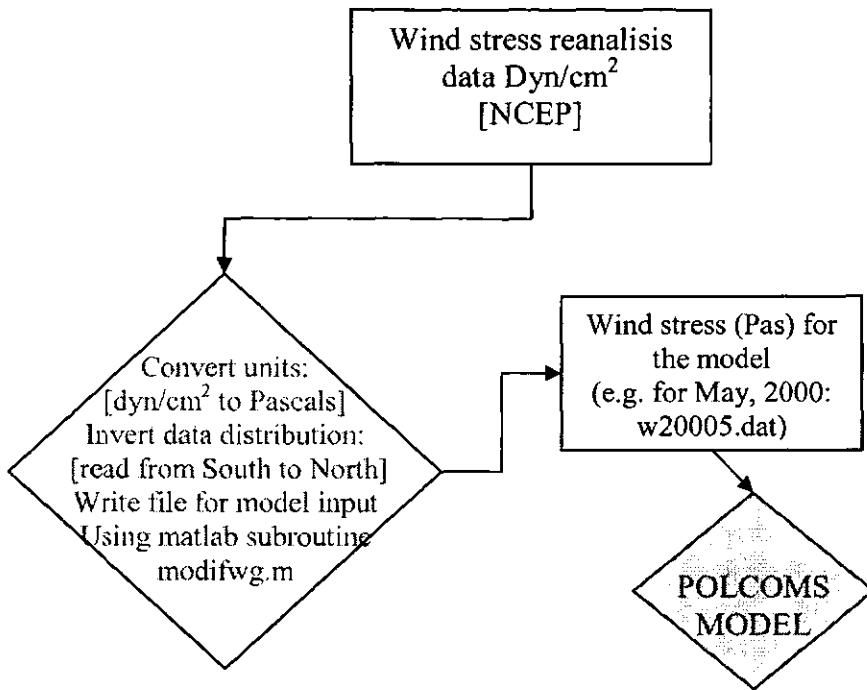
Figure 3-21 Flow chart showing the pre-processing treatment applied to the wind data for POLCOMS model.

Colour code: ☐ *Original data* ☐ *Process* ☐ *Data* ☐ *Model input data*

Figure 3-22 shows an example of the data corresponding to the 13 of May 1998 at 6:00 hrs. This plot shows approximately the typical wind pattern occurring in the Black Sea which is dominated by northerlies in the northern part of the sea veering cyclonically across the basin.
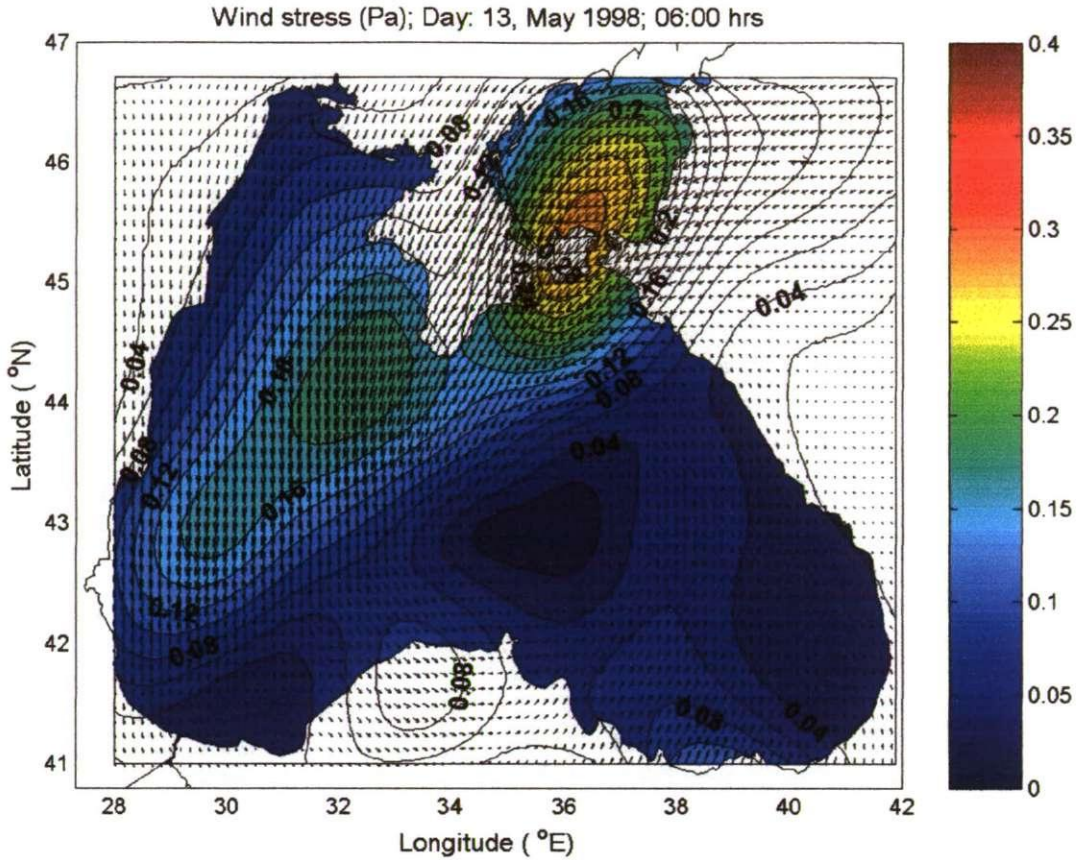
Figure 3-22 Wind stress field (Pascals) calculated from NCEP reanalysis data; [13 May1998; 6:00 hrs].

3.7. Methods of post-processing the modelled output data

The results of the model received some post-processing treatment to be transformed into practical information. The post-processing techniques which were applied to all the modelled output data will be described within this section. The summary of the post-processing applied to the modelled data together with the subroutines developed for the analysis are compiled in the Appendix.

1. The model output needs first to be interpolated vertically from s-coordinates to preselected horizontal levels (original z-coordinates). For this process the Matlab subroutine *treatg.m* was developed.

2. Once the data are in z-coordinates a series of maps and plots for visualisation were obtained with subroutines *mapspp.m* and *transpp.m*. The first one creates maps of temperature, salinity and current velocities at pre-selected depths. Subroutine *transpp.m* creates vertical transects of temperature, salinity and current velocity at the locations shown in Figure 3-8.

3. The basin averaged total kinetic energy was monitored and was calculated with:

$$TotKE = \iiint \frac{1}{2} \rho \left(u^2 + v^2 \right) dxdydz$$

where u and v are the zonal and meridional components of the velocity and the density ρ is taken as $1027 \ ^{kg}/_{m^{-3}}$. The subroutine *eking.m* was developed for this purpose.

The above procedures are the ones applied to all the modelled experiments. The methodologies describing analysis techniques which were applied for a particular analysis will be described together with the corresponding result.

CHAPTER 4. ANALYSIS OF OBSERVATIONS

4.1. Introduction

This chapter includes analysis of observational data, namely CTD measurements from a hydrographic campaign in the north-eastern part of the Black Sea (carried out by Prof. A. Zatsepin from the Shirshov Institute of Oceanology, Moscow and his research team) and a series of NOAA AVHRR sea surface temperature images. The data was used to support and provide evidence of the dynamic processes of the Black Sea and more importantly to give a basis for a qualitative comparison of the model output for verification. The 3-D thermo-haline structure in the region of the *in situ* measurements and the distribution of geostrophic currents were obtained from the data.

The satellite imagery provides a 2-D view of the temperature field covering the whole basin giving information on the surface current structure, spatial scales and intensity of mesoscale activity. Moreover, the images provide information beyond that of a snapshot, making it possible to follow the time evolution of mesoscale structures, allowing the approximation of dynamical characteristics such as speed of displacement and orbital velocities.

Within this chapter we describe the Black Sea dynamics using the results of the observational analysis to:

- Describe the general thermo-haline distribution and current structure of the Black Sea basin.

- Present the thermo-haline distribution and geostrophic currents in the north-eastern part of the Black Sea during November 2000.

- Describe the mesoscale activity in the upper layer during October-November 2000.

4.2. Upper layer hydrodynamics

4.2.1. Temperature distribution

A succession of analysed Sea Surface Temperature (SST) images from the 25 of October to the 14 of November 2000 together with measurements in the north-eastern part of the Black Sea during November 2000 offered the possibility to characterise the temperature distribution and some of the circulation features present in the Black Sea basin during that period of time. Figure 4-1 is an example of the set of SST images analysed. This almost cloud-free image can be used to illustrate the main features of the hydrodynamics. There is a lateral temperature gradient with colder water in the north-west and much warmer water in the south-east of the Black Sea basin, where temperature values reach approximately 20°C. The Rim Current acts as the border between the central basin, dominated by cyclonic eddies, and the coastal areas, dominated by anticyclonic features. The coldest waters during the 26 of October of 2000 are located in the centre of the basin at the south of the Crimean peninsula and in the north-western shelf close to the coast with temperatures down to less than 15°C. There is evident mesoscale activity throughout the area with clear meanders and filaments developing from the Rim Current and well delimited parcels of water indicating the presence of anticyclonic (warm) or cyclonic (cold) eddies. The images also show that in the coastal areas the temperature appears to be advected along the coast in the direction of the main current.

From the *in situ* measurements we can see that during November 2000 the surface water temperature near the north-eastern coast is relatively warm, reaching 16.9°C (Figure 4-2a), and decreases towards the sea. The minimum temperature measured at the surface is 14°C.
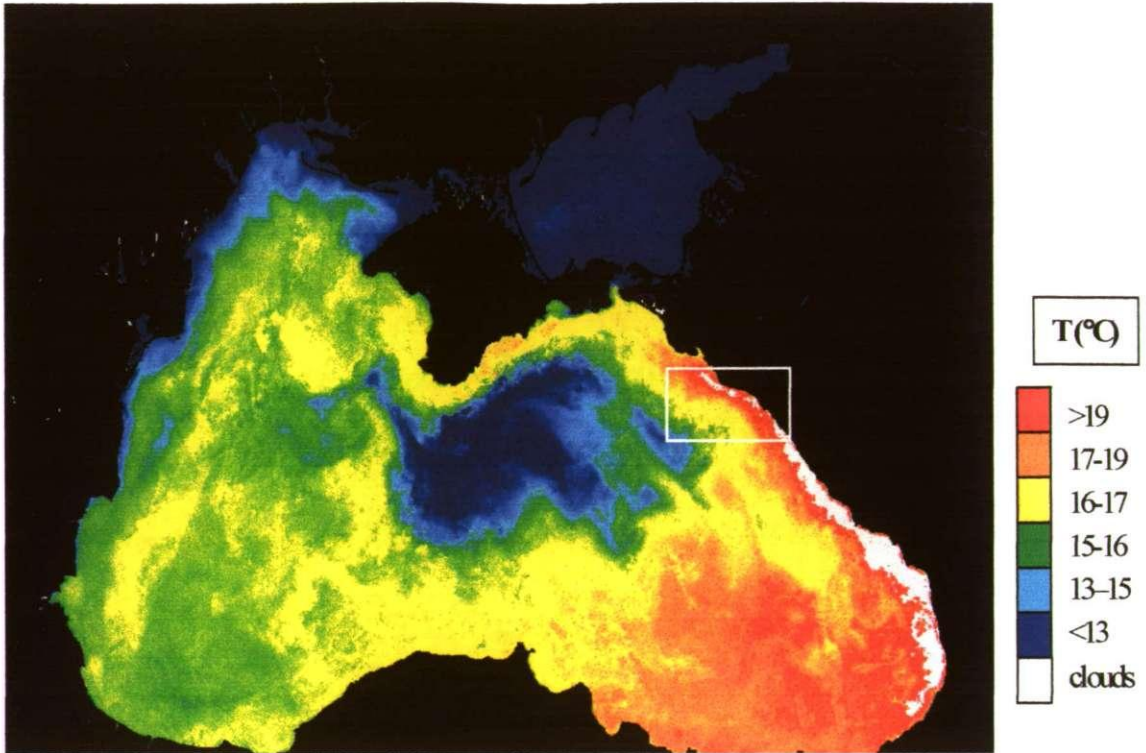
Figure 4-1 AVHRR image showing the mean sea surface temperature for the week beginning the 26 October 2000. This figure also shows the surveyed area (white rectangle)

4.2.2. Salinity distribution

The fresher waters are located in the coastal regions, especially in the north-western area where the main rivers discharge and followed by a cross-shelf salinity gradient. The CTD measurements show the salinity gradient and the fresher coastal water extending north-westward along the coast in the direction of the Rim Current (Figure 4-2b). The salinity variations at the surface are between 17.7 *psu* near the coast and 18.2 *psu* away from the coast. There is a weaker along-shelf salinity gradient in the north-eastern coast where salinity increases away from the rivers so that the saltier coastal water is in the north.

In general the results agree with the climatic salinity distribution for the month of November in Staneva's data set (Figure 4-3).

76

Map of temperature (C) at 0m depth

Map of salinity (psu) at 0m depth
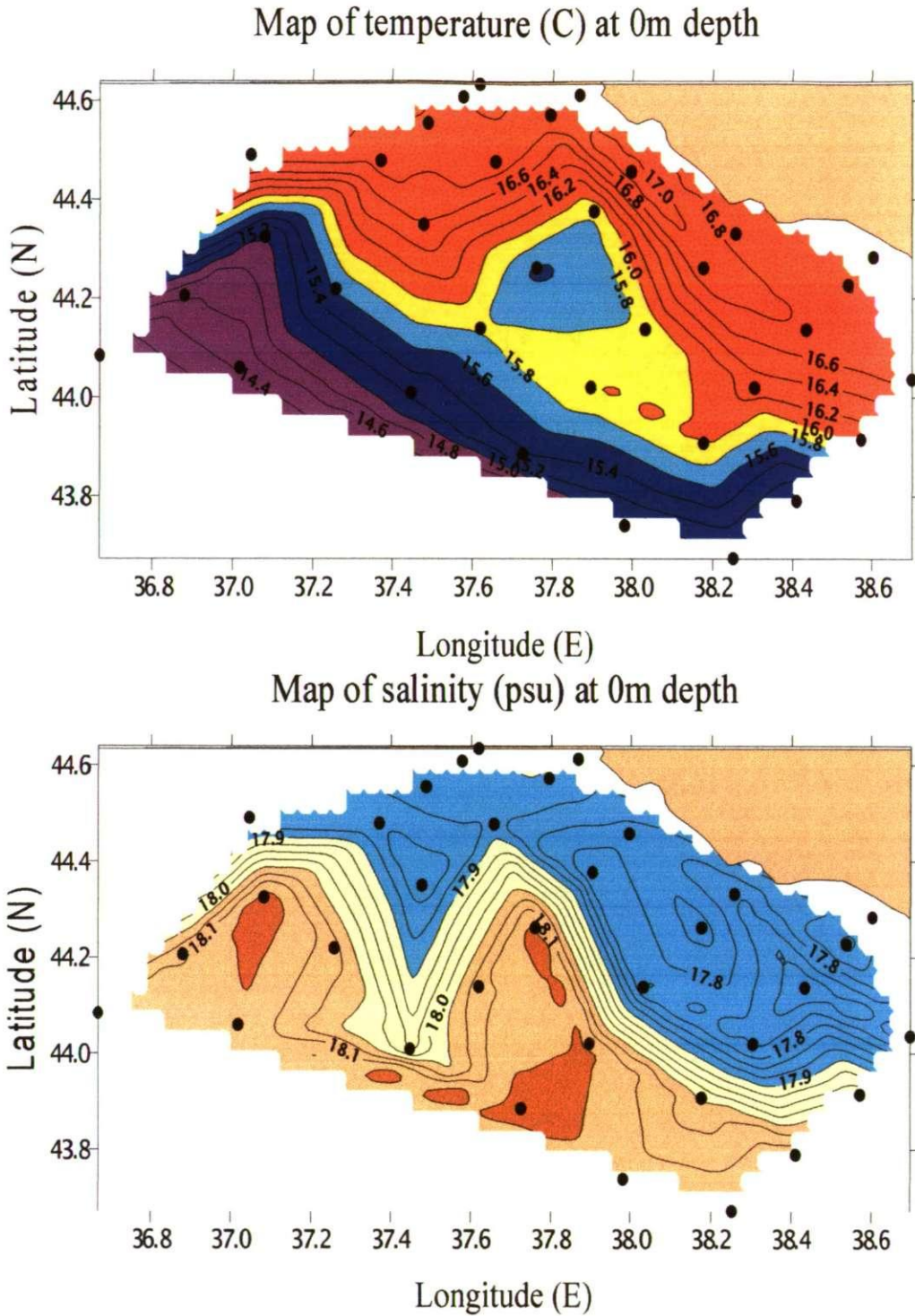
Figure 4-2 Hydrographic maps of temperature (°C) (top panel) and salinity (bottom panel) at the surface during the field campaign (17 to 20 of November 2000) in the NE part of the Black Sea. Data provided by A. Zatsepin, Shirshov Institute of Oceanology, Moscow.
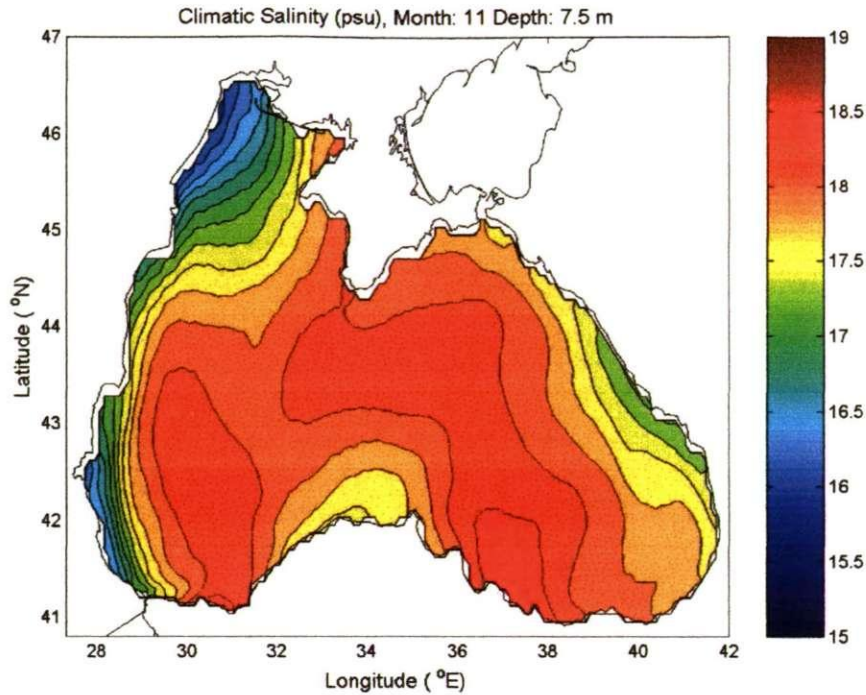
Figure 4-3 November climatic sea surface salinity distribution from Staneva's data (Staneva and Stanev, 1998)

4.2.3. Mesoscale circulation

During the 25 and 26 October a meander of the Rim Current was close to the north-eastern coast. When this situation occurs, the coastal anticyclonic mesoscale circulation diminishes and the current flows very close to the coast. This was verified by Zatsepin et al. (2002) presenting results from three expeditions carried out in the north-eastern part of the Black Sea during the Autumn of the years 1999, 2000 and 2001. The upper layer circulation in the north-east is shown by the geostrophic velocity map (Figure 4-4). The method for calculating the current fields is described in Section 3.2.2. There is a well defined meandering current (the Rim Current), flowing to the north parallel to the isobaths, reaching velocities of 1 m/s in the narrowest areas. Closer to the coast the current flows to the south.

78

Due to the equidistant spacing between the isopycnals through the water column, the same circulation pattern throughout the depth is expected (Figure 4-4b). The geostrophic maps confirm the presence of the Rim Current with velocity decreasing with depth. It is also possible to identify anticyclonic near-shore features close to the coastal area and also manifested on the higher surface height values in the dynamic topography.
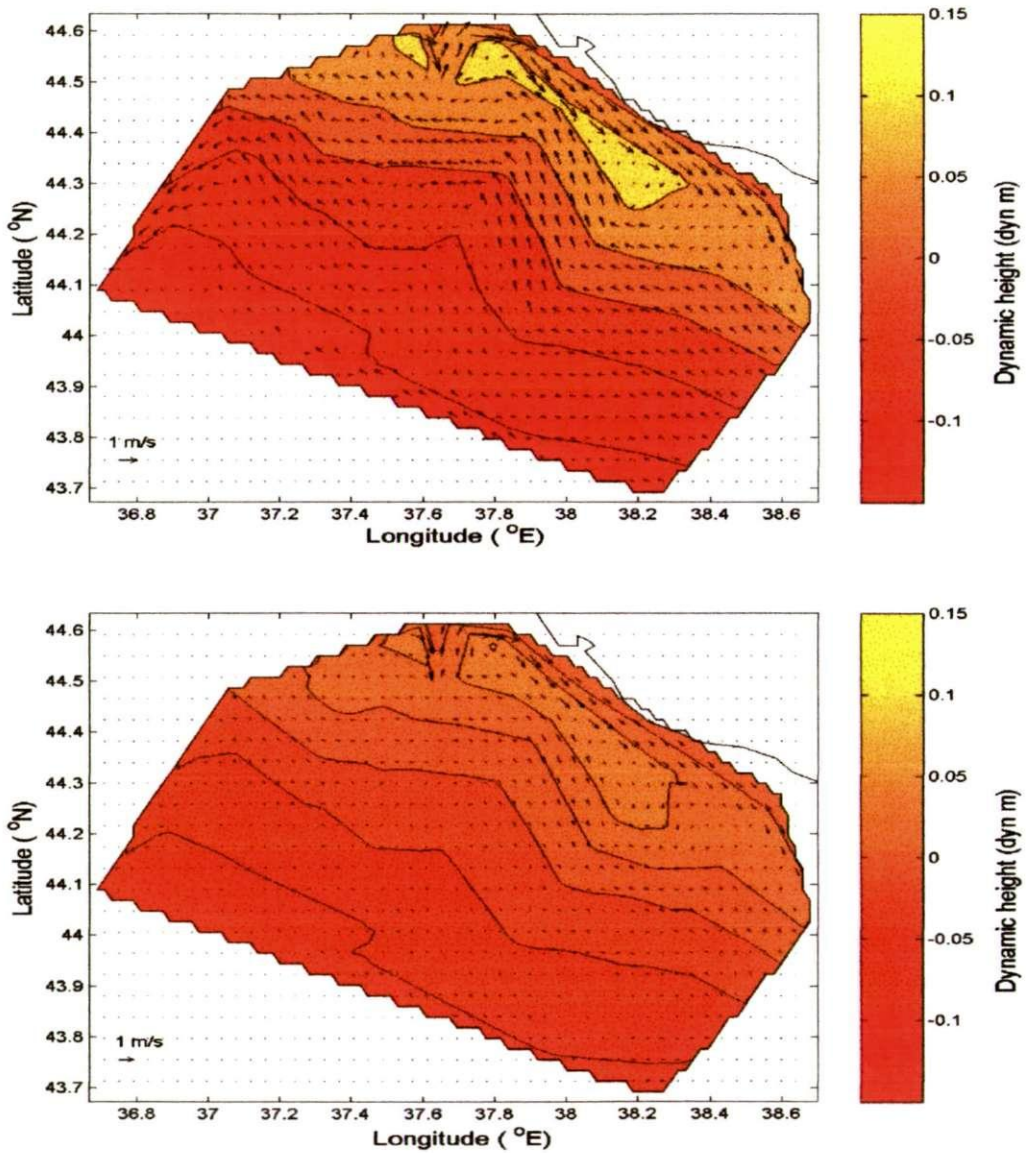
Figure 4-4 Maps of geostrophic velocity (m/s) during the field campaign (17-20 November 2000) in the NE part of the Black Sea at the surface (top) and at 100 m depth (bottom). The map has contours of dynamic topography (dyn m) relative to 500 m depth.

During the *in situ* measurements a cyclonic eddy was located very close to the coast and it is shown in Figure 4-2a as a patch of cold water at the centre of the study area (~44.3 °N, 37.75 °E). It is manifested in Figure 4-4 as a meander of the main current. It is proposed in this study that the feature is actually a cyclonic eddy sitting on the Rim Current so that the left side of the eddy (flowing to the south) decreases the mean velocity flowing to the north. The analysis of this cyclonic eddy was expanded with the SST images covering the CTD sampling dates. The centre of the eddy was identified at station 176 (Figure 4-5) and has colder, more saline and therefore denser water than its neighbour stations.
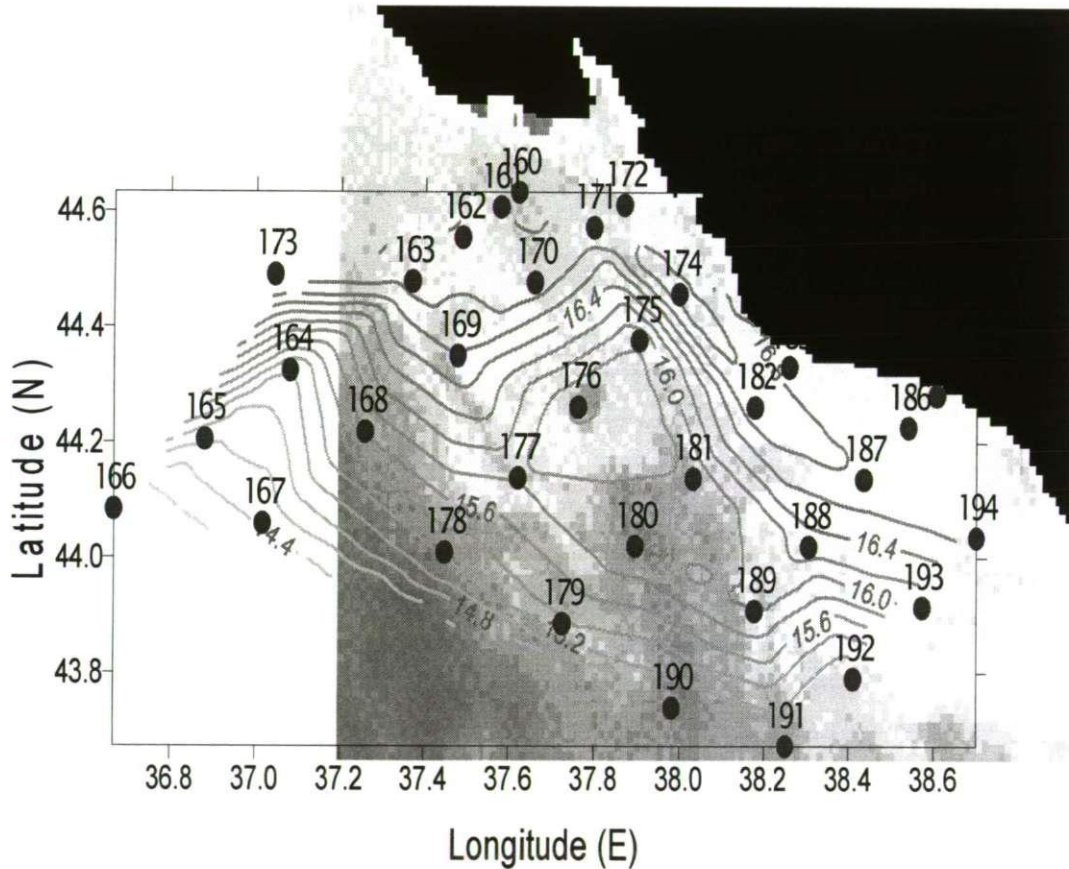
Figure 4-5 AVHRR SST image from the 17th of November 2000, showing the cyclonic eddy present during the hydrographic campaign. Overlapped there are temperature contours (°C) from the in situ measurements.

From the SST image of November 17th (Figure 4-6) we can see that the diameter of the core of the eddy is approximately 11 km and after one day it travelled to the north-west with a drifting velocity of approximately 0.36 m/s. Because this cyclone was present during the hydrographic campaign, its vertical structure was characterised and it is presented in Section 4.3.
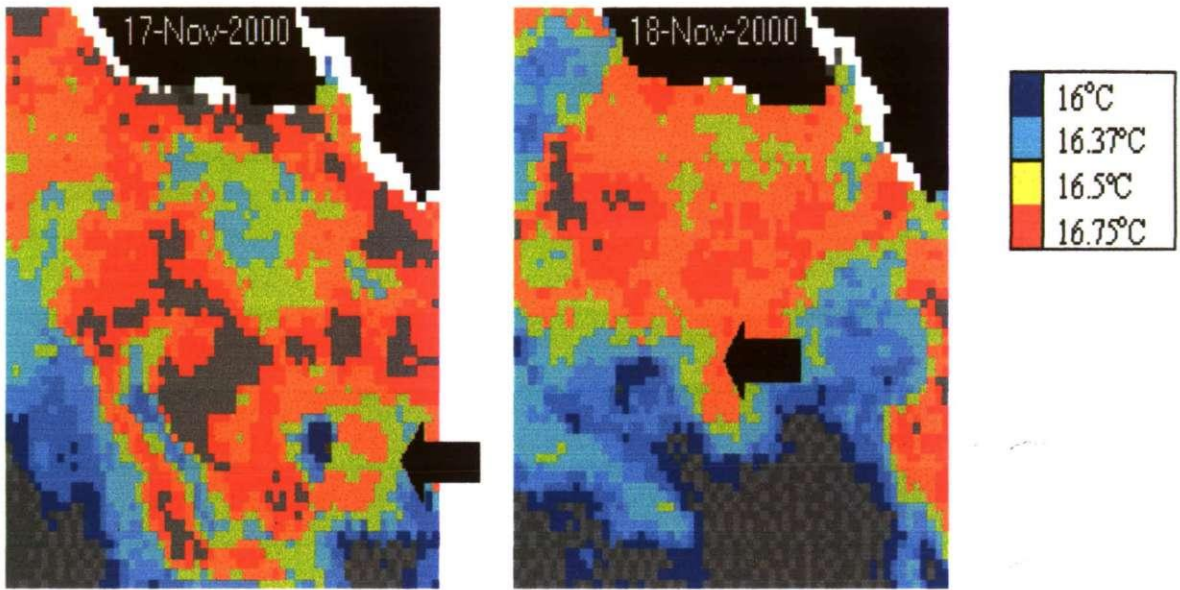
Figure 4-6 AHRR SST images showing the evolution of the mesoscale cyclonic eddy present in the NE part of the Black Sea from the 17th to the 18th of November 2000.

Other mesoscale features were present during the time period but outside the area or time of the measurements, so that there is no information on their vertical structure. Nevertheless the images are able to provide useful information on scale and velocities of mesoscale features. Some examples of these are below.

One cyclonic structure was evident the 25 of October in the north-eastern part of the Black Sea, with approximately 51 km diameter. In one day it travelled approximately 9 km

towards the north-west and increased its diameter to 62 km (Figure 4-7). By the 28 of October, when the south-eastern part of the Black Sea was clear from clouds, this cyclone was no longer evident and probably dissipated between other cyclonic fingers and meanders in the area. Most eddies seem to have life spans of a few days to one week [Zatsepin, 2002].
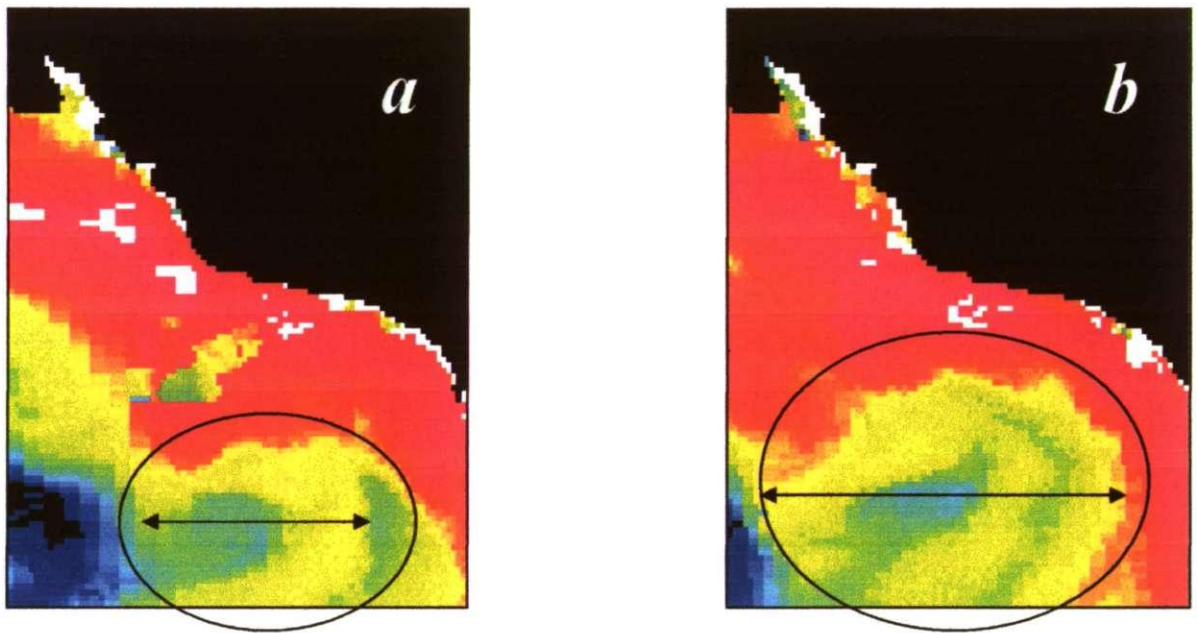
Figure 4-7 AVHRR SST images showing the evolution and displacement of cyclonic eddy in the eastern coast of the Black Sea: a) 25 October, 2000 and b) 26 October, 2000. The arrows show the diameter of the eddies delimited by the ellipses.

The southern coast is also characterised by the presence of coastal anticyclones and the period of October-November 2000 was not an exception. Several anticyclones are evident throughout the month as shown in Figure 4-8. They have diameters between 30 and 80 km. From October 30, the meandering of the Rim Current retracted to a more central region, away from the east and north-eastern coast, so it is possible to see some anticyclonic features near the coast as shown in Figure 4-9. In the same image, among the mesoscale

eddies located throughout the basin, we can distinguish a dipole system. It is a 'mushroom-like' feature.
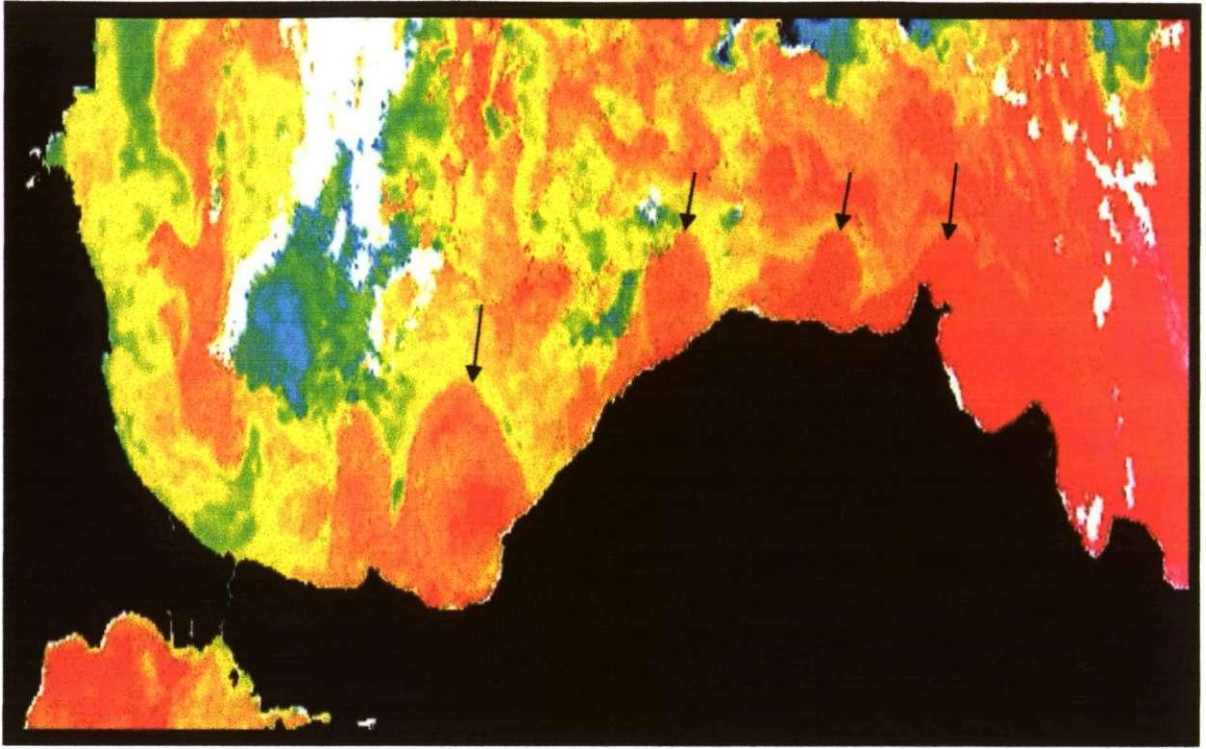
Figure 4-8 AVHRR SST image of the southern part of the Black Sea for the 30th of October of the year 2000, showing the coastal anticyclonic eddies which are normally present in this area (some of them are pointed out by arrows).

The concept of mushroom-like eddies was introduced by K.N. Fedorov (1986). This particular feature has been reported in the past, consisting of an anticyclonic eddy and a cyclonic eddy near the north-eastern part of the basin. The eddies are coupled by the Rim Current and filaments, forming the stem and cap of the mushroom-eddy system (Oguz et al., 1994). In our results it was only evident during the first few days of November. Also in the north-eastern area of the Black Sea, it was possible to follow with the satellite images one particular cyclone for 6 days (from the 13th to the 18th of November), allowing the approximation of its trajectory and velocity. It propagated to the west with an approximate drifting velocity of 0.14 m/s. Its orbital velocity, calculated by comparing the images from 13 and 14 of November (Figure 4-20), was approximately 0.17-0.20 m/s.
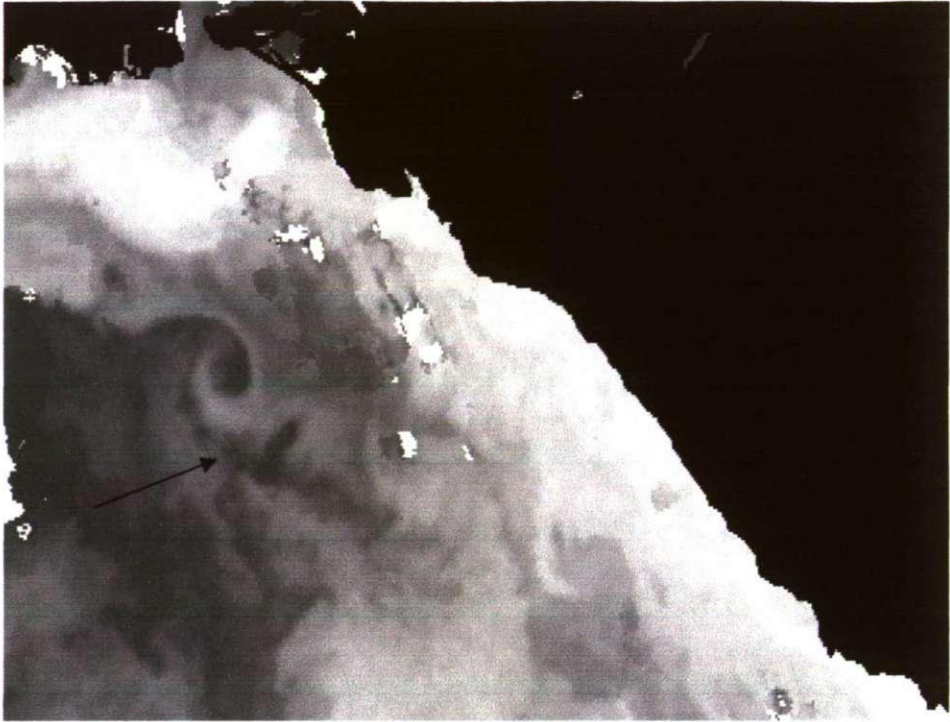
Figure 4-9 AVHRR SST image for 2nd of November 2000 in the NE part of the Black Sea, showing the mushroom eddy structure which has been observed in the past in that area (Oguz et al., 1994)
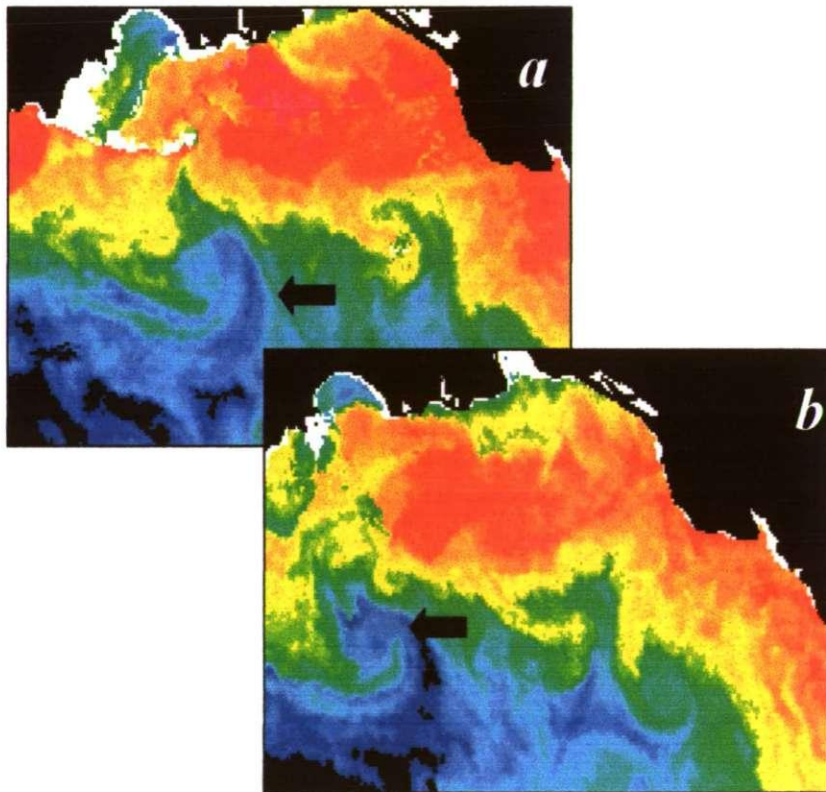
Figure 4-10 AVHRR SST images showing the evolution of cyclonic eddy from the 13th (a) to the 14th of November 2000 (b).

4.3. Vertical thermo-haline structure

4.3.1. Water masses

Generally the Black Sea has three layers of water with very distinctive characteristics (e.g. (Leonov, 1960):

1. A top layer with warmer water and low salinity

2. A cold intermediate layer, CIL, with the lowest temperature and low salinity

3. A lower layer with cold temperature and higher salinity

These three water masses are clearly distinguished in the T-S diagrams as shown in Figure 4-11. This figure includes all the stations and it is clear that the stations located near the coast only have the upper layer water mass of fresher water with salinity ~18 *psu* and with temperature slightly decreasing with depth.

The distribution of temperature, salinity and density in the water column can be seen from the vertical profiles at each station, such as the one for station 163 in Figure 4-12 and also in the vertical transects at different locations of the studied area (e.g. Figure 4-13). The map showing the transect locations is in Chapter 3, Figure 3-8.

4.3.2. Temperature distribution

The top layer is a mixed layer which extends from the surface to a variable depth depending on a combination of different physical phenomena. In the north-eastern part of the Black Sea during the field campaign (17 - 20 of November 2000), the surface mixed layer reached depths of 15 to 25 m in the stations located further from the coast and about 40 m depth in the stations located closer to the coast.
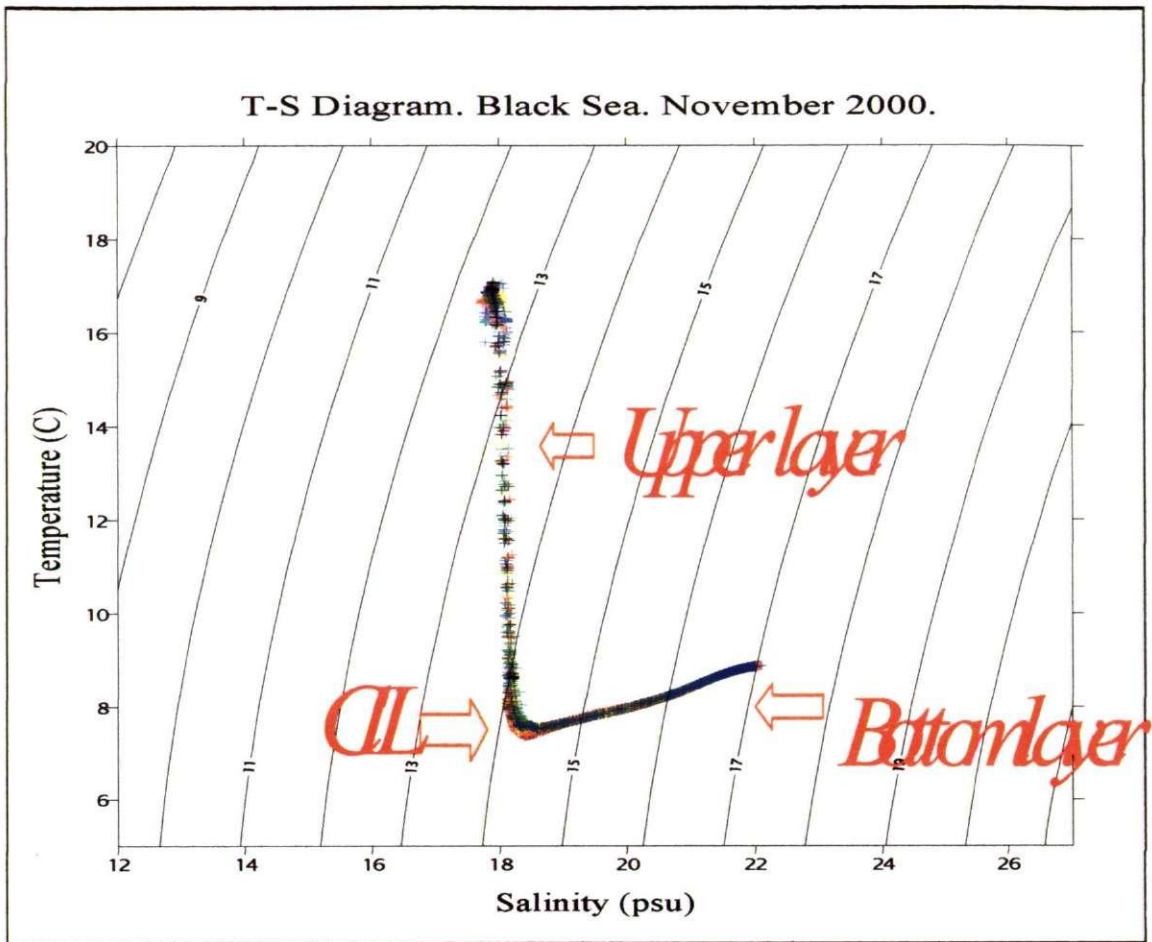
Figure 4-11 T-S diagram including all the stations measured during the hydrographic campaign in the NE Black Sea during November 2000. The different colours represent different stations.

Below the surface mixed layer there is a strong thermocline of approximately 20 – 25 m width, in which the temperature falls abruptly from ~15 to 8 °C. It is located between 12 and 24 m in the deep water and between 36 and 58 m at stations closer to the coast as can be seen in Figure 4-13. Below the thermocline the presence of the CIL is very clear, containing the minimum temperature of the water column. It is located approximately at a depth of 50 m in deep waters and at about 100 m depth near the boundaries. The core of the CIL in this region and during this time has temperatures of 7.3-7.5 °C, with 8 °C

isotherms assumed to be its lower and upper boundaries. Below the CIL the temperature slightly increases up to about 8.8 °C in the deeper sampled areas (510 m).

4.3.3. Salinity distribution

The salinity distribution in the north-eastern part of the Black Sea during the hydrographic campaign consists of a surface mixed layer which has the lowest salinity values in the water column. This layer goes from the surface to about 35 m depth. Below the mixed layer is the halocline where the salinity increases abruptly from 17-18 *psu* to approximately 21.5 *psu* at a depth of about 350 m. Below the halocline the salinity continues to increase with depth but at a much lower rate. The maximum salinity is measured at the bottom reaching values of 22 *psu*.

4.3.4. Density distribution

The density field from the *in situ* measurements clearly shows the strong stratification resulting from the strong dilution of the surface waters, primarily due to rivers (Stanev et al., 1997) which characterises the Black Sea. The σ_t distribution consist of a surface mixed layer followed by a gradual increase from approximately 12.5 kg/m^3 at the surface to about 16.6 kg/m^3 at the lower part of the pycnocline located at approximately 200 m depth. Below the pycnocline the change in density towards the bottom is very small with increasing σ_t at a rate of 0.2 kg/m3 every 100 m and reaching approximately 17 kg/m^3 at 500 m depth.
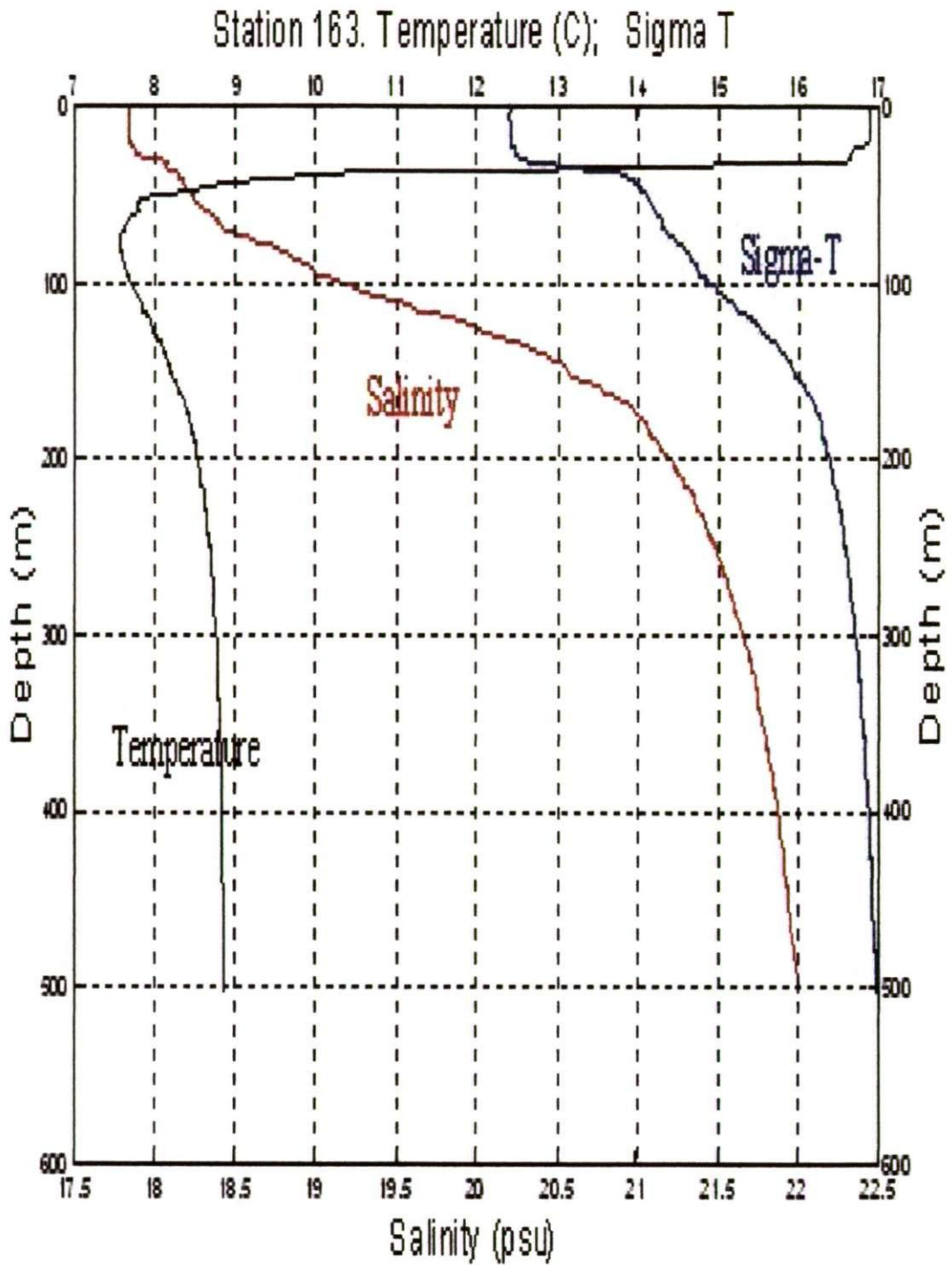
Figure 4-12 Vertical profile of temperature (°C), salinity (psu) and sigma-T. Note that the bottom axis shows the scale for salinity and the top axis shows the scale for temperature and sigma-t.

Figure 4-13 shows cross-shelf vertical transects of temperature, salinity and sigma-t. Within these cross-sections the presence of the surface mixed layer and the marked vertical stratification below it can be verified. The inclination of the isolines in the transects results from the influence of the Rim Current which flows cyclonically along the shelf edges. Cyclones in the northern hemisphere generate a slope where the sea level rises away from the centre. The pressure gradient force is therefore directed towards the centre of the cyclones and the low pressure at the core determines the rising of the isolines from below.

4.3.5. Vertical structure of the sampled cyclonic eddy

The vertical structure of the cyclonic eddy which was present in the measured area during the field campaign is shown in along-shore vertical cross-sections in Figure 4-14. It was mentioned before that the core of the eddy has colder and saltier water than the surrounding water. This is also evident in the cross-sections. The centre of the eddy shows a mixed layer from the surface down to approximately 20 m depth with a temperature of 16°C, (more than 0.5 °C colder than the surrounding waters) and a salinity of more than 18 *psu* (exceeding the surrounding water salinity by more than 0.3 *psu*). All the isolines (thermocline, halocline and pycnocline) rise in the centre of the eddy, showing at the surface water with properties of deeper water (upwelling). The influence of this eddy reaches depths of more than 200 m.
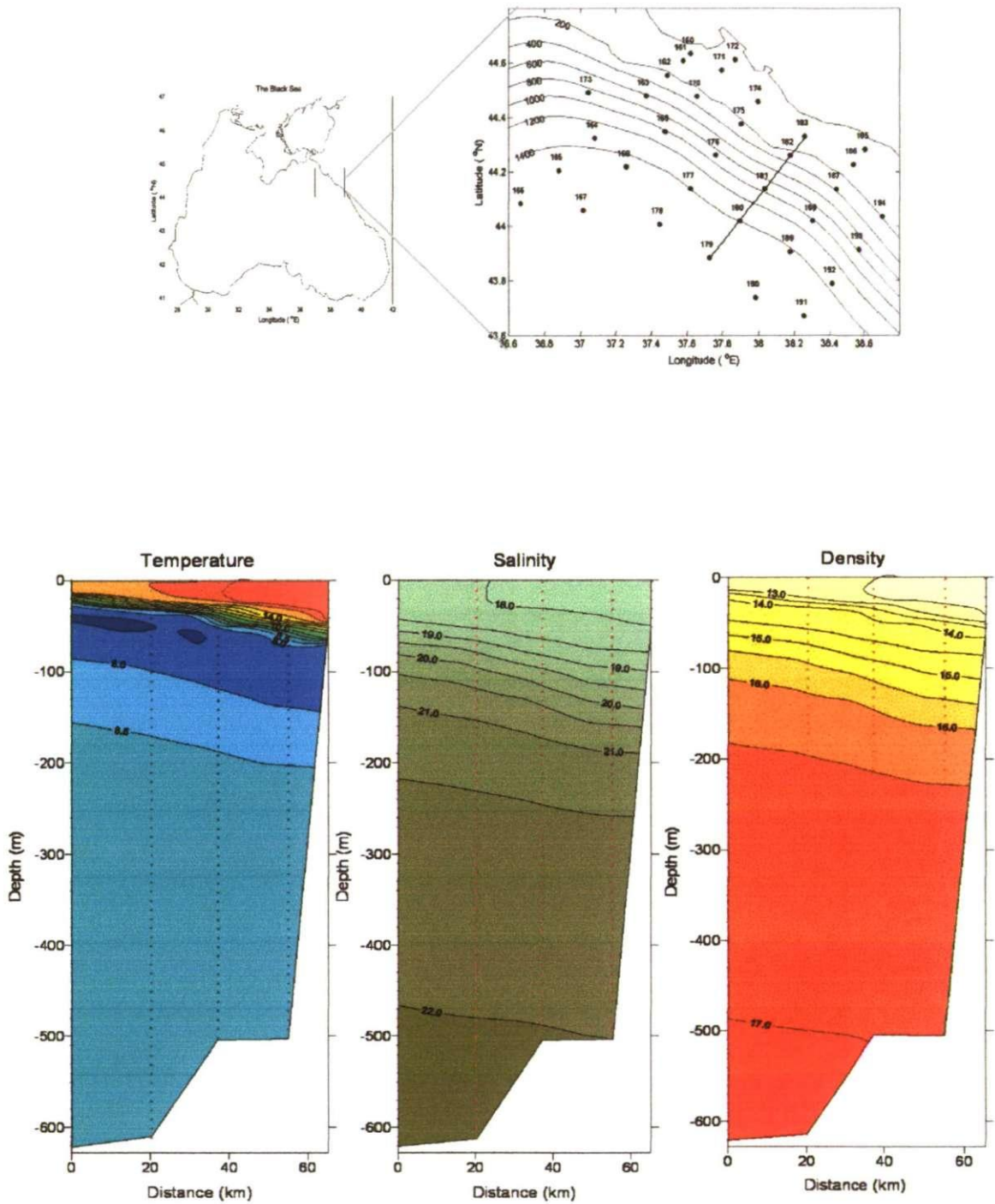
Figure 4-13 The top panel shows the location of the 3 vertical cross- sections (bottom panel) during November 2000 showing the temperature (° C), salinity (psu) and sigma-t vertical structure. The red dots represent the location of the measurements. The bottom axis shows the distance from Stn 179 landwards.
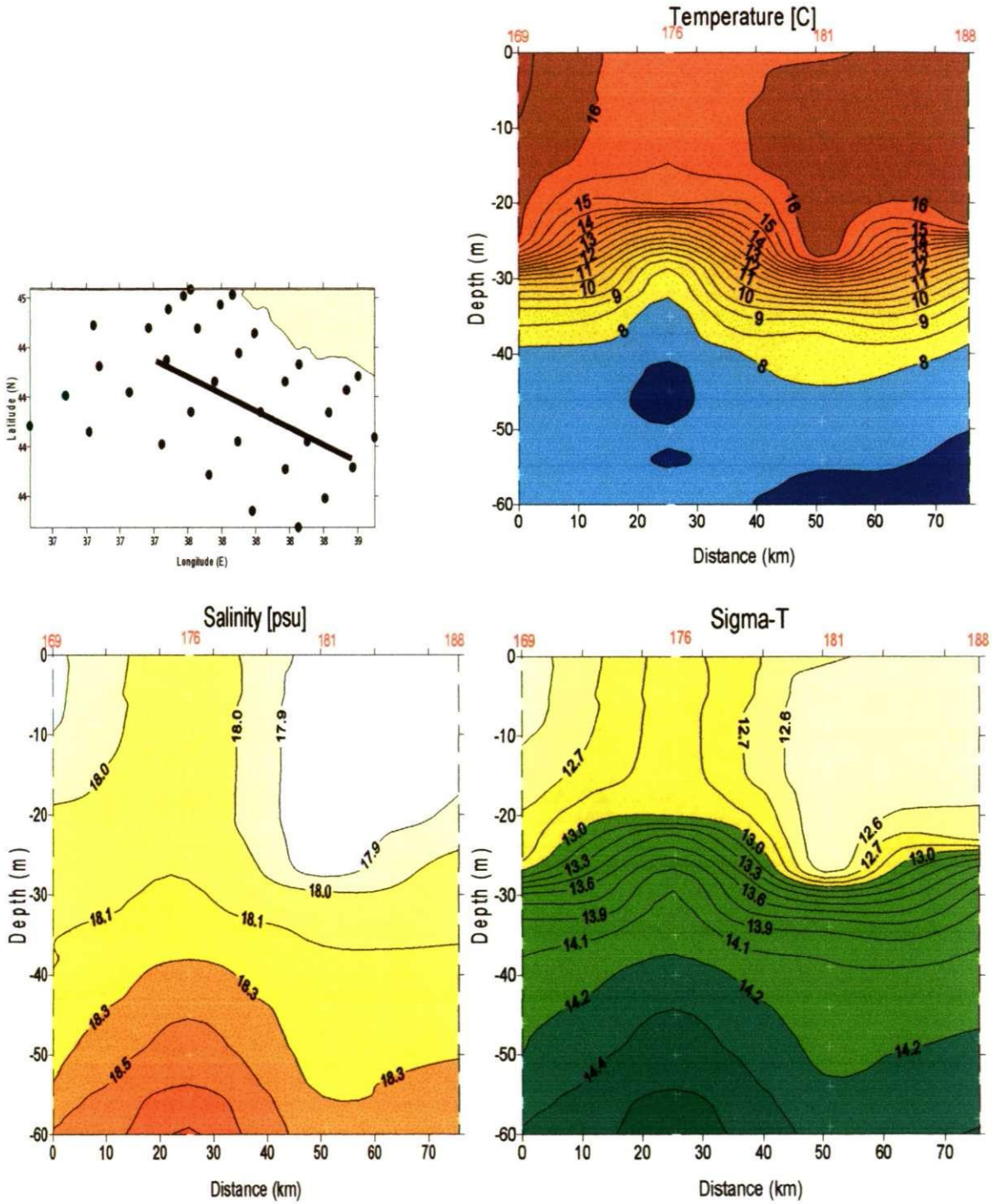
Figure 4-14 Vertical along-shore cross-sections across the cyclonic eddy present during the hydrographic campaign in the NE part of the Black Sea during November 2000. The transects show temperature, salinity and sigma-t of the water column in the location specified in the top left panel.

4.4. Summary

From the analysis of observational data this chapter presents the general and mesoscale dynamics in the Black Sea during October and November 2000. The hydrodynamics in the Black Sea during this time coincide with the general structure which characterises this area:

- The SST images show the presence of a lateral temperature gradient from the north-west to the south-east which is typical throughout the year.

- In the north-eastern area the CTD data show cross-shelf salinity gradient from the coast due to freshwater discharge and a weaker along-shelf gradient extending to the north-west with higher salinity values in the north of the sampled area.

- The central basin was dominated by cyclonic circulation (from remote sensing data) and the cyclones generate a lifting of the isotherms below them (from *in situ* measurements).

- The vertical transects (CTD data) show the surface mixed layer, the strong stratification and the CIL dividing the upper layer from the bottom layer.

- The circulation included the Rim Current flowing cyclonically around the basin, mesoscale eddies in the central and coastal areas and meanders and filaments all over the Black Sea area.

The analysis showed additional results which were observed during the studied time:

- The presence of a cold patch covering a large area (about the size of the Crimean peninsula) in the northern-central basin during October 2000.

- In November 2000 the stream of the Rim Current was strong and flowing very close to the coast in the north-eastern part of the Black Sea.

- One small cyclonic eddy was present in the north-eastern area at the time of the hydrographic campaign and was characterised from the results of both, CTD and remote sensing analysis obtaining its dimensions, vertical structure and drifting velocity.

- Additionally in the SST images several mesoscale eddies were identified in the basin during this period of time.

- The size, shape and velocity of mesoscale structures were determined from the SST images. The size of the features identified range between 10 and 90 m in diameter. The drifting velocities of mesoscale eddies approximated from the images ranged between 0.1 and 0.15 m/s. The orbital velocity of a mesoscale cyclonic eddy during the 13 and 14 of November 2000 was approximately 0.18 m/s. These estimates are within the values of velocities previously reported in the literature.

CHAPTER 5. SENSITIVITY TESTS

5.1. Introduction

As an important component of numerical modelling studies, the model needs to be tested to evaluate its stability and the sensitivity to parameters which may have a considerable influence on the results. The results of the model should then be validated, which is the comparison of model output with current knowledge (Dyke Ph., 1996) usually coming from observations. This chapter covers the results of the sensitivity tests and the validation will be presented in Chapter 6.

Sensitivity analysis should be done whenever there is a new set up for a numerical model in order to be able to trust the model results. Although there are a substantial number of modelling studies of the Black Sea basin, this is the first use of POLCOMS model applied to that sea. Therefore, the sensitivity tests are crucial for the model setup. This study includes sensitivity tests analysing the effect of bottom topography, grid resolution, time step and horizontal diffusion coefficient on the model results. These effects are evaluated by monitoring the total kinetic energy of the basin and by comparing the modelled currents with the available knowledge of the dynamics of the Black Sea basin.

5.2. Numerical experiments

A total of 19 numerical experiments (Table 5-1) were carried out to test sensitivity to different parameters. All the experiments start from a state of rest (zero velocities) and no external forcing is included throughout the runs.

Experiments 1, 2 and 3 test the response of the model to bottom topography. These experiments are initialised with a homogeneous density distribution. Hence, the whole basin has an initial temperature of 18° and a salinity of 20 *psu*. Experiment 1 has a flat

94

bottom at 1500 m depth. Experiments 2 and 3 use the real Black Sea bottom topography with coarse and fine resolution grids respectively. The characteristics of the different grids are given in Table 5-2.

Experiments 4 to 15 investigate the sensitivity to the barotropic and baroclinic time steps. All these experiments are initialized with temperature and salinity corresponding to the climatic distribution of May, and with the real Black Sea bathymetry at the bottom boundary. Experiments 4 to 8 are performed with the coarse resolution grid and use a fixed barotropic time step of 20 s with a varied range of baroclinic time steps. Experiments 5, 9 and 10 use the coarse grid and have a fixed baroclinic time step of 400 s while varying the barotropic time step. Experiments 11 to 13 use the fine grid and have a fixed barotropic time step of 20 s varying the baroclinic step. Experiments 13 and 14 use the fine grid and have fixed baroclinic time step of 200 s varying the barotropic time step.

Experiments 5, 13 and 16 were used to find the effects of the mesh resolution on the hydrodynamic results. The runs are initialized with temperature and salinity climatic May distribution, and with the real Black Sea bathymetry at the bottom boundary. Experiment 5 uses a coarse grid, experiment 13 a fine grid and experiment 16 an extra-fine grid. The characteristics of each one of the grids are listed in Table 5-2.

Experiments 14, 17, 18 and 19 are used to test the model sensitivity to different values of the horizontal diffusion coefficient. The four runs use the fine grid and are initialized with temperature and salinity climatic May distribution and the real Black Sea bathymetry at the bottom boundary. The barotropic time step is 20 s and baroclinic time step 200 s.

No	Grid	Bottom Topography	Barotropic Time step (s)	Baroclinic Time step (s)	AHC[1] (m/s)	AHCrit[2] (m²/s)	Initial T - S	Run Length
1	Coarse	Flat	20	400	0.2	600	Unif.[3]	12 months
2	Coarse	Real	20	400	0.2	600	Unif.[3]	6 months
3	Fine	Real	20	400	0.2	600	Unif.[3]	6 months
4	Coarse	Real	20	200	0.2	600	May	1 months
5	Coarse	Real	20	400	0.2	600	May	1 month
6	Coarse	Real	20	600	0.2	600	May	1 month
7	Coarse	Real	20	800	0.2	600	May	1 month
8	Coarse	Real	20	1200	0.2	600	May	1 month
9	Coarse	Real	10	400	0.2	600	May	1 month
10	Coarse	Real	40	400	0.2	600	May	1 month
11	Fine	Real	20	400	0.2	600	May	1 month
12	Fine	Real	20	300	0.2	600	May	1 month
13	Fine	Real	20	200	0.2	600	May	1 month
14	Fine	Real	10	200	0.2	600	May	1 month
15	Fine	Real	10	100	0.2	600	May	1 month
16	X-Fine	Real	5	25	0.2	600	May	8 days
17	Fine	Real	20	200	0.5	600	May	1 month
18	Fine	Real	20	200	1.0	600	May	1 month
19	Fine	Real	20	200	0.1	600	May	1 month

Table 5-1 List of numerical experiments for the sensitivity tests.

[1] *The horizontal diffusion coefficient is calculated as the product of the predefined constant AHC by the depth at each particular grid point.*

[2] *The horizontal diffusion coefficient is the minimum value between the predefined critical value AHCrit and the product of AHC by the depth at each grid point.*

[3] *Uniform density distribution with temperature of 18°C and salinity of 20 psu.*

Grid	Latitudinal Resolution	Longitudinal Resolution	Approximate dx	Total No. of wet grid points
Coarse	1/4°	1/3°	~ 25.5 km	12,048
Fine	1/16°	1/12°	~ 6.7 km	194,040
X-Fine	1/31°	1/24°	~ 3.4 km	790,752

Table 5-2 Space discretisation of the different grids

5.3. Sensitivity to bottom topography

Bottom topography plays a very important role in oceanic circulation, especially for barotropic flows where the density is homogeneous and hence there is no horizontal density gradient and no vertical shear, while in a stratified fluid the friction between layers tends to mitigate these effects (Kantha and Clayson, 2000).

The evolution of the currents generated in a homogeneous density fluid in response to the bottom topography is described in this section. In a flat-bottomed basin using the coarse grid with a uniform temperature and salinity distribution (Test 1) no velocities were generated after a 1 year simulation. This test shows that the model is stable and does not generate noise or false velocities because a fluid with uniform density distribution in a flat bottomed basin can only be driven by an external forcing.

The next step was to introduce the bottom topography, again without any external forcing and using uniform temperature and salinity distribution throughout the basin. The response of the model to the real Black Sea bottom topography is very different for the coarse (Test 2) and for the fine grid (Test 3). The evolution of the basin averaged total kinetic energy was monitored for both tests and it is clear that the coarse grid generates noise and allows the noise to grow continuously with time (dotted line in Figure 5-1). This situation is probably because the coarse grid, having low space resolution, deals with much greater

difference in depth from point to point and therefore it is more sensitive to steep topographic changes than the high resolution grid. After only 10 days of simulation using the coarse grid, the model develops currents with velocities of about 0.01 m/s. These perturbances are growing and propagating to the rest of the basin so that after 6 months the noise has spread, with maximum velocities reaching 0.7 m/s in the north-western shelf as shown in Figure 5-2.
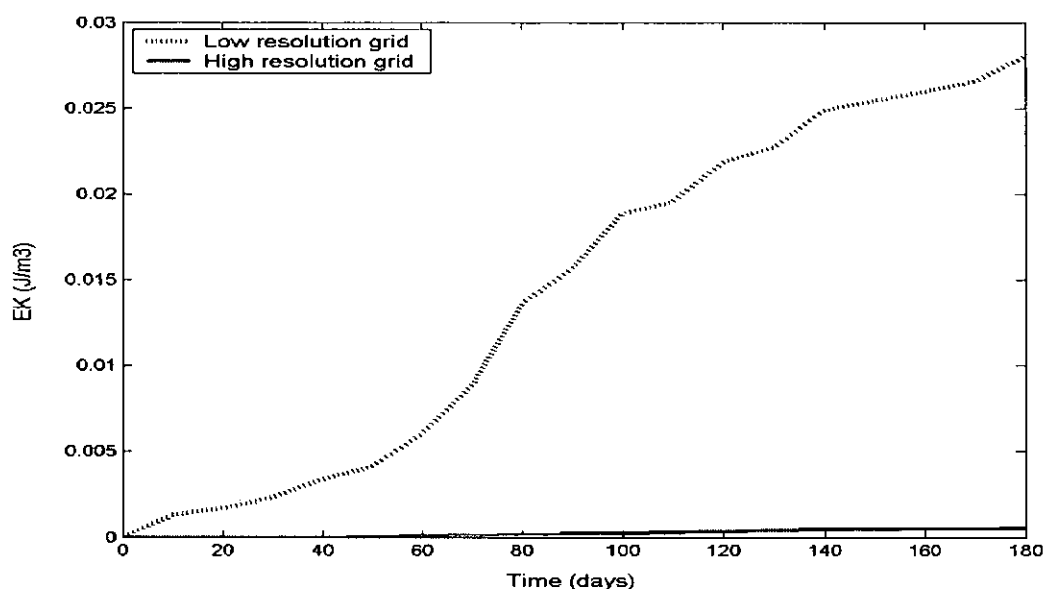
Figure 5-1 Time series of daily basin averaged total kinetic energy using the real bottom topography and homogeneous T-S distribution as initial condition. Dotted line=coarse grid (test 2), dark line=fine grid (test 3).

On the other hand, with the fine grid, the model runs for 55 days without generating velocities anywhere in the domain: the total kinetic energy is equal to 0 throughout this time (Figure 5-1). After 60 days of running a few isolated grid cells develop a small amount of noise (velocities less than 0.01 m/s). Nevertheless most of the basin remains stationary and the noise is restricted to a very small number of grid points (Figure 5-2b). Hence the use of the fine grid gives much more stability to the model than the use of the coarse grid.
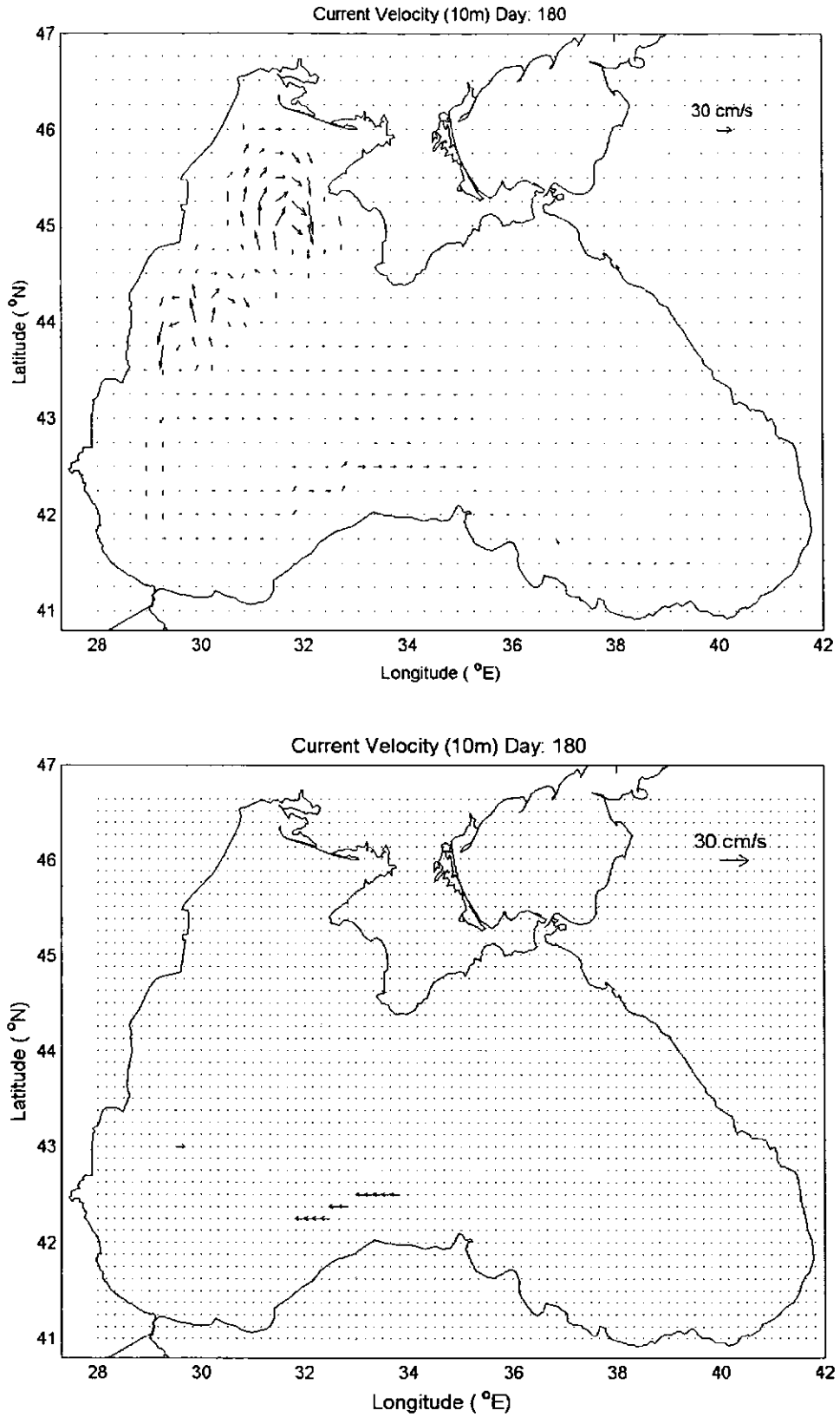
Figure 5-2 Noise surface velocities generated by the model using real bottom topography after 180 days of modelling with the coarse grid (test 2) in the upper panel and with the fine grid (test 3) in the lower panel.

The evolution of the total kinetic energy shows that the perturbance from the fine grid does not increase significantly (Figure 5-1) nor propagates to the whole basin after 6 months of running (Figure 5-2). Because the time scales of mesoscale processes are of the order of weeks to a couple of months, the 6-month stability shown within this test is a satisfactory result for this study.

5.4. Sensitivity to time step

Problems involving time and space require integration, step by step, forward in time from known initial conditions, seeking solutions that satisfy the boundary conditions demanded in the physical domain. The stability and accuracy of a numerical scheme to solve a set of differential equations depends on the space discretization, the time step and the relation between them. The Courant-Friedrichs-Lewy (CFL) condition states that given a space discretisation, a time step must be kept small enough so that information has enough time to propagate through the grid points. This means that for a chosen grid size, one cannot propagate numerical solutions forward in time faster than a disturbance itself would propagate across the grid. It is imperative then to find the best time step for the chosen grid. Because the system we are using is non-linear, the exact values for the time step in the pre-defined set up can only be obtained by experimenting.

POLCOMS model uses a splitting method which separates the baroclinic and barotropic calculations. The barotropic part (explicit scheme) requires a very small time step as the barotropic external gravity waves are very fast ($\sim$ hundreds of metres per second). The baroclinic part (implicit scheme) can use a much bigger time step as the baroclinic internal gravity waves are much slower ($\sim$1-2 metres per second).

Because the time step must decrease when increasing the resolution of the space discretization, the results of the tests are separated to show the more adequate time steps for each grid.

5.4.1. Coarse grid

This section examines the response of the model to different time steps using the coarse grid. All the runs used for this test (No. 4-10) use the coarse grid and start from a state of rest with the climatic 3-D initial temperature and salinity distribution of May (Staneva and Stanev, 1998) and with no external forcing included. Tests 4 to 8 have a barotropic time step of 20 s combined with different values of baroclinic time steps: 200, 400, 600, 800 and 1200 s. The development of the currents varies significantly between the tests. The top panel in Figure 5-3 shows daily values of the basin averaged total kinetic energy generated by runs 4, 5, 6 and 7. It is clear that the results are strongly dependent on the baroclinic time step. When the barotropic time step is fixed the velocity of the currents grows considerably while increasing the baroclinic time step. Moreover, the magnitude of the currents grows continuously with time (Figure 5-3). Spatially, this increase of the velocities is mainly localised in the area of the north-western shelf break and within the Rim Current along the southern coast as shown in Figure 5-4. This figure presents surface currents after 19 days of modelling under each one of the tests 4, 5, 6 and 7 which correspond to the four different scenarios of the top panel in Figure 5-3. At this time (after 19 days of running) there is a difference of about 12 J/m^3 in the basin averaged total kinetic energy when using a baroclinic time step of 200 s (Run 4) or of 400 s (Run 7). Only the runs 4 and 5 seem to reach a saturation point.
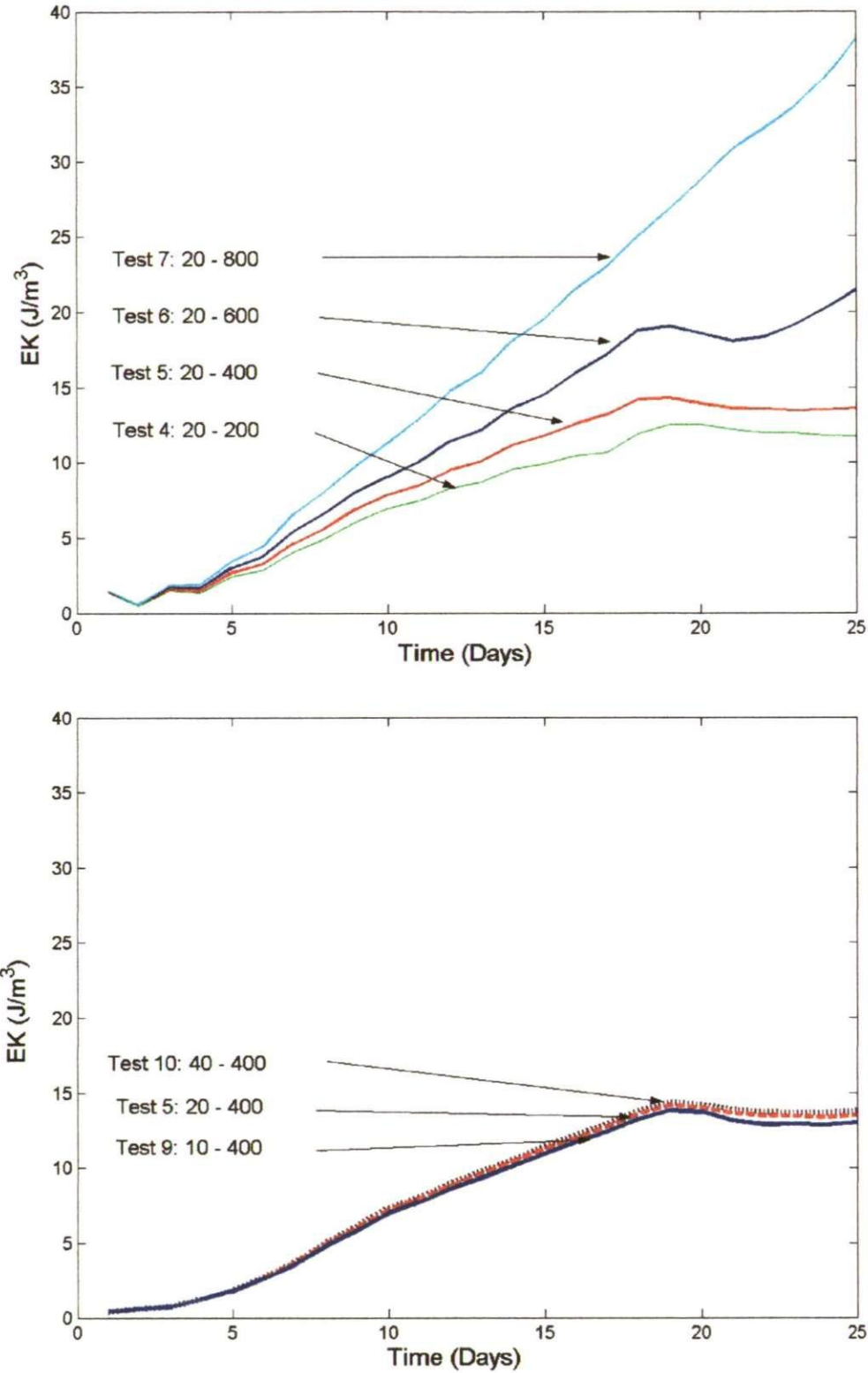
Figure 5-3 Time series of daily basin averaged total kinetic energy using the coarse grid under different time steps. The top panel has a barotropic time step of 20s with varying baroclinic time steps. The bottom panel has a baroclinic time step of 400s with varying barotropic time steps (in seconds).

The results of runs 5, 9 and 10 were used to test the model sensitivity to the barotropic time step. They use a baroclinic time step of 400 s and barotropic time step of 10, 20 and 40 s respectively. The model results clearly are independent to reasonable variations of the barotropic time step as shown in the bottom panel of Figure 5-3. Therefore, with the coarse grid, when the baroclinic time step is 400 s or less and barotropic time step of 20 s or less, the currents build up from the initial state of rest and reach some stability. The time to achieve this equilibrium is approximately 19 days of simulation.
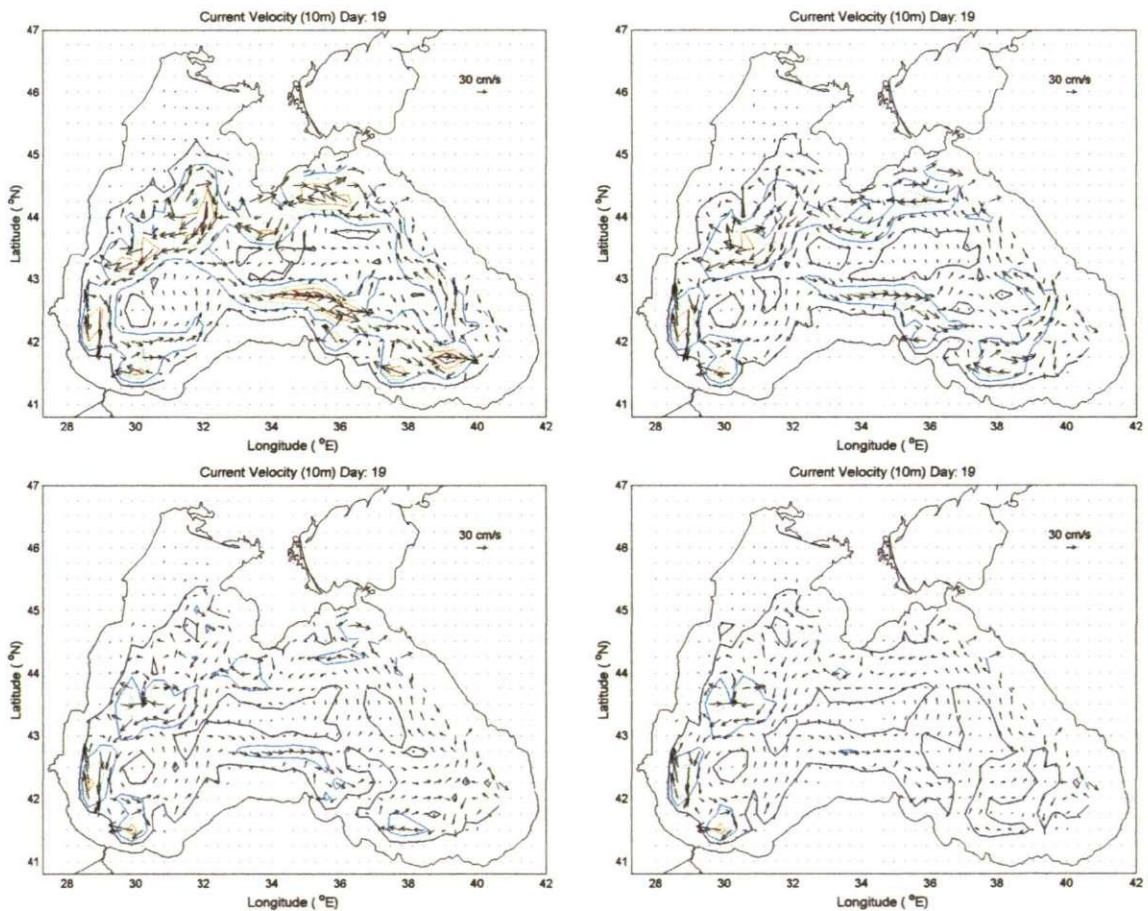
Figure 5-4 Surface velocities after 19 days of modelling using coarse grid using different time steps: top-left barotropic time step of 20s and baroclinic time step of 800s (test 7) top-right barotropic time step of 20s and baroclinic time step of 600s (test 6) bottom-left barotropic time step of 20s and baroclinic time step of 400s (test 5) bottom-right barotropic time step of 20s and baroclinic time step of 200s (test 4)

5.4.2. Fine grid

To test the model sensitivity to the baroclinic time step when using the fine grid we used the results of runs 11, 12, 13 and 15 (Table 5-1). Runs 11, 12 and 13 use a barotropic time step of 20 s and baroclinic time steps of 400, 300 and 200 s respectively. Run 15 has barotropic time step of 10 s and baroclinic time step of 100s.

When using the fine grid, as with the coarse grid, the results are highly influenced by changes in the baroclinic time step (Figure 5-5). The magnitude of the current velocities is higher with the use of bigger baroclinic time steps. This is evident by looking at the magnitude of the current fields, such as in Figure 5-6, which shows currents at day 25 of the simulations of tests 11, 12, 13 and 15. The kinetic energy starts to differ between the different runs after approximately five days of running. The difference in the basin averaged total kinetic energy after 30 days of running is of approximately 2 J/m^3 when using a baroclinic time step of 100 s or one of 400 s.

The results of the runs 13 and 14 were used to test the sensitivity to the barotropic time step. They both have a prescribed baroclinic time step of 200 s and their barotropic time steps are 20 and 10 s respectively. Again, the results are independent of barotropic time step changes, as shown in Figure 5-5. With the fine grid, the kinetic energy reaches stability much faster than with the coarse grid (about 5 or 6 days with the fine and 19 days with the coarse). In summary, when using the fine grid, a baroclinic time step of 200 s or less is needed to avoid the development of unrealistic velocities. Using the appropriate time steps (20 s barotropic and 200 s baroclinic) the model results are realistic and the basin averaged total kinetic energy saturates within about 5 days and maintains an approximate equilibrium thereafter.
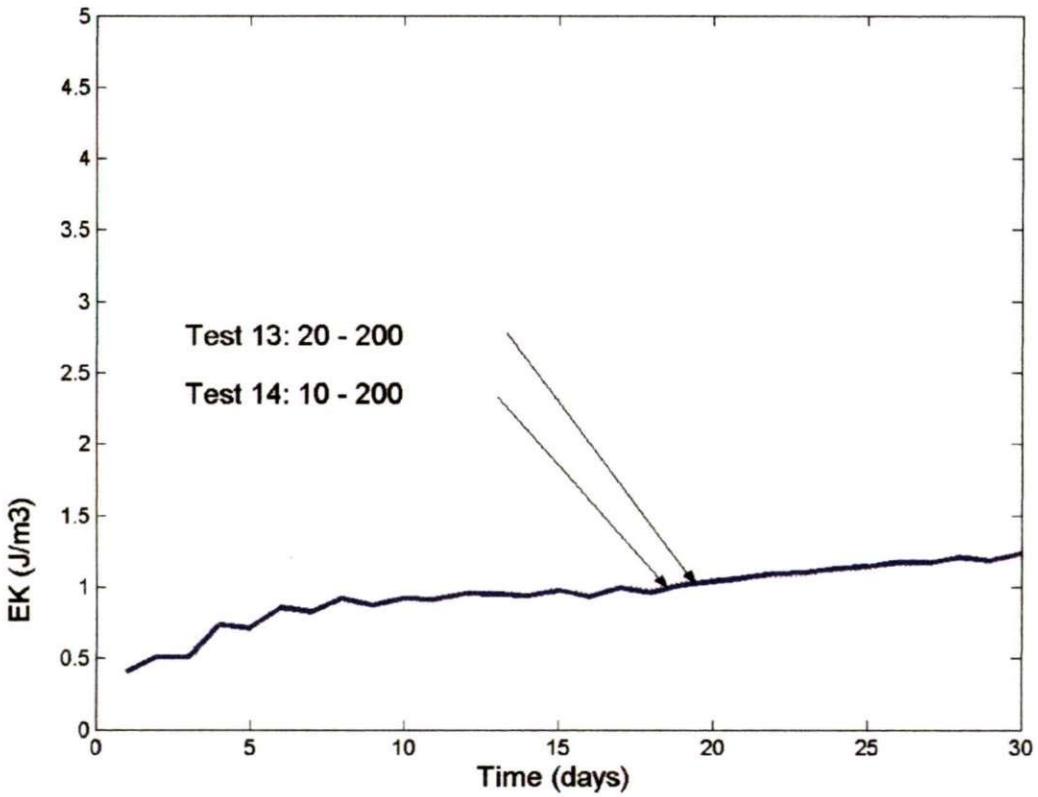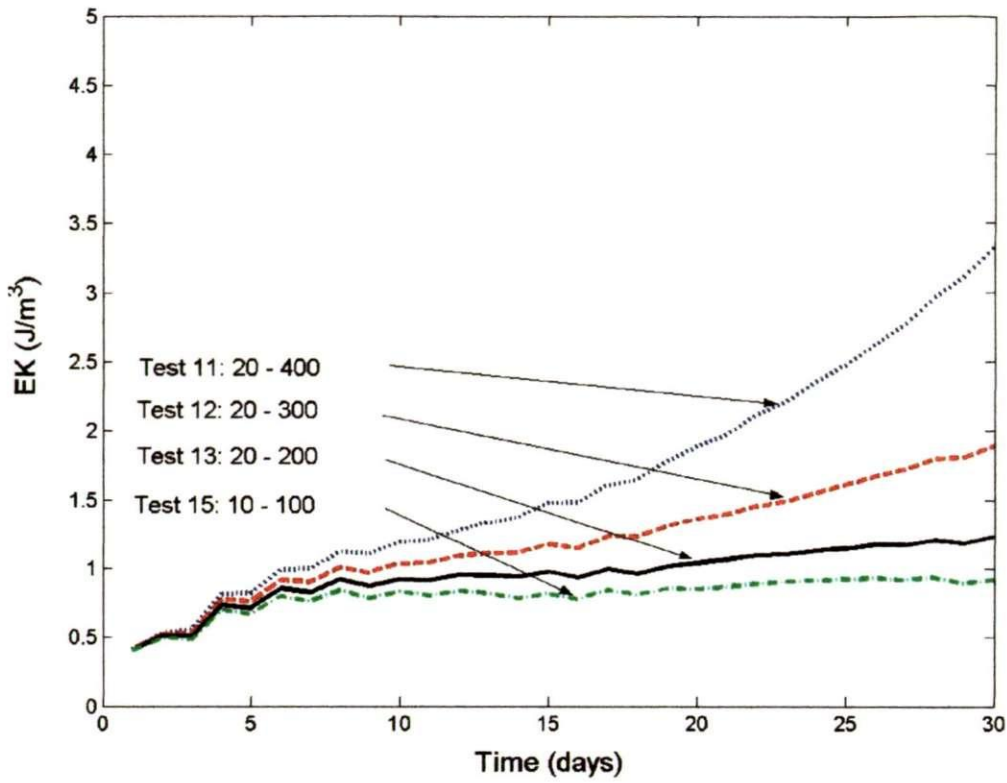
Figure 5-5 Time series of daily basin averaged total kinetic energy using the fine grid under different time steps. The top panel has a barotropic time step of 20s with varying baroclinic time steps and the bottom panel has baroclinic time step of 200s with varying barotropic time steps. The figures show results of a snapshot every 24 hrs.

105
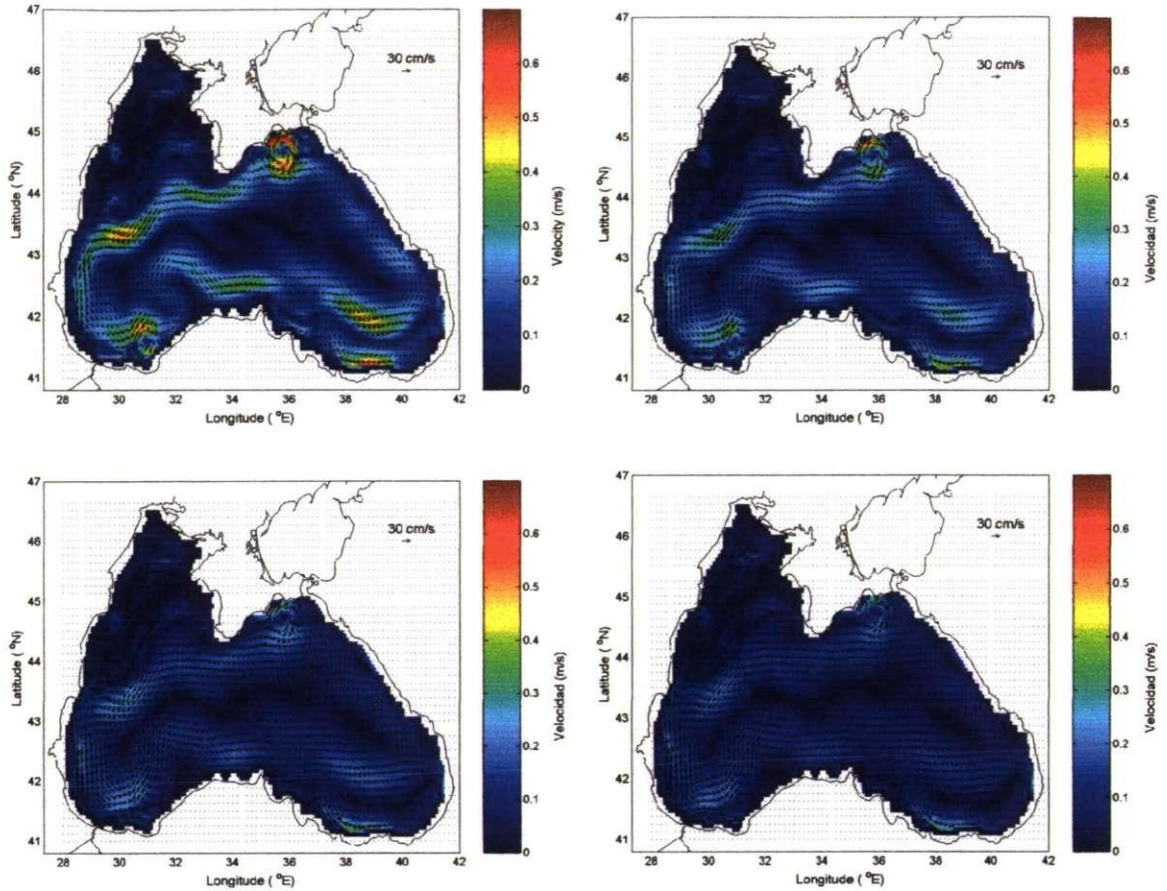
Figure 5-6 Surface velocities after 25 days of modelling using the fine grid under different time steps: top-left barotropic time step of 20s and baroclinic time step of 400s (test 11) top-right barotropic time step of 20s and baroclinic time step of 300s (test 12) bottom-left barotropic time step of 20s and baroclinic time step of 200s (test 13) bottom-right barotropic time step of 10s and baroclinic time step of 100s (test 15). The velocity vectors are plotted every second grid point.

5.5. Sensitivity to grid resolution

This section examines the model response to different resolution grids. The currents resulting from low, high and extra-high resolution grid during 8 days of simulations are discussed in this section. The characteristics of each one of the grids was presented at the beginning of this chapter in Table 5-2.

To analyse the model performance using grids of different resolution we compared the results of test 5 and test 13, described in the previous sections, with a third run which used an extra-fine resolution grid (test 16). Both test 5 and test 13 used the optimal time steps for their corresponding grid resolution. The first result encountered was that the use of the x-high resolution grid is extraordinarily expensive in terms of computational time. The evolution of the basin averaged kinetic energy produced by each one of the three grids is shown in Figure 5-7. Within 8 days of simulation we can clearly see the non-stable nature of the kinetic energy of the coarse grid and the stability of the fine and extra-fine grids. For these tests, the total kinetic energy is calculated and plotted at hourly intervals and therefore it shows high frequency variations which were not visible in the tests of the previous sections. Regardless of the grid resolution, the results show oscillations which have a frequency corresponding to the inertial frequency of the Black Sea. The inertial period at a particular location is $\frac{2\pi}{f}$, where f is the local Coriolis parameter, $f = 2\Omega \sin(latitude)$ and Ω is the angular velocity of the earth about its axis (approximately 7.29 x 10^{-5} s^{-1}). These oscillations will be addressed in detail in Chapter 6 as part of the validation of the model.

The model reproduction of the current velocities is significantly improved when changing from the coarse to the high resolution grid but little improvement was observed when changing from high to x-high resolution grid as shown in Figure 5-8. In fact, the currents obtained with both the fine and x-fine grids are very similar to the typical current scheme in the Black Sea area (Figure 2-13). At this point, and before deciding to use the fine grid for the main numerical experiments, it was needed to ensure that the difference between the results of the modelling when using the fine and the x-fine grid are not significant. This was determined after a series of analysis which are presented in Section 5.5.1.
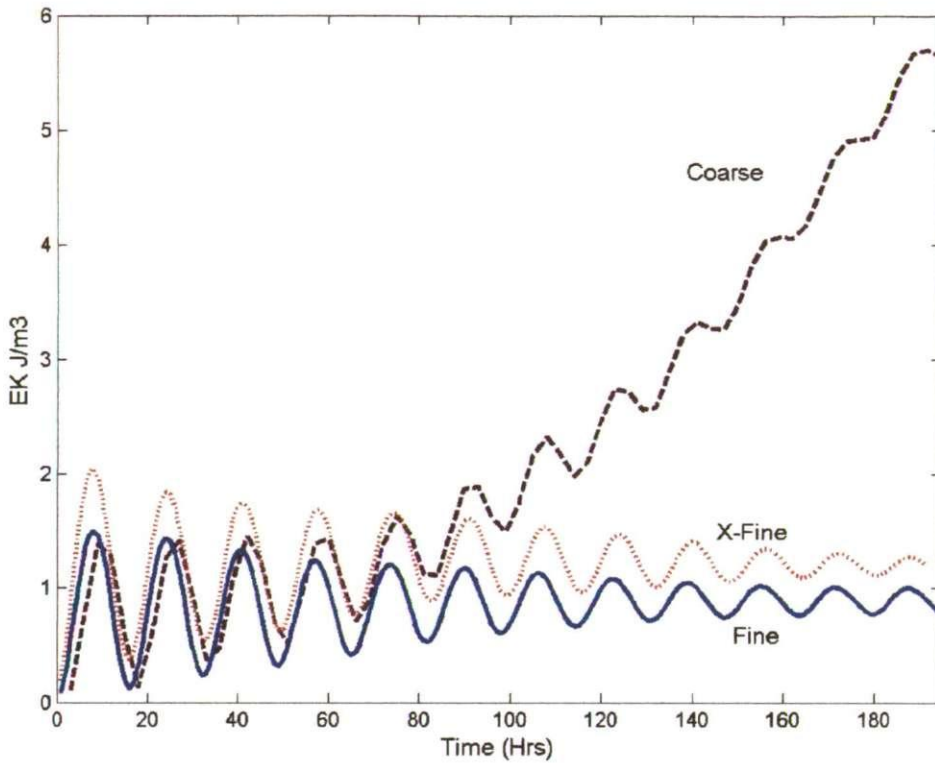
Figure 5-7 Hourly basin averaged kinetic energy (fine grid) under different grid resolution: Coarse grid ¼ °(~ 25km) , fine grid 1/14 ° (~6km) and x-fine grid 1/24 ° (~ 3 km)

5.5.1. Difference between the x-fine and fine grids

Within this section it is demonstrated that there is no significant difference between the results obtained when using the fine and the x-fine grids and that the fine grid is therefore the best option for this study.

The differences between the two grids were determined by subtracting each variable (temperature, salinity and velocity) of the fine grid from the average of the 4 cells from the x-fine grid which cover the same area.

The mean and standard deviation of the differences were obtained and are presented in Table 5-3.
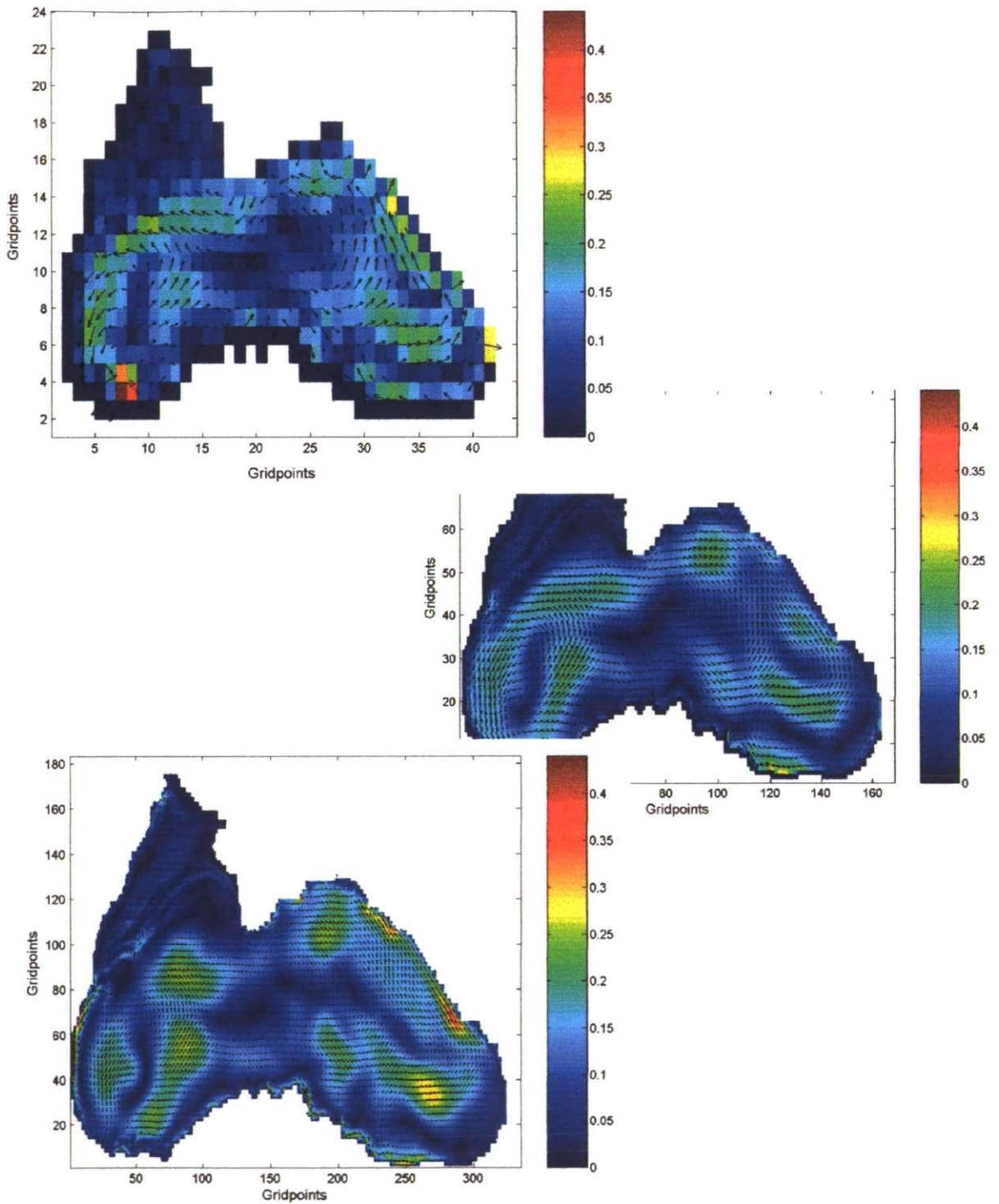
Figure 5-8 Surface velocities after 127 hours of modelling. Top: using the coarse grid (test 5); Middle: using the fine grid (test 13), with velocity vectors plotted every second grid point; Bottom: using the x-fine grid (test 16), with velocity vectors plotted every fourth grid point.

109

X-Fine less Fine	Mean	Std
Temperature	-0.017 °	0.167 °
Salinity	-0.008 *psu*	0.079 *psu*
Velocity	0.012 (m/s)	0.038 (m/s)

Table 5-3 Statistics of the difference between the fine and x-fine grids

For the temperature, salinity and velocity fields we obtained histograms of the difference between the grids (Figures 5-9, 5-12 and 5-15 respectively).

For the temperature and salinity the relative error was calculated by dividing the difference in temperature/salinity between the two grids by the temperature/salinity calculated with the x-fine grid and is expressed as error percentages (Figures 5-10 and 5-13). This is done by:

$$\%E = \frac{Var_{xf} - Var_f}{Var_{xf}} * 100$$

where Var_{xf} is the variable (temperature, salinity or velocity) from the x-fine grid and Var_f is the variable from the fine grid. This analysis is not suitable for the difference in the velocity fields as it is clear from the equation that the percentage error will tend to infinity where the velocity on the x-fine grid tends to zero. Another way to visualise the differences is to plot the correlation and calculate the correlation coefficient, R^2, between the results of both grids. By doing this, the proximity to the 1:1 correspondence would correspond to a R^2 equal to 1. The results of the correlations are shown in Figures 5-11, 5-14 and 5-16 for the temperature, salinity and velocity respectively.

It is clear that for the temperature and salinity the results between the grids are very well correlated. In the temperature field about 60 % of the data differs by less than 0.1 degree, more than 90 % of the data has less than 5 % of error and the correlation coefficient is 0.9738 (Figure 5-11). For the salinity field, the situation is even better with the results being nearly the same when using x-fine and fine grids. 90% of the data has less than 1% error and there is an excellent correlation coefficient of 0.9937 (Figure 5-14). The case for the velocity fields has slightly different results, even when it is clear from the histogram that the majority of the data (more than 70 %) has differences of less than 0.05 m/s, the correlation coefficient is much lower (0.52). This is because although the difference is concentrated in localised small areas, the difference is noticeable. Figure 5-17 shows the spatial distribution of the difference in velocities at different depths. This figure shows 6 slices which are maps of the differences at the depths of 30, 50, 100, 150, 300 and 800 m. The slices show the Black Sea basin at each particular depth and the view is from the south-western side of the area. It shows that all the differences are concentrated in the periphery of the basin and very close to the boundaries. The currents studied in this research are located further away from the coast and hence it is safe to say that this difference does not affect our results. The use of the x-fine grid requires approximately 30 times more computational time than the fine grid. This is because not only the number of grid points is increased by a factor of 4 but due to the smaller distance between the grid points, a much smaller time step is required for a finer grid as mentioned in section 5.4. Therefore, considering that the use of the x-fine grid is extremely expensive in terms of computational time and storage capacity it was regarded as not suitable for this study.
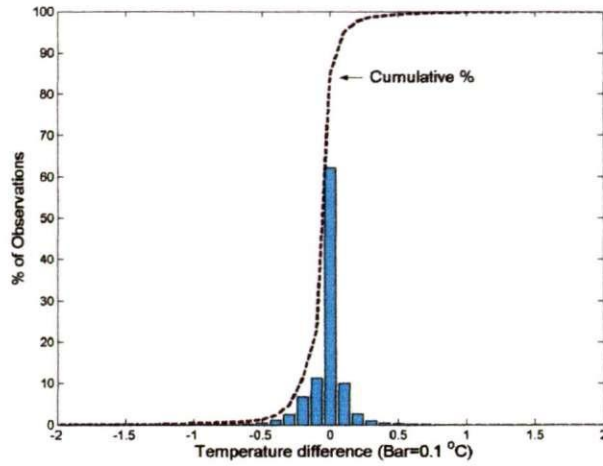
Figure 5-9 Histogram of the difference between the temperature of the x-fine grid and the fine grid for the entire basin
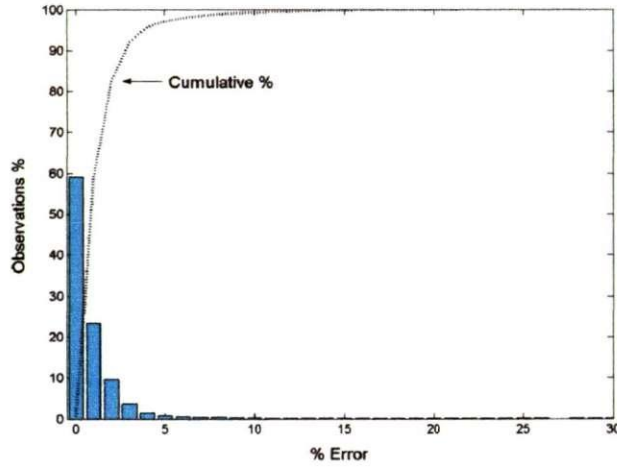
Figure 5-10 Histogram of the percentage error calculated from the difference between the temperature of the x-fine grid and the fine grid for the entire basin
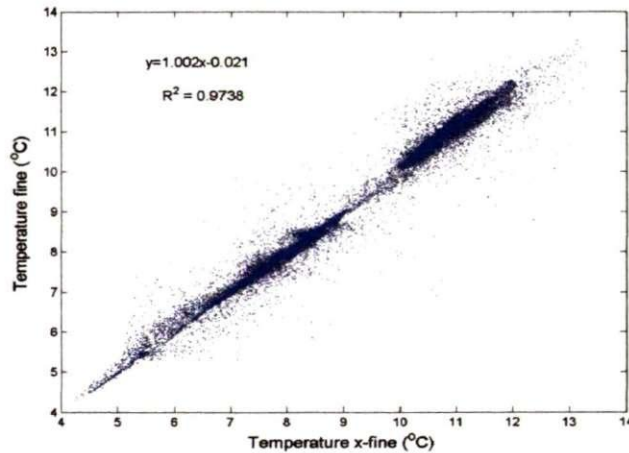
Figure 5-11 Temperature of the x-fine grid against the temperature of the fine grid.

112
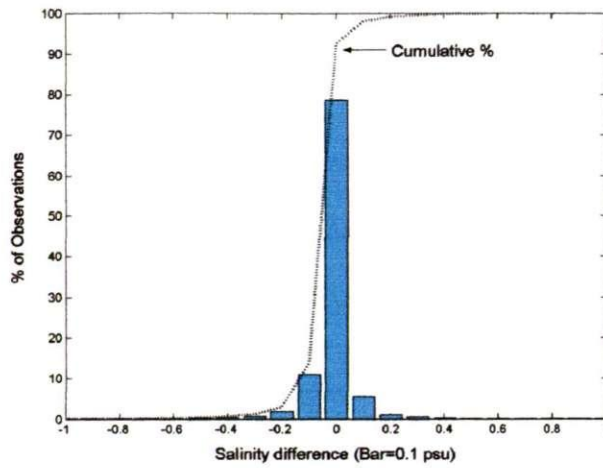
Figure 5-12 Frequency histogram of the difference in salinity between x-fine and fine grid for the entire basin
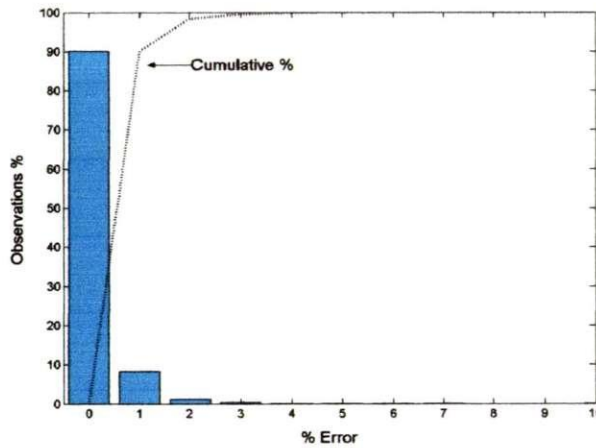
Figure 5-13 Histogram of the percentage error calculated from the difference between the salinity of the x-fine grid and the fine grid for the entire basin
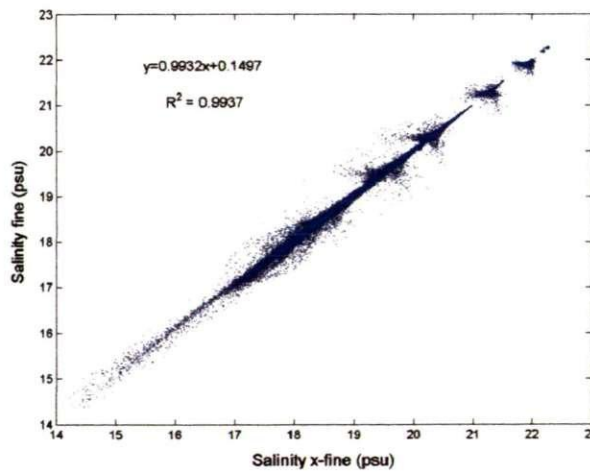
Figure 5-14 Salinity of the x-fine grid against the salinity of the fine grid

113
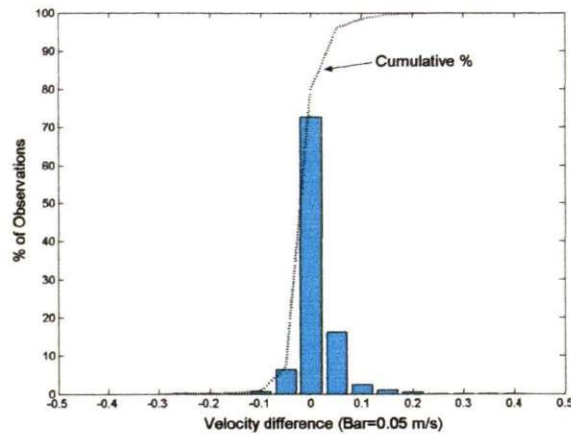
Figure 5-15 Frequency histogram of the difference in velocity between x-fine and fine grid for the entire basin
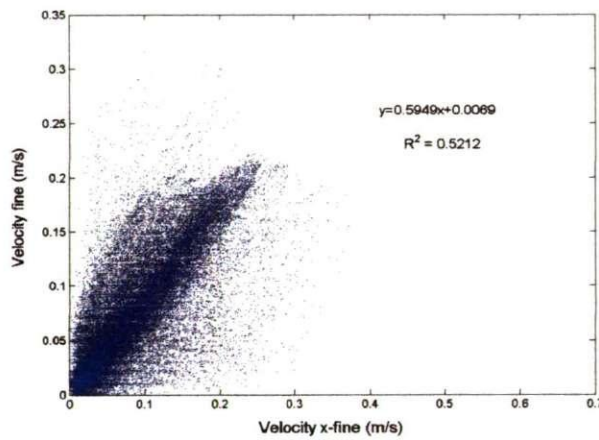
Figure 5-16 Velocity of the x-fine grid against the velocity of the fine grid
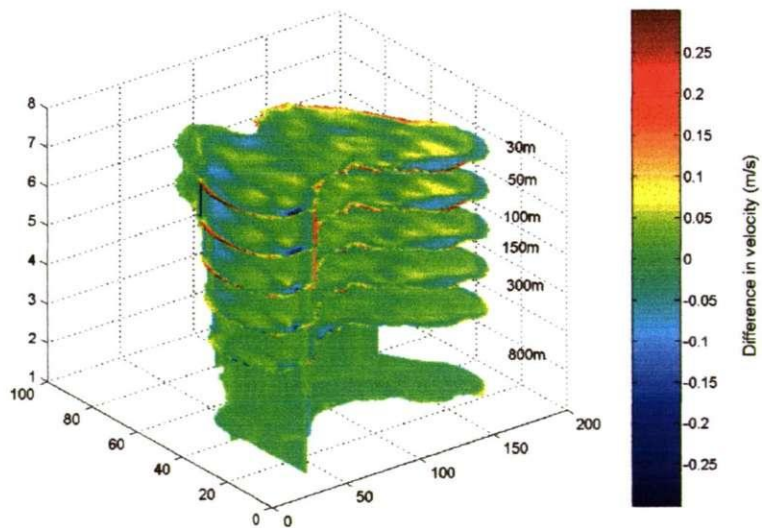
Figure 5-17 Difference in velocity between the x-fine and fine grids. The plot shows slices of the Black Sea basin at the depths of 30, 50, 100, 150, 300 and 800 m viewed from the south-western side of the area

114

5.6. Sensitivity to the horizontal diffusion coefficient

The water in seas and oceans is turbulent: its averaged motion is disturbed by continuously randomly varying eddies, whirls, oscillations or spurts transferring smaller volumes of substance in every direction. These turbulent motions are responsible for mixing the fluid and for smoothing the average velocities in the flow. The velocity fluctuations occur on different timescales (from seconds to days) and therefore the method of computing the turbulent viscosity should serve to define the average velocity profile of the turbulence. The constant of proportionality, diffusion coefficient, used to calculate the friction arising from the turbulent flow is not a physical parameter and depends on temperature, pressure, salinity and the scale of the eddies that should be counted as turbulence. Therefore care should be taken when assigning its value. There are different coefficients for the horizontal and vertical diffusion because the horizontal mixing is generally much bigger than the vertical. This is because the intensity of the vertical turbulence depends on the stratification and the vertical shear on the current field. Vertical turbulence is therefore only present in the upper ocean layer and is largely limited by the inhomogeneities in the density structure. POLCOMS model uses the Mellor-Yamada-Galperin level 2.5 turbulence closure scheme (Mellor and Yamada, 1974; Galperin et al., 1988) to estimate the vertical eddy viscosity and diffusivity. The horizontal diffusion coefficient (A_H) in POLCOMS is calculated as a function of depth and is taken to be the minimum value between a prescribed critical value *AHCrit,* and the product of a prescribed constant *AHC* and the depth at each grid point.

The test of sensitivity to the horizontal diffusion coefficient involved the results of four numerical experiments, runs 14, 17, 18 and 19 (Table 5-1). These runs were prescribed with different values of the constant *AHC* to assess the influence on the resulting currents. As one would expect, results show that with higher values of *AHC* the magnitude of the velocities slightly decreases and at the same time the width of the currents increases as can

be seen in Figure 5-18. The difference between the runs in the test of sensitivity to the horizontal diffusion coefficient is not as dramatic as the differences found on the sensitivity tests to time step and grid size. Nevertheless the best resemblance to the real Black Sea currents in terms of typical velocities and scale of the Rim Current and mesoscale eddies is obtained when using $AHC = 0.2$ m/s with a critical value $AHCrit$ of 600 m^2/s. Therefore these parameters were used in the calculation of the horizontal diffusion coefficient for all the subsequent numerical experiments.
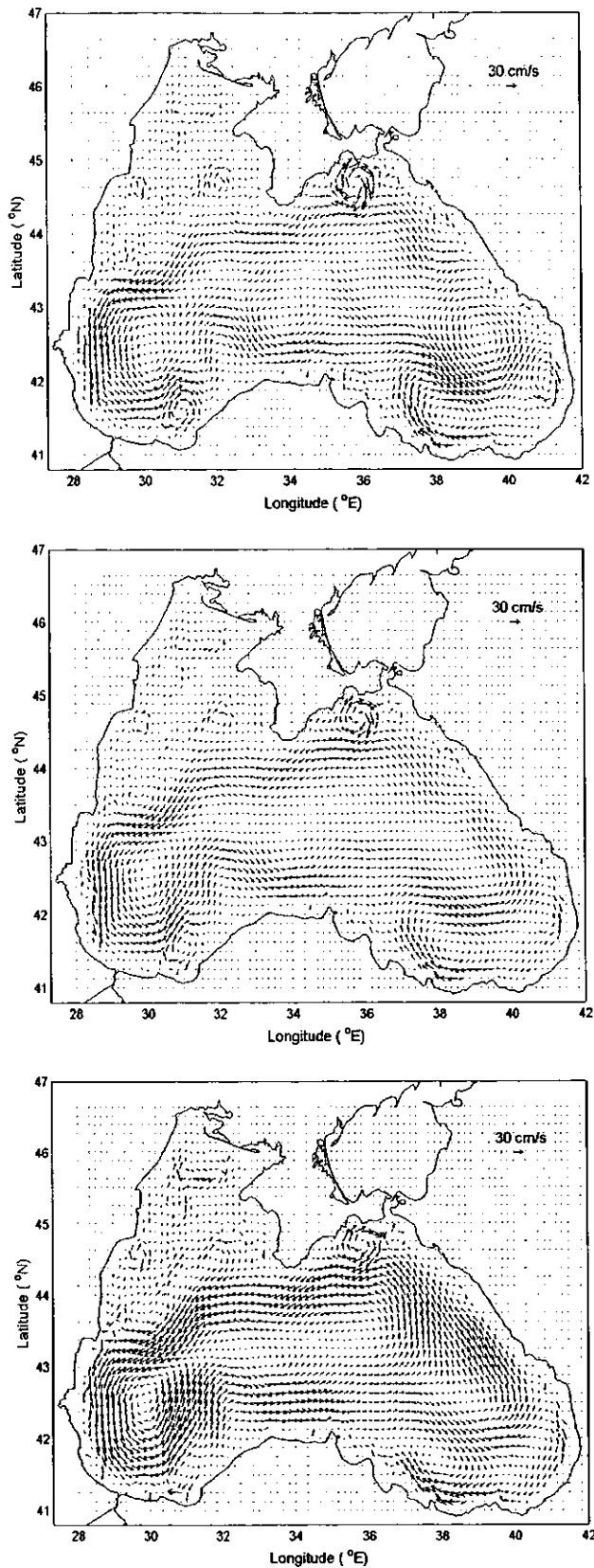
Figure 5-18 Current velocities after 30 days running using (a) AHC=0.1m/s (test 19) (b) AHC = 0.2 m/s and (c) AHC = 1.0 m/s.   Velocity vectors are shown every second grid point

117

5.7. Summary

This chapter presented the results of the series of sensitivity tests applied to find the best set up of the model POLCOMS for the Black Sea environment.

The variables analysed were:

1. The impact of the bottom topography on the results.

2. The influence of using different barotropic and baroclinic time steps on the hydrodynamics.

3. The grid size which gives the optimal performance with the resolution needed.

4. The way in which changes in the horizontal diffusion coefficient affect the modelled output.

Results show that the fine grid with approximately 6.7 km resolution (Table 5-2) has the resolution which best copes with the Black Sea bottom topography used in the model. A higher resolution grid with approximate dx of 3.4 km (x-fine grid) does not improve the modelled results and the excessive computational time makes it unsuitable for performing the nature of the experiments for this research project. A coarser grid with approximately 25.6 km resolution does not give good results for studying mesoscale phenomena as it is not able to resolve mesoscale eddies and is not stable in combination with the existing bottom topography. Nevertheless, this coarse resolution grid gives some reproduction of the general circulation which includes the Rim Current and some of the semi-permanent gyres in the deep sea. Hence the coarse grid was used as a preliminary model for all the subsequent tests due to the enormous time saved when using the coarse grid. The fine grid therefore proved to be the one with the optimal characteristics for exploring the mesoscale circulation giving an accurate reproduction of the circulation of the Black Sea.

It was found that the model is very sensitive to variations in the baroclinic time step but not so sensitive to variations of the barotropic time step. This situation allows a certain range

of flexibility to save computational time. The best time steps to use with each different grid were detected. Using the coarse resolution grid, the best performance is obtained when using a barotropic time step of 20 s or less and a baroclinic time step not exceeding 400 s. The fine resolution grid works adequately when the barotropic time step is 20 s or less and when the baroclinic time step does not exceed 200 s.

From the sensitivity test to the horizontal diffusion coefficient it was noticed that the increase of the coefficient leads to smoothing the currents, obtaining lower magnitudes of the velocity and wider currents. The best and more realistic result in terms of magnitude and scale of the currents was obtained with *AHC*=0.2 m/s and a critical value of *AHCrit* = 600 m^2/s.

CHAPTER 6. GEOSTROPHIC ADJUSTMENT AND VALIDATION

6.1. Introduction

As the model starts running, the medium suffers perturbations due to a number of reasons. The first one is owing to the fact that the model is initialised with temperature and salinity distributions (Staneva and Stanev, 1998) which were produced by a numerical model using a different bathymetry than the one used for this study. The disparity between bathymetries lead to a number of empty grid points in some corners of the model domain which needed to be filled (Section 3.5.8). Moreover, the initial density field corresponds to a climatic situation which is dynamic (involves currents), while the model starts with zero velocities. When a stably stratified fluid at rest is disturbed, both barotropic and baroclinic waves are radiated out and the resulting motions are eventually dissipated by friction to return to a state of equilibrium. After reaching this state of 'equilibrium' the results of the model may then be validated by comparing them with observations. The validation within this research includes the qualitative comparison of the modelled hydrodynamics with the well known circulation and thermo-haline characteristics of the Black Sea and a quantitative comparison of the nature of the high frequency oscillations of the velocity components at some pre-selected points within the trajectories of drifters from the drifter experiment during the year 1999 (Zhurbas et al., 2004).

This chapter describes the process of geostrophic adjustment followed by the validation of the model results.

6.2. Geostrophic adjustment

The model was initialised using the geostrophic adjustment approach which is achieved when the perturbation at the moment of the initialisation is dissipated by friction to return

to a state of equilibrium. The rotation of the earth has a profound influence on how the medium adjusts when perturbed and the final state is not a state of rest but that of geostrophic equilibrium (Kantha and Clayson, 2000). To achieve geostrophic adjustment the model was prescribed with initial climatic distribution of temperature and salinity of May (Staneva and Stanev, 1998). This distribution corresponds to a dynamical situation involving currents whose velocities were not available for this study. Hence the initial velocities were set to zero everywhere in the domain and the model was run without any external forcing until the geostrophic adjustment was achieved. The parameters used in the run (No. 17) are listed in Table 6-1. The model was integrated forward during 1 month which should be enough time for the circulation to be consistent with the prescribed water density structure.

No	Grid	Bottom Topography	Barotropic Time step	Baroclinic Time step	AHC	AHCrit	Initial T - S	Run Length
17	Fine	Real	20 s	200 s	0.5 m/s	600 m^2/s	May	1 month

Table 6-1   Parameters used in the model during the geostrophic adjustment

To assess when the equilibrium state is reached the total kinetic energy was monitored. The basin averaged total kinetic energy was calculated every hour from the modelled output velocity components and the time series is plotted in Figure 6-1. It is clear that the kinetic energy does not have an increasing trend but it shows a strong oscillatory signal. The frequency of the oscillations is approximately 17 hrs which corresponds to the inertial frequency of the Black Sea. The amplitude of the oscillations tends to decrease with time. It is beyond the interest of this research to investigate the origin of the oscillations but their

characteristics (energy and frequency) were compared with observations as part of the model validation as will be described later in this chapter.

The criteria used to consider the medium as adjusted is to measure the time at which the amplitude of the oscillation is less than the mean value of the total kinetic energy. This is achieved within approximately 127 hours (Figure 6-1) as the mean kinetic energy is 0.86 J/m^3 and the difference between the crest (1.075) and the trough (0.725) of the oscillation at that time is 0.350 J/m^3. The amplitude after 127 hrs is nearly $1/5^{th}$ of the average of the kinetic energy. Hence, the velocity field after 127 hrs of adjustment can be taken as the initial velocity field for the main modelling experiments.
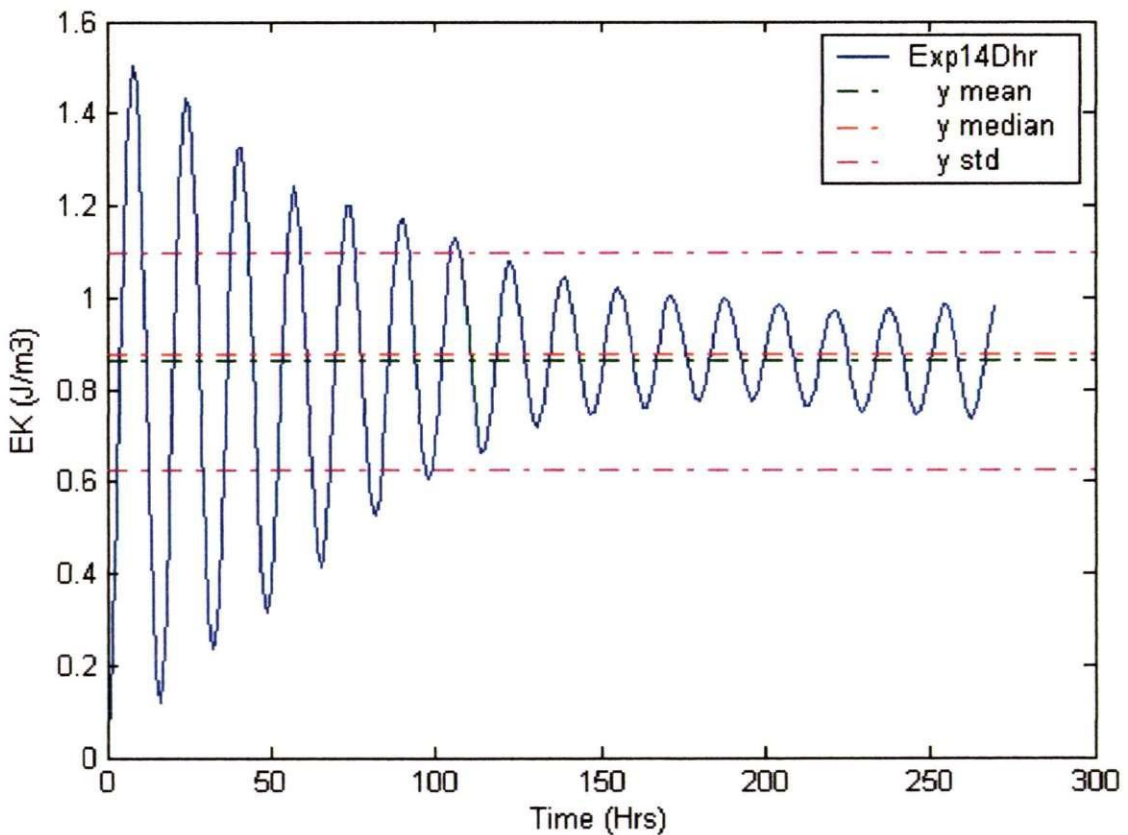
Figure 6-1 Evolution of the basin averaged kinetic energy (hourly output)

6.2.1. Check of similarity between the T-S fields before and after geostrophic adjustment

The water mass structure after the model initialisation process (described in 6.2) has been completed must be similar to the initial one in order to use the result to initialise the main modelling experiments. Therefore a check was made to assess the similarity between the temperature and salinity fields before and after geostrophic adjustment. Figure 6-2 shows the maps of temperature at 10 m depth before and after the geostrophic adjustment. The process of adjustment did not alter the overall temperature distribution. The lateral gradient with minimum temperature in the north-western shelf and maximum in the south-eastern part of the basin is conserved although the fronts of warmer water in the eastern part are not as sharp after adjustment as they were in the climatic data (initial). In the central area there is also evidence of mixing processes so that the water is slightly colder after the adjustment than before adjustment. The salinity field at the surface was less disturbed during the process of geostrophic adjustment. Figure 6-3 shows the salinity distribution before and after geostrophic adjustment at a depth of 10 m. The fresher water in the north-western shelf, the sharp salinity gradient from the coast to the sea and the saltier water in the locations of the western and eastern central cyclonic gyres are all nearly untouched by the adjustment. In the vertical the structure also preserves the temperature and salinity distribution. Figures 6-4 to 6-6 show vertical cross-sections of temperature, salinity and current velocity at the location of transects number 1, 3 and 5 (Figure 3-8 – Chapter 3). The surface mixed layer reaches approximately 30 m depth. The cold intermediate layer is located between depths of 30 and 100 m. The minimum salinity is at the surface and it increases with depth. The velocities resulting from the geostrophic adjustment penetrate down to depths of more than 300 m in the areas where the Rim Current is stronger.
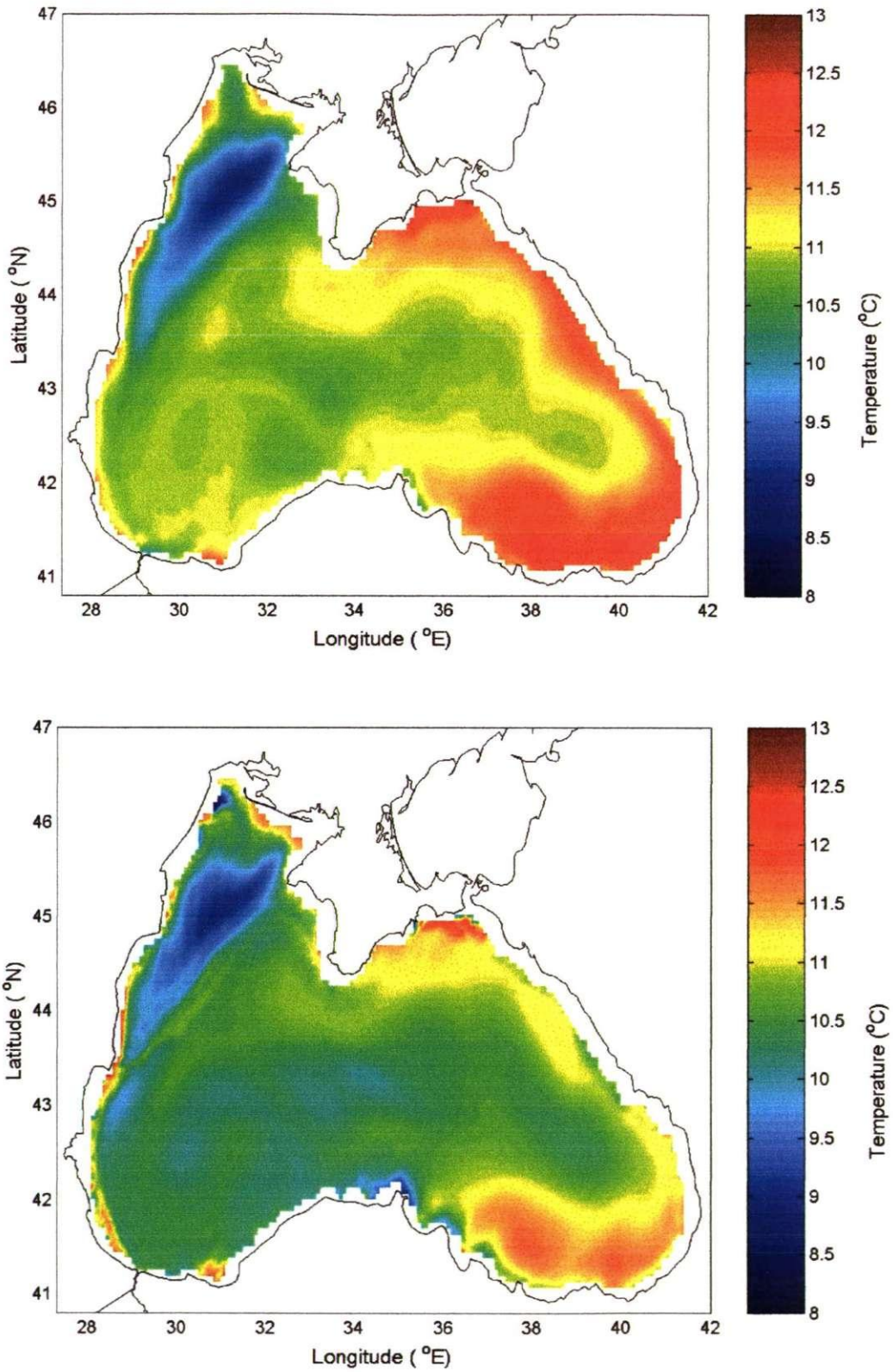
Figure 6-2 Modelled maps of temperature at 10 m depth a) before geostrophic adjustment (initial) b) after geostrophic adjustment (after 127 hrs).
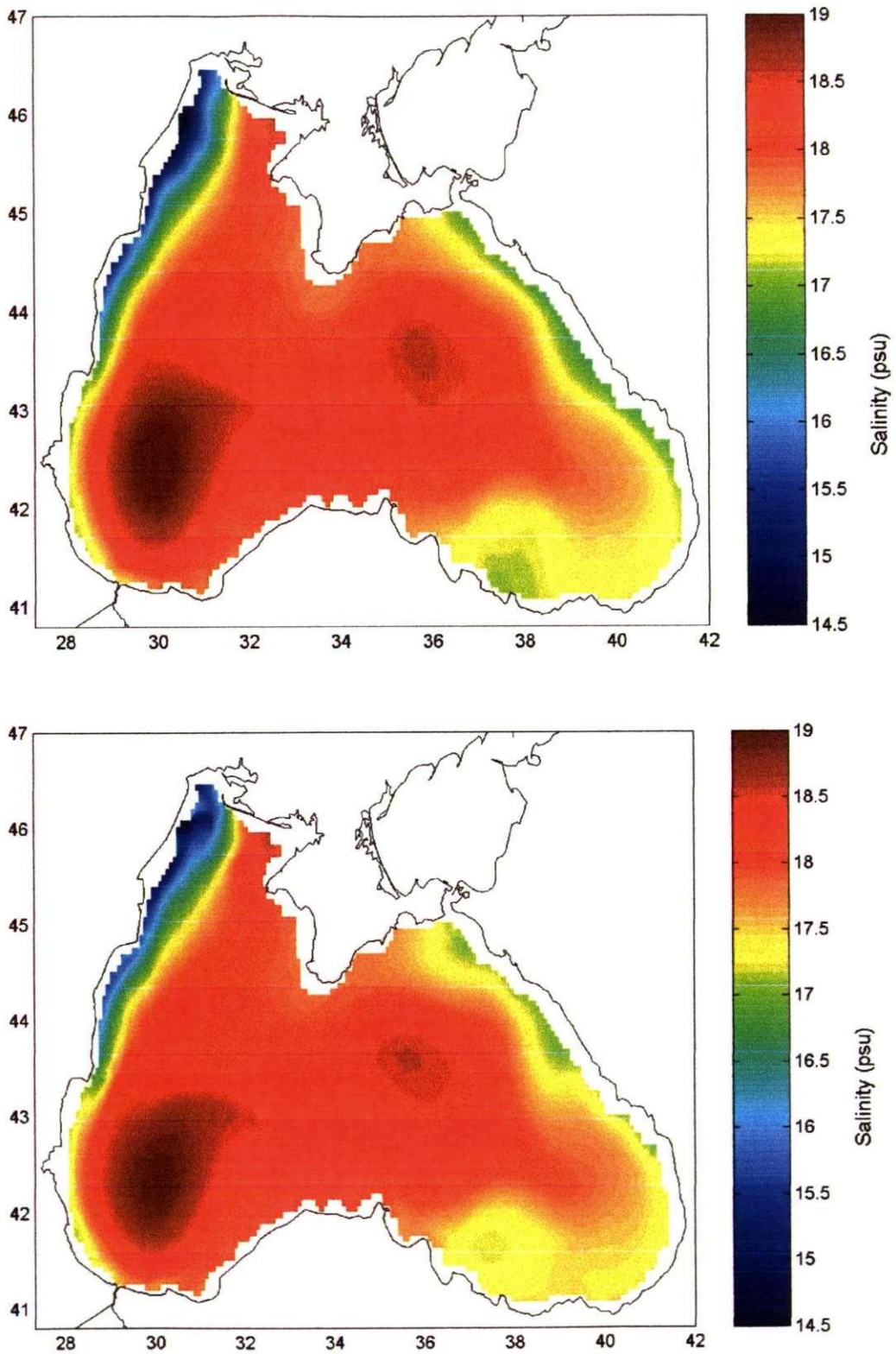
Figure 6-3 Modelled map of salinity at 10 m depth a) before geostrophic adjustment b) after geostrophic adjustment

Although the qualitative check does not show significant alterations in the thermohaline distribution resulting from the geostrophic adjustment, a quantitative check of the difference between the temperature and salinity fields before and after the geostrophic adjustment was carried out. The statistics of the differences for the whole basin, for only the active layer (upper 300m) and for only the bottom layer (deeper than 300m) are presented in Table 6-2 and the histograms of the difference in temperature before and after geostrophic adjustment are shown in Figures 6-7 and 6-8. In general during geostrophic adjustment the temperature decreases in some areas, increases in some other areas and remains the same in the majority of the basin. Figure 6-8 shows that the differences are concentrated in the top 50 m of the basin. The surface layer (top 10 m) loses some heat during the adjustment while the sub-surface layer (10 to 50 m which includes the cold intermediate layer) suffers an increase of temperature. Below 50 m and down to the bottom (1500 m) the changes are negligible.

To quantitatively assess the difference resulting from the adjustment process, the correlation between the modelled temperature after 127 hrs of geostrophic adjustment and the climatic temperature of May which was used to initialise the model is plotted in Figure 6-9. The correlation coefficient, R^2 is equal to 0.98 which relates to a very good agreement. The differences are concentrated in the upper layer and it is clear from Figure 6-10 that within the interior of the basin the magnitude of the difference is small and relates to normal mixing processes resulting from the currents. Bigger differences are concentrated only in the periphery of the basin very close to the boundaries.

As with the temperature, most of the difference between the salinity after and before geostrophic adjustment occurs within the upper 50 m of the basin. The histogram of the difference is plotted in Figure 6-11. The salinity field gives also a very good correlation coefficient of 0.99 (Figure 6-12). Figure 6-13 shows the location of the salinity differences,

which are mainly located in front of the Bosphorus Strait and in the shallowest part of the north-western shelf. These are the two more vulnerable areas with larger salinity gradients.
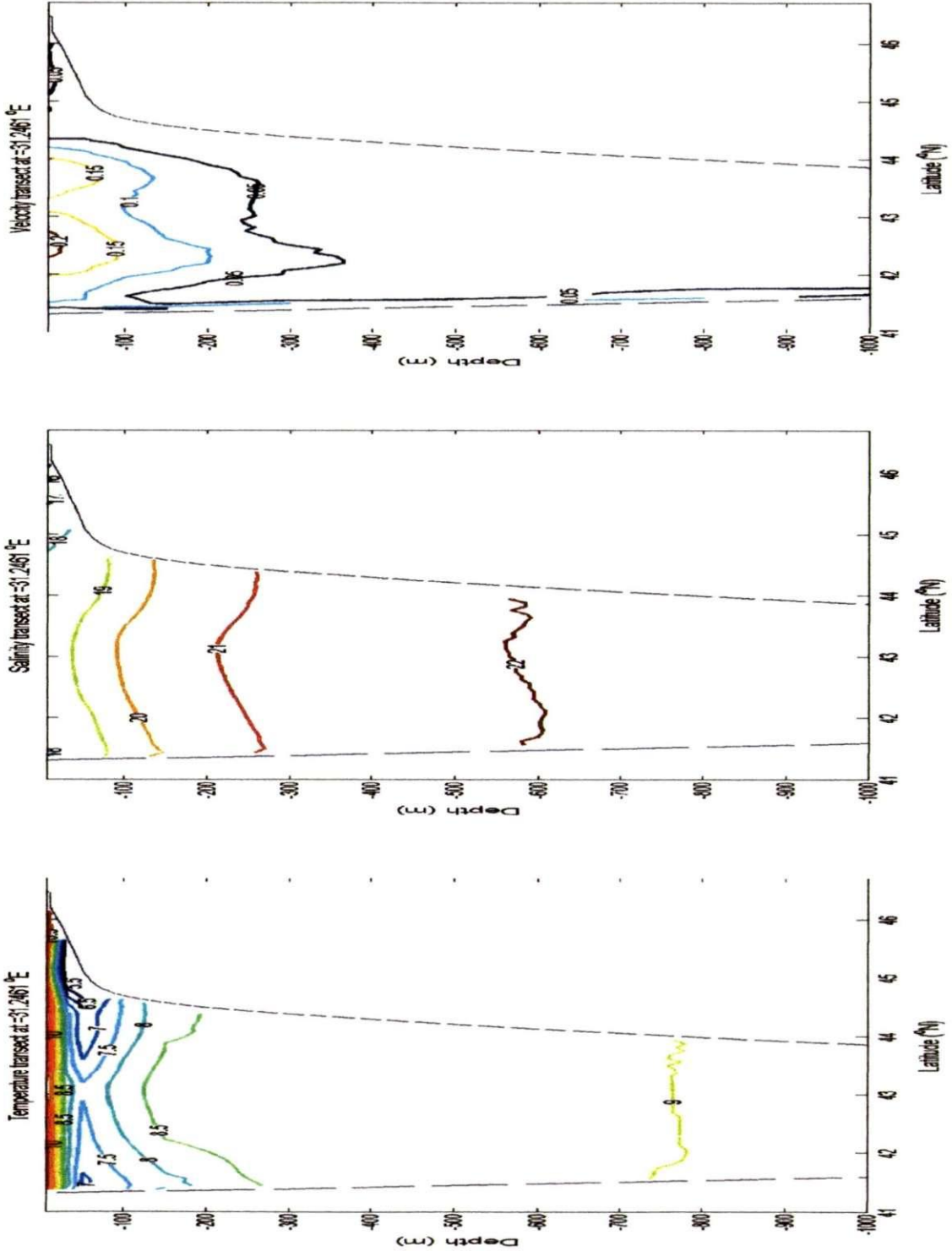
Figure 6-4 Meridional sections at Longitude 31.246°E after geostrophic adjustment showing (a) temperature (°C), (b) salinity (psu) and (c) current velocity (m/s)
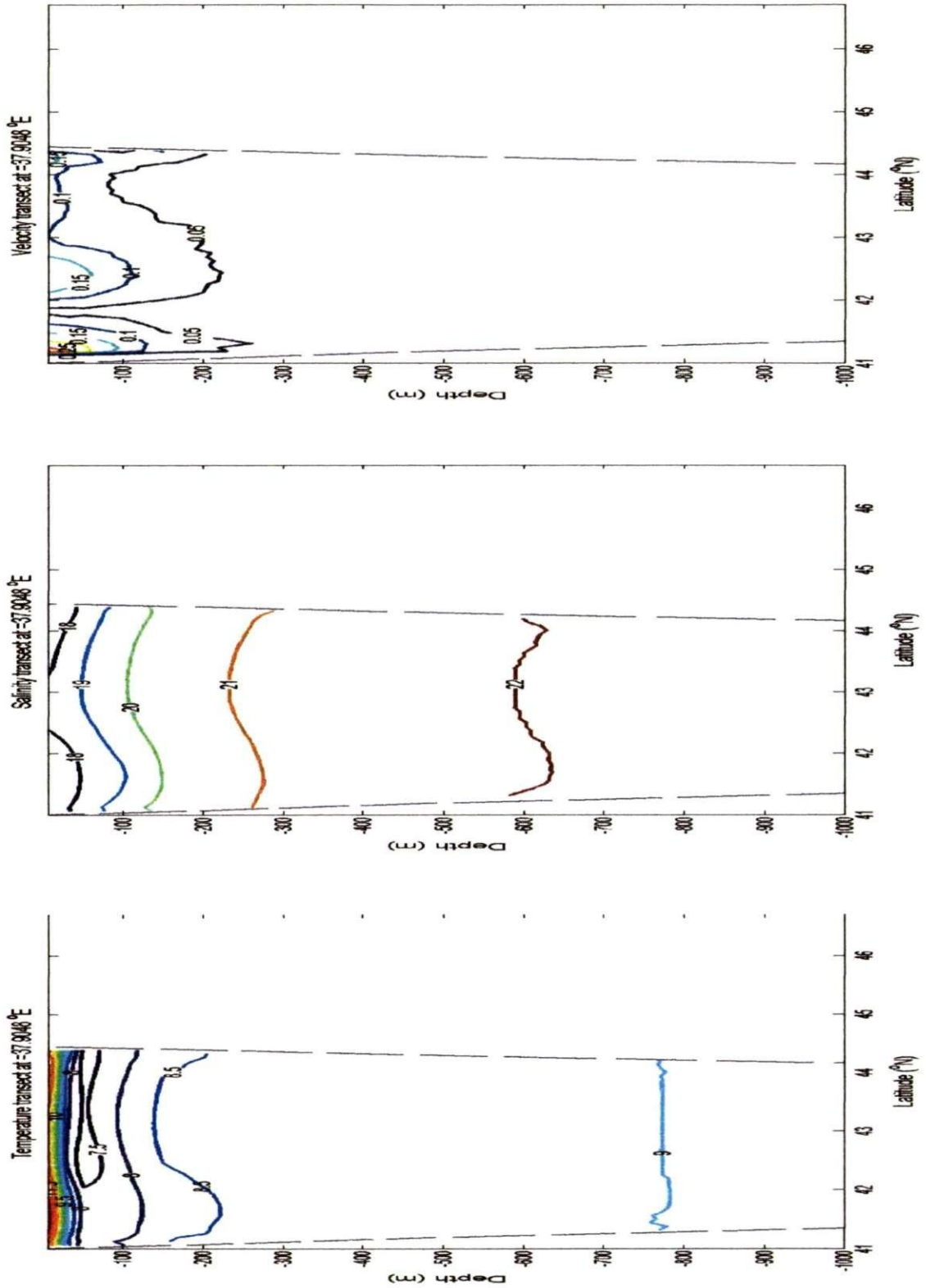
Figure 6-5 Meridional sections at Longitude 37.9°E after geostrophic adjustment showing (a) temperature (°C), (b) salinity (psu) and (c) current velocity (m/s)
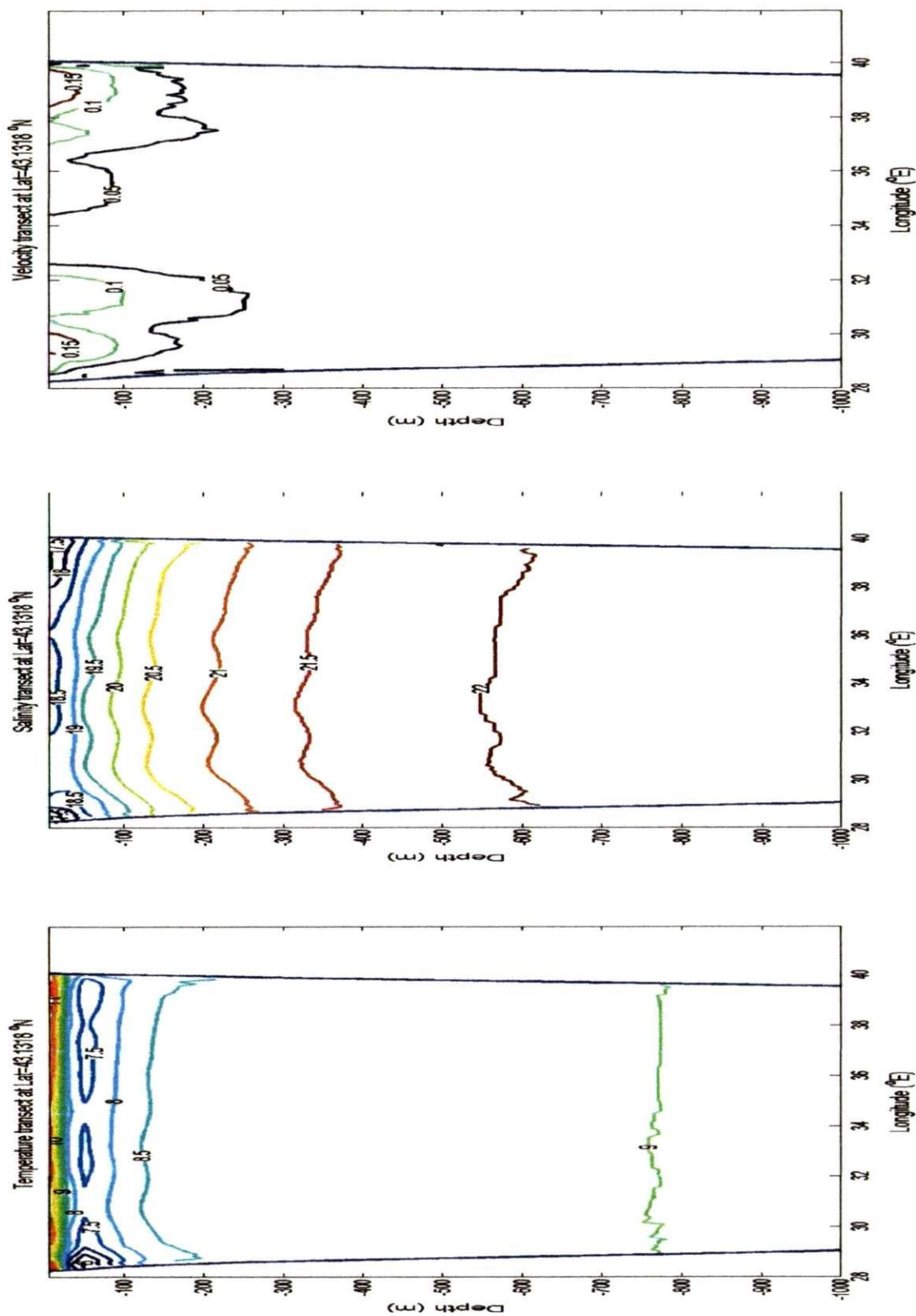
*Figure 6-6 Zonal sections at Latitude 43.13°N after geostrophic adjustment showing
(a) temperature (°C), (b) salinity (psu) and (c) current velocity (m/s)*

	May after GA less Climatic May (Initial)	
	Mean	**Std**
Difference in temperature whole basin	-0.0751	0.3316
Difference in temperature active layer (300m)	-0.0987	0.3779
Difference in temperature bottom layer (>300m)	-0.0014	0.0060
Difference in salinity whole basin	0.0065	0.0899
Difference in salinity active layer (300m)	0.0097	0.1025
Difference in salinity bottom layer (>300m)	-0.0034	0.0205

Table 6-2 Statistics of the difference between the adjusted and initial temperature (°C) and salinity (psu) distribution

6.3. Validation of the model

6.3.1. Qualitative comparison of the hydrodynamics

To validate the model the output was qualitatively compared with the general knowledge of the Black Sea hydrodynamics. As a first step, we used the results of the run that was set up for the geostrophic adjustment (No. 17). The parameters of that run are listed in Table 6-1. The model results show good agreement between the modelled and the known scheme of the Black Sea circulation (Figure 6-14a). To illustrate this agreement the results corresponding to day 15 of the run are presented in this section.
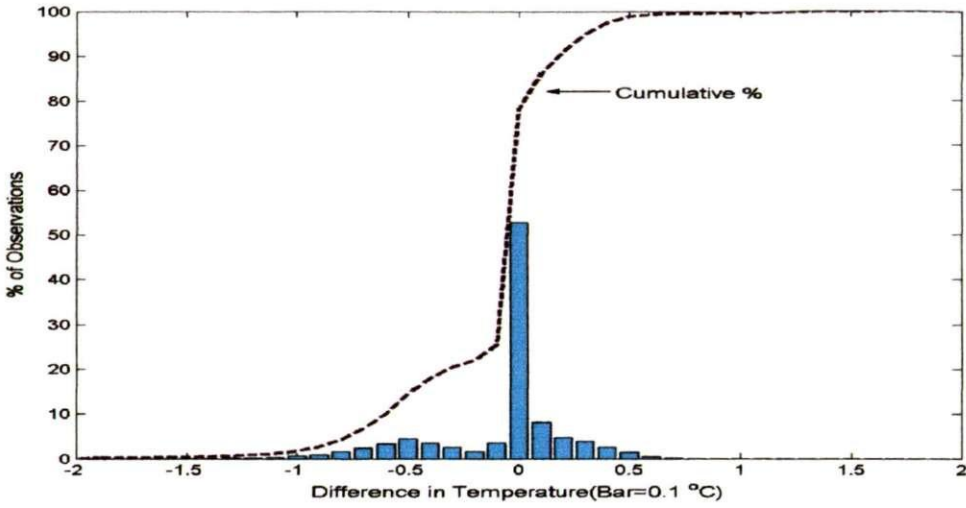
Figure 6-7 Histograms of the difference in temperature of the whole basin May time=127 hrs less May time=0 hrs (after and before geostrophic adjustment)
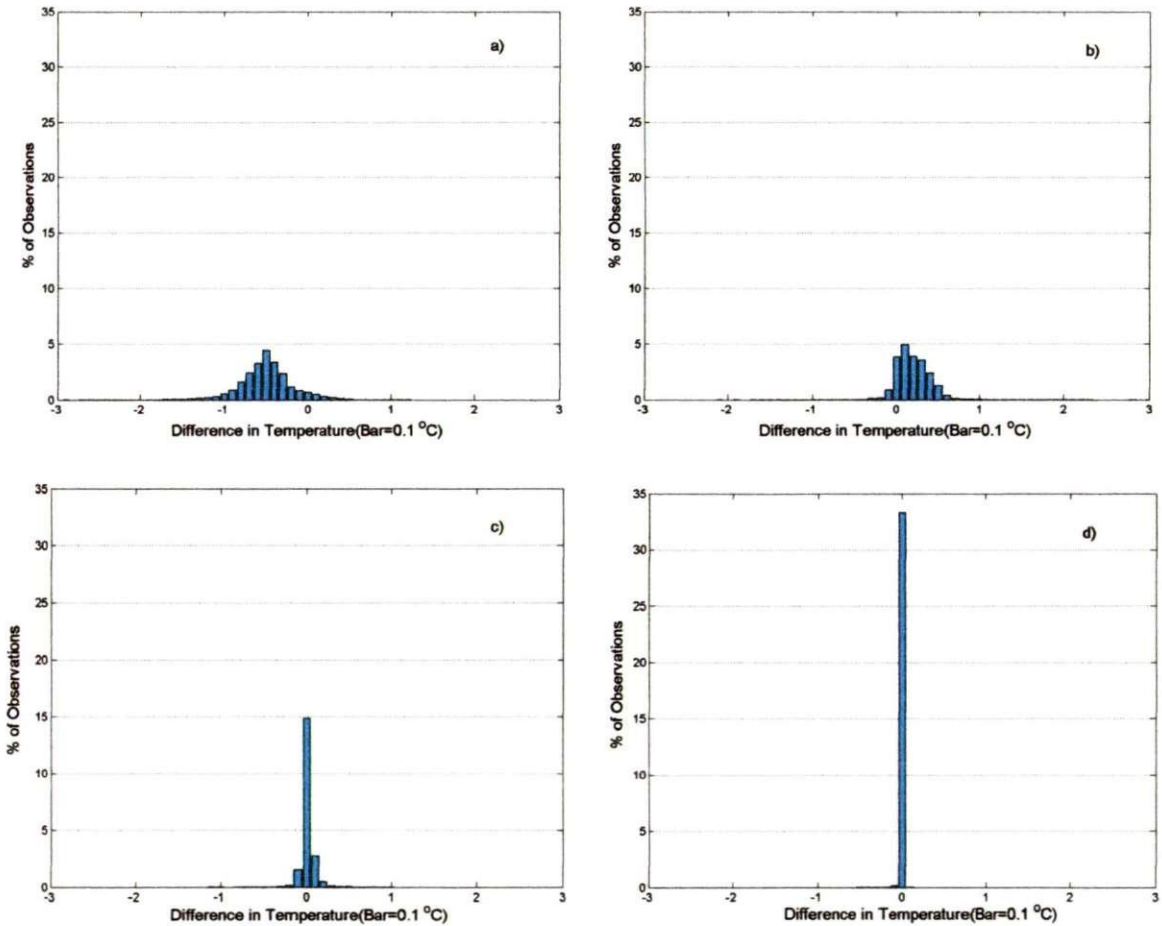
Figure 6-8 Histograms of the difference in temperature before and after geostrophic adjustment. The data were divided into four different layers a) top 10m depth b) from 10 to 50m depth c) from 50 to 150m depth and d) from 150 to 1500m depth. Bar width=0.1°C.

131
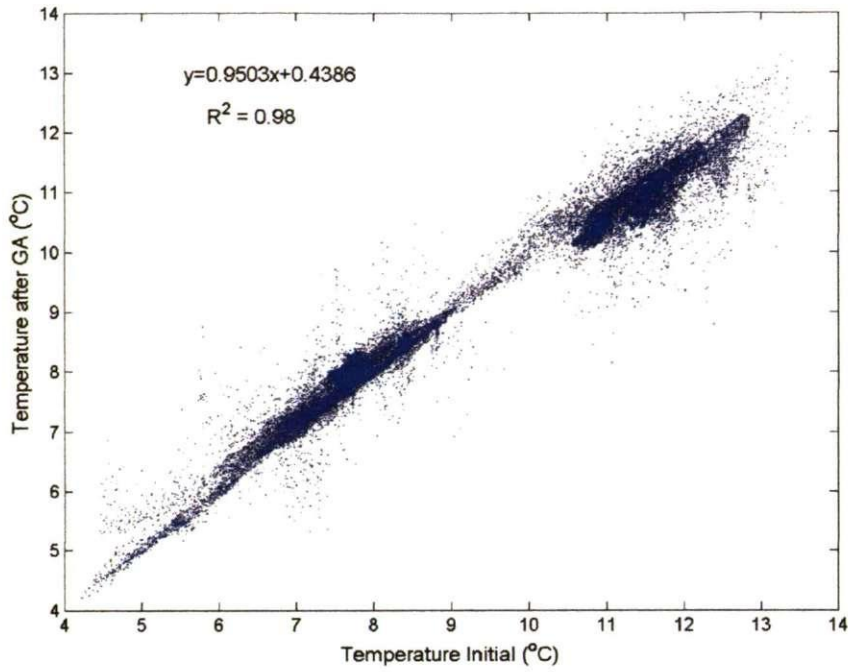
Figure 6-9 Initial temperature against temperature after geostrophic adjustment.
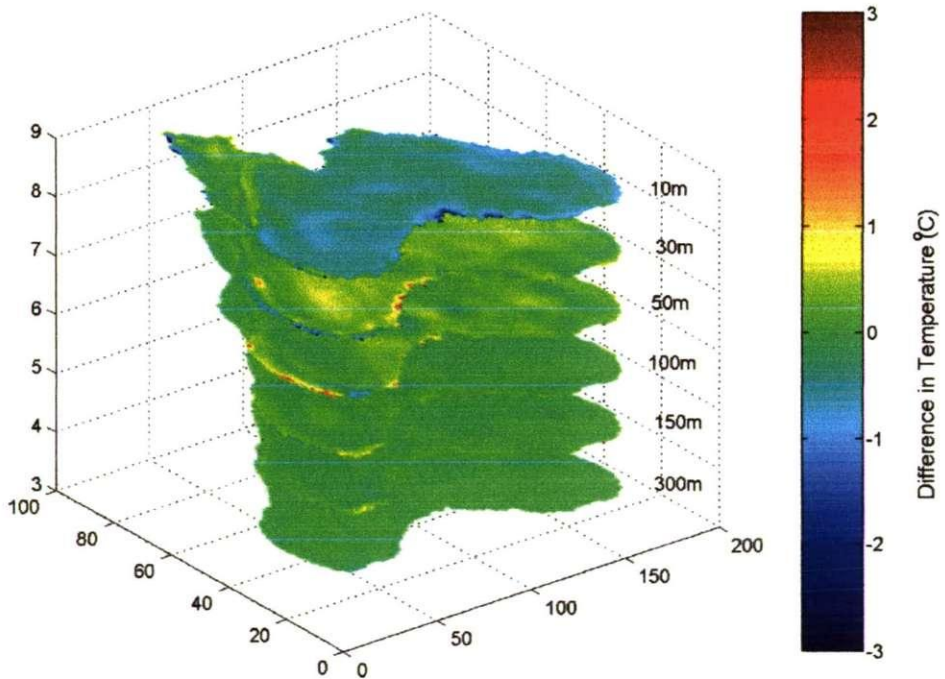
Figure 6-10 Distribution of the difference in temperature before and after geostrophic adjustment. The plot shows slices of the Black Sea basin at the depths of 10, 30, 50, 100, 150 and 300 m viewed from the south-western side of the area.
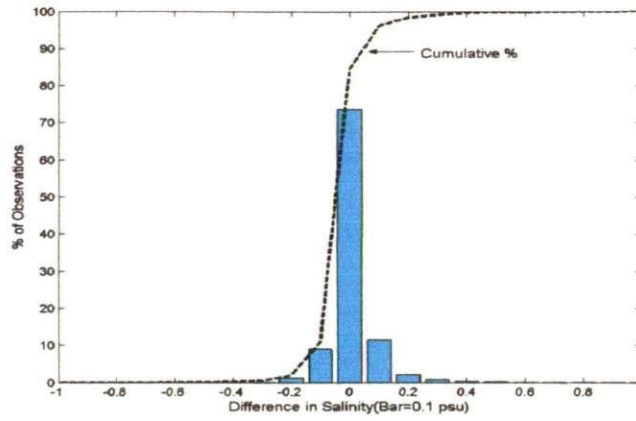
Figure 6-11 Histogram of the difference in salinity of the whole basin between May at time=0 and May at time=127 hrs (before and after geostrophic adjustment)
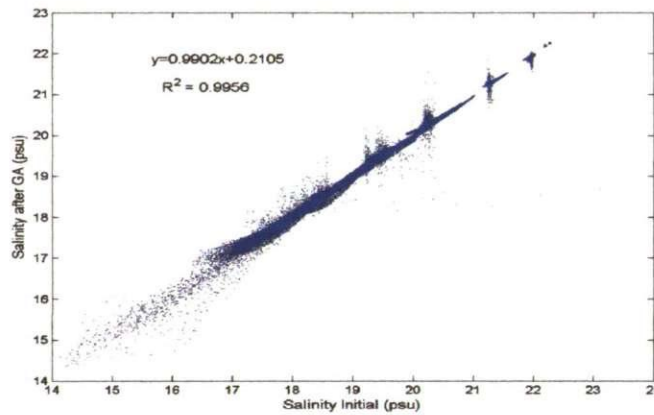
Figure 6-12 Initial salinity against salinity after geostrophic adjustment
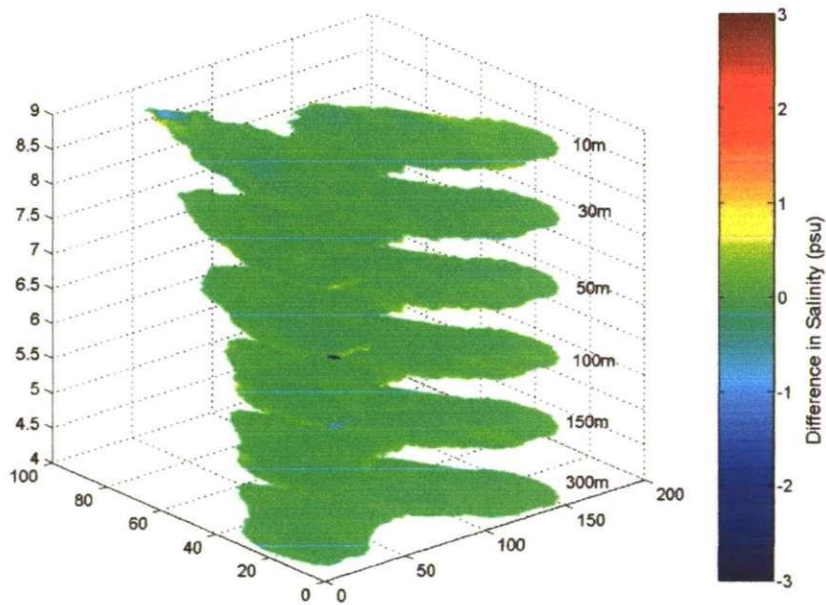
Figure 6-13 Plot showing the distribution of the difference in salinity before and after geostrophic adjustment at different vertical levels

133

Figure 6-14b shows the upper layer circulation after 15 days of running. The main feature of the upper layer circulation is the basin scale boundary current, Rim Current, which is satisfactorily reproduced by the model. The current flows cyclonically around the basin developing meanders and gyres with velocities of 0.1 to 0.22 m/s. The cyclonic gyres at the centre of the basin and coastal anticyclones are also reproduced by the model with sizes and velocities which are well correlated with observed ones. Some of the semi–permanent features such as the Sevastopol, Crimea, Kali-Akra, Batumi and Caucasus anticyclones, as well as several anticyclonic meanders and eddies in the south of the sea are present in the results.

The thermohaline distribution also shows a good agreement with the Black Sea structure. The coldest water is located in the north-western shelf with gradually increasing temperature towards the south-eastern part of the sea, reaching 12° C (Figure 6-2). The salinity distribution is presented in Figure 6-3. The fresher water is located in the coastal area, especially in the north-western shelf where the major rivers discharge. The central part of the sea is bounded by the Rim Current and has saltier waters with values of more than 18.5 *psu*. The vertical distribution of temperature and salinity along the pre-selected transects (Figure 3-8 – Chapter 3) presented in Figures 6-4 to 6-6 show the strong stratification, the Cold Intermediate Layer and the dome shape of the isolines due to the cyclonic circulation. Colder and fresher water from the north-western shelf extends down to the lower levels of the shelf and within the Cold Intermediate Layer.

6.3.2. Analysis of the inertial oscillations of the Black Sea

During the sensitivity tests to grid resolution a high temporal output resolution (1 hour) was required. From that moment it was clear that there is a well defined high frequency (less than 1 day) oscillation in the modelled circulation (Figure 6-1).
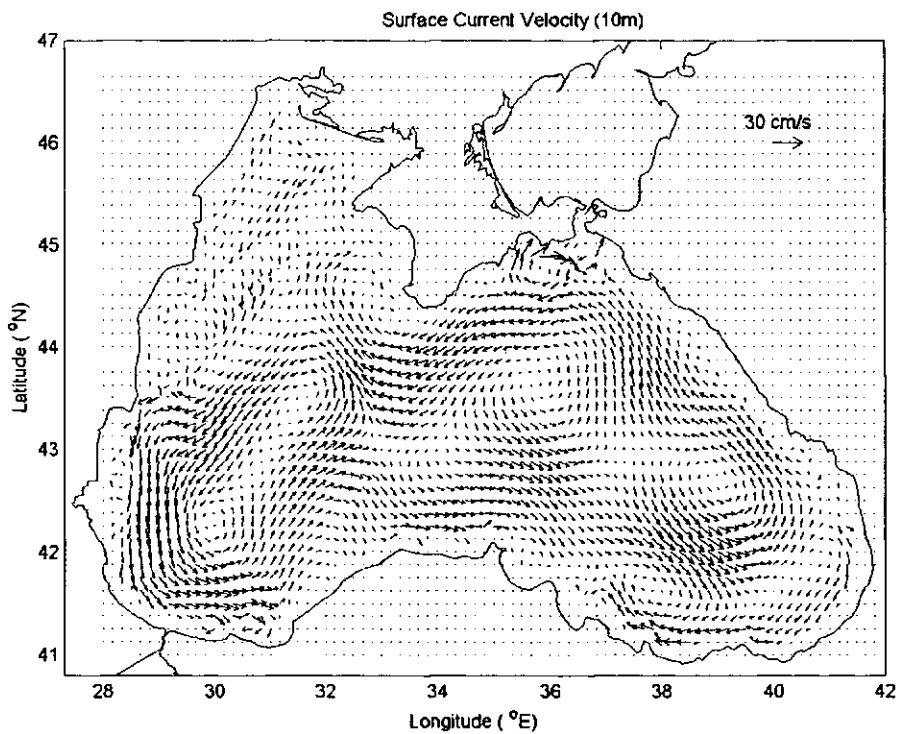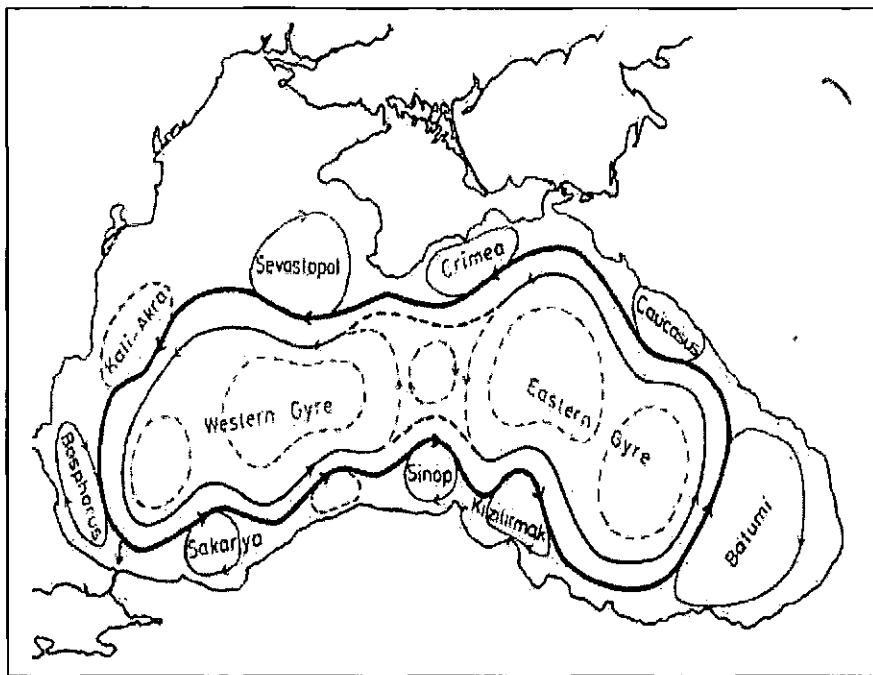
Figure 6-14 Upper layer circulation. The top panel shows the schematisation of the circulation from (Oguz et al., 1993). The bottom panel shows the modelled current velocity field at 10 m depth after 15 days of the run. Velocity vectors are plotted every second grid point.

To assess whether it was a real or a numerical oscillation, it was necessary to identify the frequency and amplitude of the oscillations and compare with observations. It is not easy to have access to observational data measured at high frequency but fortunately a drifter experiment was carried out recently in the Black Sea, from September 1999 to September 2002 (Zhurbas et al., 2004). They collected long term high frequency data and calculated the frequency and energy of oscillations of the measured velocities. To compare our model results with the drifter measurements a run (No. 19) was set up with the parameters listed in Table 6-3. The run was initialised with the temperature, salinity and velocity distribution obtained from the geostrophic adjustment process. This run includes all the forcing data available for this study, namely heat flux, evaporation, precipitation and river data for May and the wind stress during May of the year 1999.

Run name	Experiment No. 19
Initial Condition	Real bottom topography, 3-D T-S distribution and velocity field obtained from geostrophic adjustment.
Forcing data	Heat fluxes[1], Evaporation[1], Precipitation[1], Rivers[1], Wind[2] (1999) [1] Climatic [2] High frequency (every 6 hrs) NCEP re-analysis.
Run length	33 days
Starting date	1st May 1999
Barotropic *dt*	20 s
Baroclinic *dt*	200 s
AHC	0.2 m/s
AHCrit	600 m^2/s

Table 6-3 Parameters used in the run for validation of the oscillations.

The results from the drifter experiment are lagrangian measurements of the velocity and some caution should be taken while comparing with the eulerian data of the model at any one point. Figure 6-15 presents the tracks of the drifters during the experiment. The approach followed to evaluate the oscillations was to compare the modelled high frequency oscillations of the velocity components from a number of selected points along the drifter trajectories with the corresponding drifter results. In order to achieve this, the following methodology was applied to the modelled velocity results:

1. A total of 15 points from the Black Sea model's domain were selected to calculate from them the frequency and energy of the oscillations. The location of the points is presented in Figure 6-16. All the points are located approximately along the trajectories of the drifters, which are shown in Figure 6-15.

2. From each one of the selected points a time series of the modelled u and v components of the velocity at 15 m depth was extracted (e.g. Figure 6-17a). The length of the time series is 720 hrs starting after geostrophic adjustment so that the initial time is hour 127.

3. For each velocity component the mean part ($\overline{u(t)}$ and $\overline{v(t)}$) was removed from the time series (Figure 6-17b).

4. Once 'demeaned', the trend was removed from the time series (Figure 6-17c).

5. The next step was to calculate the energy spectra of the month long time series of the velocity components to identify the frequency of the oscillations.

6. The high frequency part ($T < = 24$ hrs) of the velocity fluctuations was extracted from the velocity time series using a high-pass / low-pass filter (Fast Fourier Transformation technique) (Figure 6-20).

7. Then the total kinetic energy per unit mass was calculated for only the high frequency part of u *(t)* and v *(t)* (Figure 6-21).

137
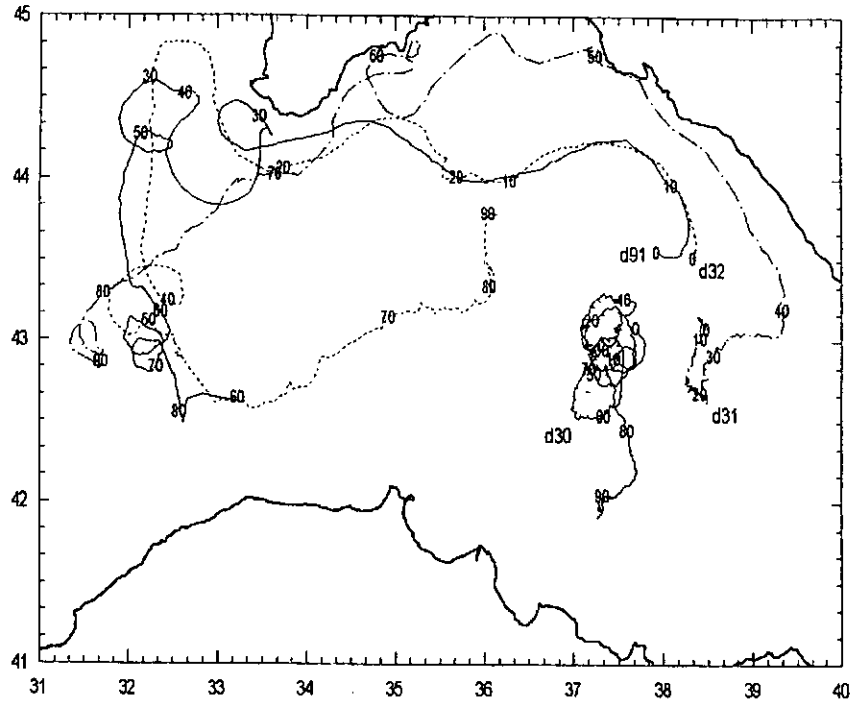
Figure 6-15 Trajectories of four of the drifters during the drifter experiment (Zhurbas et al., 2004).
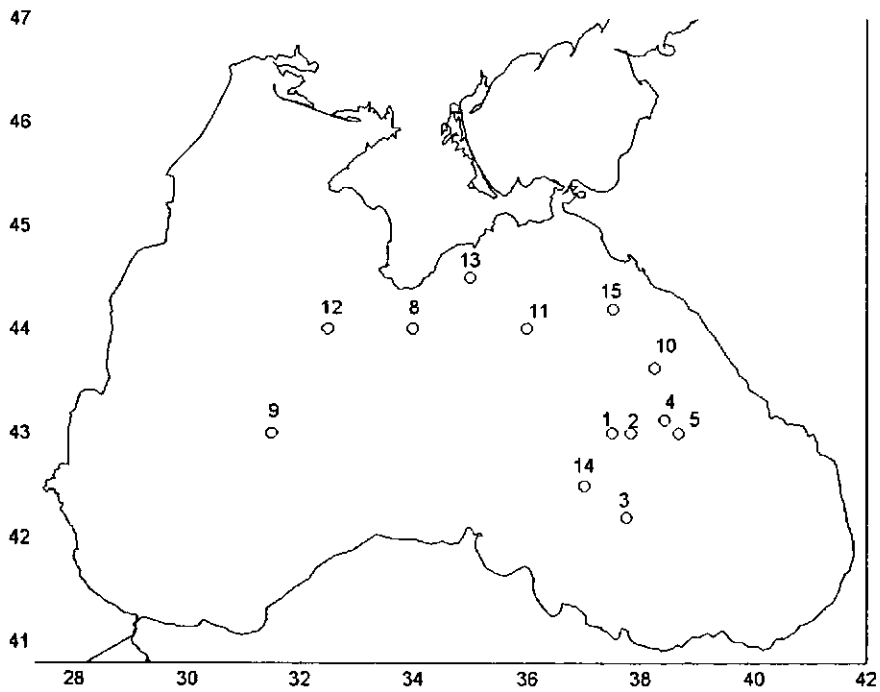
Figure 6-16 Plot showing the location of the points at which time series of the modelled velocity components at 15 m depth were extracted to compare with the drifter data.

The spectral analysis was calculated using the Matlab function 'spectrum' which uses the Welch's averaged periodogram method for the calculation of the power spectral density function.

From the one month run, the length of the time series is 720 and the sampling frequency is 1 hr. The time series were zero-padded to achieve a length of 2^n (n being the number of samples). In this case the final length is 1024. A Hanning window was used with a size covering 10 days in order to get a closer match to the way in which Zhurbas et al. (2004) made their calculations. They used a window size wide enough to allow some mesoscale frequencies to be included in the spectrum although the widening of the window gave them 6 degrees of freedom which is very small. The number of degrees of freedom resulting from the window size in our time series is 8.22. Figure 6-18 shows the power spectrum of the velocity at point No. 1. The spectra of the modelled velocity components from the selected points have the dominant peak located in the inertial frequency band (period ~ 17 hrs). The frequency at which the peak of the high frequency oscillation occurs did not change when the power spectrum was obtained using a smaller window size which would cover 2 days, increasing the degrees of freedom to 57.88.

There are two smaller peaks located at periods of 256 hrs and 36 hrs. Both are in the domain of the periods of mesoscale eddy motions which according to Stanev and Beckers (1999) are frequently between 2 and 15 days. Both the modelled data and the drifter data have peaks within the inertial and the mesoscale frequency bands as shown in Figure 6-19. Finally the kinetic energy of the oscillations was obtained following the approach of Zhurbas et al. (2004). In their study the frequency of the oscillations was obtained from the power spectra but the energy of the inertial oscillations was calculated directly from the velocity components due to the large confidence intervals.
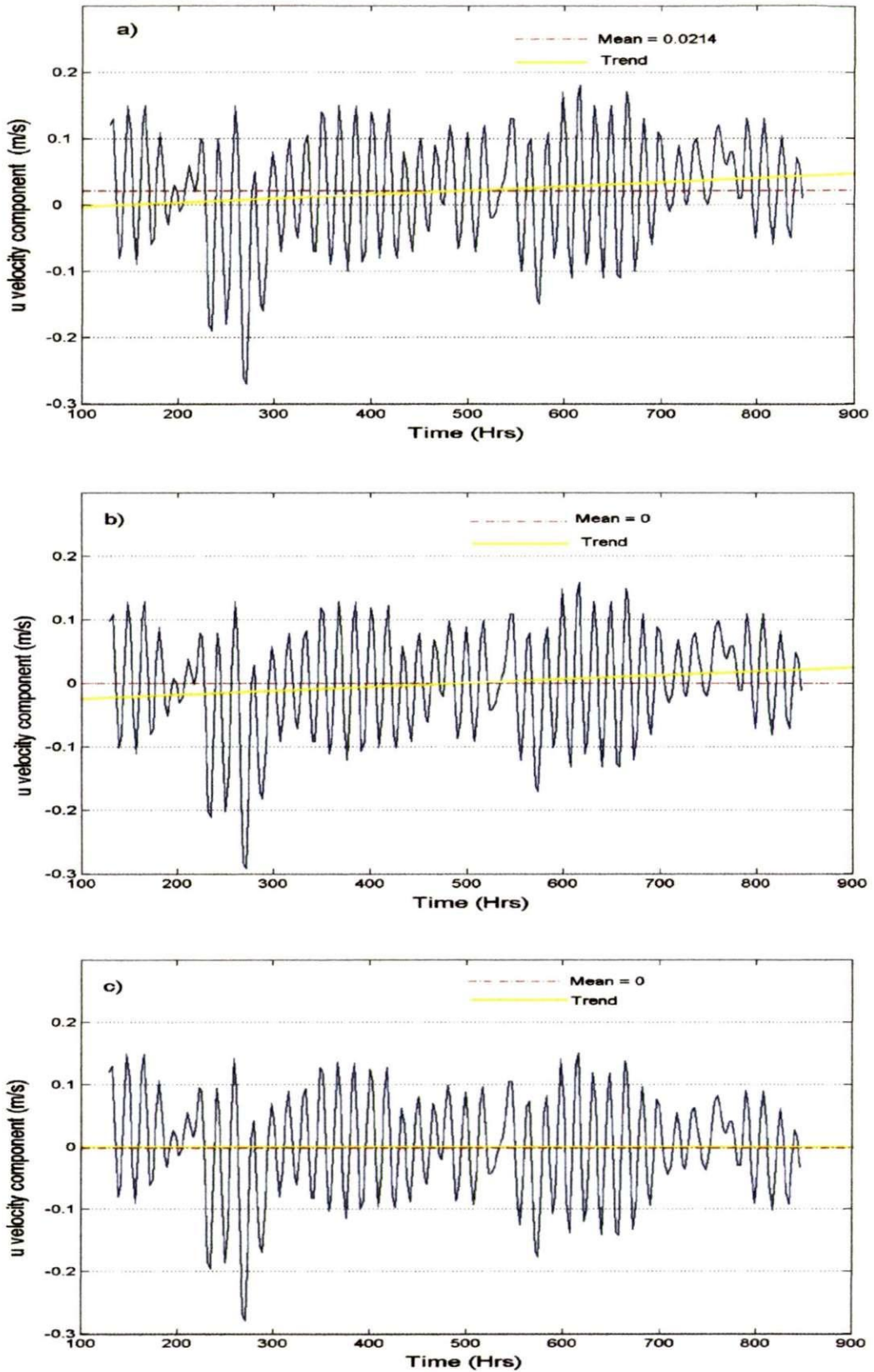
Figure 6-17 Time series of the u(t) component of the velocity at point No. 1 (Figure 6-16) and at 15m depth a) true model output b) mean removed c) mean and trend removed

The result of the averaged total kinetic energy at each one of the selected points is listed in Table 6-4. The energy of the modelled inertial oscillations is compared with the drifter experiment results which relate to the average of the measurements collected by each drifter during limited periods of time (Zhurbas et al., 2004). In general the energy of the modelled inertial oscillations is within the range of the observed values during the drifter experiment. The averaged energy of the modelled inertial oscillations from the selected points is 3.47×10^{-3} m^2/s^2 and the averaged energy of the drifters is 4.25×10^{-3} m^2/s^2. Our results are also similar to the results obtained by E. Stanev and J. Beckers (1999). They used numerical modelling to study the barotropic and baroclinic oscillations of the Black Sea. In their spectral analysis the inertial oscillations are represented in a peak of energy at about 15 – 16 hrs period. This peak however is not very energetic in their study and they attributed the 'very low spectral maximum' to the fact that they used smoothly varying seasonal wind forcing and therefore the inertial oscillations were not effectively excited, which is not the case within this study. Their results also show oscillations with periods very close to the smaller two peaks of our spectra: In this research the peaks are approximately at 36 hrs and 10 days while in their study there are peaks at 29 hrs and 11 days.
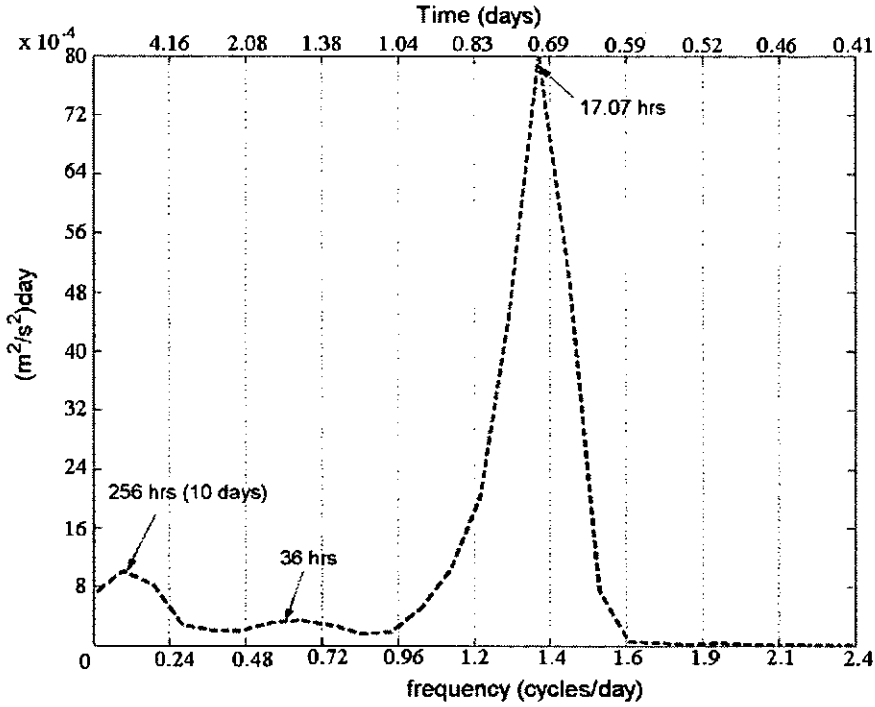
Figure 6-18 Power spectrum of the modelled v component of the velocity at point No. 1 (the location of the points is shown in Figure 6-16) using a window size m=80.
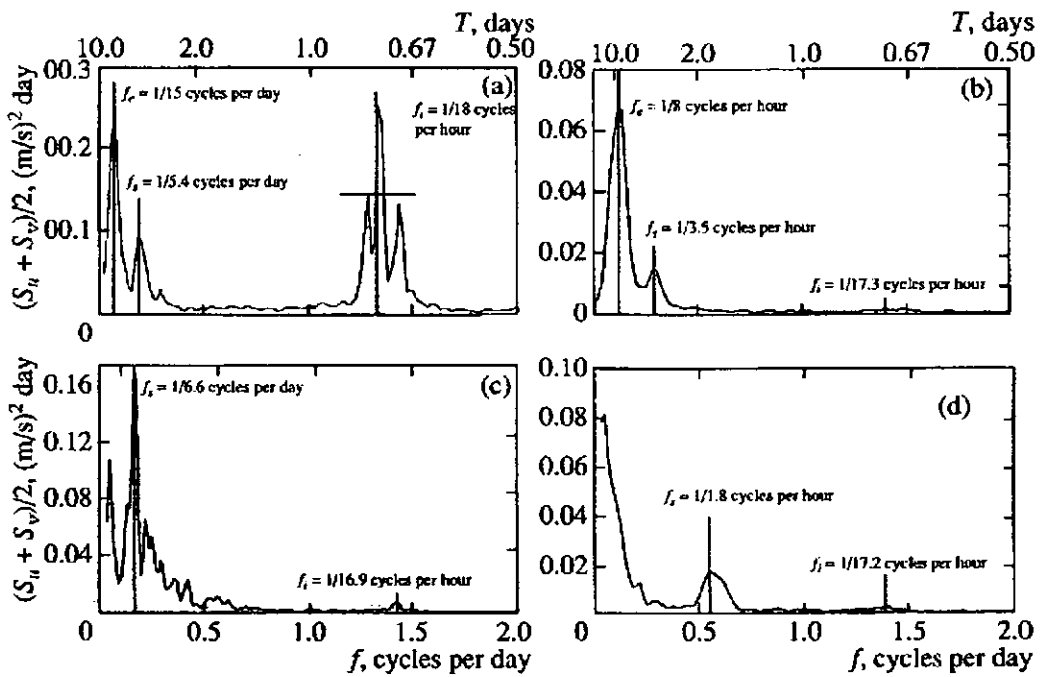
Figure 6-19 Power spectra of the drifter velocity components of four of the drifters (Zhurbas et al., 2004) a) drifter 30; b) drifter 91; c) drifter 31; d) drifter 29.
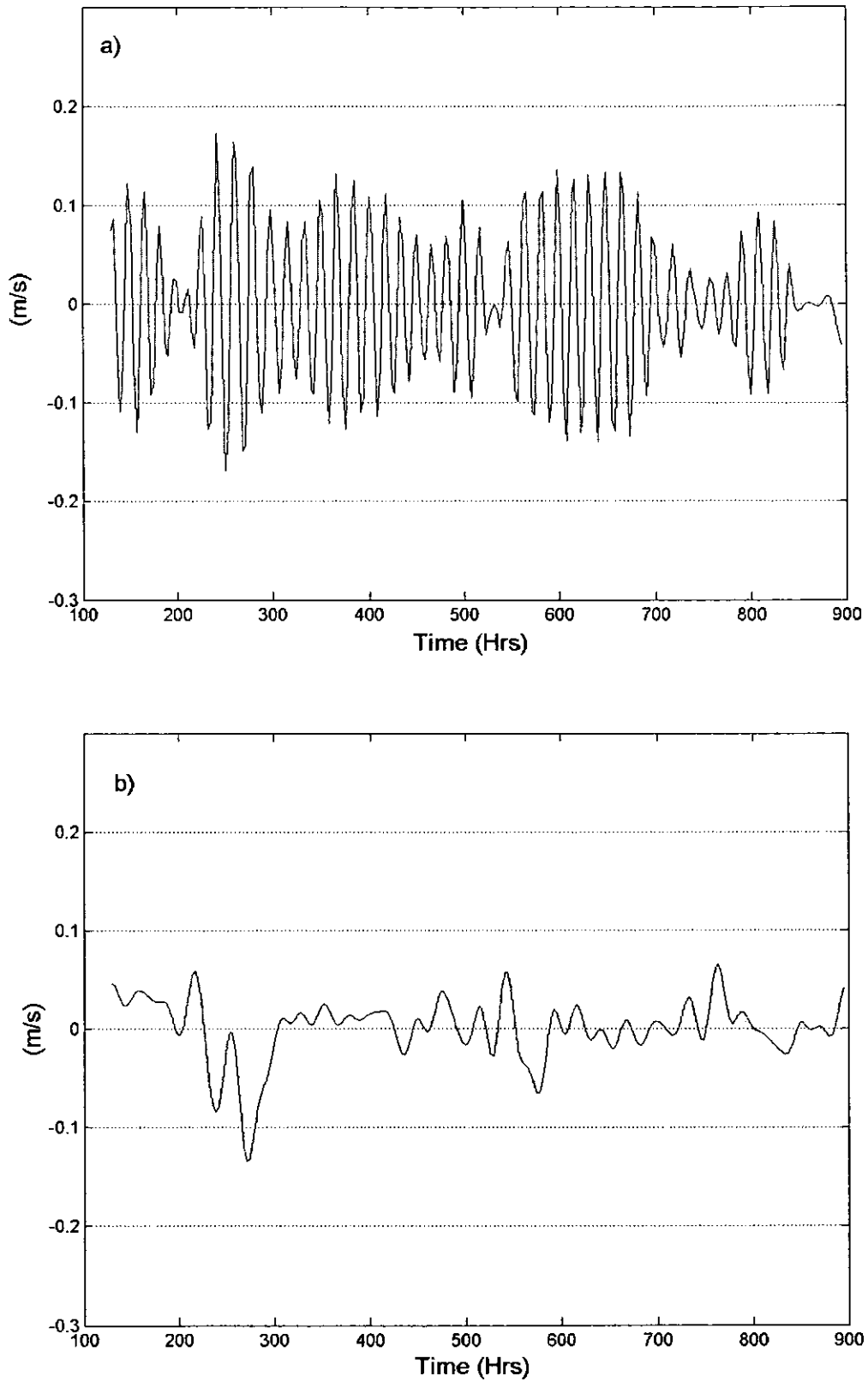
Figure 6-20 Time series of the filtered u(t) component of the velocity at point No. 1 at a depth of 15 m a) high frequency part (T<=24hrs) b) low frequency part (T>24 hrs)

143
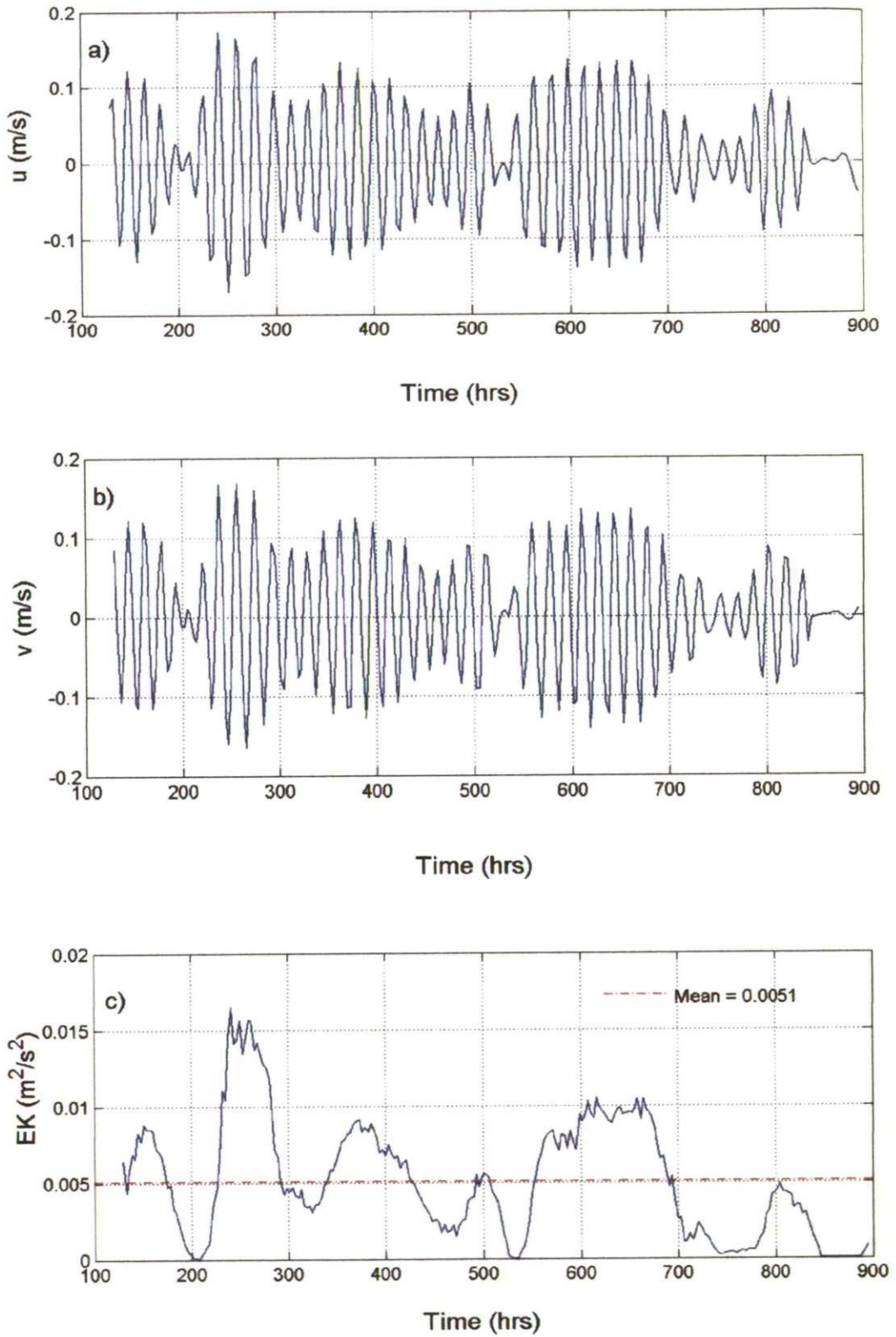
Figure 6-21 Time series of the high frequency part of a) u component of velocity b) v component of velocity and c) kinetic energy calculated from the filtered high frequency velocity components from point No. 1 at 15 m depth.

Point No.	Latitude (°N)	Longitude (°E)	Row	Col	Average of the TKE from H.F. oscillations $\left(\times 10^{-3}\, m^2\!/_{s^2} \right)$	Corresponding drifter No / mean TKE measured by drifter $\left(\times 10^{-3}\, m^2\!/_{s^2} \right)$
1	43	37.5	33	115	5.1	
2	43	37.78	33	119	4.26	Drifter 30
3	42.2	37.7	20	118	3.59	7.02
14	42.5	37	25	109	3.5	
4	43.1	38.4	35	126	3.39	Drifter 31a
5	43	38.65	33	129	3.02	5.49
8	44	34	49	73	3.18	Drifter 31b
9	43	31.5	33	43	2.8	5.32
13	44.5	35	56	85	2.1	
10	43.6	38.2	43	124	4.02	Drifter 91
11	44	36	49	97	4.2	
12	44	32.5	49	55	3.2	1.56
15	44.2	37.5	52	115	2.8	
Average of all points/drifters					3.47	4.25

Table 6-4 Location of the points from which the velocity components were extracted from the model results, the kinetic energy of the inertial oscillation at each of the extracted points and the kinetic energy of the inertial oscillation of the corresponding drifter (Zhurbas et al., 2004).

6.4. Summary

There are perturbations resulting from the initialisation of the model such as starting with zero velocities in a dynamical condition of the temperature and salinity distribution which in turn do not match the bottom topography. The perturbations generate motions which are eventually dissipated by friction. Due to the rotation of the earth the final state is not a state of rest but that of geostrophic equilibrium (Kantha and Clayson, 2000). The process is called geostrophic adjustment.

In order to detect when the geostrophic equilibrium is achieved the basin averaged total kinetic energy was monitored. The results show that the kinetic energy does not have an obvious increasing trend but oscillates and the amplitude of the oscillations is much bigger in the beginning of the run and decreases for some time before it reaches stability. The time to achieve geostrophic equilibrium using the fine resolution grid was 127 hrs, time at which the amplitude is nearly $1/5^{th}$ of the average of the oscillation. The process of adjustment did not alter the overall temperature and salinity distributions. The results include:

- A lateral gradient with minimum temperature in the north-western shelf and maximum in the south-eastern part of the basin.

- The front of warmer water in the eastern part is less sharp after adjustment than in the climatic data (initial).

- In the central area the water is slightly colder after the adjustment due to the mixing resulting from the currents.

- The fresher water is located in the north-western shelf with a sharp salinity gradient from the coast to the sea.

- The saltier water is present in the locations of the western and eastern central cyclonic gyres.

- The surface mixed layer reaches approximately 30 m depth.

- The cold intermediate layer is present in the basin between depths of 30 and 100 m.

- The minimum salinity is located at the surface and it increases with depth.

The effect of the process of geostrophic adjustment on the temperature and salinity fields is restricted to the upper layer and the changes are the following:

- The surface layer (top 10 m) loses some heat while the sub-surface layer (10-50 m), which includes the Cold Intermediate Layer, increases its temperature. From 50 m depth and down to the bottom (1500 m) the changes are negligible.

- The correlation between the modelled temperature after 127 hrs of geostrophic adjustment and the climatic temperature of May, which was used to initialise the model, gives a coefficient (R^2) of 0.98 which relates to a very good agreement.

- The effect of the adjustment on the salinity field is very small giving a correlation coefficient of 0.99.

- The velocity field generated during the adjustment process includes the Rim Current flowing cyclonically around the periphery of the basin developing meanders and gyres with velocities of 0.1 to 0.22 m/s.

- The cyclonic gyres at the centre of the basin and coastal anticyclones are accurately reproduced by the model with sizes and velocities which are well correlated with observed ones.

- Some of the semi–permanent features such as the anticyclones: Sevastopol, Crimea, Kali-Akra, Batumi and Caucasus gyres are present as well as several anticyclonic meanders and eddies in the south of the sea.

• The velocities resulting from the geostrophic adjustment penetrate down to depths of more than 300 m in the areas where the Rim Current is stronger.

To further validate the model performance the oscillations of the modelled velocity components were analysed. The frequency and amplitude of the modelled oscillations were compared with observational data from a drifter experiment carried out in the Black Sea from September 1999 to September 2002 (Zhurbas et al., 2004). The power spectra of the modelled velocity components showed a dominant peak located in the inertial frequency band (T~17 hrs). Two smaller peaks were located at periods of 256 hrs and 36 hrs which are typical for mesoscale eddy motions (T~2-15 days). The peaks obtained in the spectral analysis occur at similar frequencies to those found in previous modelling studies of the Black Sea (Stanev and Beckers, 1999). The kinetic energy of the high frequency part of the oscillations was calculated directly from the velocity components. The energy of the inertial (high frequency) modelled oscillations (average of all the selected points) is 3.47×10^{-3} m^2/s^2 and the averaged energy of the drifters is 4.25×10^{-3} m^2/s^2.

The results presented in this chapter show that the model adequately represents the hydrodynamics of the Black Sea basin and therefore the results from the numerical experiments are reliable.

CHAPTER 7. INTERANNUAL MESOSCALE VARIABILITY OF THE BLACK SEA

7.1. Introduction

It is now known that the real circulation in the Black Sea varies from the mean scheme and that the mesoscale variability is a very significant component of the variability. The mesoscale variability is not easily accessible to observations due to its spatial (order of 10 km) and temporal (order of days-weeks) resolution. To gain insight into the multi-scale circulation and its elements, within this research we represent the mesoscale variability of the circulation in the Black Sea based on modelling results.

Recently it has been suggested that the wind forcing is the major factor responsible for the variability of the mesoscale currents, although there is some debate on whether it is the curl of the wind stress (Zatsepin et al., 2002) or the wind stress itself (G. Shapiro, personal communication, 2000) which mostly affect the Black Sea mesoscale circulation. Contemplating these statements this study evaluates the interannual variability of the hydrodynamics by forcing the model with wind data from different years. This chapter presents the results of three numerical experiments which were forced with exactly the same climatic heat flux, evaporation, precipitation and river data but using high frequency (T=6 hr) wind forcing for three different years (1998, 1999 and 2000).

Within this chapter, Section 7.2 describes the numerical experiments. Then to assess the variability of the mesoscale circulation, the characteristics of the wind circulation in the Black Sea area during the months of May and June for the three years used in the experiments are presented in Section 7.3. Finally Section 7.4 has the results of the hydrodynamics and the interannual variability of the general and mesoscale circulation of the Black Sea during May and June using wind forcing of the years 1998, 1999 and 2000.

7.2. Numerical simulations

To evaluate the wind-driven response of the Black Sea hydrodynamics and in particular its inter-annual variability, 3 numerical experiments were carried out. All three experiments were initialised after geostrophic adjustment (described in Chapter 6). They were forced with climatic heat fluxes, evaporation, precipitation and river inflow starting from the 1st of May and ran forward for 60 days. The wind data used to force the experiments (described in Chapter 3) correspond to the years 1998, 1999 and 2000. The main parameters used for these experiments are listed in Table 7-1 and were determined based on results of the sensitivity tests (Chapter 5) corresponding to run No. 13 (Table 5-1).

The model output was averaged for 17 hour intervals in order to filter the inertial oscillations.

Barotropic Time step (s)	Baroclinic time step (s)	*AHC (m/s)*	*AHCrit (m^2/s)*	Wind data	Other forcing data	Run length
20	200	0.2	600	1998	Climatic[1]	60 days
20	200	0.2	600	1999	Climatic[1]	60 days
20	200	0.2	600	2000	Climatic[1]	60 days

Table 7-1 List of numerical experiments. [1] The climatic data includes: heat flux, evaporation, precipitation (Staneva and Stanev, 1998), and river discharge (Altman and Kumish, 1986).

7.3. Characteristics of the wind fields

In addition to the observations, it is possible at the present to obtain wind data from numerical weather forecast models such as the National Centres for Environmental Prediction, NCEP, (http://www.cru.uea.ac.uk/cru/data/ncep/), the European Centre for Medium-Range Weather Forecasts, ECMWF, (http://www.ecmwf.int/) or the Fleet

Numerical   Meteorology   and   Oceanography   Centre,   FNMOC,

(https://www.fnmoc.navy.mil/). Each one of the data sets is subject to their own errors

even if they may represent part of the real signal. Wind data sets and computations of wind

stresses may be affected by many sources of errors. Observations are mainly taken from

land stations (near the shores) and wind values at the sea are extrapolated from these

samples. The measurements carried out in the sea are sporadic and coarse. It is beyond the

scope of this research to analyse the reliability of the different wind data sets in the Black

Sea but it is recognised that large discrepancies may occur with the use of different wind

data sources.

According to A.K. Leonov (1960) in Rachev et al. (1991), the wind field in the Black Sea

during the spring time (April-June) is less intense than during the winter time and therefore

the spring is the season with the strongest wind variability and without a particularly

predominant direction. In general the wind is more intense in the western part of the basin

throughout the year and the areas with minimum wind speeds are the south of the Crimean

peninsula and off the Caucasian coast (Oguz and Malanotte-Rizzoli, 1996). The strong

wind events occur about every 5-10 days (Besiktepe et al., 2001).

Using the wind data from the NCEP reanalysis data set (described in Chapter 3) we

calculated the characteristics of the wind field over the Black Sea during May and June

from the years 1998, 1999 and 2000. The parameters obtained were the wind stress (τ),

the curl of the wind stress, the kinetic energy of the wind and the enstrophy (square of the

curl). The reasons for using these parameters in this study are discussed in Section 8.6.

The large-scale ocean circulation at mid-latitudes is controlled by the curl of the wind

stress (Molcard et al., 2002) so that if the curl of the wind stress has positive values within

the basin, then the circulation may be composed of cyclonic gyres and of anticyclonic

gyres with negative wind stress curl values.

The curl of the wind stress, $\mathrm{curl}\,\tau$, is the vertical component of the vorticity of the wind friction stress. Vorticity is a characteristic of the kinematics of fluid flow which expresses the tendency for portions of the fluid to rotate.

When the vorticity is measured relative to the Earth, it is called relative vorticity and the vertical component in the horizontal plane is

$$\mathrm{curl}_z V = \frac{\partial v}{\partial x} - \frac{\partial u}{\partial y}.$$

Correspondingly, the wind stress curl is calculated by

$$\mathrm{curl}_z \tau = \frac{\partial \tau_y}{\partial x} - \frac{\partial \tau_x}{\partial y},$$

where τ_x and τ_y are the zonal and meridional components of the wind stress respectively.

The enstrophy represents the variance of the vorticity and, as well as the kinetic energy, was obtained using the grid nodes belonging to the Black Sea basin only.

To illustrate the variability of the wind data we describe the behaviour of the wind during a one-month period (from 7 May to 5 of June) extracted from the 2-month data set used in the numerical simulations. The basin averaged total kinetic energy of the wind for the 3 different years is shown in Figure 7.1. From the kinetic energy it is clear that the wind varies significantly in small periods of time so that each one of the years has a period of time during which it is more intense than the other two years. The wind of the year 1998 was in general the more energetic during that month and especially during the first week, from the 7 to the 14 of May (Figure 7.2). The wind of the year 1999 is the weaker of the three years and is more intense during the second week of that period of time, from the 15 to the 21 of May. The wind of the year 2000 was similar in intensity to the one of the year 1999 but slightly more energetic with minimum strength during the second week and maximum strength during the last week of that month (from the 29 of May to the 5 of June). As well as the magnitude, the direction of the wind is very important.
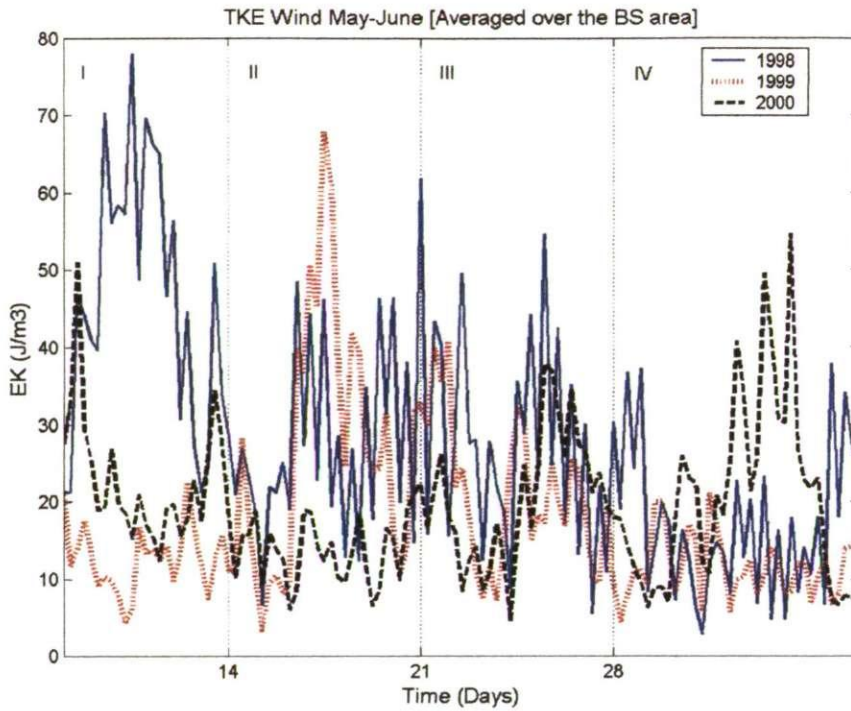
Figure 7.1 Time series of the averaged total kinetic energy of the wind from the 7 of May to the 5 of June of the years 1998, 1999 and 2000. The wind data is NCEP reanalysis covering the Black Sea area. The calculation of the kinetic energy covers only the area above the sea and excludes the land.
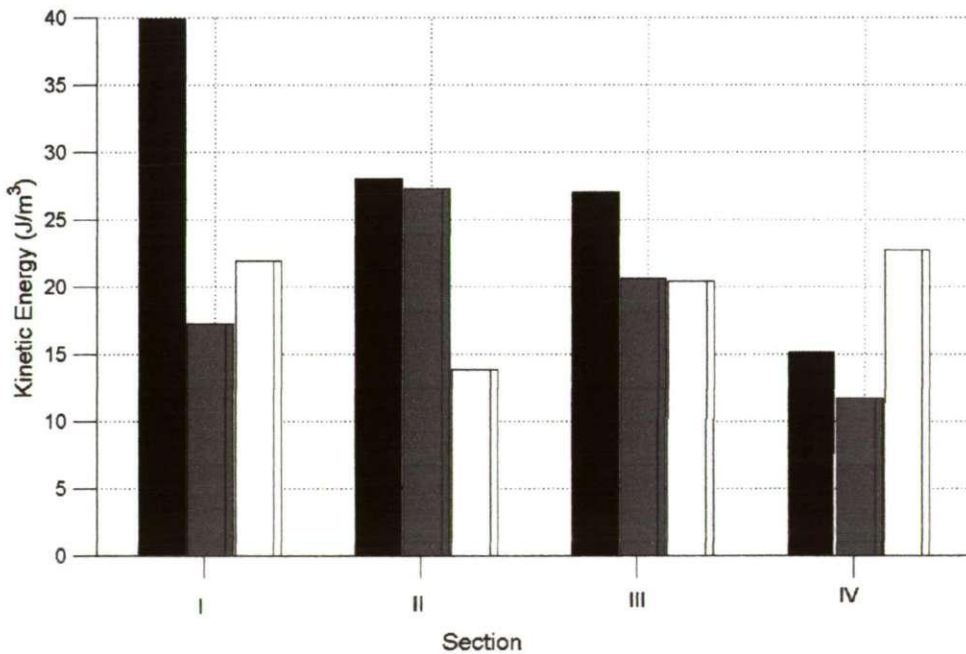
Figure 7.2 Averaged kinetic energy of the wind during: I) 7 to 14 of May (week 2); II) 15 to 21 of May (week 3); III) 22 to 28 of May (week 4); IV) 29 of May to 5 of June (week 5). The bars correspond to the years 1998 (black), 1999 (grey) and 2000 (white).

153

In general the wind is more intense when it is coming from the north and has a cyclonic tendency. This is shown in Figure 7.3a presenting the wind stress of 1998 averaged during the week of the 7 to the 14 of May. During that week most of the basin is dominated by strong north-easterlies except for the south-eastern part of the Black Sea. On the other hand, when the wind is of an anticyclonic nature it is in general less energetic, for example during the week of the 15 to the 21 of May of the year 2000 (Figure 7.3b). This analysis shows that the curl of the wind stress and the magnitude of the wind stress are inter-related in the Black Sea area.

The spatial distribution of the wind curl is shown in Figure 7.4. The wind curl distribution averaged during the week of the 7 to 14 May 1998 (Figure 7.4a) showing two areas with negative values, located at the south-east of the Crimean peninsula and along the Bulgarian coast, and two areas with positive values, located in the north-eastern part of the sea and in the south western area. These distribution resembles the typical wind curl distribution dominating the Black Sea region through the year according to Rachev et al. (1991). Contrastingly, the wind curl pattern shown in Figure 7.4b which is the average from the 15 to the 21 of May of the year 2000 presents a very different distribution, with positive values in the coastal areas and negative values in most of the central area of the Black Sea basin.

The maximum and minimum values of enstrophy (Figure 7.5) were found during the events of maximum and minimum energy (7 – 14 May 1998 and 15 – 21 May 2000 respectively).
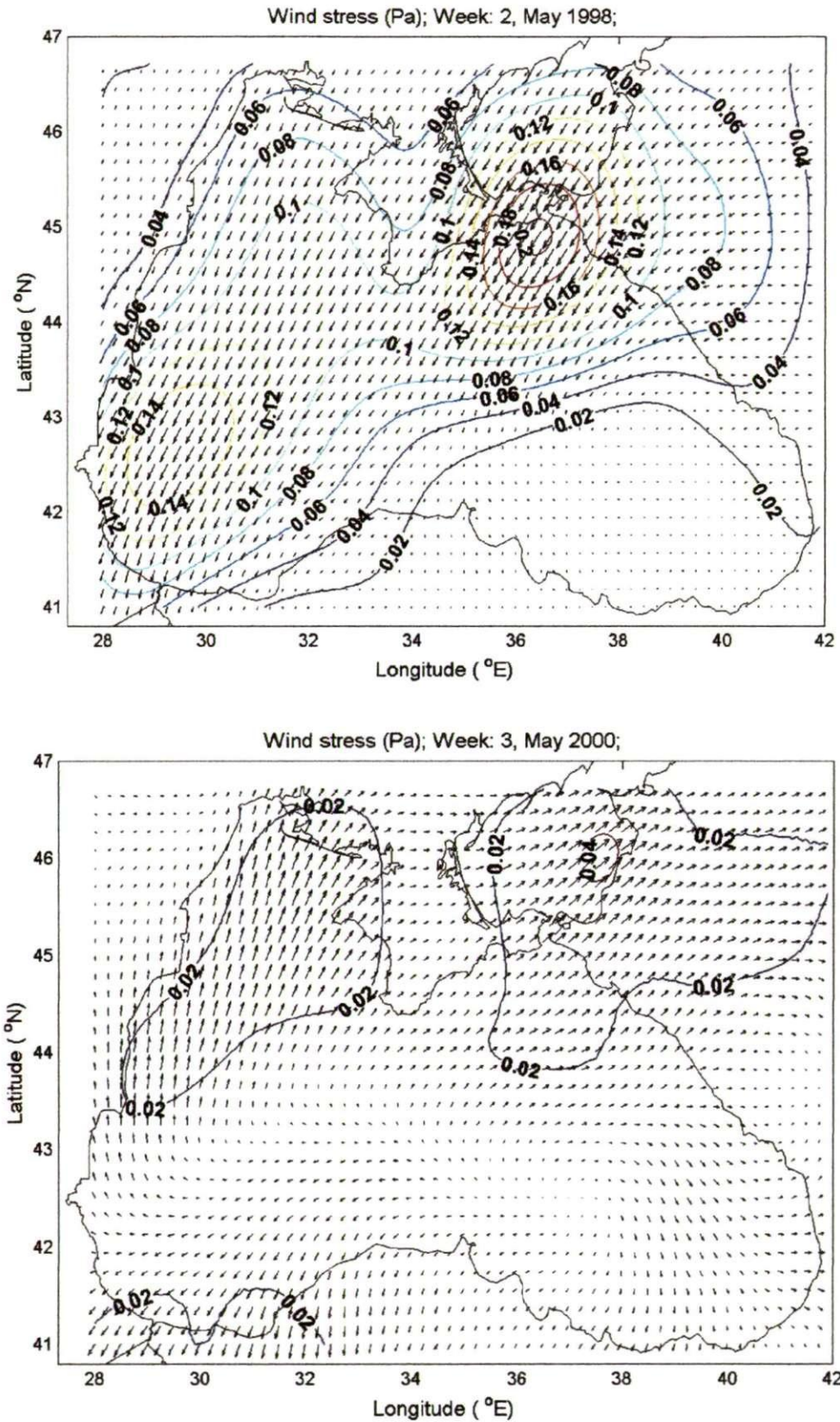
Figure 7.3 Wind stress fields averaged during the weeks of a) 7-14 May of 1998 and b) 15-21 May of 2000. The vectors are plotted every third grid point and the contours show the magnitude of the wind stress (Pa).
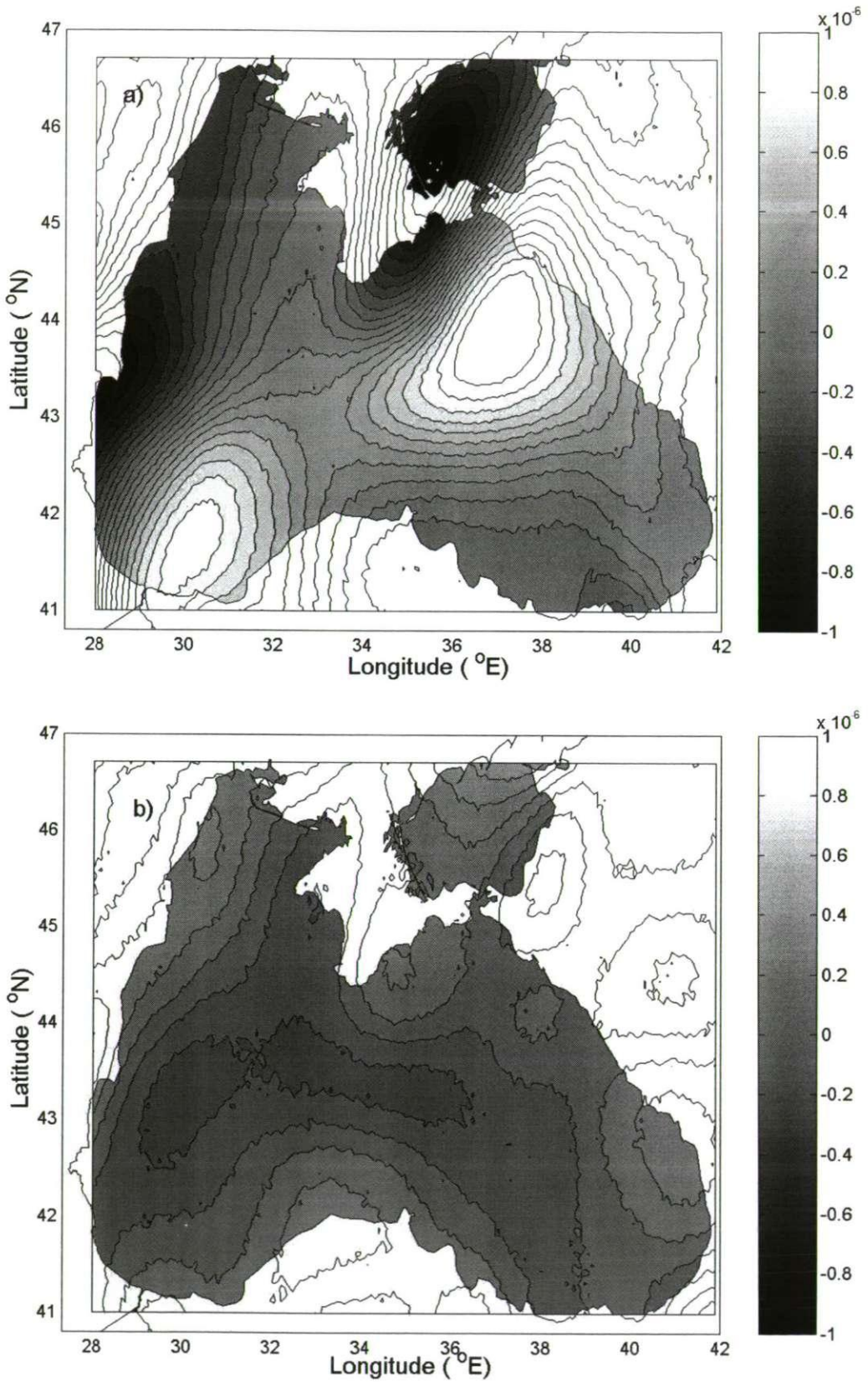
Figure 7.4 Wind stress curl fields (N/m³) averaged during the weeks of maximum and minimum enstrophy which are respectively a) 7-14 May of 1998 and b) 15-21 May of 2000.
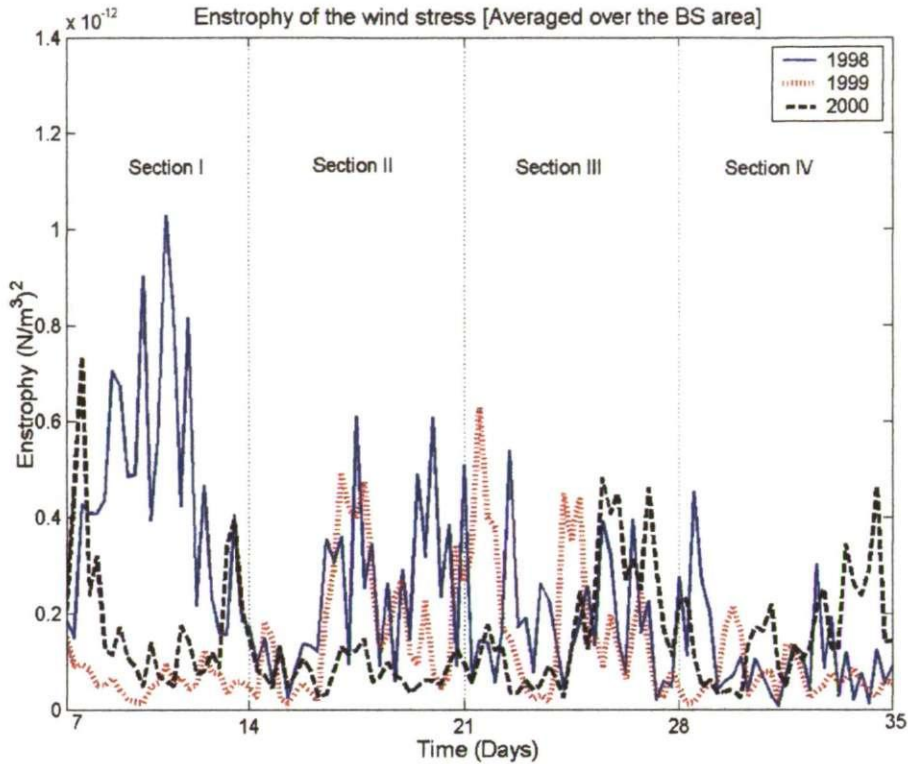
Figure 7.5 Time series of the enstrophy of the wind averaged over the Black Sea area from the 7 May to the 5 of June

7.4. The Black Sea modelled hydrodynamics during May – June of the years 1998, 1999 and 2000

The hydrodynamics of the Black Sea during May and June of the years 1998, 1999 and 2000 as well as the interannual variability during those three years are presented based upon the numerical simulations described in Section 7.2. The results presented are mainly related to the time period from day 7 to day 35 of the simulation (7 of May to 5 of June). This period is representative of the features, anomalies and interannual variability encountered during the simulations. In addition to the figures included in this section, a complete set of figures covering the period of the simulations (1 of May to 30 of June) is attached in the Appendix.

The figures for each one of the simulations (1998, 1999 and 2000) include:

1. Maps of temperature, salinity, current velocity, curl and enstrophy of the currents at various vertical levels (7.5, 45, 75, 105, 310 and 400 m depth) for the following days of the run: 7, 14, 21, 28, 35, 42, 49 and 56.

2. Daily maps of temperature, salinity, and current velocity at the surface (7.5 m depth).

3. Vertical transects of temperature, salinity and velocity at the selected zonal and meridional transects located as detailed in Table 7-2 and shown in (Figure 3.8 – Chapter 3).

Zonal	1	42.50° Latitude N
	2	43.13° Latitude N
	3	44.07° Latitude N
Meridional	1	31.24° Longitude E
	2	33.74° Longitude E
	3	37.90° Longitude E

Table 7-2 Location of the vertical transects.

7.4.1. Thermo-haline structure

The temperature and salinity maps corresponding to the day 35 of the numerical simulations are presented in Figure 7.6 and Figure 7.7 showing the horizontal distribution at 7.5 m depth (surface layer) and at 45 m depth (approximately at the upper boundary of the Cold Intermediate Layer) for the three different runs (1998, 1999 and 2000). These maps together with the vertical cross-sections (Figure 7.8) show the general characteristics and particular features of the thermohaline distribution present in the runs. The highest

158

temperatures at the surface were located in the south-east and in the northern part of the north-western shelf with temperatures reaching 13° C with the warmest patches found especially at the centres of anticyclones. The coldest water in general is in the areas of the shelf break all around the basin except for the south-eastern part of the basin.

The surface temperature maps provide a reflection of the nature of the currents, e.g. the stream of the Rim Current in the eastern coast advecting warmer water to the north-west, the presence of gyres (e.g. warmer patch in the south-western part of the central basin) and mesoscale features (e.g. the cold finger meandering anticyclonically at the east of the Crimean peninsula).

The general circulation was more intense in the year 1998, with a stronger defined Rim Current and sharper zonal temperature gradient than during 1999 and 2000 (Figure 7.6. Left panel). A stronger Rim Current jet is more able to delimit the coastal area restricting the coastal-deep sea interaction. The same figure shows that the surface temperature in the western area was lower during the year 1998 than during the other two years. At 45 m depth (plots of the right hand side of Figure 7.6) in the western area the water is warmer during 1998 than during 1999 and 2000. During these two years the warm patches in that area are more localised in the places where anticyclones are present along the shelf break. In the north-eastern area the temperature gradient between the coast and the central part is smooth in the years 1999 and 2000 (plots of the right hand side of Figure 7.6). The salinity maps (Figure 7.7) show some common characteristics between runs: The fresher water at the surface is present in the north-western area resulting from the major river discharges. Moving away from the coast a steep salinity gradient follows towards the sea. The saltier water is located mainly in the central part of the basin and the maximum salinity values are found within patches corresponding to the cyclonic gyres.

The analysis of the interannual variability of salinity shows that the general circulation in the year 1998 simulation was stronger than in the other two years. This is reflected in the more 'confined' coastal waters in the north-eastern part of the basin during 1998. The fresher coastal water occupies a wider area in the results of 1999 and 2000 with a weaker zonal salinity gradient than in the 1998 case (Figure 7.7. Right panel).

At 45 m depth only the year 1998 shows a clear signal of the eastern central cyclonic gyre, lifting the isolines underneath so that the water at its centre is colder and saltier (Figure 7.7. Right panel). Another obvious feature at this depth is the anticyclonic mesoscale eddy at the east of the Crimean peninsula which is well defined in the simulation of the year 2000; there is a weaker signal of it in the simulation of the year 1999 and it is not evident in 1998.

In the vertical (Figure 7.8), the temperature distribution shows that the surface mixed layer reached higher depth in the 1998 run than in 1999 and 2000 (Arrow No.1 in Figure 7.8). During 1998 it reached approximately 25 m in the central part of the basin and down to about 60 m in the area of the western part of the Rim Current. During the other two simulations the surface mixed layer reached about 15 – 30 m depth. The thermocline (Arrow No. 2 in Figure 7.8) is located below the mixed layer and it is sharper during 1999 and 2000 than during 1998. It has a width of about 50 m in all the three scenarios. The Cold Intermediate Layer (Arrow No. 3 in Figure 7.8) is below the thermocline and in the three simulations it is located approximately between 50 and 125 m depth and going deeper in the western part, below the Rim Current jet. Within the Cold Intermediate Layer, the coldest water is located in the western side. The patch of coldest water during 1998 is contained in the shelf by the steep slope of the thermocline in that area while in the years 1999 and 2000 the patch is detached from the shelf break. Below the CIL the temperature

increases with a much smoother gradient than the one above it and the rate of change decreases considerably with depth.

The vertical salinity field shows little difference between the runs. The variations are confined to the upper layer (down to 50 m) with more homogeneous waters during the year 1998 than 1999 and 2000.

7.4.2. Circulation

The multi-scale circulation in the Black Sea is very dynamic and changes within hours. The overall description of the large scale and mesoscale structure of the hydrodynamics and the general differences between the runs is as follows:
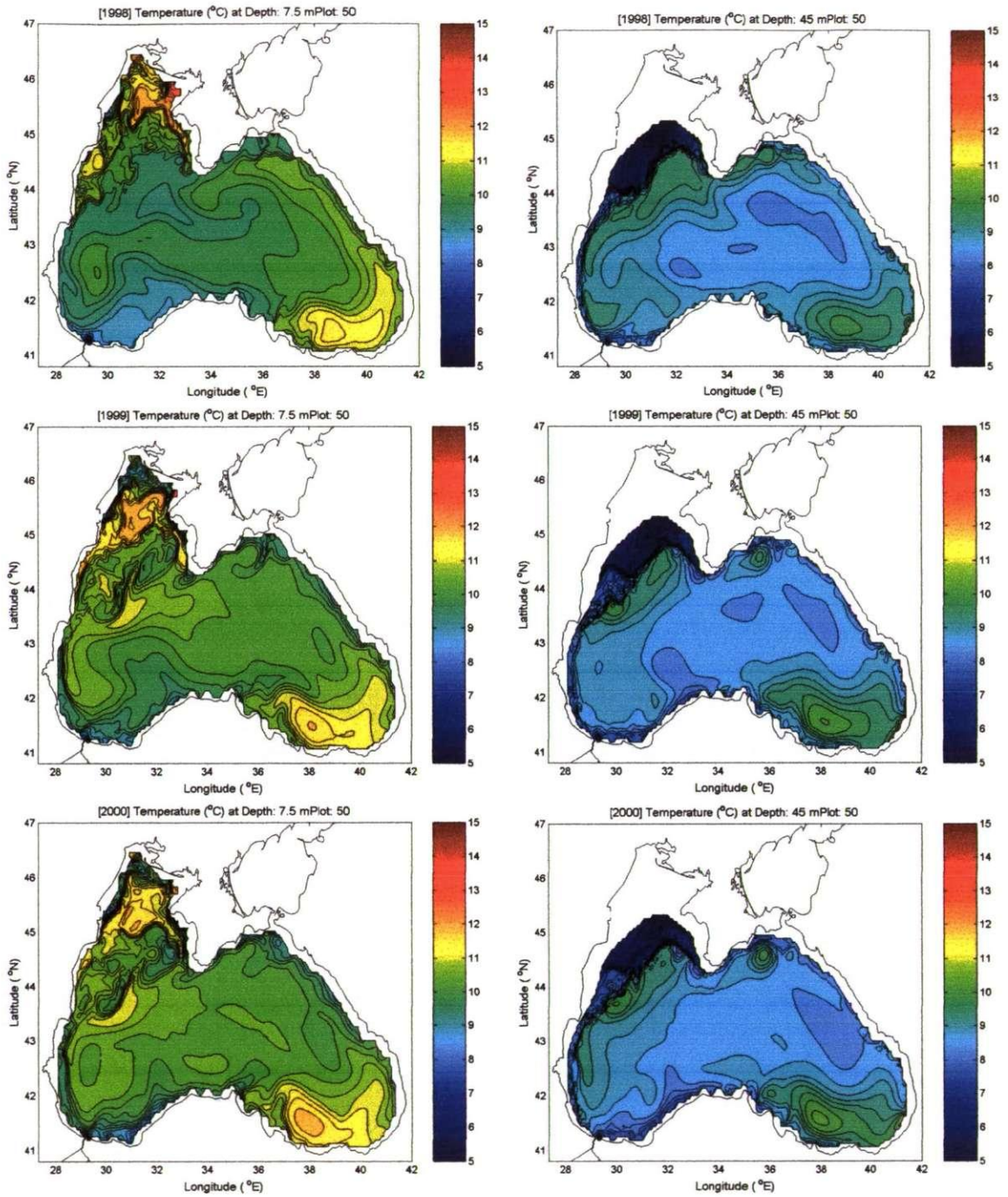
Figure 7.6 Maps of temperature distribution at the depths of 7.5 m (left figures) and 45 m (figures at the right) during the years 1998 (top), 1999 (middle) and 2000 (bottom). All the maps show the distribution at day 35 of the run, which corresponds to the 5 of June.
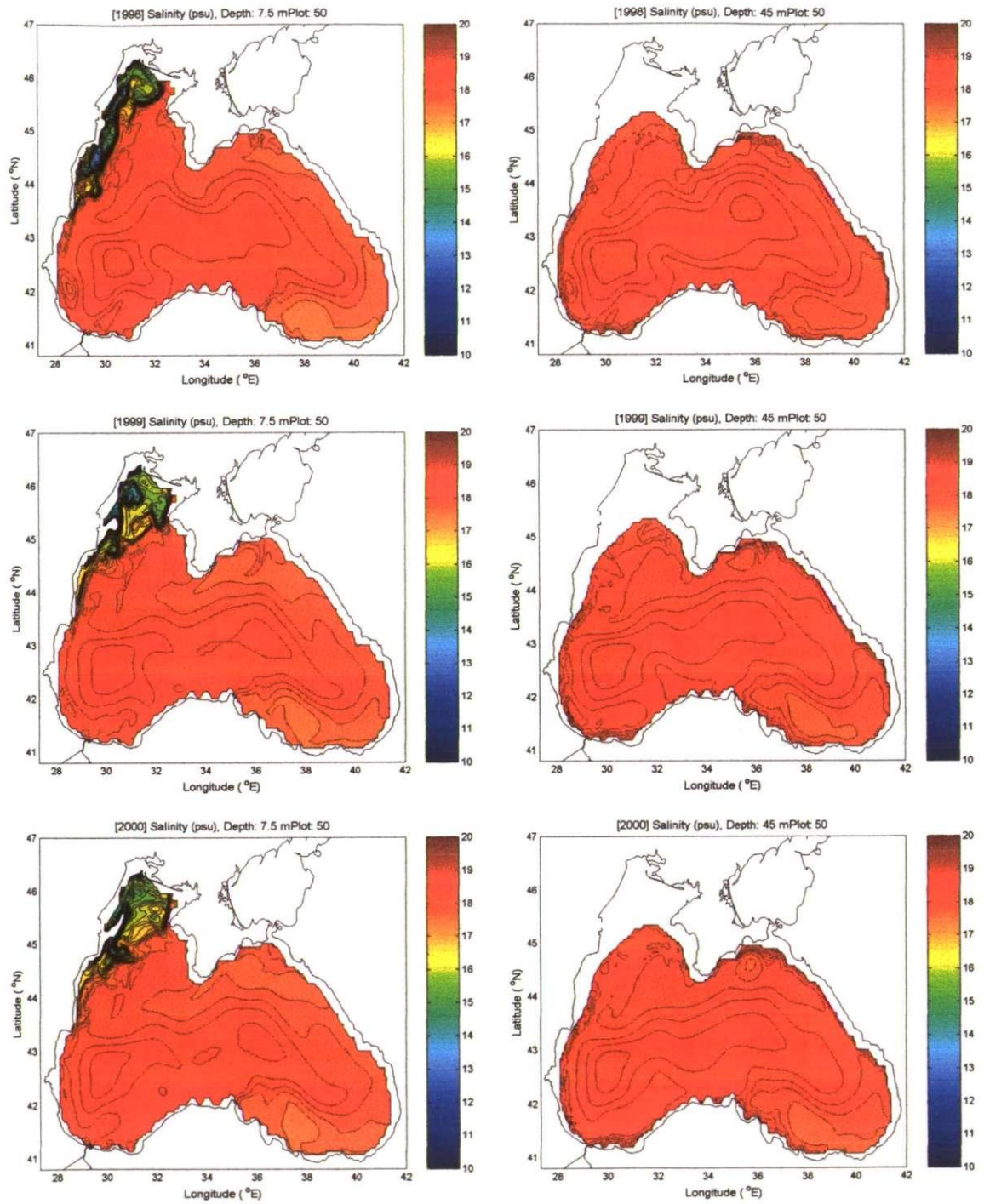
Figure 7.7 Maps of salinity distribution at the depths of 7.5 m (left figures) and 45 m (right figures) during the years 1998 (top), 1999 (middle) and 2000 (bottom). All the maps show the distribution at day 35 of the run, which corresponds to the 5 of June.
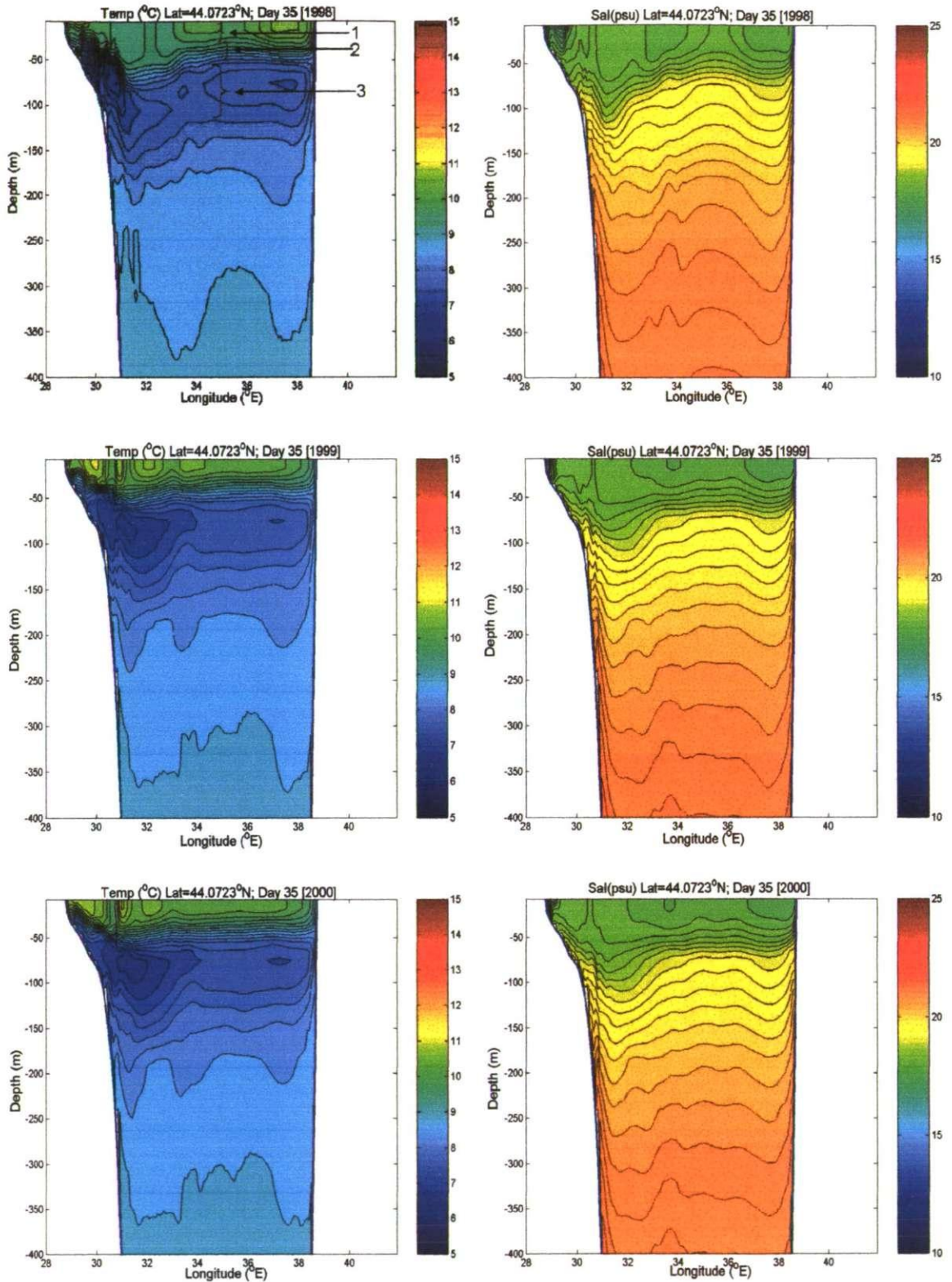
Figure 7.8 Vertical transects of temperature (left panel) and salinity (right panel) from a zonal cross-section at latitude 44°N during the years 1998 (top), 1999 (middle) and 2000 (bottom). All the maps show the distribution at day 35 of the run, which corresponds to the 5 of June.

From the numerical experiments, the wind of 1998 provides the more energetic circulation (Figure 7.9) principally during the first month. The experiments using wind of 1999 and 2000 are similar to each other in terms of energy. As expected, the kinetic energy is larger in the upper layer with high frequency variations occurring down to approximately 100 m depth in all the experiments as shown in Figure 7.10.

During the first week of the simulation, the temperature, salinity and velocity fields gradually become more settled and coherent. Therefore the results presented in this section mainly correspond to the period beginning from day 7 and up to day 35 of the simulations. The circulation patterns at 7.5 m depth corresponding to the 14th, 21st, 28th of May and 5th of June are shown in Figure 7.13. The large, sub-basin and mesoscale surface circulation include the basin wide cyclonic current, Rim Current, flowing around the basin, the sub-basin cyclonic gyres in the central part of the sea and eddies and meanders which differ in number and characteristics within the three years. The Rim Current is approximately 40-60 km wide with speed at the core between 25 and 35 cm/s and reaching maximum velocity of up to 45 cm/s in places where it merges with an anticyclonic eddy.

The Rim Current during 1998 (Figure 7.11) is well defined all around the basin. It meanders in the south and flows well attached to the eastern coast. This pattern of circulation is predominant during the whole first week (7 to 14 of May) which is the week that follows the strongest wind event in the simulations. Therefore during that time the mesoscale activity was not very active with no mesoscale anticyclonic eddies in the coastal zones (Figure 7.11a).
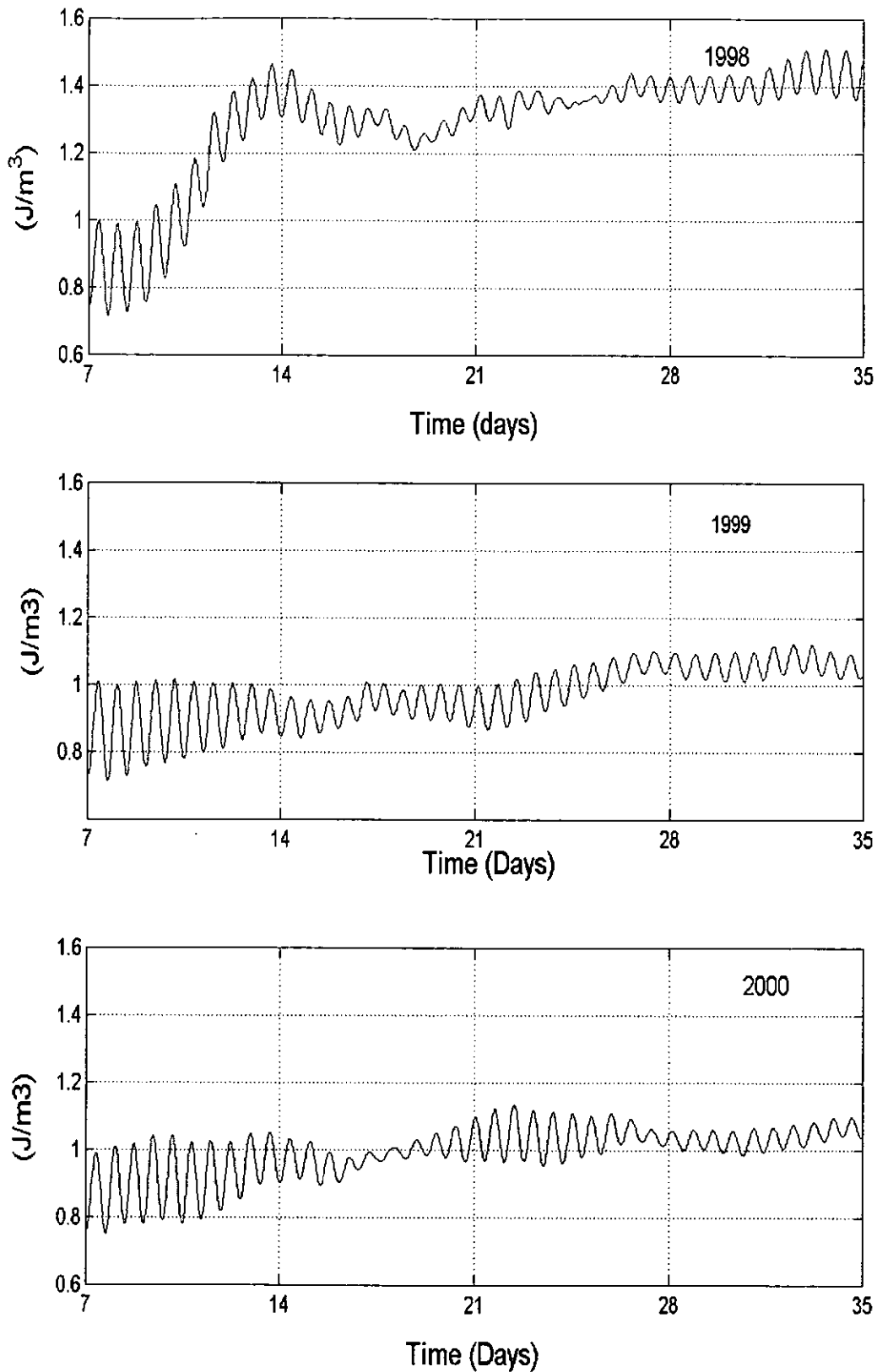
Figure 7.9 Time series of the basin averaged total kinetic energy per unit volume of the modelled currents from the 7 of May to the 5 of June of the years 1998, 1999 and 2000
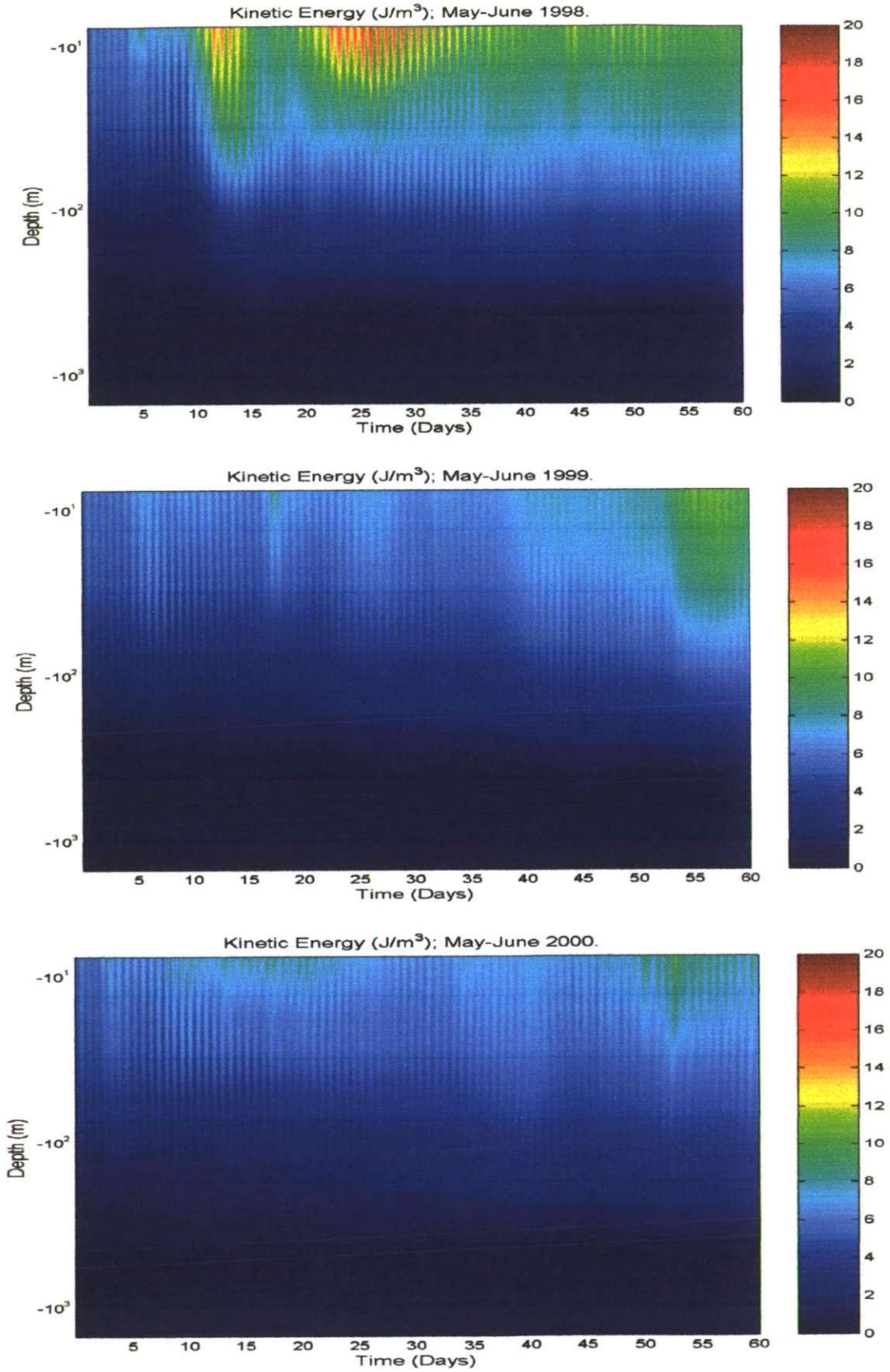
Figure 7.10 Temporal evolution of the averaged kinetic energy and its variation with depth for the years 1998, 1999 and 2000.

During the following weeks of the 1998 simulation the mesoscale activity increased considerably. A total of 12 eddies were identified in the circulation of the 21 of May (Figure 7.11b), namely 2 cyclonic gyres (in the western and eastern central basin) and 10 anticyclones (3 of them were small). Some of these mesoscale eddies are also evident in the temperature field. Their presence is particularly evident at 45 m depth, which is approximately the location of the upper limit of the thermocline highlighting the effect of the lifting and lowering of the isotherms by the cyclones and anticyclones respectively. Some strong gyres may influence the water column down into the pycnocline. For example it is possible to detect the big anticyclones (in the south-eastern area) in the temperature maps at 310 m depth.

During 1999 the circulation (Figure 7.12) was very different than during 1998. The first week (7 to 14 May) shows more mesoscale activity than the first week of 1998. At this time the Rim Current is well defined but it loses continuity in the eastern side of the sea during the second week (Arrow in Figure 7.12b). By the 21 of May the eastern part of the basin seems more like a set of gyres flowing attached to each other. Under these circumstances, the 'boundary' between the central and coastal areas is interrupted close to the middle of the Caucasian coast. The central cyclone (located approximately between 42 and 43° N) gets closer to the coast having the coastal anticyclones at its north and south. The currents at the western side of the basin do not differ from the 'typical' circulation scheme but also show high mesoscale activity.

During the third week of the 1999 simulation the Rim Current approximately recovers its continuity and by the 5 of June it is well defined all around the basin (Figure 7.12c).

The circulation pattern during the year 2000 (Figure 7.13) is somehow an intermediate state between the other two simulations. The Rim Current has more meanders and

instabilities than the year 1998 but does not lose its continuity during the studied period of time, as the 1999 simulation did, and the mesoscale activity is evident all the time.

On the whole, the mesoscale activity during the 1999 and 2000 simulations exceed that of 1998 which had less mesoscale features. In the modelling results, the first evidence of the degree of mesoscale activity in the basin seems to be the number of mesoscale anticyclones (or anticyclonic meanders) close to the shelf break in the north-western area and close to the coast elsewhere. This is very clear when plotting the curl of the currents such as in Figure 7.14 in which negative values reflect anticyclonic vorticity and positive values show cyclonic vorticity.

The more remarkable mesoscale features appearing in the modelling are listed in Table 7-3 and are shown in Figure 7.15. Some of them are present all the time in the three simulations for instance the Crimean anticyclone at the east of the Crimean peninsula, the anticyclones in the south-eastern coast, and the western and eastern central cyclonic gyres. Other features were also present in the three runs but did not last for the full two months, for example the Sevastopol eddy at the west of the Crimean peninsula and some anticyclones along the southern coast. Some other eddies were detected only in one or two of the simulations and for a small time period, such as the Caucasus anticyclone in the north-eastern coast and the Bosphorus anticyclone in the south-western coast.

The depth of penetration of the eddies varies from a couple of metres to more than 400 m depth, as can be seen in Figure 7.16.

Several smaller features which are not listed in Table 7-3, specifically meanders and short lived (couple of days) small eddies, were also detected in the modelled hydrodynamics, being more abundant in the runs of 1999 and 2000.
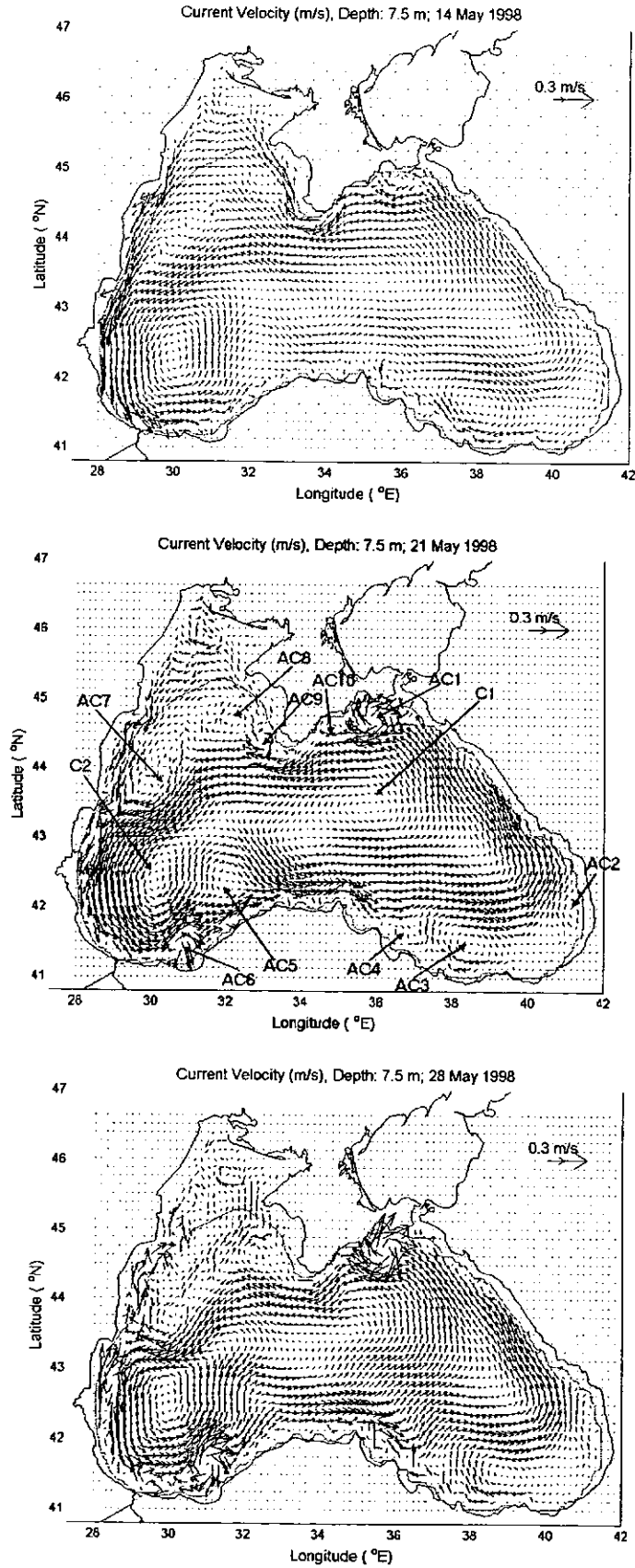
Figure 7.11 Current velocity at 7.5m depth during a) 14 of May; b) 21 of May; arrows show the mesoscale eddies; c) 28 of May of the year 1998.
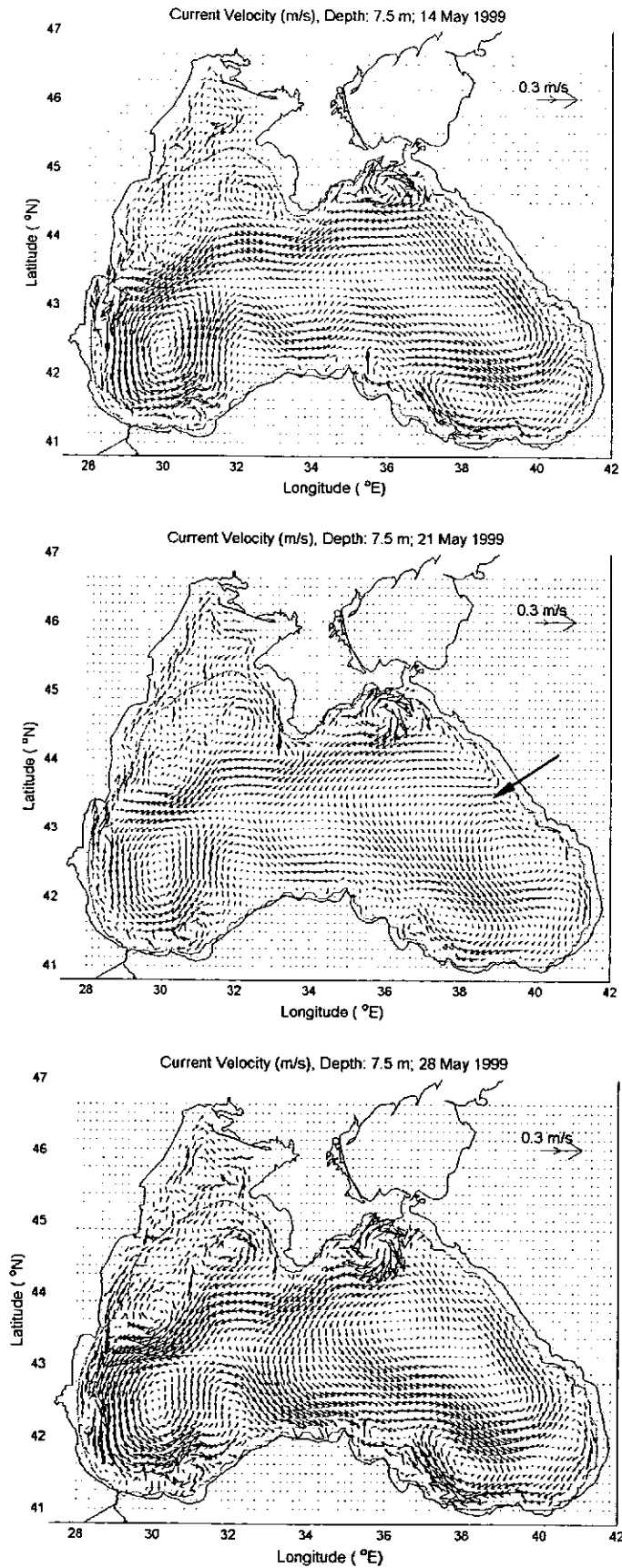
Figure 7.12 Current velocity at 7.5m depth during a) 14 of May; b) 21 of May; c) 28 of May of the year 1999.

171
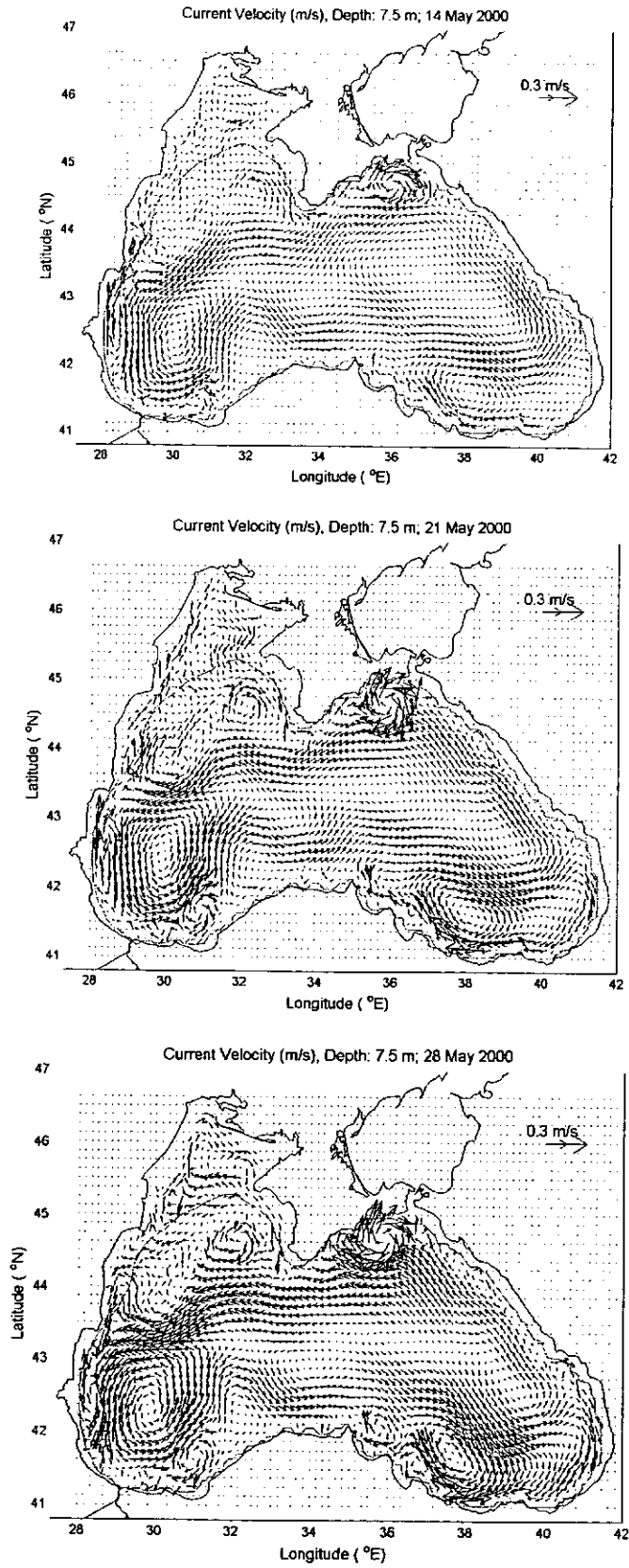
Figure 7.13 Current velocity at 7.5m depth during a) 14 of May; b) 21 of May; c) 28 of May of the year 2000.
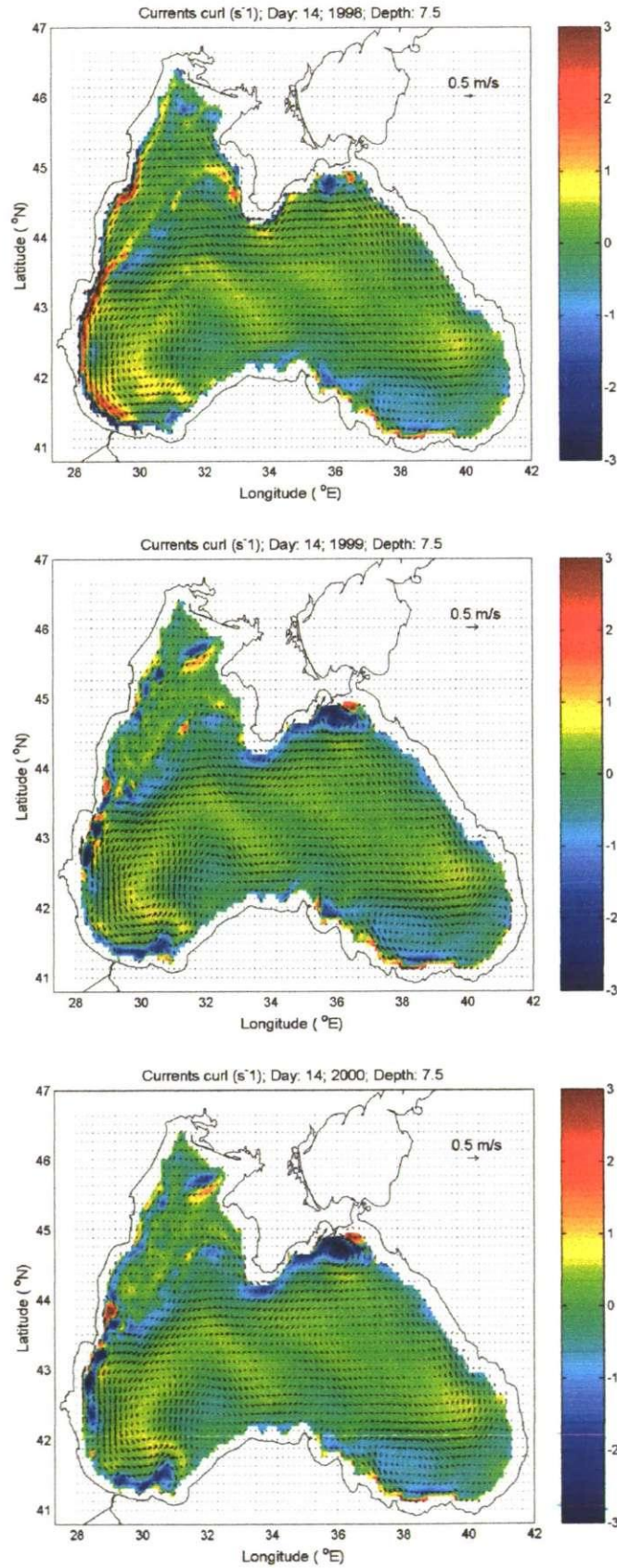
Figure 7.14 Maps showing the curl of the currents (1/s) at 7.5 m depth during the 14 of May of the years a) 1998, b) 1999 and c) 2000.

No.	Mesoscale Structure	Location	Velocity (m/s)	Depth of penetration[1]	Comments
1	Crimean AC	East of Crimean peninsula	.10-.40	350 m	Present all years all the time
2	Caucasus AC	NE coast	.10-.15	100 m	Present in 1999 and 2000 and not all the time
3	Batumi eddy	South-eastern corner	.10-.18	400 m	Present in 1999 and 2000 all the time.
4	Anticyclone	South coast at 38 E	.10-.30	~200 m	In 98 is smaller, rounder and located more to the east than in 99 and 00. Present all the time.
5	Kizilirmak anticyclone	South coast ~ 35 - 36 E	.10-.30	~200 m	In 98 and 99 is not well defined as in 2000.
6	Sakarya anticyclone	South coast at ~31 E	.15-.25	> 800 m	Is more energetic in 98. Present all the time.
7	Bosphorus AC	SW coast	.15-.35	~200 m	Present all years but not all the time.
8	Kali-Akra AC	Western coast at ~ 44 N	.10-.25	-	Present all years but not always well defined in 1998
9	Sevastopol AC	West of Crimean peninsula	.10-.20	~400m	Present all years but not always well defined in 1998
10	Western cyclonic gyre	Central south western part	.10-.30	-	Present all years all the time
11	Eastern cyclonic gyre	Central eastern area	.10-.20	-	Present in 1999 and 2000.

Table 7-3 Mesoscale eddies present in the runs

[1] *Vertical penetration of the eddies during the day shown in Figure 7.15*
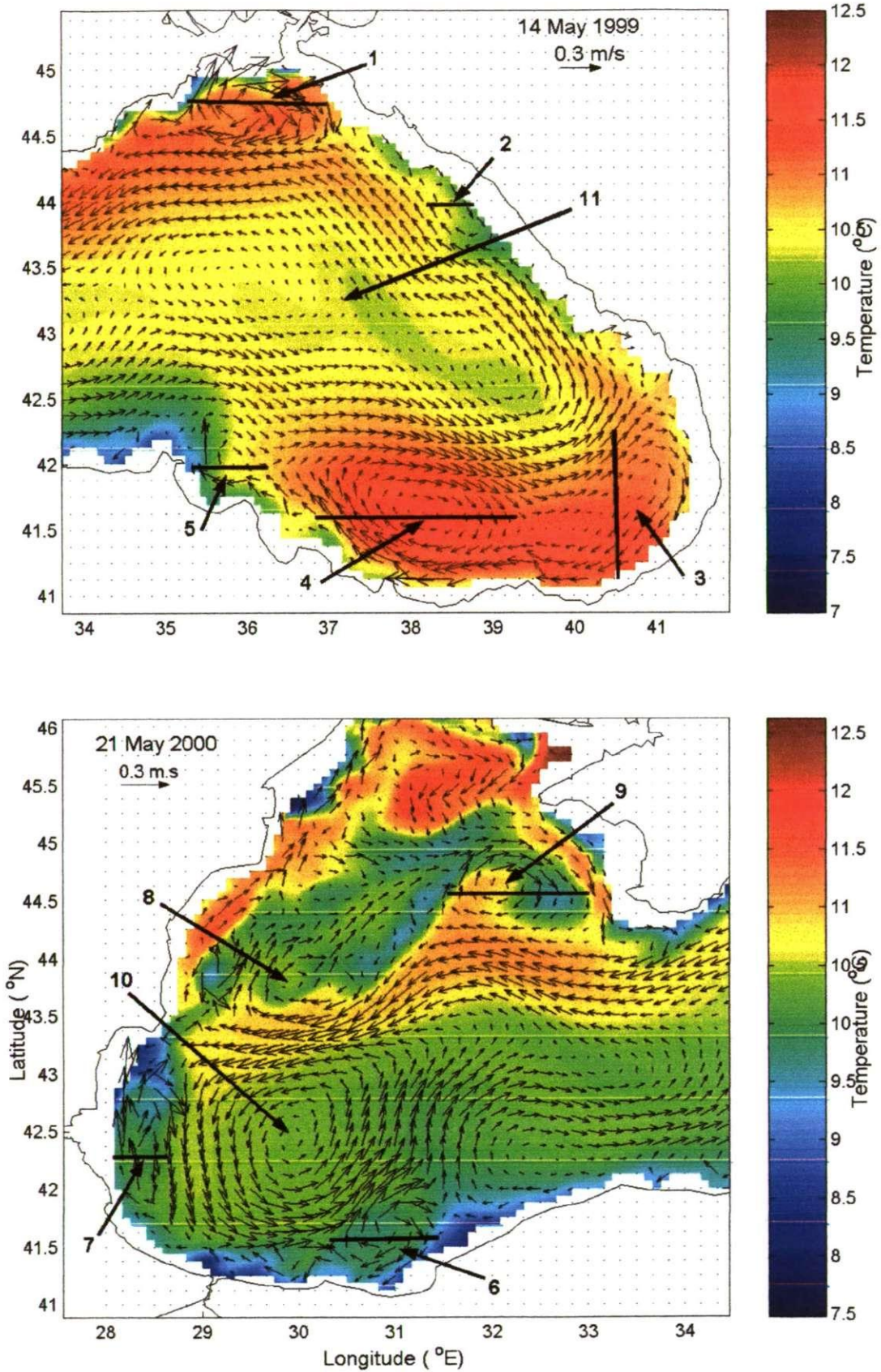
Figure 7.15 Mesoscale features present in the modelling. Numbers corresponding to Table 7-3 and dark lines showing the location of vertical transects.

175
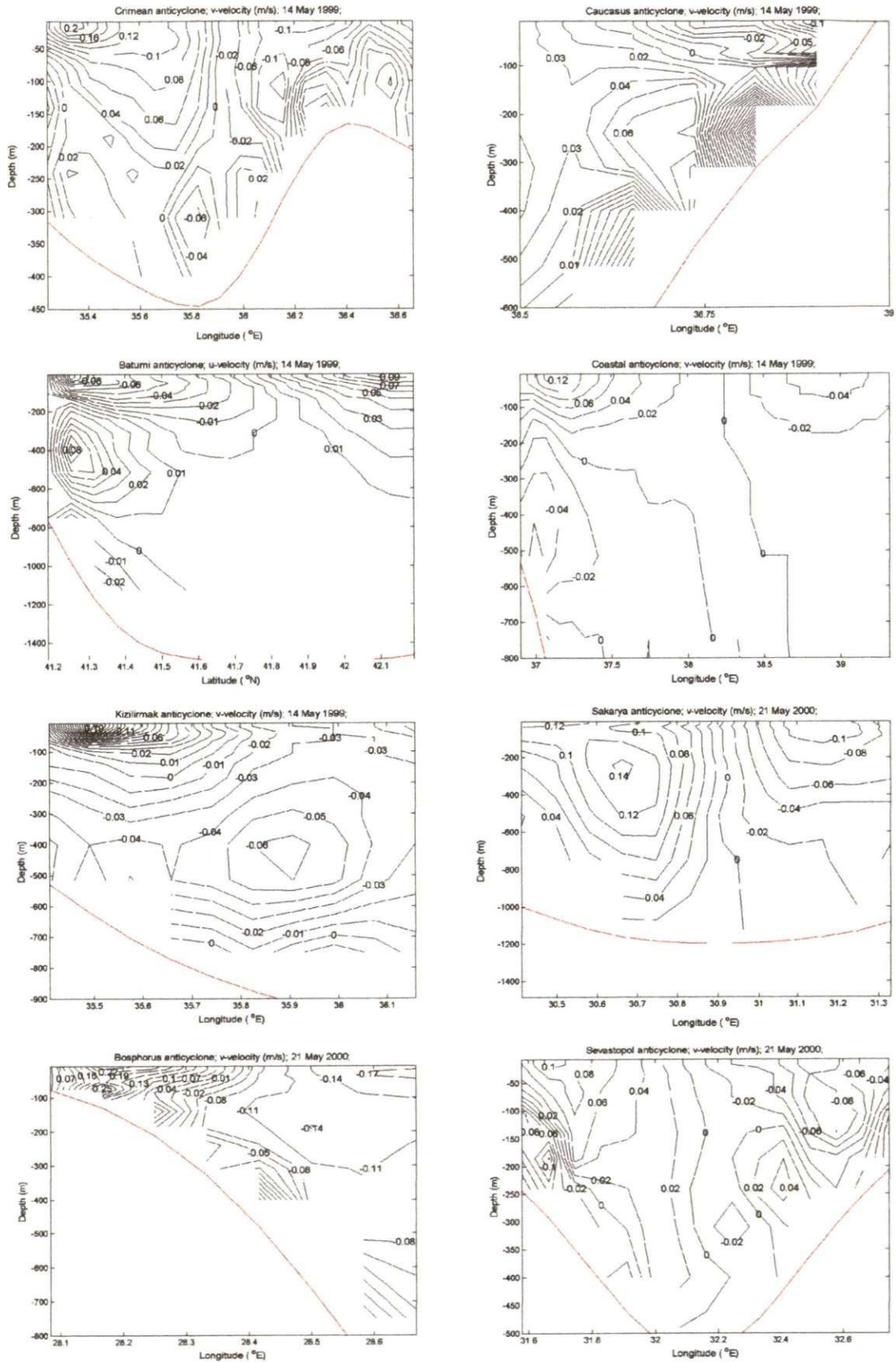
Figure 7.16 Vertical cross-sections of the horizontal velocity structure of mesoscale eddies No. 1, 2, 3, 4, 5, 6, 7, and 9 (Table 7-3). Location of the transects is shown in Figure 7.15

7.5. Summary

This chapter presents the results of the numerical experiments carried out to study the general and mesoscale circulation of the Black Sea. Following the hypothesis suggesting that the wind forcing is the major responsible on the variability of the mesoscale circulation (Zatsepin et al., 2002) the interannual variability of the hydrodynamics was evaluated by forcing the model with wind data from three different years, 1998, 1999 and 2000 and with climatic heat flux, evaporation, precipitation and river data. The wind fields during May and June of the years 1998, 1999 and 2000 were analysed. The wind of the year 1998 was in general the more energetic and had a cyclonic tendency. It had also the highest value of enstrophy and maximum values of wind curl. The wind fields during 1999 and 2000 shows similar characteristics between them in terms of energy, curl and enstrophy. However, the wind during 2000 was slightly more energetic than the one of the year 1999.

The thermo-haline distribution resulting from the numerical experiments show that the highest temperatures at the surface are in the south-east and in the northern part of the north-western shelf with temperatures reaching 13° C. The coldest patches at the surface are located especially at the centres of the anticyclones and near shelf break all around the basin except for the south-eastern part of the basin. The temperature maps show the Rim Current, the sub-basin scale gyres and several mesoscale eddies. The salinity maps show the fresher water close to the coast of the north-western shelf followed by a steep salinity gradient towards the sea. The saltier water is located mainly in the central part of the basin and the maximum salinity concentrations are within patches corresponding to the cyclonic gyres. In the vertical, the temperature distribution shows that the surface mixed layer is deeper in the 1998 run than in 1999 and 2000. The thermocline is located below the mixed

layer and it is sharper during 1999 and 2000 than during 1998. It has a width of about 50 m in all the three scenarios. The CIL is below the thermocline and in the three simulations it is located approximately between 50 and 125 m depth and going deeper in the western part, below the Rim Current jet.

The current fields resulting from the experiments show that the one using wind of 1998 was the more energetic. The large, sub-basin and mesoscale surface circulation include the Rim Current, the sub-basin cyclonic gyres in the central part of the sea and eddies and meanders which differ in number and characteristics within the three years. The Rim Current is approximately 40-60 km wide with speed at the core between 25 and 35 cm/s. The 1999 and 2000 the circulation show much more mesoscale activity than the 1998.

CHAPTER 8. DISCUSSION AND CONCLUSIONS

8.1. Introduction

The aim of this research is to investigate the mesoscale circulation in the Black Sea based on numerical modelling experiments with emphasis on establishing if mesoscale activity is directly influenced by the temporal and spatial variability of the wind in the Black Sea area. Prior to this research most of the numerical studies have used climatic wind forcing data, which is considerably smoother than the real wind. To evaluate the significance of the influence of the wind variability on the mesoscale variability of the currents, we used NCEP re-analysis high resolution (6 hr) wind allowing the inclusion of the spatial and temporal variability of the wind fields in the model forcing.

The findings of the present research are of particular significance since they provide an unprecedented account of the influence of the wind variability on the mesoscale activity in the Black Sea. This was achieved by:

- Characterising the mesoscale circulation during October-November 2000 in the Black Sea from observational data (Chapter 4).

- Using the POLCOMS 3-D numerical model to simulate the Black Sea hydrodynamics (Chapter 5).

- Validating the Black Sea model against observations (Chapter 6).

- Using the Black Sea model to simulate the hydrodynamics and to study the interannual variability of the circulation by using wind forcing data from different years (Chapter 7).

In this chapter we examine these results and their significance in the context of existing knowledge.

8.2. Mesoscale circulation in the north-eastern part of the Black Sea during October-November 2000.

Hydrographic data measured at high spatial resolution provide a 3 dimensional 'snapshot' of the complex dynamical activity occurring in an area. This kind of study is considerably expanded if it is complemented with remote sensing data analysis, which expands the spatial coverage and provides the time evolution of processes by compiling sequences of 'snapshots' to produce animations. However, the remote sensing only gives information at the surface and the time-evolution of the water column can not be obtained.

The general and mesoscale hydrodynamics during October-November 2000 were characterised with the combined analysis of CTD data from the north-eastern part of the Black Sea and sea surface temperature images of the whole Black Sea (Chapter 4). Results of the analysis showed pronounced mesoscale activity in most of the basin except for the north-eastern area where mesoscale activity was scarce. The temperature structure showed a clear lateral gradient from the north-west to the south-east which is the typical distribution throughout the year (Oguz et al., 1993). The circulation of the Black Sea during this time showed several features from the general circulation including the Rim Current flowing cyclonically around the basin, mesoscale eddies in the central and coastal areas, and meanders and filaments all over the Black Sea basin.

The central basin was mainly dominated by cyclonic circulation. A striking feature was a cold patch covering a large area (about the size of the Crimean peninsula) which was identified in the SST images in the northern central basin. The cyclones generate lifting of the isotherms below them and may erode the thermocline.

Results from CTD analysis verify the vertical characteristics of the Black Sea including the surface mixed layer, the strong stratification and the Cold Intermediate Layer dividing the upper layer from the bottom layer.

The Rim Current appeared strong and well defined. The geostrophic velocities in the north-eastern part of the Black Sea coincide with typical velocities of the Rim Current in that area and show that the stream of the Rim Current was flowing very close to the coast. According to Zatsepin et al. (2002b) the intensification of the Rim Current and its location close to the coast in the north-eastern part of the sea during the autumn of 2000 were due to the cyclonic vorticity of the wind over the Black Sea on that area during the summer and autumn of that year. When the Rim Current is either deflected far from the coast or too close to the coast, it may allow other currents such as eddies to exchange material or properties between the coastal and the open sea water masses, having important implications on mixing and transport processes.

Several mesoscale eddies were identified in the Black Sea basin during the autumn of 2000. Their diameters varied from about 10 to about 90 km, and their drifting velocities ranged from 0.1 to 0.15 m/s. One of those eddies was present in the north-eastern area at the time of the hydrographic campaign and was characterised from the results of both CTD and remote sensing analysis. The dimension, vertical structure and drifting velocity of this small eddy were obtained from the analysis. Small eddies with similar characteristics to this one have been observed in the area (e.g. Krivosheya et al., 1998b).

In general the form, scale and velocities of mesoscale structures obtained from this analysis agree with observations reported in the literature (e.g. Ginzburg et al., 2002a; Ginzburg et al., 2002b; Krivosheya et al., 1998; Oguz et al., 1994; Zatsepin et al., 2003).

8.3. Set up of POLCOMS model for the Black Sea

Our ability to comprehend and explore oceanic processes, monitor the currents, and to a limited extent even predict their future state is vastly increased by using numerical ocean models in combination with observed data. When the models are properly validated their results can be trusted and they may be used as laboratories for numerical experiments opening more windows into our knowledge, e.g. it is not possible to modify the direction or magnitude of the wind in nature to evaluate the impact on the ocean currents, while with the aid of numerical models one can study a huge range of different scenarios.

The choice of a particular ocean model depends very much on the intended application and the computational and pre- and post-processing capabilities available. The degree of success of the modelling depends on the fidelity with which it can simulate the targeted processes. As a guide, a comprehensive review of the coastal and shelf-sea modelling in the European context is given by J. E. Jones (2002), including an inventory of models, model inter-comparisons, different modelling techniques presently used and other relevant information.

We chose to use the Proudman Oceanographic Laboratory Coastal Ocean Modelling System (POLCOMS), which is a three dimensional baroclinic model. The more relevant reasons to select POLCOMS model for our studies include:

i. The Black Sea has large areas of continental shelves and deep sea and POLCOMS model has been developed to incorporate features suitable for the modelling of baroclinic processes on the shelf, at the shelf slope and in ocean regions, allowing coupled ocean-shelf simulations. POLCOMS has been successfully applied to various seas including the North Sea (Holt and James, 2001) and more recently, the European Shelf, the Irish Sea, the Liverpool Bay and the San Quintin Bay in the Mexican Pacific (A. Souza, personal communication, 2004).

ii. Because the target of this research is the mesoscale circulation, it is important to be able not only to resolve, but also to preserve eddies. POLCOMS model includes a sophisticated advection scheme, the "Piecewise Parabolic Method", which has excellent feature-preserving properties. It has been very successful simulating river plumes (James, 1997), fronts (Proctor and James, 1996), transport of tracers from localized sources (Holt and James, 1999), thermohaline structure and currents (Holt and James, 2001), etc. Moreover, the model is formulated on an Arakawa B grid (1966) in contrast to the C grid used in many shelf sea models. The B grid is more commonly used in deep ocean models and is well suited to the modelling of horizontal density variations since the Coriolis term can be calculated without averaging. This helps prevent the dispersion of the velocity features associated with fronts, in contrast with the C grid which requires averaging over a number of points to calculate this term (Holt and James, 2001).

iii. We judged convenient the use of σ - or s-coordinates in the vertical, which follow the bottom topography, to avoid the step like representation of the sea bed resulting from z-coordinate models. Because a large area of the Black Sea is very deep (more than 2000 m), the use of s-coordinates was more appropriate since they are a refinement of the σ -coordinate scheme which attempt to increase resolution in the surface layer or in any other area of interest.

One of the well-known disadvantages of σ - and s-coordinates is that the levels are inclined in areas of steep bottom topography. The horizontal pressure gradients on these levels acquire a vertical component which may generate false circulation in the results. POLCOMS model deals with this problem by first interpolating the different parameters (e.g. density) in the vertical so that they are at the same depth level and the pressure

183

gradients are calculated in z-levels and not in σ-levels. Nevertheless, because the Black Sea has a very steep continental slope a test was carried out specifically to evaluate the effect of the bottom topography in the modelled currents (Chapter 5- Section 5.3) and the results are discussed below.

This is the first study using POLCOMS model to simulate the Black Sea hydrodynamics and therefore it is compulsory to perform sensitivity tests to build an adequate set up which gives reliable results. The parameters tested were the bottom topography, the time steps, the grid discretisation and the horizontal diffusion coefficient.

All these parameters proved to have an effect on the modelled results. Moreover, these variables are linked and related to each other so that the best set up has to be the combination of the more suitable parameters.

Based on the results of the sensitivity tests the best set up achieved was the Run No. 13 (Table 5-1) which used a fine grid with latitudinal resolution of 1/16° and longitudinal resolution of 1/12°, corresponding to a spatial resolution of approximately 6.7 km, a barotropic time step of 20 s, a baroclinic time step of 200 s, and *AHC* of 0.2 m/s (factor multiplied by the depth at each point to obtain the horizontal diffusion coefficient), with a critical horizontal diffusion coefficient value of 600 m²/s (*AHCrit*). Therefore this was the set up which was used for the main numerical experiments.

Sensitivity to grid resolution

The fine grid with spatial resolution of approximately 6.7 km is the best option for these studies giving good results in reasonable computing time. A higher resolution grid of approximately 3.4 km (x-fine grid) did not improve the modelled results and its use was extremely expensive in terms of computational time and storage capacity. Therefore it was regarded as not suitable for performing the nature of the experiments for this research

project. A coarser grid with approximately 25.6 km resolution does not give good results for this kind of study since is not able to resolve mesoscale eddies and is not stable in combination with the existing bottom topography. It does give some reproduction of the general circulation which includes the Rim Current and some of the semi-permanent gyres in the deep sea. Therefore it was used as a preliminary model for all the subsequent tests.

Sensitivity to bottom topography

As an initial test, the model's performance with the Black Sea bottom topography was evaluated by running the model for 6 months with homogeneous density. This avoided the vertical friction that a stratified fluid would have, mitigating the effect of the bottom topography. Using the fine grid (Table 5-2) the model performance was satisfactory but with the coarse grid false velocities were generated in areas near the shelf break where there are steep changes in the bottom topography.

Sensitivity to time step

The best time steps to use with each different grid were investigated. From these tests the main result was to find that the model is very sensitive to variations in the baroclinic time step but not so sensitive to variations of the barotropic time step. This situation allows a certain range of flexibility to save computational time. This result is not only valid for the Black Sea set up since based on our findings, the results of a completely different study using the POLCOMS code to model the hydrodynamics of the Irish Sea were significantly improved (P. Osuna-Canedo, personal communication, 2004). For the preliminary tests with the coarse resolution grid, the best performance is obtained when using a barotropic time step of 20 s or less and a baroclinic time step not exceeding 400 s. For the main

numerical experiments, which used the fine resolution grid, the barotropic time step should be 20 s or less and the baroclinic time step no more than 200 s.

Sensitivity to horizontal diffusion coefficient

The sensitivity tests to the horizontal diffusion coefficient showed that with higher values of this coefficient, the results have lower magnitude velocities, but wider currents.

The use of *AHC* = 0.2 m/s gave the more realistic result in terms of magnitude and scale of the currents.

8.4. Inertial oscillations in the Black Sea (numerical study)

Once the optimal set up for the Black Sea model was obtained, the model was initialised using the geostrophic adjustment approach and the results were validated against current meter measurements analysing the high frequency oscillations (periods of less than 24 hrs) of the basin (Section 6.3.2) and by qualitatively comparing the model output with the general knowledge of the Black Sea hydrodynamics (Section 6.3.1).

The current measurements arose from the drifter experiment in the Black Sea during September-December 1999 (Zhurbas et al., 2004) and provided the frequency and energy of the oscillations from the measured velocities. The model results are based upon the calibrated simulation (Run No. 19) initialised by geostrophic adjustment and subsequently forced with monthly climatic heat fluxes, evaporation, precipitation and river data for May and high frequency (T=6 hr) wind forcing of May of the year 1999 as detailed in Table 6-3. Although the comparison between eulerian velocities from the model output with lagrangian measurements of the drifters may add a source of error to the results, the modelled output in terms of the frequency and energy of the inertial oscillations is in good agreement with the measurements. The spectral analysis of the modelled velocities show a

dominant peak at 17 hrs corresponding to the inertial frequency of the Black Sea and two smaller peaks at periods of 36 hrs and 256 hrs which are typical for mesoscale eddy motions. These peaks occur at similar frequencies to those found in observations (Zhurbas et al., 2004) (Figure 6-19) and also agree with the results of the modelling study on the oscillations of the Black Sea basin carried out by E. Stanev and J. Beckers (1999).

The kinetic energy of the inertial oscillations was calculated from the velocity components and the average of all the selected points from the model is 3.47×10^{-3} m^2/s^2 while the averaged energy of the drifters is 4.25×10^{-3} m^2/s^2.

The biggest difference between the model and the measurements was with drifter 30 (Figure 6-15). A possible reason for such a difference is that during the measurements this drifter was located in the centre of an anticyclonic eddy which is not present in the model results. It is known that the areas of anticyclonic vorticity in the ocean (frontal interfaces on the sides of waters with smaller density, warm rings of the Gulf Stream and others) represent a kind of a trap for inertial oscillations, whose energy may increase almost by an order of magnitude compared to the adjacent waters (Kunze, 1985).

Overall, our results show that the large scale circulation features, including the Rim Current are not evident permanently in instantaneous 'snapshots' as they were described in the traditional literature, but they are perfectly clear as residual currents when averaging during one inertial period. Other investigations support this result stating that the Rim Current represents neither a stationary nor a continuous current (Zhurbas et al., 2004; Zatsepin et al., 2002b; Zatsepin et al., 2003; Latun, 1989).

To look at the mesoscale currents more accurately and in order not to process an unreasonably large amount of data, the model output from the main simulations was averaged for 17 hr intervals (approximately the inertial period in the Black Sea).

8.5. Circulation and thermo-haline structure in the eddy-resolving Black Sea hydrodynamic model.

A qualitative synoptic assessment of the model prediction of the circulation and thermo-haline distribution over the Black Sea domain was made. The description is based on the results from the main simulations, which after geostrophic adjustment (detailed in Section 6.2) were forced with monthly climatic heat fluxes, evaporation, precipitation and river data for May and high frequency (T=6 hr) wind forcing data of May for three different years, 1998, 1999 and 2000.

The results show that the model is able to accurately generate and maintain the structures of the current, temperature and salinity fields which characterise the Black Sea basin as described in Chapter 2.

The upper layer circulation shows large, sub-basin and mesoscale circulation features. The Rim Current flows cyclonically around the basin developing meanders and gyres with velocities of 0.1 – 0.22 m/s. The central part of the sea has mainly cyclonic circulation and the coastal areas are dominated by anticyclonic circulation. All of the semi-permanent eddies included in the 'typical circulation scheme' presented by Oguz, (1993) (Figure 6-14) appear at least during some period of time in the simulations as detailed in Table 7-3. These eddies include the Sevastopol, Crimea, Kali-Akra, Batumi, Caucasus, Kizilirmak and Sakarya anticyclones, the eastern and western cyclonic gyres in the central basin and a number of smaller and short-lived eddies all around the Black Sea. Their shapes, sizes and velocities are in well agreement with *in situ* and remote sensing observations during October-November of 2000 (described in Chapter 4) and during other seasons as described in the literature review (Chapter 2).

The modelled temperature field also agrees with the Black Sea temperature structure. In general the maximum temperature at the surface is located in the south-east and in the northern part of the north-western shelf with temperatures reaching 13°C, with the warmest patches at the centres of the anticyclones. The coldest water in general is in the areas close to the shelf break all around the basin except for the south-eastern part. It is also clear the presence of cold water in areas with high current velocities such as the places in which an anticyclone coincides with the Rim Current. This situation is especially evident with the Crimean and Sevastopol anticyclones.

The salinity fields show that the fresher water at the surface is in the north-western area where the major rivers discharge. In general the coastal water has lower salinity and further from the coast there is a steep salinity gradient. The saltier water is located in the central part of the basin and the maximum salinity concentrations are within patches corresponding to the cyclonic gyres.

The temperature and salinity structure at 45 m depth show a clear signal of some of the mesoscale features. For example the central cyclonic gyres generate lifting of the isolines below so that the water at its centre is colder and saltier. The anticyclones produce the opposite effect.

In the vertical the temperature distribution shows a surface mixed layer reaching between 15 and 35 m depth in the simulations using the wind of 1999 and 2000, while in the 1998 simulation, the mixing attained higher depths (approximately 25 m in the central part of the basin and down to about 60 m in the area of the western part underneath the Rim Current). The thermocline is located below the mixed layer and it is sharper during the years 1999 and 2000 than during 1998. It has a width of about 50 m in all the three scenarios.

The Cold Intermediate Layer is below the thermocline between 50 and 125 m depth and lies deeper in the western part, below the Rim Current jet. Within the Cold Intermediate

Layer, the coldest water is located in the western side. In 1998 it appears that the cold water cascades from the continental shelf, and further extends its propagation towards the rest of the basin. The cascading event seems similar to those observed worldwide (Shapiro et al., 2003)

Below the Cold Intermediate Layer the temperature increases with a much smoother gradient than the one above it and the rate of change decreases with depth, reaching temperatures of approximately 9.1 °C.

The salinity always increases with depth. At the surface the salinity ranges between near 0 *psu* at the river mouths to more than 18 *psu* in the central basin. The increase in salinity is small in the surface mixed layer, then the halocline has the biggest rate of change and in the deeper layer the salinity smoothly increases down to the bottom. For example, the vertical salinity profile during day number 17 of the 1998 simulation at one location (43.4° latitude N and 32° longitude E) shows the following rates of change of the salinity with depth: in the surface mixed layer (between 7.5 and 30 m) the salinity increases approximately 6.7×10^{-4} *psu* every metre; in the steeper part of the halocline (from 30 to 200 m) the rate of change is 1.3×10^{-2} *psu*/m; between 200 and 500 m depth the salinity increases at a rate of 3.3×10^{-3} *psu* per metre and from 500 m down to the bottom the changes are much smaller (about 6.7×10^{-4} *psu*/m).

8.6. Interannual variability of the wind and hydrodynamics in the Black Sea during May-June (1998, 1999 and 2000)

It is known from *in situ* observations, satellite images and laboratory experiments that the wind is a very important factor influencing the water circulation, but there has been a debate on the degree to which different properties of the wind affect the currents. In the

Black Sea basin two different properties of the wind have been proposed as the major influence on the variability of the mesoscale circulation, namely the curl of the wind stress (Zatsepin et al., 2002a), and the wind stress itself (G. Shapiro, personal communication, 2000).

Knowing the characteristics of the wind fields during 1998, 1999 and 2000 it is possible to understand the differences between the modelled hydrodynamics forced by those winds. The averaged distributions of the circulation and thermohaline structure were presented in Section 8.5 and in this section we will focus only on the variations from the mean situation. To determine the relationship between the wind and the mesoscale circulation we analysed different characteristics of the modelled currents and the wind used to force the model simulations, corresponding to May and June of the years 1998, 1999 and 2000. The parameters analysed include the wind stress, the curl of the wind stress, the current fields, the vorticity of the currents, and, from both wind and currents, the total kinetic energy and the enstrophy. It has been suggested that the total kinetic energy and the enstrophy could be primary indicators of mesoscale variability in the Black Sea (Shapiro, personal communication, 2003). According to principles of geophysical fluid dynamics, the total mechanical energy of an isolated body of fluid can only be changed by external forcing of frictional dissipation. A similar statement is approximately valid for the conservation of potential enstrophy (vorticity). In the shallow water approximation on the β-plane the integral form of the quasigeostrophic potential vorticity gives (Pedlosky, 1998),

$$\frac{\partial}{\partial t} \iint [(\xi - f\psi)] dx dy = 0$$

where $\xi - f\psi$ is the potential vorticity, the relative vorticity is $\xi = \dfrac{\partial v}{\partial x} - \dfrac{\partial u}{\partial y}$, f is the Coriolis parameter and ψ is the stream function of the current.

As changes in the Coriolis parameter across the Black Sea are relatively small, (from $f=1.05 \times 10^{-4}$ s^{-1} in the North to $f=0.95 \times 10^{-4}$ s^{-1} in the south, with a variability less than 7%) then the main term in the equation is related to the integral value of relative vorticity. Any changes in the basin averaged relative vorticity,

$$\bar{\xi} = \frac{1}{Volume} \iiint \xi dx dy dz$$

are indicators of changes in the circulation due to external forcing.

Our results (detailed in Section 7.3) show that both the magnitude and the direction of the wind stress are very important in determining the currents and, even when the approaches by A. Zatsepin and G. Shapiro are based on different physical principles, the results are not dissimilar because in the Black Sea the curl of the wind is interrelated with its magnitude.

Variability of the wind

There is significant high frequency variability in the wind as shown in the time series of the integral total kinetic energy. The wind of May and June of the year 1998 was in general the more energetic and had a cyclonic tendency. It had also the highest value of enstrophy (maximum values of wind curl) especially during the first month than the other two years. The winds of 1999 and 2000 have in general similar characteristics in terms of energy, curl and enstrophy. The wind of the year 1999 is the weaker of the three years and its maximum intensity was during the week of the 15 to the 21 of May. The wind of the year 2000 was slightly more energetic than that of 1999. Its minimum strength was during the week of the 15 to the 21 of May and its maximum strength was from the 29 of May to the 5 of June. The highly energetic wind of 1998 generated an intense general circulation with a well defined Rim Current and big energetic sub-basin gyres. The mesoscale activity during that year was smaller than in the years 1999 and 2000.

In general the wind is more intense when is coming from the north and has a cyclonic tendency (Figure 7.3a). Results show that the wind of 1998 during the selected period (10 of May to 5 of June) has more cyclonic events and the duration of those events is longer than in the other two years. The areas of intensity are also different within the years; in 1998 the wind is generally stronger in the western part of the basin and weaker in the south-east. In 1999 the spatial distribution shows that the centre of vorticity is dominantly located in the south of the sea. During this year the wind has only one cyclonic event from the 15 to 20 of May, followed by an anticyclonic event from the 20 to 23 of May. Except from these two events, the wind is very weak. The impact of the cyclonic wind circulation is very clear in the evolution of the total kinetic energy (Figure 7.1) so that the year 1999 shows only one strong event approximately between days 16 and 19. During 2000 the anti-cyclonic circulation dominates during the first part of the selected period of time (from day 10 to 25) and it was cyclonic and more intense during the last week (day 30 to 35).

The overall results give a clear indication of the interannual variability of the wind field which must be taken into account for studies of a mesoscale nature.

Variability of the currents

The mesoscale circulation shows much more variability between the different years than the large and sub-basin scale circulation. Nevertheless even the Rim Current, which is considered to be the more 'stable' and strong feature of the Black Sea circulation, shows substantial differences between the simulations. These differences are more evident in the eastern branch of the Rim Current (along the Caucasian coast) which in our results appears to be the more vulnerable area to the wind variations.

During 1999 and 2000 there are more mesoscale eddies than during 1998. In the year 2000 there is a great amount of meanders and curls all over the basin but the number of well defined eddies is smaller than during the year 1999.

Because the wind forcing was the only variable between the three experiments, all the differences in the resulting currents are related to the wind variations. Overall, our results confirm that the variability of the wind has a significant effect on the mesoscale circulation. When the wind forcing has long lasting strong cyclonic events or in general, most of the Black Sea area is dominated by northerlies, the large scale circulation is reinforced. When this happens, there is an evident decrease in the mesoscale activity reflected mainly in the number of eddies and meanders present in the Black Sea basin. On the other hand during periods of weak wind forcing and when the wind field is anticyclonic the large scale circulation is less intense and the mesoscale activity increases.

This study verifies the importance of taking into account the wind variability in numerical modelling studies because the use of smoothed seasonal or monthly wind forcing could severely underestimate the contribution of some important physical processes that control the ocean response to the atmospheric forcing. Moreover, the impact of the variability not only affects the mesoscale dynamics but has other important implications such as the reduction of the evaporative flux as a result of averaging the winds reducing the rates of ocean convection and therefore reducing the production of the cold intermediate water as demonstrated by Stanev et al., (1995).

8.7. Conclusions

The major achievements resulting from this research are:

➢ Setting up a fully working 3-D Black Sea eddy resolving model to simulate the general and mesoscale hydrodynamics.

➢ Finding that the Black Sea model is sensitive to different parameters and detecting through sensitivity tests the optimal set up which is stable and gives reliable results.

➢ Showing that the model gives accurate and realistic results of the temperature and salinity structure and of the shape, size and velocity of currents through validation against AVHRR SST images, CTD data and available observational and modelling studies from the literature.

➢ Demonstrating that the model accurately reproduces the oscillations of inertial frequency in the Black Sea basin as compared with *in situ* current meter measurements.

➢ Confirming the hypothesis stating that the significant interannual variability in the mesoscale circulation in the Black Sea results mainly from the strong variability of the wind field.

8.8. Further Research

Several lines for further research, which could improve the results and understanding, have been detected:

- It is known that the bottom topography has an important effect on the nature of the hydrodynamics. The effects of the detailed bathymetric features (without smoothing or cutting) on the resulting barotropic oscillations and their influence on the mesoscale circulation would be of particular interest. Hence the results can be expanded by including the real bottom topography in the numerical experiments.

- The modelling of the temperature structure in the upper layer of the sea needs some attention. The heat flux in the present modelling experiments was introduced with an exponential decay. It is recommended to try alternative methods of heat assimilation at the sea surface to improve the accuracy of the modelled temperatures.

- It would be interesting to carry out long term runs to assess the model capability to replicate seasonal trends and to verify the stability of the Cold Intermediate Layer which is very vulnerable and subject to be eroded in numerical studies.

- The effect of different properties of the wind field (magnitude, direction, curl, etc) can be best understood by carrying out numerical experiments using synthetic wind fields.

List of References

Altman, E. N. and N. I. Kumish. 1986. *Interannual and seasonal variability of the Black Sea fresh water balance.* Trudy Gos. Okeanograph. Instituta.145 pp.

Arakawa, A., "Computational design for long-term numerical integration of the equations of fluid motion: Two-dimensional imcompressible flow. Part I.," *Journal of Computational Physics* 1: 119-143 (1966).

Besiktepe, S. T., C. J. Lozano, and A. R. Robinson, "On the summer mesoscale variability of the Black Sea," *Journal Of Marine Research* 59 (4): 475-515 (2001).

Besiktepe, S. T., E. Ozsoy, and M. A. Latif, "Sewage Outfall Plume in the 2-Layer Channel - An Example of Istanbul Outfall," *Water Science and Technology* 32 (2): 69-75 (1995).

Blatov, A. S. et al. 1984. *Variability of hydrophysical fields of the Black Sea.* St. Petesburg. 240 pp.

Blumberg, A. F. and Mellor, G. L. A description of a three dimensional coastal ocean model. Heaps N.S. [4], 1-16. 1987. Washington, D.C., AGU. Three-Dimensional Coastal Ocean Models, Coastal and Estuarine Studies.
Ref Type: Serial (Book,Monograph)

Brown J. et al. 2002. *Ocean Circulation.* Edited by Bearman G.The Open University. 238 pp.

Colella, P. and P. R. Woodward, "The Piecewise Parabolic Method (Ppm) for Gas-Dynamical Simulations," *Journal of Computational Physics* 54 (1): 174-201 (1984).

Degens, E. T. and D. A. Ross. 1974. *The Black Sea; Geology, Chemistry, and Biology.* Edited by Degens E.T. and Ross D.A. Oklahoma, USA: The American Association of Petroleum Geologists. 633 pp.

Demyshev S. and Korotaev G., "Numerical Modeling of the Seasonal Trend of Synoptic Variability of the Black Sea," *Izvestya, Atmospheric and Oceanic Physics* 32 (1): 99-106 (1996).

Dyke Ph. 1996. *Modelling Marine Processes*. London: Prentice Hall. 152 pp.

Efimov, V. V. and M. V. Shokurov, "Spatiotemporal structure of the surface wind field over the Black Sea," *Izvestiya Atmospheric And Oceanic Physics* 38 (4): 421-430 (2002).

Efimov, V. V. and Timofeev, N. A. Investigation of the Black Sea and Azov Sea heat balance. 1-237. 1990. Ukraine, Ukranian Academy of Science, Sevastopol.
Ref Type: Report

Efimov, V. V. et al., "Estimate of the Ocean-Atmosphere Heat and Moisture Exchange Coefficient," *Izvestiya Akademii Nauk Sssr Fizika Atmosfery I Okeana* 21 (7): 735-743 (1985).

Emery W. and Thomson R. 2001. *Data Analysis Methods in Physical Oceanography*. Second ed.Elsevier Science B. V. 638 pp.

EOWEB. *Daily Sea Surface Temperature from the Black Sea, derived from NOAA AVHRR.* 2000. Germany, German Aerospace Center (DLR) -. *Sea surface temperature data from the Mediterranean Sea.*
Ref Type: Map

Fedorov, K. N. and A. I. Ginzburg, ""Mushroom-like" (vortex dipole) currents in the ocean and in a laboratory tank.," *Ann.Geophys.* 4 (B5): 507-516 (1986).

Fedorov, K. N. and A. I. Ginzburg. 1992. *The near-surface layer of the ocean.* Edited by Utrecht VSP. Netherlands. 259 pp.

Filippov, D. M., "The cold intermediate layer in the Black Sea," *Oceanology* 5: 47-52 (1965).

Galperin, B. et al., "A quasi-equilibrium turbulent energy model for geophysical flows.," *Journal of Atmospheric Sciences* 45: 55-62 (1988).

Ginzburg, A. I. et al., "Peculiarities of the water dynamics and chlorophyll a distribution in the northeastern part of the Black Sea in Autumn 1997," *Oceanology* 40 (3): 316-328 (2000).

Ginzburg, A. I. et al., "Mesoscale eddies and related processes in the northeastern Black Sea," *Journal Of Marine Systems* 32 (1-3): 71-90 (2002a).

Ginzburg, A. I. et al., "Anticyclonic eddies in the northwestern Black Sea," *Journal Of Marine Systems* 32 (1-3): 91-106 (2002b).

Gunnerson, C. G. and E. Ozturgut, "The Bosphorus," *The Black Sea - Geology, Chemistry and Biology* 20: 99-113 (1974).

Holt, J. T. and I. D. James, "A simulation of the southern North Sea in comparison with measurements from the North Sea Project Part 2 Suspended Particulate Matter," *Continental Shelf Research* 19 (12): 1617-1642 (1999).

Holt, J. T. and I. D. James, "An s coordinate density evolving model of the northwest European continental shelf - 1, Model description and density structure," *Journal Of Geophysical Research-Oceans* 106 (C7): 14015-14034 (2001).

Holt, J. T., I. D. James, and J. E. Jones, "An s coordinate density evolving model of the northwest European continental shelf - 2, Seasonal currents and tides," *Journal Of Geophysical Research-Oceans* 106 (C7): 14035-14053 (2001).

Huthnance, J. M., "Circulation, exchange and water masses at the ocean margin: The role of physical processes at the shelf edge.," *Progress In Oceanography* 35: 353-431 (1995).

Ibraev, R. A., "A study of the sensitivity of the model of the Black Sea current dynamics to the surface boundary conditions," *Oceanology* 41 (5): 615-621 (2001).

Ivanov, L. and I. Shkvorets, "Thermohaline structure of deep and near bottom waters of the Black Sea. (In Russian).," *Marine Hydrophys.J.Sevastopol.* 5: 54-63 (1995).

Ivanov, L. I. and A. S. Samodurov, "The role of lateral fluxes in ventilation of the Black Sea," *Journal Of Marine Systems* 31 (1-3): 159-174 (2001).

James, I. D., "Advection schemes for shelf sea models," *Journal Of Marine Systems* 8 (3-4): 237-254 (1996).

James, I. D., "A numerical model of the development of anticyclonic circulation in a gulf-type region of freshwater influence," *Continental Shelf Research* 17 (14): 1803-1816 (1997).

Jaoshvili, Sh. The Rivers of the Black Sea. Khomerki I., Gigineishvili G., and Kordzadze A. 71, 1-58. 2002. Denmark, European Environment Agency. 52 pp.
Ref Type: Report

Jones, J. E., "Coastal and Shelf-Sea Modelling in the European context.," *Oceanography and Marine Biology: an Annual Review.* 40: 37-141 (2002).

Kantha, L. H. and C. A. Clayson. 2000. *Numerical Models of Oceans and Oceanic Processes.* Vol. 66. Academic Press. 940 pp.

Kazmin, A. S. and V. E. Sklyarov, "Some peculiarities of the Black Sea circulation inferred from the Meteor satellite (in Russian)," *Issledovanie Zemli iz kosmosa* 5: 56-64 (1982).

Knipovich, N. M. The Hydrological Investigations in the Black Sea. 10, 1-274. 1932. Russia, Trudy Azova-Dhernomorskoy Nauchnopromyslovoy Ekspeditsii.
Ref Type: Report

Korotenko, K. A., D. E. Dietrich, and M. J. Bowman, "Modeling of the circulation and transport of oil spills in the Black Sea," *Oceanology* 43 (4): 474-484 (2003).

Krivosheya, V. G. et al., "Features of water dynamics and hydrological structure in the northeastern Black Sea in Autumn 1993.," *Oceanology* 37: 321-326 (1997).

Krivosheya, V. G. et al. 1998a. Experimental studies of eddy structures within the Rim Current zone in the north-eastern part of the Black Sea. In *Ecosystem Modeling as a Management Tool for the Black Sea*. Vol. 2. Edited by L. M. IVANOV and T. Oguz. Netherlands: Kluwer Academic Publishers.

Krivosheya, V. G. et al., "Meandering of the Main Black Sea Current and eddies formation in the north-eastern part of the Black Sea in summer 1994," *Okeanologiya* 38 (4): 546-553 (1998b).

Kundu, P. K. and J. S. Allen, "Some Three-Dimensional Characteristics of Low-Frequency Current Fluctuations near the Oregon Coast," *Journal Of Physical Oceanography* 6: 181-199 (1976).

Kunze, E., "Near-Inertial Wave-Propagation in Geostrophic Shear," *Journal Of Physical Oceanography* 15 (5): 544-565 (1985).

Latun, V. S., "Studying and Modeling the Hydrophysical Processes in the Black Sea," *Gidrometeoizdat, Moscow [in Russian]*: 40-49 (1989).

Leonov, A. K. 1960. *Regional Oceanography*. Vol. I. St. Petesburg. 765 pp.

Mee, L. D. 2001. Eutrophication in the Black Sea and a basin-wide approach to its control. In *Science and Integrated Coastal Management*. Edited by Bodungen B. and Turner R.K.Dahlem University Press.

Mellor, G. L., "An Equation of State for Numerical-Models of Oceans and Estuaries," *Journal of Atmospheric and Oceanic Technology* 8 (4): 609-611 (1991).

Mellor, G. L. and T. Yamada, "A Hierarchy of Turbulence Closure Models for Planetary Boundary Layers.," *Journal of Atmospheric Sciences* 31: 1791-1806 (1974).

Meschanov, S. L. and G. I. Shapiro, "A young lens of Red Sea Water in the Arabian Sea," *Deep-Sea Research Part I-Oceanographic Research Papers* 45 (1): 1-13 (1998).

Molcard, A. et al., "Wind driven general circulation of the Mediterranean sea simulated with a Spectral Element Ocean Model," *Dynamics Of Atmospheres And Oceans* 35 (2): 97-130 (2002).

Neumann, G., "Die Absolute Topografie des Physikalischen Meeresniveaus und die Oberflachen-Stromungen des Schwarzen Meeres," *Ann.Hydrogr.Berl.* 70: 265-282 (1942).

Oguz, T. et al., "Mesoscale circulation and thermohaline structure of the Black - Sea - observed during HYDROBLACK-91," *Deep-Sea Research Part I-Oceanographic Research Papers* 41 (4): 603-& (1994).

Oguz, T. and S. Besiktepe, "Observations on the Rim Current structure, CIW formation and transport in the western Black Sea," *Deep-Sea Research Part I-Oceanographic Research Papers* 46 (10): 1733-1753 (1999).

Oguz, T. et al., "Circulation in the surface and intermediate layers of the Black Sea," *Deep-Sea Research Part I-Oceanographic Research Papers* 40 (8): 1597-1612 (1993).

Oguz, T. and P. Malanotte-Rizzoli, "Seasonal variability of wind and thermohaline-driven circulation in the black sea: Modeling studies," *Journal Of Geophysical Research-Oceans* 101 (C7): 16551-16569 (1996).

Oguz, T., P. Malanotte-Rizzoli, and D. Aubrey, "Wind and Thermohaline Circulation of the Black Sea driven by yearly mean climatological forcing," *Journal Of Geophysical Research-Oceans* 100 (C4): 6845-6863 (1995).

Ozsoy, E. et al., "Fluorescent Dye Measurements of the Mixing and Transport of Waste-Water Discharge in the Bosporus," *Water Science and Technology* 32 (2): 61-68 (1995).

Ozsoy, E. and U. Unluata, "Oceanography of the Black Sea: a review of some recent results," *Earth-Science Reviews* 42 (4): 231-272 (1997).

Ozsoy, E., U. Unluata, and Z. Top, "The Evolution of Mediterranean Water in the Black-Sea - Interior Mixing and Material Transport by Double-Diffusive Intrusions," *Progress In Oceanography* 31 (3): 275-320 (1993).

Pedlosky, J. 1998. *Ocean Circulation Theory*. 1 ed. Berlin: Springer-Verlag.

Preisendorfer, R. W. 1988. *Principal Component Analysis in Meteorology and Oceanography*. Vol. 17. Edited by C. D. Mobley. The Netherlands: Elsevier Science Publishers B. V. 425 pp.

Proctor, R. and I. D. James, "A fine-resolution 3D model of the Southern North Sea," *Journal Of Marine Systems* 8 (3-4): 285-295 (1996).

Rachev, N. H., Roussenov V., and E. Stanev, "The Black Sea Climatological Wind Stress," *Bulgarian Journal of Meteorology and Hydrology* 2 (3-4): 72-79 (1991).

Rhines, P.B. 2000. Turbulence and Diffusion: Mesoscale Eddies. University of Washington. Available from:http://www.ocean.washington.edu/research/gfd/eddies-ap/eddies-ap-weba.htm [Accessed 2 December 2004].

Robinson, A. R. and M. Golnaraghi, "Circulation and Dynamics of the Eastern Mediterranean-Sea - Quasi-Synoptic Data-Driven Simulations," *Deep-Sea Research Part Ii-Topical Studies in Oceanography* 40 (6): 1207-1246 (1993).

Shapiro, G. I. et al., "Transport of fine sediment with mesoscale currents in the shelf-slope zone of the sea," *Oceanology* 40 (3): 305-311 (2000).

Shapiro, G. I., J. M. Huthnance, and V. V. Ivanov, "Dense water cascading off the continental shelf," *Journal Of Geophysical Research-Oceans* 108 (C12): 20-1-20-19 (2003).

Shapiro, G. I. and S. L. Meschanov, "Distribution and Spreading of Red-Sea Water and Salt Lens Formation in the Northwest Indian-Ocean," *Deep-Sea Research Part A-Oceanographic Research Papers* 38 (1): 21-34 (1991).

Shapiro, G. I. and S. L. Meschanov, "Spreading pattern and mesoscale structure of Mediterranean outflow in the Iberian Basin estimated from historical data," *Journal Of Marine Systems* 7 (2-4): 337-348 (1996).

Shapiro, G. I. et al., "Self-Similarity of the Meddy Family in the Eastern North- Atlantic," *Oceanologica Acta* 18 (1): 29-42 (1995).

Simonov, A. I. and E. N. Altman. 1991. *The Black Sea, Gidrometeoizdat.* Vol. IV. Edited by Simonov A.I. and Altman E.N. 430 pp.

Song, Y. and D. Haidvogel, "A Semi-implicit Ocean Circulation Model Using a Generalized Topography-Following Coordinate System," *Journal Of Geophysical Research-Oceans* 115: 228-244 (1994).

Stanev, E., Staneva, J. V., Bullister, J. L., and Murray, J. W. Ventilation of the Black Sea pycnocline. Parameterization of convection, numerical simulations and validations against observed chlorofluorocarbon data. Deep-Sea Research Part I- Oceanographic Research Papers . 2004.
Ref Type: In Press

Stanev, E., J. V. Staneva, and Roussenov V., "On the Black Sea Water mass formation. Model ensitivity Study to Atmospheric forcing and parameterisations of Physical processes," *Jounal of Marine Systems* 13: 245-272 (1997).

Stanev, E. V., "On the Mechanisms of the Black-Sea Circulation," *Earth-Science Reviews* 28 (4): 285-319 (1990).

Stanev, E. V. and J. M. Beckers, "Barotropic and baroclinic oscillations in strongly stratified ocean basins - Numerical study of the Black Sea," *Journal Of Marine Systems* 19 (1-3): 65-112 (1999).

Stanev, E. V. et al., "Control of Black Sea intermediate water mass formation by dynamics and topography: Comparison of numerical simulations, surveys and satellite data," *Journal Of Marine Research* 61 (1): 59-99 (2003).

Stanev, E. V., P. Y. Le Traon, and E. L. Peneva, "Sea level variations and their dependency on meteorological and hydrological forcing: Analysis of altimeter and surface data for the Black Sea," *Journal Of Geophysical Research-Oceans* 105 (C7): 17203-17216 (2000).

Stanev, E. V. and N. H. Rachev, "Numerical study on the planetary Rossby modes in the Black Sea," *Journal Of Marine Systems* 21 (1-4): 283-306 (1999).

Stanev, E. V. et al., "Sea Response to Atmospheric Variability - Model Study for the Black-Sea," *Journal Of Marine Systems* 6 (3): 241-267 (1995).

Stanev, E. V. and J. V. Staneva, "The sensitivity of the heat exchange at sea surface to meso and sub-basin scale eddies - Model study for the Black Sea," *Dynamics Of Atmospheres And Oceans* 33 (3): 163-189 (2001).

Staneva, J. V. et al., "Rim current and coastal eddy mechanisms in an eddy-resolving Black Sea general circulation model," *Journal Of Marine Systems* 31 (1-3): 137-157 (2001).

Staneva, J. V. and E. Stanev, "Oceanic response to atmospheric forcing derived from different climatic data sets. Intercomparison study for the Black Sea.," *Oceanologica Acta* 21 (3): 393-417 (1998).

Sur, H. I. and Y. P. Ilyin, "Evolution of satellite derived mesoscale thermal patterns in the Black Sea," *Progress In Oceanography* 39 (2): 109-151 (1997).

Sur, H. I., E. Ozsoy, and U. Unluata, "Boundary Current Instabilities, Upwelling, Shelf Mixing and Eutrophication Processes in the Black-Sea," *Progress In Oceanography* 33 (4): 249-302 (1994).

Suvorov, A. M., Eremeev, V. N., Belokopytov, V., Khaliulin, A. H., Godin, E. A., Ingerov, D. R., Palmer, D. R., and Levitus, S. Rivers of the Black Sea. 2004. Environmental Services Data and Information Management Program, Marine Hydrophysical Institute of the National Academy of Sciences of Ukraine. Digital Atlas: Physical Oceanography of the Black Sea; CD-ROM.
Ref Type: Map

Trukhchev, D. and A. S. Sarkisyan, "Hydrodynamic diagnosis of climatic temperature, salinity and currents of the Black Sea," *Izvestiya Akademii Nauk Fizika Atmosfery I Okeana* 31 (6): 809-819 (1995).

Unluata, U. et al. 1990. On the physical oceanography of the Turkish Straits. In *The Physical Oceanography of Sea Staits.* Edited by L. J. Pratt. The Netherlands: Kluwer Academic Publishers.

Whitney, F. and M. Robert, "Structure of Haida eddies and their transport of nutrient from coastal margins into the NE Pacific Ocean," *Journal of Oceanography* 58 (5): 715-723 (2002).

Wilson, C. and R. G. Williams, "Why are eddy fluxes of potential vorticity difficult to parameterize?," *Journal Of Physical Oceanography* 34 (1): 142-155 (2004).

Yuce, H., "Mediterranean Water in the Strait of Istanbul (Bosphorus) and the Black Sea Exit," *Estuarine, Coastal and Shelf Science* 43: 597-616 (1996).

Zatsepin, A. G. et al., "Observations of Black Sea mesoscale eddies and associated horizontal mixing," *Journal Of Geophysical Research-Oceans* 108 (C8): art-3246 (2003).

Zatsepin, A. G. et al., "Variability of water dynamics in the northeastern Black Sea and its effect on the water exchange between the near-shore zone and open basin," *Oceanology* 42: S1-S15 (2002).

Zhurbas, V. M. et al., "Water circulation and characteristics of currents of different scales in the upper layer of the Black Sea from drifter data," *Oceanology* 44 (1): 30-43 (2004).

Appendix A. Subroutines developed for pre-processing data for the modelling

A.1 Bathymetry and Mask

The methodology for the bathymetric data treatment is as follows;

1. Extract the Black Sea domain from the bathymetry of the mediterranean using Matlab

2. In surfer linearly interpolate to fit the model's grid:

	min	max	spacing	No. of lines
x	28	41.9		168
y	41	46.76		92

3. Cut to a max depth of 1500 m.

4. Smooth the bathymetry by running average filtering using a window size of 5 by 5 using Matlab

There are no subroutines for the bathymetric data processing.

Methodology for the mask file for POLCOMS:

1. From the bathymetric file select the wet points and assign them the value=1 in Mask.dat. Assign value=0 to the rest of the grid points.

2. Check that every wet point has a corresponding initial temperature and salinity value (different from cero).

A.2 Temparature and Salinity

The methodology for the TS treatment is as follows;

1. Select the month from which the model will be initialized
   and generate 24 output files for surfer (corresponding to the 24 vertical Z-levels of Staneva's original data.
   The files have 4 columns with: [x (longitudes) y (lats) tem (C) sal (psu)]

2. In surfer open each file and interpolate in the horizontal using krigging to fit this study's grid:

	min	max	spacing	No. of lines
x	28	41.9		168
y	41	46.76		92

and use the option of output grid file as: ASCII XYZ (*.dat)

3. Use the subroutine Interscoord1.m
   * loads Matlab workspace mascara.mat
   (which contains the bathymetry and mask saved from Mask.dat and Bathy.dat)
   * loads the interpolated TS from Matlab workspace TSextrapolZlevels.mat (step 4)
   * generates a 3-D matrix of depths (in meters) at the s-coord grid points called (zzz3 [92,168,22]).
   This matrix is manually saved in the Matlab workspace mascara.mat together with the mask and the bathymetry.

4. Run subroutine Interscoord2.m
   * Uses the variable zzz3 {from step 5} and the land mask by loading the Matlab workspace mascara.mat
   * Uses the variables tem and sal {from step 4} by loading TSextrapolZlevels.mat

   * generates 3-D variables of:
        temperature (deg. C) at the s-coord grid points called (temi2 [92,168,22]))
        salinity   (psu)   at the s-coord grid points called (sali2 [92,168,22]))
        [example for the month of may in the file TS_S_levels.mat]

5. With wts.m generate the file for POLCOMS
   * uses temi2 and sali2 {from step 6}by loading the Matlab workspace TS_S_levels.mat
   * generates T and S with 24 vertical levels in s-coordinates and writes them in the output file for POLCOMS:
   * output ---> iniTSmay.dat.

■■■

%   Interscoord1.m

% This subroutine generates a 3-D matrix of depths (in meters) at the s-coord grid points (zzz3).
% It needs the bathymetry and mask matrixes present in the workspace as
% variables: bat(i,j) and mas(i,j), which can be loaded from the file
% mascara.mat
load mascara
load TSextrapolZlevels
% Define the s-coord parameters
hc=300;
cc=1;
theta=8;
bb=1;

```
% Number of vertical levels
N=24;
sig=linspace(-1+0.5/(N-2),-0.5/(N-2),N-2);
sigo=linspace(-1,0,N-1);
zzz=zeros(92,168,22);
for i=1:92
  for j=1:168
   if mas(i,j)==1
            if bat(i,j)<=hc

        sc=sig;
        sco=sigo;

            else
        sco(1)=-1;
        sco(N-1)=0.;
            for k=2:N-2

        %FFH=0.5*(Hs-HC+sqrt((Hs-HC).^2+4.*cc^2));
            FFH=(bat(i,j)-hc)./bat(i,j);

        Cs=(1-bb)*(sinh(theta*sigo(k)))./sinh(theta)+...
            bb*(tanh(theta*(sigo(k)+0.5))-tanh(0.5*theta))./...
            (2.*tanh(0.5*theta));
            sco(k)=sigo(k)+FFH*(Cs-sigo(k));
            %disp([k FFH*(Cs-sigo(k))])
            end

        sc(1)=-1.+(sco(2)+1)/2;
            for k=2:N-2
            sc(k)=0.5*(sco(k)+sco(k+1));
            end

     end
   zzz3(i,j,:)=sc.*bat(i,j);

 else
    zzz3(i,j,:)=0;
  end
end
end
```

%   **Interscoord2.m**

% It needs the 3-D array of depths of the s-levels [zzz3]and the mask.
load mascara
load TSextrapolZlevels.mat
y=92; %Number of rows (latitudes)
x=168; %No. of columns (longitudes)
s=22; %No. of vertical levels - 2 (excluding the top and bottom)
N=25; %No. of vertical z-levels of original data files

% Depths of the original Staneva's data's z-levels:

z=[2.5;7.5;12.5;17.5;25;35;45;55;65;75;85;105;140;185;240;310;400;515;750;1125;1485;
1755;1940;2070];

% VERIFY THAT THE ARRAYS SHOULD BE FIRST BOTTOM AND LAST
SURFACE!

```
temi2=zeros(92,168,22);
sali2=zeros(92,168,22);

for k=1:24
    sall(:,:,k)=sal(:,:,25-k);
    tem1(:,:,k)=tem(:,:,25-k);
    zeta5(k)=-z(25-k);
end
tem1(:,:,25)=tem1(:,:,24);
sall(:,:,25)=sall(:,:,24);
zeta5(25)=0;

for i=1:92
  for j=1:168
    if mas(i,j)==1

        for k=1:22
           zz(k)=zzz3(i,j,k);
        end

        for k=1:25
          s(k)=sall(i,j,k);
          t(k)=tem1(i,j,k);
        end


        temi2(i,j,:)=interp1(zeta5,t,zz);
        sali2(i,j,:)=interp1(zeta5,s,zz);

    end
```

```
   end
end
```

■■■

% Subroutine wts.m

% This writes the file for POLCOMS iniTSmay.dat

```
load TS_Slevels.mat
tem3=zeros(92,168,24);
sal3=zeros(92,168,24);
tem3(:,:,1)=temi2(:,:,1);
tem3(:,:,24)=temi2(:,:,22);
sal3(:,:,1)=sali2(:,:,1);
sal3(:,:,24)=sali2(:,:,22);
for k=2:23
   tem3(:,:,k)=temi2(:,:,k-1);
   sal3(:,:,k)=sali2(:,:,k-1);
end

fid=fopen('iniTSmay.dat','w');
for k=1:24
T=tem3(:,:,k)';
fprintf(fid,'%8.2f%8.2f%8.2f%8.2f%8.2f%8.2f%8.2f%8.2f\n',T);
end

for k=1:24
S=sal3(:,:,k)';
fprintf(fid,'%8.2f%8.2f%8.2f%8.2f%8.2f%8.2f%8.2f%8.2f\n',S);
end
fclose(fid);
```

A.3 Heat Fluxes

The methodology for the Heatflux data treatment is as follows;

1. Run Matlab subroutine MJ2W.m which:
    Reads the original file QTOT.dat [original files from Staneva]
    converts units for the heat flux from MJ/month to Watts [J/s]
    generates output files for interpolation in surfer : qtout1.dat,
    qtout2.dat ... qtout12.dat with [x(longs) y(lats) totalheatflux(J/s) month]
    [for the month of may, the file is qtout5.dat]

3. In surfer open the file corresponding to the month to be treated (e.g. for May qtout5.dat)

211

and interpolate using kriging to fit Cecilia's model's grid:

	min	max	spacing	No. of lines
x	28	41.9	168	
y	41	46.76	92	

and use the option of output grid file as: ASCII XYZ (*.dat)
(for the month of May the file is qtkr5.dat)
[The extrapolated 12 months are in [QTextrapol.mat which has a variable
QT (92,168,12)].

4. With wqt.m generate 12 files which contain the monthly climatic total heat flux in J/s:
   [for the months of april, may and June, the files are QT4.dat, QT5.dat and QT6.dat
with the following:
           Spatial range: from 41 to 46.7 deg. N and from 28 to 41.9 deg. E.
           Dimension of the array: (92, 168)
           File format (8f8.2).
           Storage of the array:
           Origin located at the SW corner: 41N, 28E
           Increasing i's from W to E and increasing j's from south to north

5 Use program QTfine.f90 to interpolate in time to daily heat flux data
           ! Input: Three data files with monthly climatic QT {e.g. for May, the months
           !   needed are April, May and June = QT4.dat, QT5.dat and QT6.dat}
           ! Output: 1 file with daily QT data for during the month = QTmay.dat

****

%   Subroutine   MJ2W.m
% This subroutine opens the file QTOT.dat [original files from Staneva],
% and converts units for the heat flux
% from MJ/month to Watts [J/s]
% then generates output files for interpolation in surfer : qtout1.dat,
% qtout2.dat ... qtout12.dat with [x(longs) y(lats) totalheatflux(J/s) month]

```
fid=fopen('\QTOT.dat','r');
    qtot=zeros(133,76,12);

  for month=1:12
     u=fscanf(fid,'%g',[133 76]);

     qtot(:,:,month)=u.*1000000./(30*24*3600);
  end
    fclose(fid)
```

212

```
%Coordinates of Staneva's data
x=[27.38:0.1111:42.05];
y=[40.45:0.083333:46.7];

masc=zeros(133,76);
qt=qtot(:,:,1);
mas=find(qt==0);
masc(mas)=1;
%%%%%%%%%%%%%%%%%%%%%%%%%%%%%%%%%%%%%%%%%%%%%%%%%%%
%%%%%%%%%
% Generates files for surfer interpolation
k=1;
for m=1:12
for i=1:76
    for j=1:133
        if masc(j,i)==0
        qtout(k,:)=[ x(j) y(i) qtot(j,i,m) m];
        k=k+1;
        end
      end
   end
end

for mes=1:12
   name=['qtout',num2str(mes),'.dat'];
   fid=fopen(name,'w');
   a=[1:5162:56783];
   b=[5162:5162:61944];
QT=qtout(a(mes):b(mes),:)';
fprintf(fid,'%11.4f%11.4f%11.4f%11.4f\n',QT);
fclose(fid);
mes
end
```

```
%%%%%%%%%%%%%%%%%%%%%%%%%%%%%%%%%%%%%%%%%%%%%%%%%%%
```

%   Subroutine wqt.m

```
% This loads the climatic monthly total heat fluxes (J/s) from
% QTextrapol.mat and needs the land Mask from mascara.mat

% Writes 12 files:  QT1.dat, QT2.dat ... QT12.dat
% which are monthly climatic total heat flux in J/s

load QTextrapol
load mascara
for mnth=1:12
```

```
name5=['QT',num2str(mnth),'.dat']
fid=fopen([name5],'w');


for i=1:92
   for j=1:168
     if mas(i,j)==1
         ui(i,j)=QT(i,j,mnth);
      else
         ui(i,j)=0;
      end
   end
end
u=ui';
pcolor(u);colorbar;shading flat;
pause
fprintf(fid,'%8.2f%8.2f%8.2f%8.2f%8.2f%8.2f%8.2f%8.2f\n',u);
fclose(fid);

end
```

■■

Program Qtfine.F

```
! This subroutine interpolates in time to daily heat flux data
! Input: Three data files with monthly climatic QT {e.g. for May, the months
!      needed are April, May and June  = QT4.dat, QT5.dat and QT6.dat}
! Output: 1 file with daily QT data for during the month = QTmay.dat
!x=first month, x1=second, x2=the third, x3=interpolated heat flux at each
! moment in time (daily)
!d= 30 days
!dt= is a counter that goes from 15 to 1
!t= is a counter that goes from 1 to 15



real*4 x(92,168),x1(92,168),x2(92,168),x3(92,168)
integer dt,d
d=30


open(10,file='QTmay.dat',status='unknown')

open (33,file='QT4.dat', status='unknown')
11 format(8f8.2)

do i=1,92
```

```fortran
!  do j=1,168
   read(33,11) (x(i,j),j=1,168)
!  enddo
!  write(*,*)i,j
enddo
close(33)

open (33,file='QT5.dat', status='unknown')
do i=1,92
!  do j=1,168
   read(33,11) (x1(i,j),j=1,168)

!  enddo
enddo
close(33)

open (33,file='QT6.dat', status='unknown')
do i=1,92
!  do j=1,168
   read(33,11) (x2(i,j),j=1,168)

!  enddo
enddo
close(33)




!11 format(8f8.2)
dt=15
do t=1,15
      a=float(dt)/float(d)
!      write(*,*) a

      do i=1,92
        do j=1,168
          x3(i,j) = a*x(i,j)+(1.0d0-a)*x1(i,j)
        enddo
      enddo
      do i=1,92
      write(10,'(8f8.2)') (x3(i,j),j=1,168)
      enddo

      dt=dt-1
enddo

dt=30
do t=1,15
```

```
       a=float(dt)/float(d)
!      write(*,*) a


       do i=1,92
         do j=1,168
           x3(i,j) = a*x1(i,j)+(1.0d0-a)*x2(i,j)
         enddo
       enddo
       do i=1,92
       write(10,'(8f8.2)') (x3(i,j),j=1,168)
       enddo

       dt=dt-1
enddo

close(10)
write(*,*) 'Done!'
end
```

A.4 Evaporation - Precipitation

The methodology for the Evaporation-Precipitation data treatment is as follows;

1. Run subroutine ep.m which,
    * Reads data from Staneva Evaporation in MJ/month and Precipitation in mm/month.
    * Evaporation is converted to mm3/month to have same units as precipitation by:
        Evap (J/month)(1x10^9)/(latent heat of evaporation (2.5 * 10^6 J/kg)* Density of sea water (1027 kg/m^3))
    * Calculates evaporation minus precipitation in mm/month.
    * then generates output files for interpolation in surfer : epout1.dat,
       epout2.dat ... epout12.dat with [x(longs) y(lats) E-P(mm/month) month]
       [for the month of may, the file is epout5.dat]

2. In surfer open the file corresponding to the month to be converted (e.g. for May, epout5.dat)
    and interpolate using kriging to fit the model's grid:

	min	max	spacing	No. of lines
x	28	41.9	168	
y	41	46.76	92	

    and use the option of output grid file as: ASCII XYZ (*.dat)

216

[The extrapolated months of April, May and June are in [epin4.dat, epin5.dat and epin6.dat].

3. With surfin.m the extrapolated files from surfer are loaded and generates
    12 files which contain the monthly climatic Evap less Precip in mm/month:
    [for the months of april, may and June, the files are EP4.dat, EP5.dat and EP6.dat with the following:
        Spatial range: from 41 to 46.76 deg. N and from 28 to 41.9 deg. E.
        Dimension of the array: (92, 168)
        File format (8f8.2).
        Storage of the array:
        Origin located at the SW corner: 41N, 28E
        Increasing i's from W to E and increasing j's from south to north

5 Use program EPfine.f90 to interpolate in time to daily evap-precip data
        ! Input: Three data files with monthly climatic EP {e.g. for May, the months
        !   needed are April, May and June = EP4.dat, EP5.dat and EP6.dat}
        ! Output: 1 file with daily EP data for during the month = EPmay.dat

     ****

% Subroutine ep.m

%%%%%%%%%%%%%%%%%%%%   Evaporation   less   Precipitation
%%%%%%%%%%%%%%%%%%%%%%%%%%%

% Reads data from Staneva Evaporation in MJ/month and Precipitation in
% mm/month.

% Evaporation is converted to mm/month to have same units as precipitation by:
% Evap (J/month)(1810^9)/(latent heat of evaporation (2.5 * 10^6 J/kg)* Density of sea water (1027 kg/m^3))
%
% Output: 12 output files of Evaporation less Precipitation in mm/month for interpolation in surfer
% called: epout1.dat, epout2.dat ... epout12.dat with 4 columns: [x(longs) y(lats) E-P(mm/month) month]

%%
%%%%%%%%%%%%%%%%%%%%%%%%%%%%%%%%

```
fid=fopen('EVAPO.DAT','r');
fid2=fopen('PRECIP.DAT','r');

for k=1:12
    e=fscanf(fid,'%g',[133 76]);
```

```
    eva(:,:,k)=e.*(1*10^9)/((2.5*10^6)*(1027));
    p=fscanf(fid2,'%g',[133 76]);
    precip(:,:,k)=p;
    elessp(:,:,k)=eva(:,:,k)-precip(:,:,k);
 end
 fclose(fid);
 fclose(fid2);


%%%%%%%%%%%%%%%%%%%%%%%%%%%%%%%%%%%%%%%%%%%%%%%%%%%%%%%%%%%%
%%%%%%%%%%%%%%%%%%%%%%%%%%%%%%%%%%%%%%%%%%%
%Coordinates of Staneva's data
x=[27.38:0.1111:42.05];
y=[40.45:0.083333:46.7];
masc=zeros(133,76);
mas=find(e==0);
masc(mas)=1;


k=1;
for m=1:12
for i=1:76
    for j=1:133
       if masc(j,i)==0
       epout(k,:)=[ x(j) y(i) elessp(j,i,m) m];
       k=k+1;
       end
    end
 end
end

for mes=1:12
   name=['epout',num2str(mes),'.dat'];
   fid=fopen(name,'w');
   a=[1:5162:56783];
   b=[5162:5162:61944];
EP=epout(a(mes):b(mes),:)';
fprintf(fid,'%11.4f%11.4f%11.4f%11.4f\n',EP');
fclose(fid);
mes
end


***************************************************************************
```


% Subroutine Surfin.m

% Reads the Evap-Precip data files created in surfer (monthly) and generates files

% for interpolation in time to daily data files.

% Input: extrapolated E-P files from surfer: epin1.dat ... epin12.dat
%   land mask from mascara.mat
% Output: files EP1.dat, EP2.dat ... EP12.dat : monthly climatic Evap - Precip in mm/month

```
load mascara
for mes=4:6
   name=['epin',num2str(mes),'.dat'];
   load(name)
  name1=['epin',num2str(mes)];
  temp=eval(name1);
l=1;
for i=1:92
   for j=1:168
      ep(93-i,j)=temp(l,3);
      l=l+1;
   end
end

  EP(:,:,mes)=ep;
end

for mnth=4:6
name5=['EPcac',num2str(mnth),'.dat']
fid=fopen([name5],'w');


for i=1:92
   for j=1:168
     if mas(i,j)==1
        ui(i,j)=EP(i,j,mnth);
     else
        ui(i,j)=0;
     end
   end
end
u=ui';
pcolor(u);colorbar;shading flat;
pause
fprintf(fid,'%8.2f%8.2f%8.2f%8.2f%8.2f%8.2f%8.2f%8.2f\n',u);
fclose(fid);

end
```

Program Epfine.F90

```
! This subroutine interpolates in time to daily E-P data
! Input: Three data files with monthly climatic EP {e.g. for May, the months
!        needed are April, May and June = EP4.dat, EP5.dat and EP6.dat}
! Output: 1 file with daily EP data for during the month = EPmay.dat


real*4 x(92,168),x1(92,168),x2(92,168),x3(92,168)
integer dt,d
d=30


open(10,file='EPmay.dat',status='unknown')

open (33,file='EP4.dat', status='unknown')
11 format(8f8.2)

do i=1,92
!  do j=1,168
   read(33,11) (x(i,j),j=1,168)
!  enddo
!  write(*,*)i,j
enddo
close(33)

open (33,file='EP5.dat', status='unknown')
do i=1,92
!  do j=1,168
   read(33,11) (x1(i,j),j=1,168)

!  enddo
enddo
close(33)

open (33,file='EP6.dat', status='unknown')
do i=1,92
!  do j=1,168
   read(33,11) (x2(i,j),j=1,168)

!  enddo
enddo
close(33)



!11  format(8f8.2)
```

```
dt=15
do t=1,15
      a=float(dt)/float(d)
!     write(*,*) a

      do i=1,92
        do j=1,168
          x3(i,j) = a*x(i,j)+(1.0d0-a)*x1(i,j)
        enddo
      enddo
      do i=1,92
      write(10,'(8f8.2)') (x3(i,j),j=1,168)
      enddo

      dt=dt-1
enddo

dt=30
do t=1,15
      a=float(dt)/float(d)
!     write(*,*) a


      do i=1,92
        do j=1,168
          x3(i,j) = a*x1(i,j)+(1.0d0-a)*x2(i,j)
        enddo
      enddo
      do i=1,92
      write(10,'(8f8.2)') (x3(i,j),j=1,168)
      enddo

      dt=dt-1
enddo

close(10)
write(*,*) 'Done!'
end
```

A.5 Wind

The methodology for the Wind data treatment is as follows;

1. Run subroutine modifwg.m
   * Reads original data files from Y. Ratner wind stress in dynes/cm2
   * converts units to pascals by dividing by 10.
   * Inverts the data distribution from N to S to S to N

* generates output file for POLCOMS
[for the month of may, year 2000 the file is w20005.dat]

■■

% Subroutine Modifwg.m

```
%  This subroutine reads the original data files from CD which are called:
% YYYYDDDH.zta -> zonal component of the stress
% YYYYDDDH.mta  -> meridional component of the stress
% where yyyy is the year, DDD is the julian day and H is the time code:
% 0 = 0hrs,  1=6hrs,   2=12hrs and 3=18hrs

% Converts the data from din/cm2 to Pascals

% Acomodates the data files from south to North and writes one output file
% for POLCOMS { w20005.dat for the wind data of May, year 2000 }

month=5;
name5=['w2000',num2str(month),'.dat']
fid=fopen([name5],'w');

inicio=121;   % Initial Julian day No.
final=151;    % Final Julian day No.

for day=inicio:final
if day<=9
   grid=1;
end
if day>=10
   if day<=99
      grid=2;
   else
      grid=3;
   end
end

if grid==1

   for hr=1:4
      name1=['E:\200000',num2str(day,'%3i'),num2str(hr-1,'%1i'),'.zta'];
      fid2=fopen([name1],'r');
      wi=fscanf(fid2,'%g',[168 92]);
      wi=wi/10;
      for i=1:92
        wind(:,i)=wi(:,93-i);
      end
fprintf(fid,'%9.3f%9.3f%9.3f%9.3f%9.3f%9.3f%9.3f%9.3f\n',wind);
fclose(fid2);
```

```
%%%%%%%%%%%%%%%%%%%%%%%%%%%%%%%%%%%%%%%%%%%%
name2=['E:\200000',num2str(day,'%3i'),num2str(hr-1,'%1i'),'.mta'];
fid2=fopen([name2],'r');
    wi=fscanf(fid2,'%g',[168 92]);
    wi=wi/10;
    for i=1:92
      wind(:,i)=wi(:,93-i);
    end
fprintf(fid,'%9.3f%9.3f%9.3f%9.3f%9.3f%9.3f%9.3f%9.3f\n',wind);
fclose(fid2);


%%%%%%%%%%%%%%%%%%%%%%%%%%%%%%%%%%%%%%%%%%%%

end
end
%end
if grid==2
%for day=inicio:final
    for hr=1:4
       name1=['E:\20000',num2str(day),num2str(hr-1),'.zta'];
       fid2=fopen([name1],'r');
       wi=fscanf(fid2,'%g',[168 92]);
       wi=wi/10;
       for i=1:92
         wind(:,i)=wi(:,93-i);
       end
fprintf(fid,'%9.3f%9.3f%9.3f%9.3f%9.3f%9.3f%9.3f%9.3f\n',wind);
fclose(fid2);
%%%%%%%%%%%%%%%%%%%%%%%%%%%%%%%%%%%%%%%%%%%%
%%%%%%%%%%%%

name2=['E:\20000',num2str(day),num2str(hr-1),'.mta'];
fid2=fopen([name2],'r');
wi=fscanf(fid2,'%g',[168 92]);
       wi=wi/10;
       for i=1:92
         wind(:,i)=wi(:,93-i);
       end
fprintf(fid,'%9.3f%9.3f%9.3f%9.3f%9.3f%9.3f%9.3f%9.3f\n',wind);
fclose(fid2);
%%%%%%%%%%%%%%%%%%%%%%%%%%%%%%%%%%%%%%%%%%%%
%%%%%%%%%%%%

end
end
%end
if grid==3
```

```
%for day=inicio:final
   for hr=1:4
      name1=['E:\2000',num2str(day),num2str(hr-1),'.zta'];
      fid2=fopen([name1],'r');
      wi=fscanf(fid2,'%g',[168 92]);
      wi=wi/10;
      for i=1:92
        wind(:,i)=wi(:,93-i);
      end
fprintf(fid,'%9.3f%9.3f%9.3f%9.3f%9.3f%9.3f%9.3f%9.3f\n',wind);
fclose(fid2);
%%%%%%%%%%%%%%%%%%%%%%%%%%%%%%%%%%%%%%%%%%%%%%%%%%%%%%%%%
%%%%%%%%%%%%%%

name2=['E:\2000',num2str(day),num2str(hr-1),'.mta'];
fid2=fopen([name2],'r');
wi=fscanf(fid2,'%g',[168 92]);
      wi=wi/10;
      for i=1:92
        wind(:,i)=wi(:,93-i);
      end
fprintf(fid,'%9.3f%9.3f%9.3f%9.3f%9.3f%9.3f%9.3f%9.3f\n',wind);
fclose(fid2);
%%%%%%%%%%%%%%%%%%%%%%%%%%%%%%%%%%%%%%%%%%%%%%%%%%%%%%%%%
%%%%%%%%%%%%%%

end
end

%fclose(fid);

end
fclose(fid);
```

Appendix B. Subroutines developed for post-processing of the model output

1. The model output needs first to be interpolated vertically from the model's s-coodinates to the preselected horizontal levels (original z-coordinates). [Matlab subroutine: treatpp.m] (Before this, convert binary to ascii using fortran subroutine readbin.f90 because the binary formats in matlab are not compatible with those of MSDEV fortran).

2. The ouptut files are averaged every 3 outputs [Matlab subroutine matmean.m].

3. kinetic energy computations (time series) [Matlab subroutine ekinpp.m]

4. Plotting:

   • Maps of temperature, salinity and velocity of the currents at pre-selected depths = 7.5, 45, 75, 105 and 310m. [Matlab subroutine mapspp.m].

   • Transects of temperature, salinity, velocity and sigma-t at pre-selected vertical transects in the locations: latitudes = 42.5,43.1 and 44.0 N and longitudes = 31.2, 33.7 37.9 E. Corresponding to the locations in the file 'Transect location.jpg'.

     o The values of sigma-t are calculated inside the above subroutine calling to the Matlab subroutine [swstate.m]

   • Curl of the currents [Matlab subroutine Curlcurr.m]

   • Enstrophy of the currents [Matlab subroutine Enscurr.m]

■ ■

program Readbin.f90

```
character*200 filein, filein2, filein3
real*4  x(340,200,24), x2(340,200,24)
integer*4 time,timer
integer q,t,n,m,l,d,grid,cac

n=24
d=45
grid=2
timer=1
cac=15
```

```
if(grid.eq.2) then
l = 168
m = 92


      write (*,*) 'Now reading uv'
      open            (33,file='\\Wo40785221\Shared\Cecilia\EKyearrun\Exp1\uv.sep98',
status='old',form='unformatted')
            open      (34,file='\\Wo40785221\Shared\Cecilia\EKyearrun\Exp1\ts.sep98',
status='old',form='unformatted')


!                               open   (33,file='c:/MSDEV/Exp11/AA_AK_QSQ.Exp11_3',
status='old',form='unformatted')
!      open (33,file='c:/MSDEV/Exp11/AH.Exp11_3', status='old',form='unformatted')

!Numero de dias
      do t=1,d

            read(33) time
            read(34) time
            write(*,*) 'leendo timestep:',time
!           pause

! Numero de variables
            do q=1,2
!           do q=1,3
            write(filein2,12)q,t+44*4
            write(filein3,13)q,t+44*4
!           if(t.ge.632)then
!           if(time.eq.2160000)then
            open(12,file=filein2,status='unknown')
            open(13,file=filein3,status='unknown')
!           endif

!           write(filein2,12)q
! Si no necesito T y S, este if aplica, otherwise, quitarlo
!           if (q.le.2) then
!           fil_d='d:/proba/'\\filein
            12
format('C:\Cecilia\Exp18fv\ModelforEK\EKexp1\output\ascii4\uv',i2.2,i3.3,'.dat')
            13
format('C:\Cecilia\Exp18fv\ModelforEK\EKexp1\output\ascii4\ts',i2.2,i3.3,'.dat')
!           12 format('c:/MSDEV/Exp11/AH',i2.2,'.dat')
!           10 format('uvts98',i2.2,i3.3,'.dat')


            do k=1,n
         DO i=1,l
         read(33) (x(i,j,k),j=1,m)
```

```
        read(34) (x2(i,j,k),j=1,m)

    END DO
        enddo

!       if(t.ge.632)then

!       if(time.eq.2160000)then
!       write(*,*) 'time', t
        do k=1,n
          do i=1,l
      write(12,11) (x(i,j,k),j=1,m)
       write(13,11) (x2(i,j,k),j=1,m)
          enddo
          enddo
          write(*,*)'variable/dia: ',q,t,time/3600


!       pause
        close(12)
        close(13)
!       endif

    enddo


        timer=timer+1
        if(timer.eq.7)then
        timer=1
        endif
        enddo
    close (33)
        close (34)

write (*,*) 'Done!'


    end if
       end if


       end
```

. . . .

%   Subroutine treatpp.m

% Vertically interpolates to z-coordinates using linear interpolation
n=24;
m=92;
l=168;

nam='C:\Cecilia\Exp18fv\ModelforEK\EKexp1\output\ascii4\uv0';
nam2='C:\Cecilia\Exp18fv\ModelforEK\EKexp1\output\ascii4\ts0';
mkdir('C:\Cecilia\Exp18fv\ModelforEK\EKexp1\output\','matlab');

load mascara.mat

depths=[1485 1125 750 515 400 310 240 185 140 105 85 75 65 55 45 35 25 17.5 12.5 7.5].*-1;

```
for tt=178:221;
        clear t veloc nameu namev namet names

    if tt<=9
        nameu=[nam,num2str(1),'00',num2str(tt),'.dat'];
        namev=[nam,num2str(2),'00',num2str(tt),'.dat'];
        namet=[nam2,num2str(1),'00',num2str(tt),'.dat'];
        names=[nam2,num2str(2),'00',num2str(tt),'.dat'];
      end
    if tt>=10
      if tt<=99
      nameu=[nam,num2str(1),'0',num2str(tt),'.dat'];
      namev=[nam,num2str(2),'0',num2str(tt),'.dat'];
        namet=[nam2,num2str(1),'0',num2str(tt),'.dat'];
        names=[nam2,num2str(2),'0',num2str(tt),'.dat'];
       end
    end
    if tt>=100
       nameu=[nam,num2str(1),num2str(tt),'.dat'];
        namev=[nam,num2str(2),num2str(tt),'.dat'];
        namet=[nam2,num2str(1),num2str(tt),'.dat'];
        names=[nam2,num2str(2),num2str(tt),'.dat'];
      end
    fid1=fopen(nameu,'r');
    fid2=fopen(namev,'r');
     fid3=fopen(namet,'r');
     fid4=fopen(names,'r');

   for k=1:n
      ui=fscanf(fid1,'%g',[m 1]);
      vi=fscanf(fid2,'%g',[m 1]);
       ti=fscanf(fid3,'%g',[m 1]);
       si=fscanf(fid4,'%g',[m 1]);
```

228

```
                u(:,:,k)=ui;
                v(:,:,k)=vi;
                 t(:,:,k)=ti;
                 s(:,:,k)=si;
        end

        fclose(fid1);
          fclose(fid2);
            fclose(fid3);
              fclose(fid4);
%%%%%%%%%%%%%%%%%%%%%%%%%%%%%%%%%%%%%%%%%%%%%%%%%%%%%%
    for i=1:92
    for j=1:168
      if mas(i,j)==1
  zz(1)=-bat(i,j);
  zz(24)=0;

          for k=1:24
            if k<=22
              zz(k+1)= zzz3(i,j,k);
            end
            uz(k)=u(i,j,k);
            vz(k)=v(i,j,k);
             sz(k)=s(i,j,k);
             tz(k)=t(i,j,k);
          end

      scac=interp1(zz,sz,depths,'linear');
      tcac=interp1(zz,tz,depths,'linear');
     ucac=interp1(zz,uz,depths,'linear');
     vcac=interp1(zz,vz,depths,'linear');

    for k=1:20
        uzet(i,j,k)=ucac(k);
        vzet(i,j,k)=vcac(k);
        szet(i,j,k)=scac(k);
        tzet(i,j,k)=tcac(k);
        velocz(i,j,k)=sqrt((uzet(i,j,k))^2+(vzet(i,j,k))^2);
%
    end

else

    uzet(i,j,1:20)=NaN;
    vzet(i,j,1:20)=NaN;
    szet(i,j,1:20)=NaN;
    tzet(i,j,1:20)=NaN;
    velocz(i,j,1:20)=NaN;
```

```
end

 end
end
namesal=['C:\Cecilia\Exp18fv\ModelforEK\EKexp1\output\matlab\mat',num2str(tt)];
save(namesal,'uzet','vzet','velocz','tzet','szet');

%%%%%%%%%%%%%%%%%%%%%%%%%%%%%%%%%%%%%%%%%%%%%%%%%%%%%%%%%%%tt
end
```

■■

Subroutine matmean.m

```
% Coordinates of wind data
% Grid 92(lat) x 168(lon)

nam=['C:\Cecilia\Exp18fv\ModelforEK\EKexp1\output\matlab\'];
 mkdir('C:\Cecilia\Exp18fv\ModelforEK\EKexp1\output\','matmean');


for day=176:219

name1=[nam,'mat',num2str(day),'.mat'];
name2=[nam,'mat',num2str(day+1),'.mat'];
name3=[nam,'mat',num2str(day+2),'.mat'];
load (name1);
 u1=uzet;
 v1=vzet;
 vel1=velocz;
 t1=tzet;
 s1=szet;

 load (name2);
 u2=uzet;
 v2=vzet;
 vel2=velocz;
 t2=tzet;
 s2=szet;

 load (name3);
 u3=uzet;
 v3=vzet;
 vel3=velocz;
 t3=tzet;
 s3=szet;
```

```
u=(u1+u2+u3)./3;
v=(v1+v2+v3)./3;
vel=(vel1+vel2+vel3)./3;
t=(t1+t2+t3)./3;
s=(s1+s2+s3)./3;


name5=['C:\Cecilia\Exp18fv\ModelforEK\EKexp1\output\matmean\mat',num2str(day+1)];
save(name5,'u','v','vel','t','s');
day
end
```

■ ■

% Subroutine ekinpp.m

```
dx=6800;
dy=6700;
depths=[1485 1125 750 515 400 310 240 185 140 105 85 75 65 55 45 35 25 17.5 12.5 7.5];
for i=1:19
    dz(i)=depths(i)-depths(i+1);
end
 dz(20)=depths(20);

dato=1;
% volsum=0;
% for k=1:20
%     dat=find(t(:,:,k)>=0);
%     num=size(dat,1);
%     vol=num*dx*dy*dz(k);
%     volsum=volsum+vol;
% end
load volsumpp
for day=1:250
name1=['C:\Cecilia\Exp12\outputfv\matlab/mat',num2str(day),'.mat'];
load (name1)
Ek1=0;
u=uzet;
v=vzet;

    a=u.^2;
    b=v.^2;
    for k=1:20
        for i=1:92
            for j=1:168
                if a(i,j,k)>=0
                    a1(i,j,k)=a(i,j,k);
```

231

```
        else
            a1(i,j,k)=0;
        end
        if b(i,j,k)>=0
            b1(i,j,k)=b(i,j,k);
        else
            b1(i,j,k)=0;
        end
        vel=a1(i,j,k)+b1(i,j,k);
        velvol=vel*dx*dy*dz(k);
        Ek1=Ek1+velvol;
    end
  end
end

    Ekm(dato)=(Ek1*1027/2)/volsum;
    Ek1=0;
    day
    dato=dato+1;
    end

Ekm=Ekm';

dlmwrite('C:\Cecilia\Exp12\outputfv\EkGAhr.dat',Ekm);

    plot(Ekm)
    title('TKE Geostrophic Adjustment ');
    xlabel('Time (Hrs)');
    ylabel('EK (J/m3)');
    name10=['C:\Cecilia\Exp12\outputfv\EkGAhr'];
    saveas(gcf,name10,'jpg');
    saveas(gcf,name10,'fig');
```

■■■●

% Subroutine mapspp.m

```
load tierra
scale=2;

nam=['C:\Cecilia\Exp18fv\2000\output_2\figures\'];
nam2=['C:\Cecilia\Exp18fv\2000\output_2\matmean\'];

nam3=[nam,'\mapsT\'];
nam4=[nam,'\mapsS\'];
nam5=[nam,'\mapsV\'];

mkdir(nam3,'Level1');
```

```
mkdir(nam3,'Level2');
mkdir(nam3,'Level3');
mkdir(nam4,'Level1');
mkdir(nam4,'Level2');
mkdir(nam4,'Level3');
mkdir(nam5,'Level1');
mkdir(nam5,'Level2');
mkdir(nam5,'Level3');


% The original depths are:
% z=[2.5 7.5 12.5 17.5 25. 35. 45. 55. 65. 75. 85. ...
%  105. 140. 185. 240. 310. 400. 515. 750. 1125. 1485. 1755. 1940. 2070.]
% but due to the s-coord and the max depth of POLCOMS grid, only the depths 2:21 are
% available, so the new files have 20 layers from 7.5 (level 20) to 1485m (level 1) depth.

lev=[20 15 12 10 6];
depths=[7.5 45 75 105 310];
isolT=[0.5:0.25:25];
VT=[1:25];
isolS=[13:0.2:19];
VS=[13:19];
isolV=[0:0.1:1];
VV=[0:0.1:1];
month=7;
for tt=10:10:50
    name1=[nam2,'mat',num2str(tt),'.mat'];
    load (name1)
    for K=1:3
        k=lev(K);
        d=depths(K);

[C,h]=contourf(x1,y1,t(:,:,k),isolT);caxis([0 25]);colorbar;
clabel(C,h,VT,'fontsize',12,'labelspacing',250,'rotation',0);
%pcolor(x,y,tem(:,:,k)');caxis([0 25]);colorbar; shading interp;
hold on
patch(BScoastline(:,1),BScoastline(:,2),[0.969,0.969,0.969]);
set(gca,'XLim',[27.3 42],'YLim',[40.8 47]);
name=['[2000] Temperature (^oC) at Depth: ',num2str(d),' m','Plot: ',num2str(tt)];
title({name},'Fontsize',12);
xlabel('Longitude ( ^{o}E)','Fontsize',12);
ylabel('Latitude ( ^{o}N)','Fontsize',12);

%gtext('Salinity (psu)','Fontsize',12,'Rotation',90);

name5=[nam3,'Level',num2str(K),'\T',num2str(K),num2str(tt)];
% %
saveas(gcf,name5,'jpg');
```

```
saveas(gcf,name5,'fig');
hold off
%%%%%%%%%%%%%%%%%%%%%%%%%%%%%%%%%%%%%%%%%%%%%%%%%%%%%%%%%%%%%

  [C,h]=contourf(x1,y1,s(:,:,k),isolS);caxis([13 19]);colorbar;
clabel(C,h,VS,'fontsize',12,'labelspacing',250,'rotation',0);
%pcolor(x,y,tem(:,:,k)');caxis([0 25]);colorbar; shading interp;
hold on
patch(BScoastline(:,1),BScoastline(:,2),[0.969,0.969,0.969]);
set(gca,'XLim',[27.3 42],'YLim',[40.8 47]);
name=['[2000] Salinity (psu), Depth: ',num2str(d),' m','Plot: ',num2str(tt)];
title({name},'Fontsize',12);
xlabel('Longitude ( ^{o}E)','Fontsize',12);
ylabel('Latitude ( ^{o}N)','Fontsize',12);

%gtext('Salinity (psu)','Fontsize',12,'Rotation',90);

name5=[nam4,'Level',num2str(K),'\S',num2str(K),num2str(tt)];
% %
saveas(gcf,name5,'jpg');
saveas(gcf,name5,'fig');
hold off


%u(81,145,k)=0.30;
%v(81,145,k)=0;
[C,h]=contour(x1,y1,vel(:,:,k),isolV);caxis([0 0.4]);colorbar;

hold on
quiver(x1(1:2:168),y1(1:2:92),u(1:2:92,1:2:168,k),v(1:2:92,1:2:168,k),scale,'k')
patch(BScoastline(:,1),BScoastline(:,2),[0.969,0.969,0.969]);
set(gca,'XLim',[27.3 42],'YLim',[40.8 47]);
%text(39.5,46.2,'0.3 m/s','Fontsize',12);
%quiver(x1(145),y1(81),u(81,145,k),v(81,145,k));
name=['[2000] Velocity (m/s), Depth: ',num2str(d),' m','Plot: ',num2str(tt)];
title({name},'Fontsize',12);
xlabel('Longitude ( ^{o}E)','Fontsize',12);
ylabel('Latitude ( ^{o}N)','Fontsize',12);
name5=[nam5,'Level',num2str(K),'\V',num2str(K),num2str(tt)];

saveas(gcf,name5,'jpg');
saveas(gcf,name5,'fig');
hold off

end


end
```

% Subroutine transpp.m

```
load initialdata
% load mat127.mat
depths=[1485 1125 750 515 400 310 240 185 140 105 85 75 65 55 45 35 25 17.5 12.5
7.5].*-1;


for tt=50:50
nam2=['C:\Cecilia\Exp18fv\1998\output_2\matmean\'];
name1=[nam2,'mat',num2str(tt),'.mat'];
   load (name1)

for i=1:92
for j=1:168
for k=1:20
p(i,j,k)=-depths(k);
end
end
end
[svan,sigma]=swstate(s,t,p);

nam=['C:\Cecilia\Exp18fv\1998\output_2\figures\'];
 mkdir(nam,'trans');
% mkdir(nam,'transS');
% mkdir(nam,'transV');
% mkdir(nam,'transSig');
T=[0.5:0.25:25];
S=[13:0.2:23];
Sn=[13:23];
Tn=[1:25];

V=[0:0.05:1];
Vn=[0:0.05:1];

Sigl=[13:0.2:19];


pr=0;

cutx=[25 35 50];
month=5;
day=14;
for ct=1:3
   i=cutx(ct);
     clear cutt cuts cutv lin
     for k=1:20
       for j=1:168
```

```
    lin(j)=zzz3(i,j,1);
    cutt(k,j)=t(i,j,k);
    cuts(k,j)=s(i,j,k);
    cutv(k,j)=vel(i,j,k);
    cutsig(k,j)=sigma(i,j,k);
    end
end
nametem=['Temperature     transect     (^oC)     Lat=',num2str(lat2(i)),'^{o}N;
Plot:',num2str(tt)];
n"namesal=['Salinity     transect     (psu)     Lat=',num2str(lat2(i)),'^{o}N;
Plot:',num2str(tt)];%',num2str(month)];
namevel=['Velocity     transect     (m/s)     Lat=',num2str(lat2(i)),'^{o}N;
Plot:',num2str(tt)];%',num2str(month)];
namesig=['Sigma-t transect (kg/m^3) Lat=',num2str(lat2(i)),'^{o}N; Plot:',num2str(tt)];

nametem2=[nam,'\trans\T',num2str(tt),'Z', num2str(ct)];
namesal2=[nam,'\trans\S',num2str(tt),'Z',num2str(ct)];
namevel2=[nam,'\trans\V',num2str(tt),'Z',num2str(ct)];
namesig2=[nam,'\trans\Sig',num2str(tt),'Z',num2str(ct)];

[C,h]=contourf(lon2,depths,cutt,T);caxis([0 25]);colorbar;
%clabel(C,h,Tn,'fontsize',12,'labelspacing',300,'rotation',0);
clabel(C,h,'manual','fontsize',12,'rotation',0);
    % pcolor(lon2,zeta5,cutt);colorbar;shading flat;
    title({nametem},'Fontsize',12);
    xlabel('Longitude (^{o}E)','Fontsize',12);
    ylabel('Depth (m)','Fontsize',12);
    hold on
    plot(lon2,lin,'LineWidth',1.5)
    hold off
    saveas(gcf,nametem2,'jpg');
    saveas(gcf,nametem2,'fig');

  [C,h]=contourf(lon2,depths,cuts,S);caxis([13 23]);colorbar;
%clabel(C,h,Sn,'fontsize',12,'labelspacing',300,'rotation',0);
clabel(C,h,'manual','fontsize',12,'rotation',0);
    %pcolor(lon2,zeta5,cuts);colorbar;shading flat;
    title({namesal},'Fontsize',12);
    xlabel('Longitude (^{o}E)','Fontsize',12);
    ylabel('Depth (m)','Fontsize',12);
    hold on
    plot(lon2,lin,'LineWidth',1.5)
    hold off
    saveas(gcf,namesal2,'jpg');
    saveas(gcf,namesal2,'fig');

  [C,h]=contourf(lon2,depths,cutv,V);caxis([0 0.4]);colorbar;
%clabel(C,h,Vn,'fontsize',12,'labelspacing',300,'rotation',0);
```

```
clabel(C,h,'manual','fontsize',12,'rotation',0);
    %pcolor(lon2,zeta5,cuts);colorbar;shading flat;
    title({namevel},'Fontsize',12);
    xlabel('Longitude (^{o}E)','Fontsize',12);
    ylabel('Depth (m)','Fontsize',12);
    hold on
    plot(lon2,lin,'LineWidth',1.5)
    hold off
    saveas(gcf,namevel2,'jpg');
    saveas(gcf,namevel2,'fig');


    [C,h]=contourf(lon2,depths,cutsig,Sigl);colorbar;
    %clabel(C,h,Sigl,'fontsize',12,'labelspacing',300,'rotation',0);
    clabel(C,h,'manual','fontsize',12,'rotation',0);
    %pcolor(lon2,zeta5,cuts);colorbar;shading flat;
    title({namesig},'Fontsize',12);
    xlabel('Longitude (^{o}E)','Fontsize',12);
    ylabel('Depth (m)','Fontsize',12);
    hold on
    plot(lon2,lin,'LineWidth',1.5)
    hold off
    saveas(gcf,namesig2,'jpg');
    saveas(gcf,namesig2,'fig');


end

%%%%%%%%%%%%%%%%%%%%%%%%%%%%%%%%%%%%%%%%%%%%%%%%%%%%%%%%%%%%%%%%
%%%%%%%%%%%%%%%%%%%%%%%%%%%%%%%%%%%%%%
cuty=[40 70 120];
for ct=1:3
    j=cuty(ct);
    clear cutt cuts cutv lin cutsig
    for k=1:20
        for i=1:92
            lin(i)=zzz3(i,j,1);
            cutt(k,i)=t(i,j,k);
            cuts(k,i)=s(i,j,k);
            cutv(k,i)=vel(i,j,k);
            cutsig(k,i)=sigma(i,j,k);
        end
    end

    nametem=['Temperature      transect      (^oC)      Lon=',num2str(lon2(j)),'^{o}E;
Plot:',num2str(tt)];% Month ',num2str(month)];
    namesal=['Salinity  transect  (psu)  Lon=',num2str(lon2(j)),'^{o}E;  Plot:',num2str(tt)];%
Month ',num2str(month)];
```

```
namevel=['Velocity        transect        (m/s)        Lon=',num2str(lon2(j)),'^{o}E;
Plot:',num2str(tt)];% Month ',num2str(month)];
    namesig=['Sigma-t        transect        (kg/m^3)        Lon=',num2str(lon2(j)),'^{o}E;
Plot:',num2str(tt)];

    nametem2=[nam,'\trans\T',num2str(tt),'M', num2str(ct)];
    namesal2=[nam,'\trans\S',num2str(tt),'M',num2str(ct)];
    namevel2=[nam,'\trans\V',num2str(tt),'M',num2str(ct)];
    namesig2=[nam,'\trans\Sig',num2str(tt),'M',num2str(ct)];

    [C,h]=contourf(lat2,depths,cutt,T);caxis([0 25]);colorbar;
    %clabel(C,h,Tn,'fontsize',12,'labelspacing',300,'rotation',0);
    clabel(C,h,'manual','fontsize',12,'rotation',0);
    % pcolor(lon2,zeta5,cutt);colorbar;shading flat;
    title({nametem},'Fontsize',12);
    xlabel('Latitude (^{o}N)','Fontsize',12);
    ylabel('Depth (m)','Fontsize',12);
    hold on
    plot(lat2,lin,'LineWidth',1.5)
    hold off
    saveas(gcf,nametem2,'jpg');
    saveas(gcf,nametem2,'fig');

    [C,h]=contourf(lat2,depths,cuts,S);caxis([13 23]);colorbar;
    %clabel(C,h,Sn,'fontsize',12,'labelspacing',300,'rotation',0);
    clabel(C,h,'manual','fontsize',12,'rotation',0);
    %pcolor(lon2,zeta5,cuts);colorbar;shading flat;
    title({namesal},'Fontsize',12);
    xlabel('Latitude (^{o}N)','Fontsize',12);
    ylabel('Depth (m)','Fontsize',12);
    hold on
    plot(lat2,lin,'LineWidth',1.5)
    hold off
    saveas(gcf,namesal2,'jpg');
    saveas(gcf,namesal2,'fig');

    [C,h]=contourf(lat2,depths,cutv,V);caxis([0 0.4]);colorbar;
    %clabel(C,h,Vn,'fontsize',12,'labelspacing',300,'rotation',0);
    clabel(C,h,'manual','fontsize',12,'rotation',0);
    %pcolor(lon2,zeta5,cuts);colorbar;shading flat;
    title({namevel},'Fontsize',12);
    xlabel('Latitude (^{o}N)','Fontsize',12);
    ylabel('Depth (m)','Fontsize',12);
    hold on
    plot(lat2,lin,'LineWidth',1.5)
    hold off
    saveas(gcf,namevel2,'jpg');
    saveas(gcf,namevel2,'fig');
```

```
[C,h]=contourf(lat2,depths,cutsig,Sigl);colorbar;
%clabel(C,h,Sigl,'fontsize',12,'labelspacing',300,'rotation',0);
clabel(C,h,'manual','fontsize',12,'rotation',0);
%pcolor(lon2,zeta5,cuts);colorbar;shading flat;
title({namesig},'Fontsize',12);
xlabel('Latitude (^{o}N)','Fontsize',12);
ylabel('Depth (m)','Fontsize',12);
hold on
plot(lat2,lin,'LineWidth',1.5)
hold off
saveas(gcf,namesig2,'jpg');
saveas(gcf,namesig2,'fig');


end


end
```

■■

% Subroutine Curlcurr.m

```
clear
load tierra
scale=2;
  nam2=['C:\Cecilia\Exp18fv\1998\output_2\matmean\'];
  nam3=['C:\Cecilia\Exp18fv\Appendix Interannual hydrodynamics\maps98\'];

lev=[20 15 12 10 6 5];
depths=[7.5 45 75 105 310 400];

C=[-5:0.5:5];
Vn=[-0.2:0.05:0.2];
month=5;
output=[10 20 30 40 50 60 70 80];
Julday=[7 14 21 28 35 42 49 56];
%for tt=10:88
 for sample=2:2

tt=output(sample);
day=Julday(sample);

name1=[nam2,'mat',num2str(tt),'.mat'];
  load (name1)
  for K=1:6
  %K=1;
    k=lev(K);
    d=depths(K);
```

```
[Curlz,cav]=curl(x1,y1,u(:,:,k),v(:,:,k));

pcolor(x1,y1,Curlz);caxis([-2 2]);colorbar;shading interp;

%
%    [C,h]=contourf(x1,y1,Curlz,C,'w');caxis([-5 5]);colorbar;
%       clabel(C,h,Vn,'fontsize',12,'Fontweight','Bold','labelspacing',250);
    hold on
    u(81,145,k)=0.50; v(81,145,k)=0;
    quiver(x1(1:2:168),y1(1:2:92),u(1:2:92,1:2:168,k),v(1:2:92,1:2:168,k),scale,'k')
    patch(BScoastline(:,1),BScoastline(:,2),[0.969,0.969,0.969]);
    set(gca,'XLim',[27.3 42],'YLim',[40.8 47]);
    text(39.5,46.2,'0.5 m/s','Fontsize',12);
%       quiver(x1(145),y1(81),wz(145,81)',wm(145,81)','k');
    name=['Currents curl (s^-1); Day: ',num2str(day),'; 1998; ','Depth: ',num2str(d)]
    title({name},'Fontsize',12);
    xlabel('Longitude ( ^{o}E)','Fontsize',12);
    ylabel('Latitude ( ^{o}N)','Fontsize',12);
     pause

%gtext('Salinity (psu)','Fontsize',12,'Rotation',90);

name5=[nam3,'CurlLev',num2str(K),'Plot',num2str(tt)];
%
saveas(gcf,name5,'jpg');
saveas(gcf,name5,'fig');
 hold off
 end

end
```

■■

% Subroutine Enscurr.m

```
clear
load tierra
scale=2;
 nam2=['C:\Cecilia\Exp18fv\2000\output_2\matmean\'];
 nam3=['C:\Cecilia\Exp18fv\Appendix Interannual hydrodynamics\maps00\'];

lev=[20 15 12 10 6 5];
depths=[7.5 45 75 105 310 400];

Cont=[0:5:100];
Vn=[-0.2:0.05:0.2];
month=5;
```

```
output=[10 20 30 40 50 60 70 80];
Julday=[7 14 21 28 35 42 49 56];
%for tt=10:88
 for sample=1:8

tt=output(sample);
day=Julday(sample);

name1=[nam2,'mat',num2str(tt),'.mat'];
  load (name1)
  for K=1:6
  %K=1;
    k=lev(K);
    d=depths(K);

    [Curlz,cav]=curl(x1,y1,u(:,:,k),v(:,:,k));

    pcolor(x1,y1,Curlz.^2);caxis([0 30]);colorbar;shading interp;
%
%
  %  [C,h]=contourf(x1,y1,Curlz.^2,Cont,'w');colorbar;
%       clabel(C,h,Vn,'fontsize',12,'Fontweight','Bold','labelspacing',250);
    hold on
    u(81,145,k)=0.50; v(81,145,k)=0;
    quiver(x1(1:2:168),y1(1:2:92),u(1:2:92,1:2:168,k),v(1:2:92,1:2:168,k),scale,'k')
    patch(BScoastline(:,1),BScoastline(:,2),[0.969,0.969,0.969]);
    set(gca,'XLim',[27.3 42],'YLim',[40.8 47]);
    text(39.5,46.2,'0.5 m/s','Fontsize',12);
%       quiver(x1(145),y1(81),wz(145,81)',wm(145,81)','k');
    name=['Currents   enstrophy   (s^-2);   Day:   ',num2str(day),';   2000;   ','Depth:
',num2str(d)]
    title({name},'Fontsize',12);
    xlabel('Longitude ( ^{o}E)','Fontsize',12);
    ylabel('Latitude ( ^{o}N)','Fontsize',12);
    % pause

%gtext('Salinity (psu)','Fontsize',12,'Rotation',90);

name5=[nam3,'EnstLev',num2str(K),'Plot',num2str(tt)];
%
saveas(gcf,name5,'jpg');
saveas(gcf,name5,'fig');
 hold off
 end

end
```